1987

THE CHARACTERISTICS OF SYNTHETIC AND NATURAL HYDROUS IRON OXIDES IN AQUEOUS ENVIRONMENTS

Man, Vincent

THE CHARACTERISTICS OF SYNTHETIC AND NATURAL HYDROUS IRON OXIDES IN AQUEOUS ENVIRONMENTS

by

Vincent Man, B.Sc., M.Sc.

Submitted to the Council for National Academic Awards
in partial fulfilment of the requirements for the
degree of Doctor of Philosophy.

Date: June 1987

Department of Environmental Sciences,
Plymouth Polytechnic,
Drake Circus,
Plymouth PL4 8AA,
England, U.K.

in association with:

Department of Marine Science,
Plymouth Polytechnic,
Drake Circus,
Plymouth PL4 8AA,
England, U.K.

THE CHARACTERISTICS OF SYNTHETIC AND NATURAL HYDROUS IRON OXIDES IN AQUEOUS ENVIRONMENTS by V. MAN, BSc (HONS)

A B S T R A C T

The work in this thesis is concerned with the Green Rusts, which are blue-green metastable Fe(II) - Fe(III) hydroxy compounds incorporating anions such as SO_4^{2-}, Cl^- or CO_3^-. These Green Rust compounds (or Fe-GR compounds to distinguish them from the aluminium Green Rusts (Al-GRs) which are isostructural Fe(II) - Al(III) hydroxy compounds) can be produced in a consistent fashion from Fe(II) solutions by the method of induced hydrolysis using Fe(III) gel at pH 7 and under anoxic conditions. A series of sulphate and chloride Fe-GR samples were synthesised, and characterised primarily by the analytical techniques of Mössbauer spectroscopy, X-Ray diffractometry, infra-red spectroscopy, and vacuum microbalance to measure surface area using the BET N_2 adsorption method.

For comparison, a few samples of the analogous Al-GR compounds were also synthesised and characterised by the analytical techniques mentioned above.

The results in this thesis showed that the systems producing the Fe-GR compounds were of a highly complex nature, and that the amount of precipitate formed depended crucially on the starting conditions. For the 0.1 M $FeSO_4$ system, the GR formed was almost always accompanied by a goethite phase while, for the 0.1 M $FeCl_2$ system, pure GR material was only formed at initial Fe(II) - Fe(III) ratios (IFFRs) greater than 6. Any differences between the sulphate and chloride Fe-GRs can be attributed to the difference in anion-type. X-Ray diffraction in conjunction with electron microscopy and surface area measurements confirm that the Fe-GRs have a pyroaurite crystal structure, with brucite-like layers formed by a matrix of Fe^{2+} and Fe^{3+} cations and each layer bridged to the other by anions. As far as Mössbauer spectroscopy is concerned, the most important diagnostic parameter is the quadrupole splitting (QS) of the Fe(II) doublet measured at 77K for the wet, fresh precipitate (i.e. frozen material). For sulphate Fe-GRs derived from 0.1 M $FeSO_4$ the mean QS is 2.93 ± 0.05 mms^{-1}, while for the chloride Fe-GRs derived from 0.1 M $FeCl_2$ the mean QS is 2.80 ± 0.05 mms^{-1}. Surface areas for the sulphate Fe-GRs are in the range 40-65 $m^2.g^{-1}$.

The products of oxidation and ageing for the Fe-GRs indicate several transformation pathways, especially for the chloride Fe-GRs. Sulphate Fe-GRs converted to goethite on oxidation under both wet and dry conditions, while the chloride Fe-GRs converted to akaganeite on dry oxidation, and to lepidocrocite on wet oxidation. Under both wet and dry anoxic conditions, the chloride Fe-GRs converted to magnetite. In the case of the sulphate Fe-GRs, there was a suggestion that, under the right wet anoxic conditions, the material probably transformed into magnetite. These facts clearly demonstrate that the Fe-GRs are intermediaries in the thermodynamic transformation of Fe in the II oxidation state to Fe in the III oxidation state.

ACKNOWLEDGEMENTS

I would like to thank my supervisors Geoff Millward, Alan Cuttler and Doug Glasson for their help and patience. Thanks are also due to Dave Howard for typing most of the tables in this thesis, to Ken Pearson for the atomic absorption data and to all others who have helped in this research programme.

This thesis was produced on an Apple II microcomputer system using the Applewriter wordprocessor software.

CONTENTS

THE CHARACTERISTICS OF SYNTHETIC AND NATURAL HYDROUS IRON OXIDES IN AQUEOUS ENVIRONMENTS by V. MAN, BSc (HONS)

A B S T R A C T

The work in this thesis is concerned with the Green Rusts, which are blue-green metastable Fe(II) - Fe(III) hydroxy compounds incorporating anions such as SO_4^{2-}, Cl^- or CO_3^-. These Green Rust compounds (or Fe-GR compounds to distinguish them from the aluminium Green Rusts (Al-GRs) which are isostructural Fe(II) - Al(III) hydroxy compounds) can be produced in a consistent fashion from Fe(II) solutions by the method of induced hydrolysis using Fe(III) gel at pH 7 and under anoxic conditions. A series of sulphate and chloride Fe-GR samples were synthesised, and characterised primarily by the analytical techniques of Mössbauer spectroscopy, X-Ray diffractometry, infra-red spectroscopy, and vacuum microbalance to measure surface area using the BET N_2 adsorption method.

For comparison, a few samples of the analogous Al-GR compounds were also synthesised and characterised by the analytical techniques mentioned above.

The results in this thesis showed that the systems producing the Fe-GR compounds were of a highly complex nature, and that the amount of precipitate formed depended crucially on the starting conditions. For the 0.1 M $FeSO_4$ system, the GR formed was almost always accompanied by a goethite phase while, for the 0.1 M $FeCl_2$ system, pure GR material was only formed at initial Fe(II) - Fe(III) ratios (IFFRs) greater than 6. Any differences between the sulphate and chloride Fe-GRs can be attributed to the difference in anion-type. X-Ray diffraction in conjunction with electron microscopy and surface area measurements confirm that the Fe-GRs have a pyroaurite crystal structure, with brucite-like layers formed by a matrix of Fe^{2+} and Fe^{3+} cations and each layer bridged to the other by anions. As far as Mössbauer spectroscopy is concerned, the most important diagnostic parameter is the quadrupole splitting (QS) of the Fe(II) doublet measured at 77K for the wet, fresh precipitate (i.e. frozen material). For sulphate Fe-GRs derived from 0.1 M $FeSO_4$ the mean QS is 2.93 ± 0.05 mms^{-1}, while for the chloride Fe-GRs derived from 0.1 M $FeCl_2$ the mean QS is 2.80 ± 0.05 mms^{-1}. Surface areas for the sulphate Fe-GRs are in the range 40-65 $m^2.g^{-1}$.

The products of oxidation and ageing for the Fe-GRs indicate several transformation pathways, especially for the chloride Fe-GRs. Sulphate Fe-GRs converted to goethite on oxidation under both wet and dry conditions, while the chloride Fe-GRs converted to akaganeite on dry oxidation, and to lepidocrocite on wet oxidation. Under both wet and dry anoxic conditions, the chloride Fe-GRs converted to magnetite. In the case of the sulphate Fe-GRs, there was a suggestion that, under the right wet anoxic conditions, the material probably transformed into magnetite. These facts clearly demonstrate that the Fe-GRs are intermediaries in the thermodynamic transformation of Fe in the II oxidation state to Fe in the III oxidation state.

LIST OF ABBREVIATIONS USED

Compounds

GR = Green Rust

Fe-GR = iron Green Rust (= GR in appropriate context)

Al-GR = aluminium Green Rust

SO_4 = sulphate } mainly in figures

Cl = chloride } and tables

Techniques

MbS = Mossbauer spectroscopy

XRD = X-ray diffraction

IRS = Infrared spectroscopy

AAS = Atomic absorption spectroscopy

Units

A = angstrom (in appropriate context)

°C = degrees Celsius

K = degrees Kelvin

T = tesla

Others

RT = room temperature

PI = π

Mb = Mossbauer

FFR = Fe(II)-Fe(III) ratio

IFFR = Initial Fe(II)-Fe(III) ratio

LIST OF PLATES

Plate 7. Electron micrograph of the wet, fresh precipitate of chloride Al-GR sample GR19 (IFFR = 20). Magnification: X 5500

CHAPTER 1: INTRODUCTION

1.1 Interest in Iron Compounds

Iron is the fourth most abundant element in the Earth's crust (ca. 5% by weight) and it is ubiquitous in the natural environment (see Fig 1.1). The various solid and dissolved forms of iron play major roles in processes that occur in nature (Stumm & Morgan, 1981). Despite the prevalence of this element, knowledge of the mechanisms of formation of the wide range of iron solids, and their behaviour, is poorly understood. This thesis is concerned with a particular form of iron solids, namely Green Rusts, which are thought to be precursors of other important iron compounds. Throughout the thesis, the term "iron oxides" is used collectively for oxides, hydroxides, oxyhydroxides and hydroxy salts of iron, except where it is used specifically to mean the normal oxides of iron.

The study of iron oxides is important for the following reasons:

(i) The two oxidation states of iron, i.e. Fe(II) and Fe(III), play a dominant role in the chemistry of natural

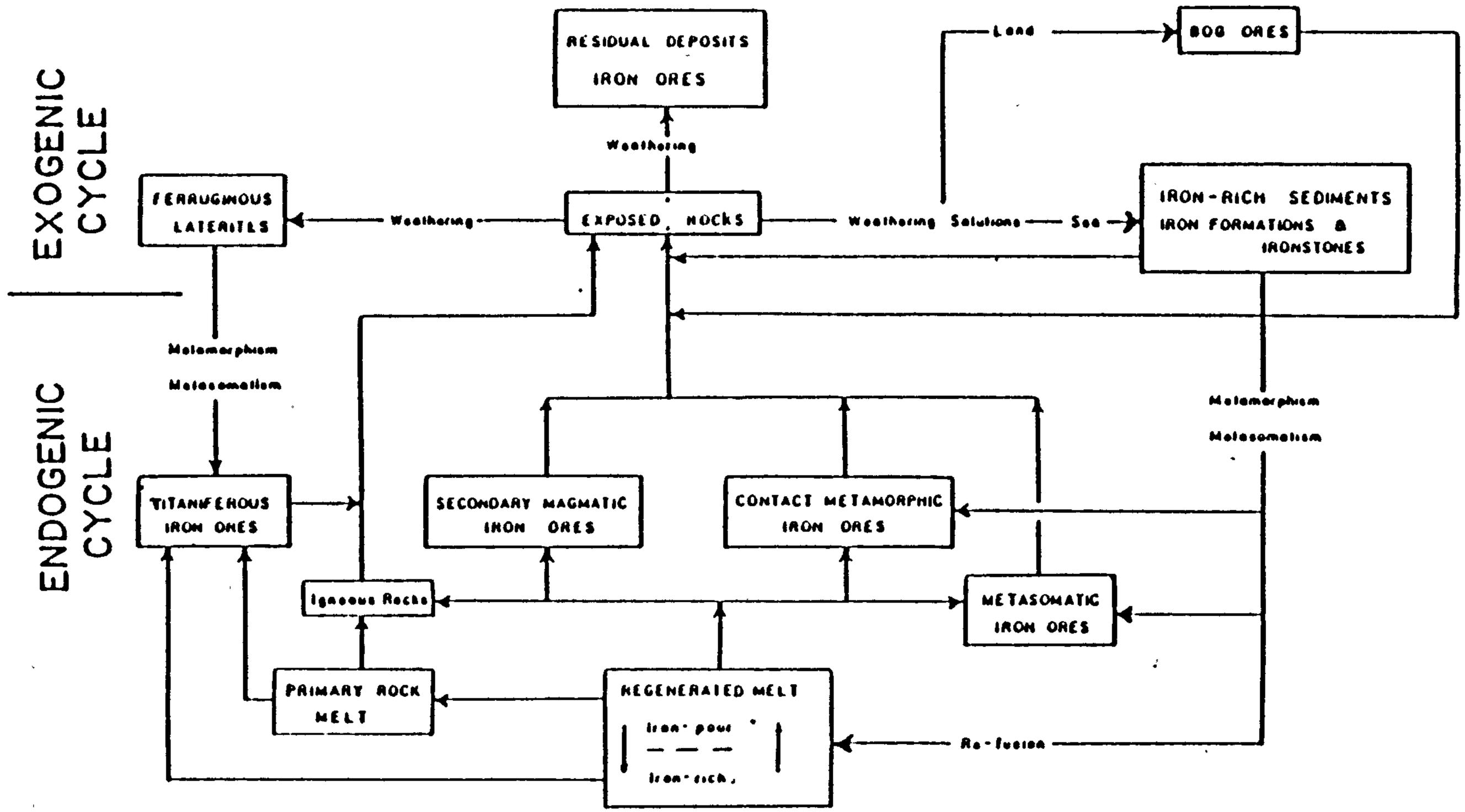

Fig 1.1 Iron cycling in the lithosphere.
(after Lepp, 1975)

waters, water supplies and waste waters (Langmuir & Whittemore, 1970). Iron solids exert their control by their surface activity which determines the partitioning of dissolved constituents between the dissolved and solid phases. The formation of iron colloids, precipitates and the presence of aged iron oxides in natural waters means that there is often considerable available surface area in the water column. The sorption properties of the solids relate to the behaviour of organic materials (Schwertmann & Taylor, 1979; Tipping; 1981; Davis, 1982) and inorganic ions and ligands (e.g. Crosby et al., 1981; Millward & Moore, 1982; Benjamin, 1983). Indeed, the control of heavy metal concentrations in seawater by iron oxides was first suggested by Goldberg (1954) and Krauskopf (1956). This has led to studies of the iron content of deep ocean sediments such as manganese nodules (Cronan, 1976) and clays (Elderfield, 1976; Johnston & Glasby, 1982; Johnston & Lewis, 1983). Furthermore the recognition of the sorption capacity of iron oxides has led to studies of the surface characteristics of natural and synthetic precipitates (Schwertmann & Fischer, 1973; Schwertmann & Taylor, 1979; Carlson & Schwertmann, 1980 & 1981; Crosby et al., 1983). However, considerably more work is needed in this area, particularly on the nature of natural iron oxides. Much more information is available on Fe(III) hydroxide which has been used for many years in the removal of phosphate from treated sewage and in waste water treatment (Gloyna &

Eckenfelder, 1970; Lijklema, 1980).

(ii) Iron oxides are important components in soils and many of the crystalline forms have been identified as the result of pedogenesis (Schwertmann & Taylor, 1977). The type and distribution of iron oxides within a soil profile often determines its colour and mechanical properties. Indeed soil colour is a crucial criterion for the naming and classification of soils (e.g. Red-Yellow Podzolic, sols rouges tropicaux, terra rossa, etc.). Iron oxides affect soil structure and texture by the formation of aggregates and cementation of other major soil components, giving rise to granules, nodules, pipe-stems or bog iron ores. The high specific surface area of iron oxides make them efficient sinks for anions such as phosphate, molybdate and silicate as well as trace elements like Cu, Pb, V, Zn, Co, Cr and Ni, some of which are essential for plant growth (Kinniburgh et al., 1976).

(iii) Geological deposits of iron ores can be of commercial value and usually consist of a mixture of iron oxides and other iron-bearing minerals, such as siderite ($FeCO_3$) and iron silicates (e.g. chamosite and greenalite), plus rock material or gangue (Baumann, 1976). The majority of deposits come from sedimentary iron formations, others are magmatic in origin. A knowledge of the characteristics and mechanisms of formation of iron oxide deposits would be useful in

establishing the type of prevailing geologic environment existing during formation. From this, the occurrence of important sedimentary iron deposits may be predicted, but currently this is not possible.

(iv) The rusting of iron in the atmosphere is intrinsically linked to the formation of iron oxides on the iron surface (Evans, 1967). A study of synthetic iron oxides would assist in the identification of the oxide phases produced and thus help in understanding the mechanism of rusting.

(v) In aqueous environments where a defiency of oxygen exists, such as in anoxic sediments, in stratified lakes and fjords and in gleyed soils, the presence of iron oxide precipitates or coatings are linked with the respiratory activities of microorganisms (Stumm & Morgan, 1981). Anoxygenic bacteria, make use of Fe(III) oxides as final electron acceptors for the oxidative decomposition of organic matter (Schwertmann & Taylor, 1977). This process results in the reduction of Fe(III) materials and give rise to dissolved Fe(II) cations in solution. In oxygenated water columns, Fe(II) can oxidise relatively quickly (i.e. mins.) to Fe(III) (Sung & Morgan, 1980). In addition, oxygenic bacteria can also participate in the oxidation process and the laying down of Fe(III) precipitates (Bowen, 1966; Chukhrov et al., 1976; Noike et al., 1983). Thus, iron oxides can function as

important intermediaries in biogenic activity and, given their adsorptive capacity, they can be a source of micronutrients which are required for plant and animal metabolism.

The following sections describe the range of iron oxides known and the details of the present understanding of their processes of formation.

1.2 Synthetic iron oxides

The chemistry of iron oxides involves the Fe(II) and Fe(III) oxidation states. Three types of oxide can result: (i) Fe(II) oxides (ii) Fe(III) oxides and (iii) mixed Fe(II)-Fe(III) oxides. The inter-relationships between the various forms are shown in Fig 1.2.

1.2.1 Fe(II) oxides

There are only two oxides in this category. One is Fe(II) oxide, FeO, which is formed when iron is heated above 848 K in a low partial pressure of oxygen (Sidgwick, 1950; Nicholls, 1973). It is only stable at high temperatures and is always cation deficient with an upper limit of $Fe_{0.74}O$ (Greenwood & Gibb, 1971). When cooled slowly, the oxide decomposes to Fe and Fe_3O_4 (magnetite). To prevent this disproportionation, the high temperature product must be quenched rapidly. Fe(II) oxide is a black substance with a melting point of ~ 1633 K. The crystalline form has a rock salt lattice and is known as wustite. Since FeO is unlikely to be encountered in aqueous environments, both in synthetic and natural systems, the oxide has therefore not been studied in this research programme.

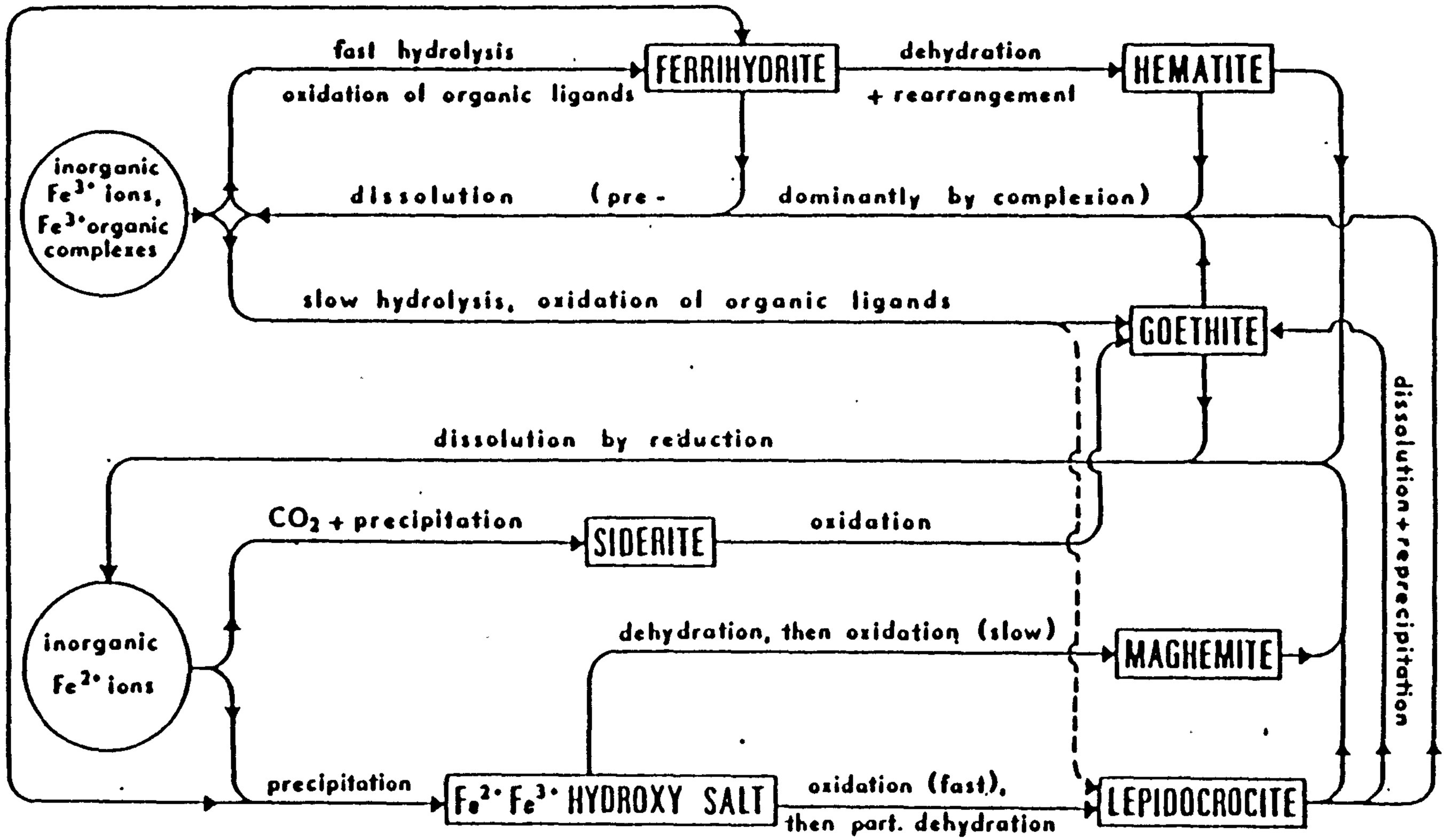

Fig 1.2 Possible pathways of iron oxide formation under near pedogenic conditions. (after Schwertmann & Taylor, 1977)

The other Fe(II) oxide is Fe(II) hydroxide, $Fe(OH)_2$, produced as a precipitate when a solution of Fe(II) salt is added to an excess of alkali under oxygen-free conditions. When pure, $Fe(OH)_2$ is white to pale greenish-white in colour but if oxygen is absorbed then it becomes a darker green due to the presence of Fe(III) cations. Fe(II) hydroxide has the CdI_2 layer structure in which every Fe atom is surrounded by six OH groups (Nicholls, 1973). It is extremely unstable in air, oxidising in a matter of minutes through a dark-green metastable phase to a reddish-brown hydrous Fe(III) oxide. This has been shown under some circumstances to give rise to lepidocrocite (γ-FeOOH) over short ageing periods (Sung & Morgan, 1980; Crosby et al., 1983). Consequently, it is a powerful reducing agent. In excess alkali conditions, $Fe(OH)_2$ converts to a black magnetic oxide which is probably magnetite/maghemite.

The solubility product of $Fe(OH)_2$ is ~ 10^{-14} (Sidgwick, 1950; Stumm & Morgan, 1981) which compares with a value of 10^{-33} for $Fe(OH)_3$. Consideration of the differences in these two solubility products indicates that the rate of nucleation of $Fe(OH)_2$ is much slower than $Fe(OH)_3$. This suggests that the precipitates derived from these two sources will have different morphologies and possibly different surface characteristics.

1.2.2 Fe(III) oxides

This group forms the largest class of iron oxides due to the high stability of the Fe(III) oxidation state under a wide range of conditions:

$$Fe^{3+} + e^- \longrightarrow Fe^{2+} \quad [\ln k\ (298\ K) = +13.2] \qquad -1.1$$

It includes the two polymorphs of Fe(III) oxide (α- and γ-Fe_2O_3), the five polymorphs of Fe(III) oxyhydroxide (α-, β-, γ-, δ- and δ'-FeOOH) and hydrous Fe(III) oxide ($xFe_2O_3.nH_2O$). Because Fe(III) oxides can be formed under a wide range of conditions, there are many methods for their preparation.

1.2.2a Fe(III) oxide (Fe_2O_3)

The two forms of Fe(III) oxide are haematite (α-Fe_2O_3) and maghemite (γ-Fe_2O_3). They are structurally and magnetically different. Haematite has the corundum (Al_2O_3) structure in which each Fe atom is surrounded octahedrally by six oxygen atoms, the latter being in hexagonally close-packed array (Nicholls, 1973; Greenwood & Gibb, 1971). It has a complex magnetic behaviour, being antiferromagnetic at low temperatures, then undergoing a transition above the Morin temperature (T_M = 260 K)

to a weak ferrimagnetic state as a result of spin canting, before finally becoming paramagnetic at high temperature. According to Kundig et al. (1966), the Neel temperature (T_N) is about 961 K. Haematite is bright red to crimson in colour with a M.P. of 1838 K.

Maghemite has the inverse spinel structure (AB_2O_4) in which the A site cations are tetrahedrally co-ordinated by oxygen and the B sites cations octahedrally co-ordinated by oxygen. It is therefore isostructural with magnetite (see section 1.2.3) except that there are insufficient Fe(III) cations to fill all the A and B sites. The stoichiometry therefore corresponds to $Fe^{3+}_{8/3}[]_{1/3}O_4$ where [] refers to a cation vacancy (Greenwood & Gibb, 1971). Like magnetite, γ-Fe_2O_3 is ferrimagnetic below the Neel temperature due to the antiparallel alignment of the A and B sublattices. Because of the similarities between magnetite and maghemite, the latter is often thought as a special case of magnetite in which the cation vacancy is at a maximum. Indeed, compounds with an intermediate composition have been shown to exist (Deer et al., 1962). Maghemite is brown to dark-brown in colour and has a bulk saturation magnetism of 83.5 $emu.g^{-1}$ at room temperature (RT). On heating in air between 670-720 K, maghemite converts to α-Fe_2O_3 (Deer et al., 1962; Taylor & Schwertmann, 1974).

1.2.2b Fe(III) oxyhydroxide (FeOOH)

Of the five polymorphs, goethite (α-FeOOH) is the most well-known and has been studied the most. It is the form which has greatest thermodynamic stability and, therefore, is the phase to which the other polymorphs would eventually transform to upon ageing in solution (Murray, 1979). Goethite has the crystal structure of diaspore (α-AlOOH) with the Fe in a distorted octahedral environment of oxygen, and a 3-dimensional structure results from the sharing of edges and corners of the octahedra (Greenwood & Gibb, 1971). It is antiferromagnetic below its Neal temperature of 403 K (Forsyth et al., 1968). Goethite dehydrates to haematite on heating to ~ 540 K or above (Francome & Rocksby, 1959). The colour of goethite can range from yellow to brown.

Akaganeite (β-FeOOH) differs from the other FeOOH phases in that it is non-stoichiometric, containing various quantities of F^-, Cl^- and H_2O. It is isostructural with hollandite (α-MnO_2) but with OH groups replacing half of the oxygen atoms (Mackay, 1960). The iron is again in an octahedral environment of oxygen. The oxyhydroxide is uniquely characterised by tunnels (~ 5 A in diameter) running parallel to the c-axis. It is

these tunnels which can accommodate a variety of anions and H_2O moleculas.. Large anions (especially Cl^-) are essential for the formation of the tunnel structure and hence β-FeOOH (Murray, 1979). Akaganeite is antiferromagnetic below 295 K, its Neel temperature (Takada et al., 1964; Rossiter & Hodgson, 1965; Dezsi et al., 1967). It is paramagnetic from 295 K to 520-670 K, at which point it decomposes to haematite (Dezsi et al., 1967; Vlasov, 1972). The colour of β-FeOOH is usually yellow to yellowish-brown.

The crystal structure of lepidocrocite (γ-FeOOH) is identical to that for boehmite (γ-AlOOH). The lattice consists of iron-centred oxygen octahedra linked together in chains by sharing diagonally opposite edges, the chains running parallel to the x-axis. These chains are in turn linked laterally to each other by sharing octahedral corners, thus forming parallel layers. The layers are held together by weak hydrogen bonding, giving rise to perfect cleavage in a given plane (Deer et al., 1962). Lepidocrocite is antiferromagnetic below the Neel temperature of 73 K (Johnson, 1969). On heating it is transformed to maghemite at 520-570 K (Murray, 1979). Typically, lepidocrocite is orange in colour but it can also be brown to orangey-brown.

Delta Fe(III) oxyhydroxide (δ-FeOOH) has no mineral name because as yet it has not been identified in the natural

environment. A modification of this phase (δ'-FeOOH) has been reported to exist in natural samples and the name feroxyhite has been proposed for it (Chukhrov et al., 1977). The structure of both δ-FeOOH and δ'-FeOOH consists of a hexagonally close-packed array of O^{2-} and OH^- anions. In δ-FeOOH, there are two Fe sites, with approximately 80% of the Fe distributed randomly in the octahedral sites and 20% similarly placed in the tetrahedral sites (Francome & Rooksby, 1959). In the case of δ'-FeOOH, the distribution of Fe occurs uniformly in half of the octahedral sites but there is disorder in the lattice as a whole (Chukhrov et al., 1977). Otherwise, the structure of δ- and δ'-FeOOH is basically the same. The lattice is somewhat similar to that of $Fe(OH)_2$ which has the CdI_2 structure. This is not surprising in view of the fact that both δ- and δ'-FeOOH can be formed topotactically from $Fe(OH)_2$. According to Dezsi et al. (1967) and Chukhrov et al. (1977), δ-FeOOH is ferrimagnetic at RT but this will depend on particle size. δ'-FeOOH is only weakly ferrimagnetic owing to its more disordered state. Bernal et al. (1959) obtained a value of ~ 19 $emu.g^{-1}$ for the saturation magnetisation of δ-FeOOH at RT. On heating in air, both δ- and δ'-FeOOH convert to haematite (α-Fe_2O_3). However, δ-FeOOH partially converts to α-FeOOH at ~ 400 K before fully transforming to haematite at ~ 510 K (Dezsi et al., 1967; Francome & Rooksby, 1959). In the case of δ'-FeOOH, conversion to haematite takes place at 513-523

K (Carlson & Schwertmann, 1980). The colour of δ-FeOOH varies from dark-brown to reddish-brown while δ'-FeOOH is usually brown to ochre-brown in colour.

1.2.2c Hydrous Fe(III) oxide ($xFe_2O_3.nH_2O$)

This is a class of Fe(III) oxides which have been termed "ferric gels" due to their gel-like nature when wet. It has also been called "amorphous ferric hydroxide". The name ferrihydrite has been given to the hydrated Fe(III) oxide with bulk composition $5Fe_2O_3.9H_2O$ (Chukhrov et al., 1971). From infrared absorption spectra, Russell (1979) suggested OH to be an essential part of the ferrihydrite structure , and arrived at the formula $Fe_2O_3.2FeOOH.2.6H_2O$. Most hydrous Fe(III) oxides, both natural and synthetic, are X-ray amorphous and therefore little is known of their structure. However, a tentative crystal structure have been proposed for ferrihydrite by Chukhrov et al. (1972) based on the work of van der Giessen (1966) and Towe & Bradley (1967). Essentially, ferrihydrite has a defect haematite structure where some oxygen atoms are replaced by OH groups and/or H_2O molecules, and less Fe occurs in the octahedral sites. This leads to a higher O/Fe ratio and the absence of the strong diffraction lines of haematite.

As with the Fe(III) oxides, ferrihydrite transforms to haematite (α-Fe_2O_3) on heating in air; the temperature of conversion being 570-670 K (Chukhrov et al., 1972; Kauffman & Hazel, 1975). Ferrihydrite is a paramagnetic oxide (the Neel temperature being just above 4 K) and is typically crimson-brown in colour when produced synthetically.

1.2.3 Fe(II)-Fe(III) oxides

Included in this group are the series of green hydrous Fe oxides, known collectively as the "Green Rusts", and the magnetic oxide, magnetite (Fe_3O_4).

1.2.3a Magnetite (Fe_3O_4)

Magnetite has an inverse spinel structure, is ferrimagnetic below the ferrimagnetic Neel temperature of 858 K and can be characterised with either of the following two formulae:

(1) $(\downarrow Fe^{3+})[\uparrow Fe^{3+}\downarrow e^{-1}]\ O_4$ (Boekema et al., 1976)

tet. oct.
A sites B sites

N.B. The arrows within the brackets show the spin orientations below the Neel temperature.

(2) Fe^{3+} $[Fe^{2+}\ Fe^{3+}]\ O_4$ (Greenwood & Gibb, 1971)
tet. oct.
A sites B sites

A transition in many of its physical properties takes place at what is known as the Verwey transition temperature (T_v = 119 K) (Verwey et al., 1947). Above T_v, magnetite is probably a degenerate semiconductor or perhaps a semimetal. Verwey et al.(1947) postulated that above T_v the conduction electrons can be considered as hopping rapidly between the Fe(II) and Fe(III) cations in the octahedral B sites (Boekema et al., 1976; Greenwood & Gibb, 1971). Others have suggested that the conduction electrons move in narrow d bands which are fully spin-polarised. Below T_v, magnetite is an insulator and has orthorhombic symmetry. Here the electrons of the octahedral B sites are confined to a particular Fe atom, giving rise to discrete valence states of Fe^{2+} and Fe^{3+}. Magnetite is normally black to greyish-black in colour and its saturation magnetisation at RT is 92-93 $emu.g^{-1}$ (Deer et al., 1962). Synthetic magnetite made from solutions at low temperature is easily oxidised in air at 473-573 K to maghemite (γ-Fe_2O_3) (van der Marel, 1951). Thereafter, at higher temperatures it is converted to haematite (α-Fe_2O_3). However, magnetite obtained synthetically by the reduction of haematite at high temperature (~ 1670 K) is a very stable product and does not convert to α-Fe_2O_3 until ~ 1070 K (van

der Marel, 1951). It does not seem to pass through an γ-Fe_2O_3 phase. This behaviour is also true for natural magnetites of magmatic origin. The difference in the two types of behaviour is attributed to irregularities in the crystal structure. The melting point of magnetite (the high temperature variety) is 1811 K (Sidgwick, 1950; Nicholls, 1970).

1.2.3b The Green Rusts

The Green Rusts are hydroxy salts of iron with the basic formula:

$$Fe^{2+}_x-Fe^{3+}_y(O^{2-}, OH^-, A)_z$$

where x = 1.95-3.6, y = 0.9-2.55 and A represents anions, such as Cl^-, Br^-, SO_4^{2-} or CO_3^{2-}, which replaces some of the OH^- groups (Taylor & McKenzie, 1980). They are metastable under normal conditions, being extremely unstable to oxidation (minimum of minutes). The crystal structure has been determined by Bernal et al., (1959) and apparently belongs to the pyrocaurite group (Taylor, 1973; Taylor, 1980; Taylor & McKenzie, 1980). The basic structure consists of Fe(II) and Fe(III) cations octahedrally surrounded by oxygen in brucite-like sheets which are separated by interlayers containing anion groups and

H_2O. The type of anion determines the degree of separation of the brucite-like sheets. Green Rusts formed from solutions containing Cl^-, Br^- or SO_4^{2-} anions and having an X-ray basal d-spacing of 7.5-8.0 A have been designated as Green Rust I (GRI) by Bernal et al. (1959). The Green Rusts formed from sulphate solutions and having a basal d-spacing of 10.6-10.9 A was termed Green Rust II (GRII). The colour of the Green Rusts vary from lime-green to dark, bluish-green depending upon the type of anion incorporated into the structure. On oxidation, Green Rusts can transform to goethite, lepidocrocite or akaganeite, and this depends upon the preparation (e.g. the type of anion present) and subsequent treatment (e.g. oxidation in dry or wet state).

Closely related to the Green Rusts are hydroxy anion compounds containing Fe(II) and Al(III) cations:

$$Fe^{2+}_x\text{-}Al^{3+}_y(O^{2-}, OH^-, A)_z$$

where x, y and A mean the same as before. These are blue-green compounds with a similar pyroaurite-like structure. They are also very unstable to oxidation in air but generally slightly more stable than the Green Rusts. These analogous aluminium compounds will be termed "aluminium Green Rusts" (Al-GRs) in the present work. Where the two types of compounds are mentioned in the

same context, the Green Rusts proper will be referred to as iron Green Rusts (or Fe-GRs) to avoid confusion.

1.3 The occurrence of iron oxides in the natural environment

The chief iron oxides in nature are the minerals magnetite (Fe_3O_4), haematite (α-Fe_2O_3) and goethite (α-FeOOH). Haematite occurs extensively as large deposits in sedimentary rocks (e.g. the Pre-Cambrian rocks of the Canadian Shield and the Lake Superior district), and is by far the most important ore of iron. Magnetite and goethite are important to a lesser extent as iron ores, and large deposits are found in certain localities. The secondary mineral, limonite, is composed mainly of goethite (Bauman, 1976; Deer et al., 1962; Lepp, 1975; Mason & Berry, 1968; Read, 1971).

Magnetite is magmatic in origin although it may also form during the oxidation of Fe(II) from solution, such as might occur in the interstitial waters of some marine sediments (Murray, 1979). Magnetite is commonly found as an accessory mineral in igneous rocks, and also occurs in metamorphic and sedimentary rocks. Large deposits of magnetite occur when large concentrations of molten magnetite segregate out from a magma prior to solidification. Often, before the solidification occurs, the large concentration of magnetite can be injected into the surrounding country rocks and solidify there. Huge deposits of magnetite, believed to be the result of

magmatic segregation, are found in Kiruna, Swaden and in the Adirondacks, New York. Thesa deposits are an important source of iron ores, especially as the iron content of magnetite is 72.4%. Indeed, the Kiruna deposits rank Sweden about seventh in world iron ore production. Magnetite is found in fairly substantial amounts in contact-metasomatic rocks, such as the skarn deposits of Scandanavia, where the magnetite has been introduced metasomatically into calcareous rocks. However, these ore deposits are of no great importance in world production. Magnetite is also a constituent of hydrothermal veins, is found in residual clays and in placer deposits - the "black sands" - formed by the degradation of earlier deposits. Magnetite is usually quite resistant down to the last stages of weathering. This is attributed to the formation of an impermeable layer of Fe_2O_3 around the magnetite (Garrels & MacKenzie, 1971).

Haematite and goethite are mainly sedimentary in origin. However, haematite occurs frequently as an accessory mineral in igneous rocks and as a minor constituent in high temperature hydrothermal veins and in contact metamorphic deposits associated with magnetite. The greatest deposits of haematite occur in the Pre-Cambrian rocks of the Lake Superior district; the principal regions are: Marquette and Menominee in Michigan; Penshee-Gogebic in Wisconsin; and Masabi, Vermilion and

Cuyuna in Minnesota. Goethite is usually found in the secondary mineral, limonite, which is really more of a rock than a mineral. Limonite not only contains goethite but also other iron oxides, such as lepidocrocite or ferrihydrite, along with absorbed clay minerals and other silicate minerals. Substantial deposits of limonite are found in the Alsace-Lorraine areas in eastern France - the extensive "Minette" iron ore - and in the "Labrador Trough", located along the Quebec-Labrador boundary in Canada.

Sedimentary iron oxides, such as haematite and goethite are probably formed as a result of the weathering of iron-bearing minerals, such as magnetite, siderite ($FeCO_3$), pyrite (FeS_2) and pyrrhotite ($Fe_{1-n}S$, with n varying from 0 to 0.2), and the iron-silicates: greenalite, chamosite and glauconite (Garrels & MacKenzie, 1971; Schwertmann & Taylor, 1977). Agents of weathering, such as wind, frost and rain, physically break up the rocks containing the iron-bearing minerals into debris, and this is then ready for attack by chemical and biological agents. Chemical agents include sulphuric, carbonic and humic acids: the first two being formed from SO_2 and CO_2 dissolving in rainwater, respectively, and the last from the decay of organic matter.

The iron present in the iron-bearing minerals is usually

in the Fe(II) oxidation state, and is readily oxidised to the Fe(III) oxidation state when released. For instance, the carbonic acid present in rainwater will react with the iron-bearing minerals, such as the iron-silicates and carbonates, in the following manner:

$$FeSiO_3 + 2CO_2 + 3H_2O \longrightarrow Fe^{2+} + H_4SiO_4 + 2HCO_3^- \quad -1.2$$

$$FeCO_3 + CO_2 + H_2O \longrightarrow Fe^{2+} + 2HCO_3^- \quad -1.3$$

The iron from the iron-bearing minerals will thus enter into solution under the action of rainwater. It will then be carried away from the site of degradation by the running rainwater, and enter streams and rivers. During this period of transport, and depending on whether the water is oxic or anoxic, the iron will either precipitate out (oxic) or remain in solution (anoxic). The precipitation is caused by the oxidation of the Fe(II) to Fe(III), which is insoluble in the pH ranges encountered in running water. As most surface running water is well-oxygenated, hydrous Fe(III) oxides or hydrous Fe(III) oxyhydroxides are usually precipitated but are carried downstream as a suspension or in colloidal form due to the momentum of the moving water. They may also be kept in suspension by the acquisition of organic ligands which prevents early flocculation. In conditions of low turbulence, the precipitated iron would probably accumulate in the sediments of the river. However, most

of the Fe(III) oxides would be deposited at the bottom of lakes, in river estuaries and on the flocr of coastal seawaters. Some of the Fe(II) material will also be transported to these places as not all maybe oxidised to Fe(III). At the bottom of the lakes and seas, anoxic zones can be prevalent, and the deposits of Fe(III) solids will then be utilised by micro-organisms as final electron acceptors to accomplish their oxidative decomposition of organic matter. The Fe(III) material is thereby reduced to the II state and thus becomes soluble. When the solubilised iron migrates to zones of oxidation, re-oxidation and subsequent re-precipitation occurs (Schwertmann & Taylor, 1977). Hence, a sort of recycling process occurs.

For underground running water, Fe(II) is the main form since anoxic conditions occur. When the waters containing the soluble iron enter oxidation zones, such as coastal seawater, the iron is precipitated.

The layers of precipitated iron will become stratified by the process of lithification over the span of geologic time. The strata of iron deposits may be brought to the surface by subsequent orogenic activity. The accompanying igneous activity may cause the metamorphism of some of the deposits of iron oxides.

Goethite is more likely to be found in rocks which are

formed from bogs and lagoons, while haematite is more widespread, occurring in shallow water sediments. Although both minerals originate from the same sort of building material, their different diagenesis has resulted in two different oxides.

Other iron oxides which are known to occur naturally, but less commonly, include maghemite (γ-Fe_2O_3), akaganeite (β-FeOOH), lepidocrocite (γ-FeOOH), feroxyhite (δ'-FeOOH) and ferrihydrite ($5Fe_2O_3.9H_2O$).

The Green Rusts and/or the Al Green Rusts may also be found in the natural environment but to date (1984) they have not been observed. The aforementioned Fe(III) oxides are sedimentary in origin, and as such they are the result of the breakdown of primary iron-bearing minerals or the weathering of existing oxides such as haematite and goethite. These Fe(III) oxides are thermodynamically unstable and will convert to haematite or goethite over the span of geologic time. Thus deposits of maghemite, lepidocrocite, ferrihydrite, etc. are relatively young formations and reflect the activity of the site of formation.

Most of the sedimentary iron oxides are found and produced in soils. Soils are the debris products of mechanical and chemical weathering, which has become a biostrata due to the action of living organisms. Here zones of oxidation and reduction are produced by the

biological activity of micro-organisms such as bacteria. Thus water containing dissolved iron will be precipitated, redissolved and reprecipitated in definite regions of the soil. This can be seen by the horizons of enriched iron oxides. Iron oxides such as haematite and goethite give soils their characteristic colouring and this is a basis for the naming and classifying of soils (e.g. Red-Yellow Podzolic, Braunerde, sols rouges tropicaux, terra rossa, etc.). Haematite gives soils a deep reddish hue while goethite make it yellowish-brown. Iron oxides also affect soils by their ability to aggregate and cement soil particles and to adsorp trace nutrients. This is an important factor for the growth of plant life in soils.

Examples of the occurrence of given types of iron oxides in the natural environment are given by Bowen (1979), Murray (1979) and Schwertmann & Taylor (1977). Table 1.1 gives some of the characteristics of iron oxide minerals.

Mineral properties	Mineral name: Hematite	Maghemite	Magnetite	Goethite	Lepidocrocite	Ferrihydrite
Formulae	α-Fe_2O_3	γ-Fe_2O_3	Fe_3O_4	α-FeOOH	γ-FeOOH	$Fe_5HO_8 \cdot 4\,H_2O$† $Fe_5(O_4H_3)_3$‡
Crystal system	Rhombohedral	Isometric or tetragonal	Isometric	Orthorhombic	Orthorhombic	Rhombohedral
Cell dimensions (Å)	a_o = 5.04 c_o = 13.77	a_o = 8.34	a_o = 8.39	a_o = 4.65 b_o = 10.02 c_o = 3.04	a_o = 3.88 b_o = 12.54 c_o = 3.07	a_o = 5.08 c_o = 9.4
Density (g cm^{-3})	5.26	4.87	5.18	4.37	4.09	3.96
Standard free energy of formation ΔG° (kcal/mole)	-177.7#	-163.6§	-243.1§	-117.0††	-114.0††	-166.5§
Solubility product‡‡ (pFe + 3 pOH)	42.2-43.3	40		43.3-44.0	40.6-42.5	37.0-39.4
Diagnostic characteristics						
X-ray spacings (Å)	2.70, 3.68 2.52	2.52, 2.95	2.53, 2.97	4.18, 2.69, 2.45	6.26, 3.29, 2.47	2.5, 2.2, 1.97, 1.71, 1.5
DTA peaks (°C)	Nil	Exotherm 600-800	See footnote¶	Endotherm 280-400	Endotherm 300-360 exotherm 370-500	Endotherm 150, loss of adsorbed H_2O
Infrared spectroscopic peaks (cm^{-1})	345, 470, 540	400, 450, 570 590, 630	400, 690	890, 797	1026, 1161, 753	Nil
Color (Munsell)	5R-2.5YR bright red	Reddish brown	Black	7.5YR-10YR yellowish-brown	5YR-7.5YR orange	5YR-7.5YR reddish-brown
Usual crystal morphology	Hexagonal plates	Cubes	Cubes	Acicular	Laths, serrated elongated plates	Spherical

† After Towe and Bradley (1967).
‡ After Chukrov et al. (1973).
§ After Garrels & Christ (1965).
¶ Magnetite converts via maghemite or directly to hematite, depending on particle size.
# After Roble & Waldbaum (1968).
†† After Mohr et al. (1972).
‡‡ Depends on particle size.
§§ At 25C and 1 bar total pressure.

Table 1.1 General characteristics of iron oxide minerals. (after Schwertmann & Taylor, 1977)

1.4 Objectives of present research

1) To investigate methods of preparation of the metastable Green Rusts and to develop a consistent method of preparation..

2) To make an in-depth study of the Green Rusts using a range of investigative techniques - viz. Mossbauer spectroscopy, X-ray diffraction, infrared spectroscopy, vacuum microbalance (surface area measurements) - with a view to characterising their properties and behaviour.

3) To study the characteristics of the synthetic iron oxides using the above techniques and use the information obtained as a reference by which to compare the Green Rusts.

4) To use all the data to develop ideas on the mechanism and modes of formation of the Green Rusts, and its significance as a pathway in the formation of iron oxides.

CHAPTER 2: ANALYTICAL TECHNIQUES

The detail study of iron oxides requires the use of several different analytical techniques. This is due to the diversity of iron oxides and their variability with regard to chemical and physical properties. A given technique can only provide certain information on a particular iron oxides. For instance, X-ray diffraction (XRD) can only provide information on crystal structure and a measure of crystallinity. However, the technique is limited if the samples have low crystallinity or are X-ray amorphous, as in the case of many naturally-occurring and synthetic iron oxides. Furthermore, impurities and low percentage of iron in natural samples can render identification by XRD very difficult.

In this thesis, four main analytical techniques have been applied to the study of the Green Rusts. These were: Mossbauer spectroscopy (MbS), X-ray diffraction (XRD), infrared spectroscopy (IRS), and vacuum microbalance (surface area measurements) to determine surface characteristics using the BET N_2 adsorption method. Where appropriate other methods, such as atomic absorption spectroscopy (AAS) and electron microscopy, have been used to supplement the main techniques. In

order to have a reference set of data, by which the Green Rusts can be compared, some of the common iron oxides were also studied by these techniques.

Since MbS is the most useful technique for the study of iron oxides, it has been the most intensely used of the analytical techniques mentioned above. This was especially true for the Green Rusts, where the low temperature facilty of MbS was extremely appropriate. A fuller discussion of the attributes of MbS is given in section 2.1.5. X-ray diffraction has been used as a method of identification only, while IRS has been used as a complementary technique to XRD. Surface areas and porosity of samples were obtained from the BET N_2 adsorption data.

The following sections explain each of the four main techniques, including a discussion of their usefulness and limitations. The explanation on MbS is more detailed than the others because it was felt that the theory behind the technique was complex enough for full familiarity and comprehension to be still lacking.

2.1 Mossbauer spectroscopy

Mossbauer spectroscopy has rapidly become a standard analytical technique in the laboratory. Its most obvicus advantage over other diagnostic techniques is that it is non-destructive: samples can be recovered and used for other analyses. The method is based upon the phenomenon of recoilless nuclear gamma resonance, discovered by Rudolf L. Mossbauer in 1957, and now known as the Mossbauer effect. It is ideal for the study of iron oxides since the Fe nucleus is one of the few nuclei that can readily partake in recoilless gamma resonance. Indeed, in terms of the literature, the Mossbauer effect in iron has been utilised in numerous studies. There are many reviews and monographs on the subject of Mossbauer spectroscopy (Bancroft, 1973; Cohen, 1976; Gibb, 1976; Greenwood & Gibb, 1971; Johnson, 1962; Vertes, 1979).

2.1.1 The Mossbauer Effect

The phenonmenon of nuclear resonant fluorescence occurs when a nucleus is excited by the absorption of a γ-ray which has an energy equal to that of the excited state. (Implicit in this statement is the fact that the source of γ-rays must be a radionuclide that can decay to the groundstate of the absorbing nucleus.) However, this

rarely happens because both the nucleus and the γ-ray are affected by recoil, which causes a mismatch in energy that is greater than the Heisenberg (or natural) linewidth of the excited state. When a γ-ray is emitted from a radioactive nucleus, the latter recoils with an energy $E_R = p^2/2M$, where p is the momentum imparted to it, which must be equal and opposite to the momentum of the γ-ray, and M is the mass of the nucleus. If the excited state has an energy level E_o, then p $= E_o/c$. Thus:

$$E_R = E_o^2/2Mc^2 \qquad -2.1$$

and the energy of the emitted γ-ray is $E_o - E_R$.

An absorbing nucleus will also recoil with the same energy E_R. Thus for resonant absorption to occur, the energy of the incident radiation must be equal to $E_o + E_R$. Hence the γ-ray is usually out of resonance by $2E_R$. For low energy γ-rays, E_R is typically 10^{-2}–10^{-3} eV which is much greater than the natural linewidths (typically 10^{-7} eV). A further complication arises from the thermal vibration of the emitting or absorbing nucleus that degrades the gamma energy even more. The spread in energy due to this thermal or Doppler broadening is given by:

$$\Delta E = [E_R . \bar{\varepsilon}]^{(1/2)} \qquad -2.2$$

where $\bar{\varepsilon}$ is the average kinetic energy of the nucleus. This is generally a factor 10^4-10^6 times greater than the natural linewidth $\Gamma = \hbar/\tau$, τ being the mean lifetime of the excited state. There is no overlap between the emission and absorption energy distributions because $2E_R$ is significantly greater than ΔE.

The Mossbauer effect provides a means of overcoming the destructive effects of recoil and thermal energies. In the preceding discussion, it was implied that the nucleus was isolated but this is usually not the case. In a crystalline solid, the nucleus would be confined to a volume of space, vibrating about a mean position, like numerous other nuclei within the lattice. In this situation, the recoil energy imparted to the nucleus could be used in three ways: (i) ejection of nucleus from lattice, (ii) excitation of lattice vibrations or (iii) transferred to the lattice as a whole. The first possibility can be ignored since E_R is too small compared to the energy required to remove the nucleus from the lattice. If E_R is used in exciting lattice vibrations (phonons), then a degrading of gamma energy would still occur. However, the phonon energy levels in a solid are quantized, and cannot be excited in an arbitrary fashion. If E_R is less than the energy required to excite the lowest phonon energy level, then the recoil energy cannot be used in exciting a phonon. Instead this energy is transferred to the whole mass of

the lattice and no recoil occurs. Thus, under the condition just described, recoil-free emission or absorption of a γ-ray can take place. A crystalline lattice may contain as much as 10^{15}-10^{17} atoms and therefore E_R and ΔE would become very small. Resonance would then occur readily.

Since E_R and the phonon excitation energies are comparable in magnitude (the latter is typically 10^{-3}-10^{-1} eV), then only a certain fraction of the emissions and absorption take place without recoil. This recoil-free fraction is largest for low-energy γ-rays (E_R tending to be small) and for tight crystal binding (i.e. for solids with a high Debye temperature, θ), and increases with decreasing temperature. On the Debye model of solids, the recoil-free fraction is given by the Debye-Waller factor:

$$f = \exp[(-3/2)(E_R/k\theta)\ X \{1 + 4(T/\theta)^2 \cdot \int_0^{\theta/T} (x\ dx)/(\exp(x)-1)\}] \qquad -2.3$$

The size of the Mossbauer effect, as determined by f, is shown in Table 2.1 for some nuclei with low energy excited states at temperatures of 4, 77 and 290 K. The Debye temperatures (θ's) were obtained from low temperature specific heat experiments. It can be seen that f is largest for ^{57}Fe and ^{169}Tm at all three temperatures.

Nucleus	E_o (keV)	E_R (eV)	θ (K)	f 4K	f 77K	f 290K
^{57}Fe	14	0.002	467	0.92	0.90	0.82
^{67}Zn	92	0.069	308	0.024	0.005	$4x10^{-8}$
^{119}Sn	24	0.0025	212[a]	0.80	0.69	0.29
^{161}Dy	26	0.0023	170	0.79	0.63	0.21
^{169}Tm	8	0.0002	170	0.98	0.96	0.87
^{191}Ir	129	0.046	287	0.06	0.02	$1x10^{-5}$
^{197}Au	77	0.016	165	0.19	0.03	$7x10^{-6}$

[a] Grey tin

TABLE 2.1 Recoil-free fractions for some Mossbauer Nuclei (after Johnson, 1962)

2.1.2 The Mossbauer Spectrum

In the previous section, it was shown that recoil-free γ-rays can be emitted from radionuclei embedded in a solid. Nuclear gamma resonance would then occur when the γ-rays are absorbed without recoil by the appropriate nuclei also embedded in a solid. The resonance process can be detected as an absorption event by placing the absorber between a nuclear detector and the source of recoil-free γ-rays. If the γ-ray energy were varied by minute amounts, then a record of events (i.e. counts) versus gamma energy, E_γ, can be obtained. This is essentially the Mossbauer spectrum. E_γ is usually varied by vibrating the source in a Doppler fashion [$\Delta E_\gamma = (v/c) E_o$] about a fixed zero so that there is a well-defined movement relative to the absorber (Fig 2.1).

At a Doppler velocity, v, where E_γ exactly matches the resonant excited state of the absorber, the probability of resonance is at a maximum. As v deviates from this point, the probability decreases and is effectively zero when v is well away from the point of maximum resonance. An absorption dip or "peak", which is often referred to as a line, is thus produced. The relative depth or intensity of this line depends upon the recoil-free fractions f_s and f_A of the nuclear transitions

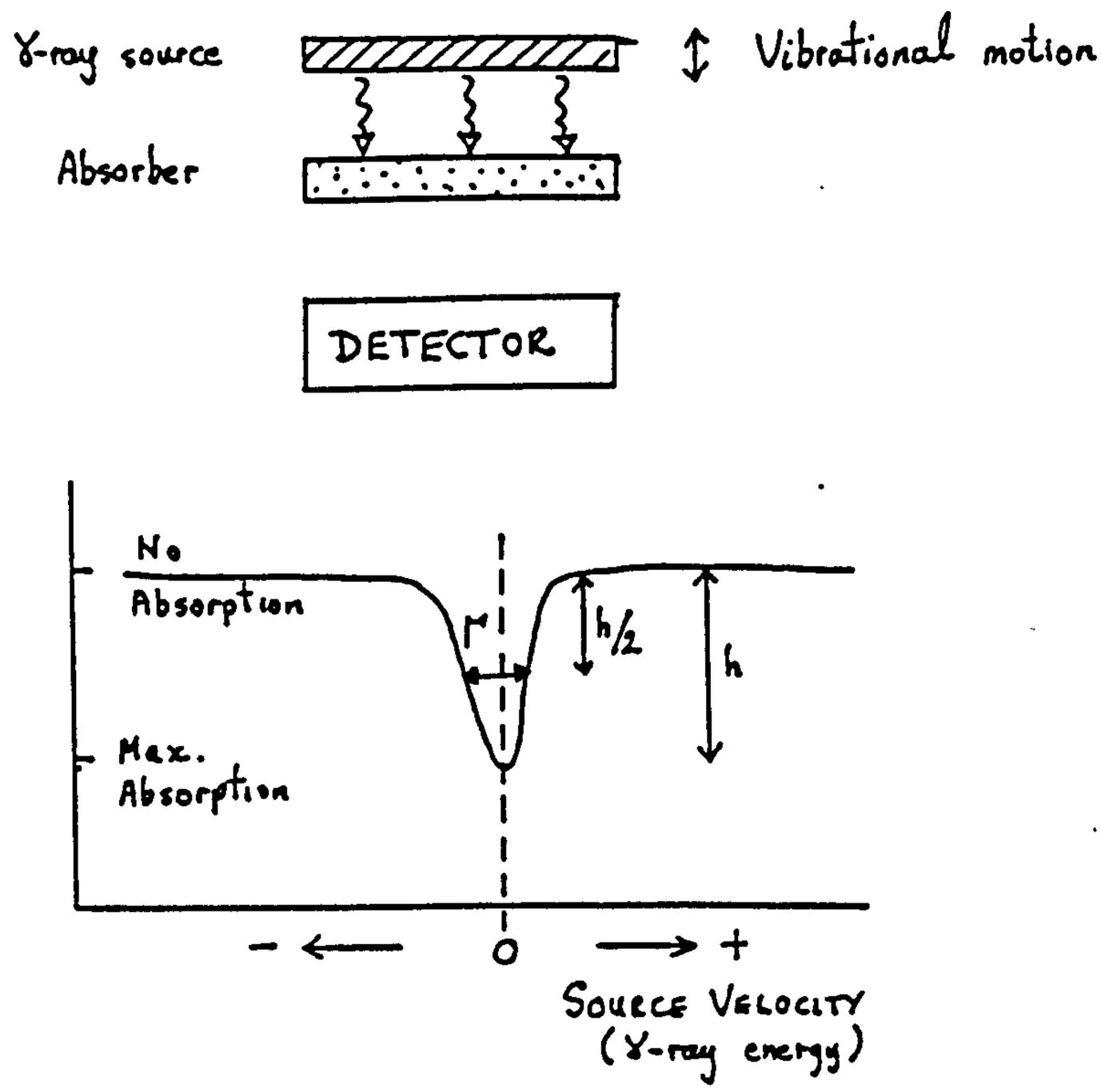

Fig 2.1 Schematic of Mossbauer spectroscopy in transmission geometry mode.

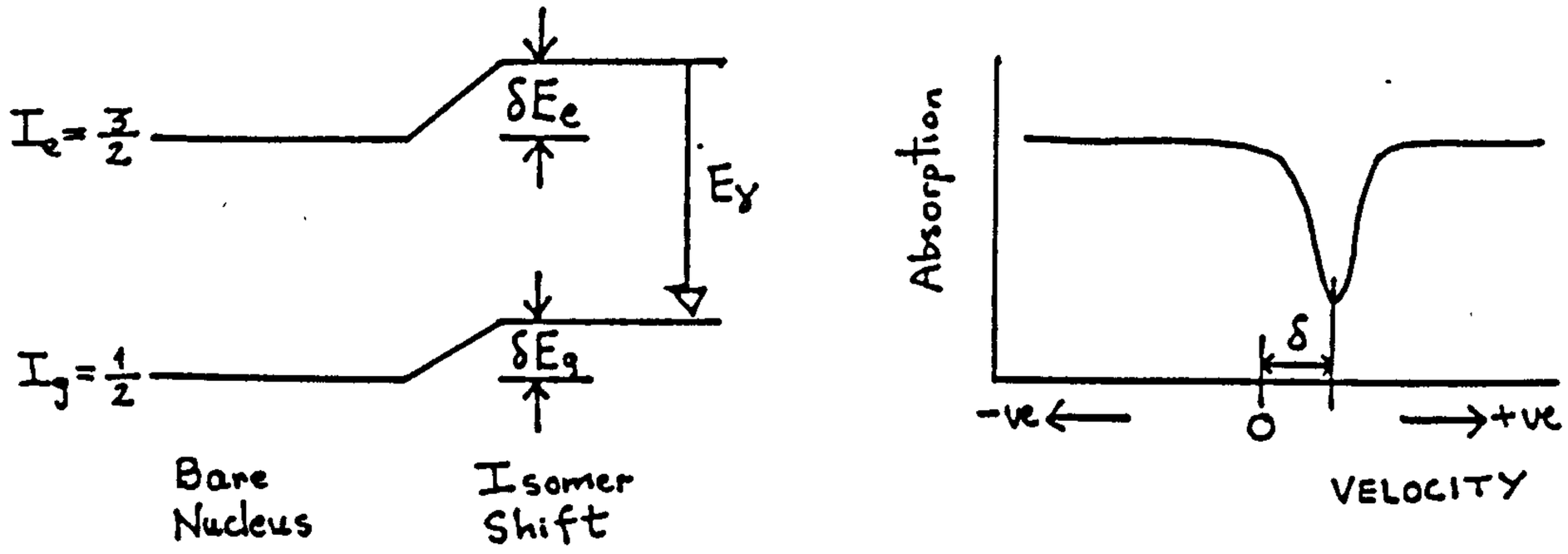

Fig 2.2 The effect of the isomer shift on the Mossbauer spectrum.

in the source and absorber, respectively. The effective absorption cross-section at maximum resonance (i.e. $E_\gamma = E_o$) is expressed as:

$$\sigma_o = f_a.(\lambda^2/2\pi I)[(2I_e + 1)/(2I_g + 1)] \times [1/(1 + a)] \qquad -2.4$$

where I_e, I_g = excited- and groundstate spins, respectively

a = internal conversion coefficient

λ = wavelength of γ-ray

The energy dependent cross-section for resonant absorption is given by the Breit-Wigner formula:

$$\sigma_a(E) = \sigma_o\ [1 + 4(E_\gamma - E_o)^2/\Gamma^2]^{-1} \qquad -2.5$$

where E_γ = incident γ-ray energy

Γ = natural linewidth (full width at half height)

This describes a Lorentzian distribution, and the lineshape in a Mossbauer spectrum conforms to this type of function very closely for thin absorbers. Of course, there may be a series of lines which arise because of the chemical environment around an absorbing nucleus. The Mossbauer spectrum can only then be described by a combination of several Lorentzian functions.

2.1.3 Hyperfine Interactions

The energy levels of a nucleus are subtly altered by its chemical environment. These perturbations in energy levels (e.g. 14.4 keV in ^{57}Fe) are of the order 10^{-7}-10^{-6} eV. They may be, however, two orders of magnitude greater than the natural linewidths of γ-rays (~ 10^{-7}-10^{-6} eV) and so can be resolved in a Mossbauer spectrum. The magnitude of the chemical perturbations, or hyperfine interactions, generally encountered is adequately covered by the Doppler velocities normally used (e.g. $v = \pm 10$ mms^{-1}, E_γ = 14.4 keV gives $\Delta E_\gamma = 4.80 \times 10^{-7}$ eV). There are three principal interactions to consider. These are the isomer shift, quadrupole splitting and magnetic hyperfine splitting.

2.1.3a Isomer shift (IS or δ)

Also known as the chemical isomer shift or centre shift, this arises from the electrostatic interaction between the charge distribution of the nucleus and those electrons which have a finite probability of penetrating the nuclear volume. This does not produce a splitting of the nuclear levels but causes a slight shift in the energy levels of a bound nucleus relative to those in a bare nucleus (Fig 2.2).

Generally, the shift in the excited state level, δE_e, is different from the shift in the groundstate level, δE_g, because of the slight difference in nuclear radius between the ground and excited state. The shift in energy levels also varies from one solid to another so that the Mossbauer transition energies may differ between source and absorber. However, the differences are very small and are easily dealt with by the Doppler velocities used in MbS. The effect is seen as a displacement of the resonant lines relative to the zero velocity point.

Only s-electrons can overlap with the nuclear charge density but they are also sensitive to the p-and d-electron densities. If $Y(0)_s$ and $Y(0)_A$ are the wave functions of the s-electrons at the nucleus in the source and in the absorber, respectively, then the observed isomer shift is given by:

$$IS = (2PI/5).Ze^2[\langle R_e^2\rangle - \langle R_g^2\rangle] \times \{|Y(0)_s|^2 - |Y(0)_A|^2\} \qquad -2.6$$

where Z = atomic number

e = electronic charge

$\langle R_e^2\rangle$, $\langle R_g^2\rangle$ = mean-square radius of nucleus in excited and groundstates, respectively.

A similar shift in the Mossbauer spectrum may arise because of a temperature difference between source and absorber. This is known as the Second Order Doppler shift. It is usually small, being ~ 0.1 mms^{-1} if the source is at 293 K and the absorber at 77 K, whereas IS is often 0.4 mms^{-1} for Fe(III) or even 1.3 mms^{-1} for Fe(II). Usually, the Second Order Doppler shift is ignored because it does not give extra information, and the observed lineshift is attributed solely to the isomer shift.

2.1.3b Quadrupole splitting (QS or Δ)

When a nucleus is located in a crystalline solid, an interaction between its electric quadrupole moment and the local electric field gradient (EFG) results in a splitting of the excited energy state (Fig 2.3). The observed spectrum consists of two or more lines of resonance.

A nucleus has an electric quadrupole moment because its charge distribution deviates from a spherical symmetry. This happens only when the nucleus is in an excited state and is true for nuclei with spin quantum number greater than $I = 1/2$, as in ^{57}Fe. The electric quadrupole moment Q can be expressed as:

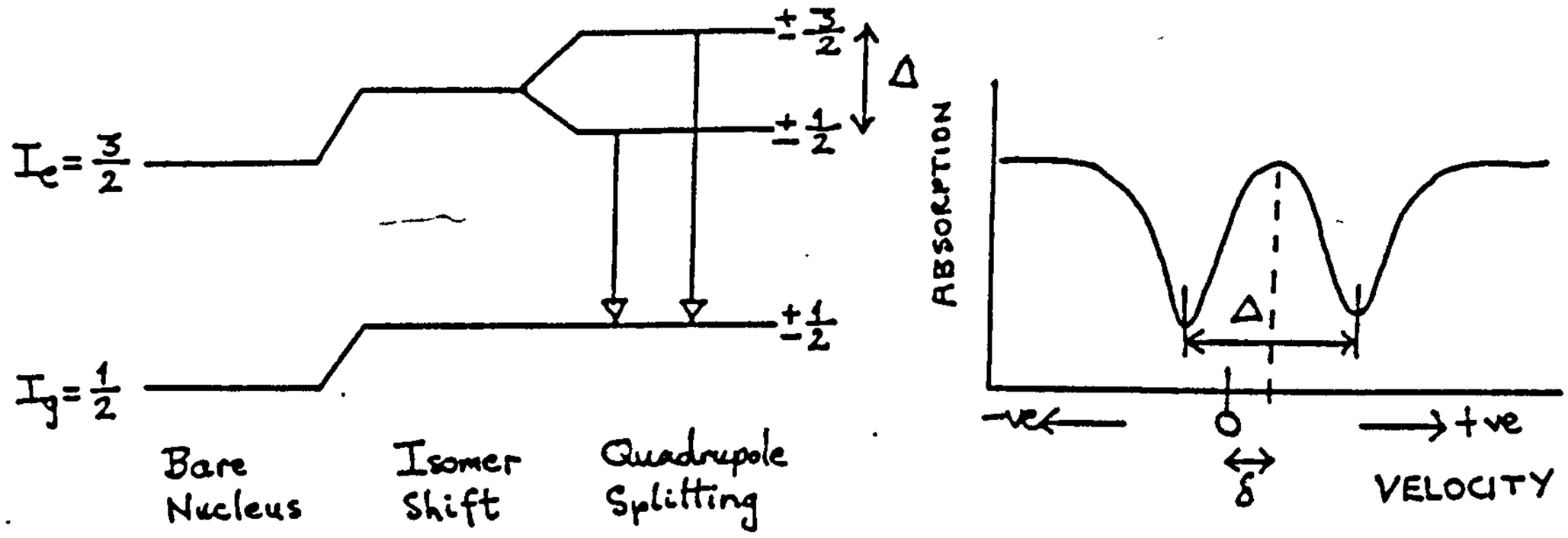

Fig 2.3 The effect of the quadrupole splitting on the Mossbauer spectrum.

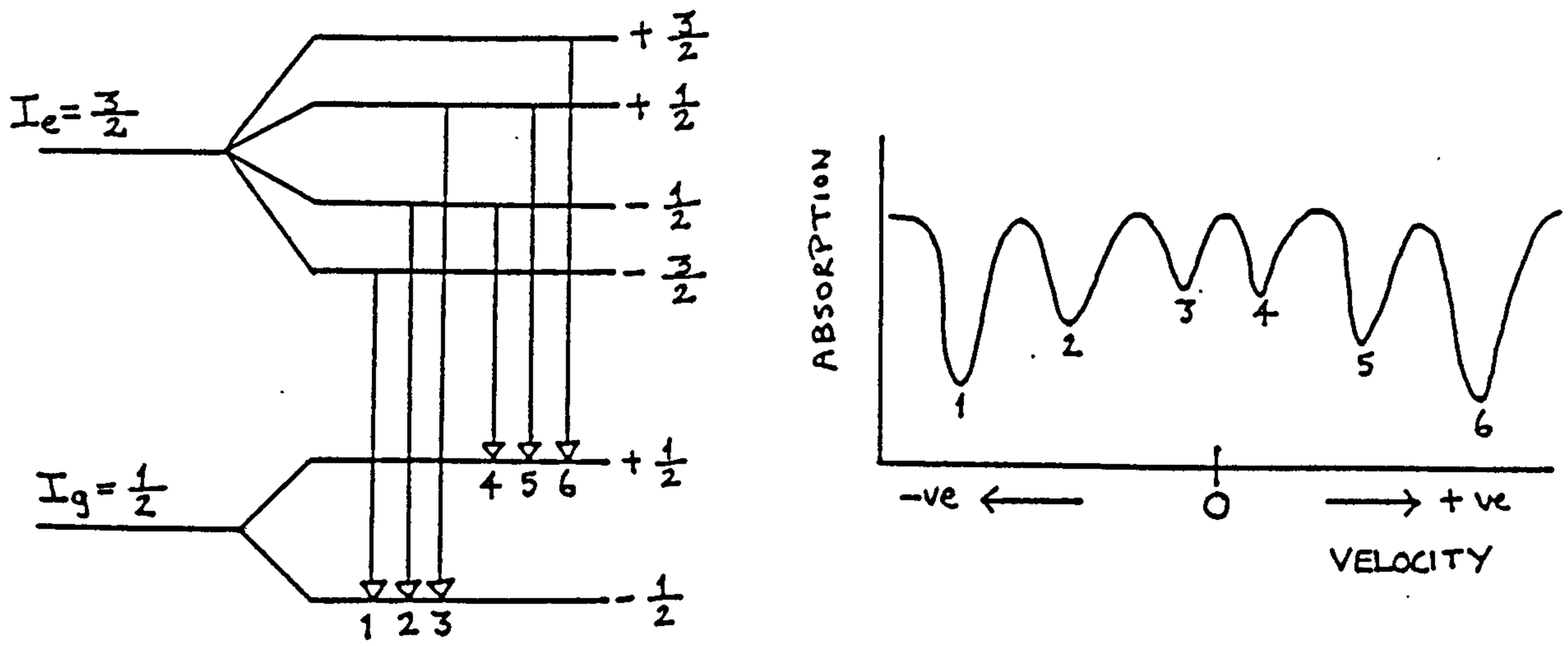

Fig 2.4 The effect of magnetic hyperfine splitting on the Mossbauer spectrum.

$$eQ = \int \rho r^2(3\cos^2\theta - 1)\, d\tau \qquad -2.7$$

where ρ = charge density in volume element $d\tau$

r = distance of volume element from centre of nucleus

θ = angle r makes with nuclear spin axis.

The interaction of Q with the local EFG due to the electronic environment is described by the Hamiltonian:

$$H = -(1/6)\ e\underset{\sim}{Q}.\underset{\sim}{\nabla E} \qquad -2.8$$

where $\underset{\sim}{\nabla E}$ = EFG tensor at nucleus

$= -V_{ij}$ $(i,j = x,y,z)$, the electric potential at nucleus.

Equation 2.8 can be re-expressed as:

$$H = [e^2\, qQ/4I(2I-1)] \quad X$$
$$[3\hat{I}_z^2 - I(I+1) + \eta(\hat{I}_x^2 - \hat{I}_y^2)] \qquad -2.9$$

where q = point charge around nucleus

I = nuclear spin

$\hat{I}_x, \hat{I}_y, \hat{I}_z$ = quantum-mechanical spin operators

η = asymmetry parameter

$= (V_{xx} - V_{yy})/V_{zz}$ (i.e. $0 \leq \eta \leq 1$)

For an asymmetric EFG ($\eta > 0$), an exact expression for the

nuclear energy levels can only be obtained for the case I = 3/2 (e.g excited state for ^{57}Fe) and this is:

$$E_q = [e^2\, qQ/4I(2I-1)] \quad X$$

$$[3I_z^2 - I(I+1)]\{1+\eta^2/3\}^{(1/2)} \qquad -2.10$$

where E_q = nuclear energy level due to quadrupole interaction

I_z = spin quantum number relative to z-axis (which is taken as symmetry axis)

= I, I-1, ..., -I

For the groundstate of ^{57}Fe, I = 1/2 and so I_z = $\pm$ 1/2. Therefore, E_q = 0 and no splitting in energy level occurs. In the excited state, I = 3/2 and I_z = $\pm$ 3/2 or $\pm$ 1/2 which gives:

$$E_q = \pm\, e^2\, qQ/4.(1+\eta^2/3)^{(1/2)} \qquad -2.11$$

Therefore, there are two, two-fold degenerate levels for the excited state of ^{57}Fe due to the quadrupole interaction, as shown in Fig 2.3. The quadrupole splitting for the transition I = 3/2 -> I = 1/2 is thus defined as $\Delta = E_q + E_q- = 2E_q$.

2.1.3c Magnetic hyperfine splitting (MHS)

The nucleus has a magnetic moment which can couple with magnetic fields at the nucleus. This causes a splitting of the nuclear ground and excited states, if the spin I > 0, and results in a multiline Mossbauer spectrum (Fig 2.4).

For ^{57}Fe, a six-line spectrum is generally produced. The transitions are governed by a selection rule so that the change in spin quantum number must be 0 or 1. The levels are not populated equally but give rise to the type of pattern shown in Fig 2.4 (a ratio of 3:2:1:1:2:3 for a randomly orientated powder).

The interaction between the nuclear magnetic moment, $\underset{\sim}{\mu}$, and a magnetic field, $\underset{\sim}{B}$, can be expressed by the Hamiltonian:

$$H = -\underset{\sim}{\mu}.\underset{\sim}{B} = -g\mu_N.\underset{\sim}{I}.\underset{\sim}{B} \qquad -2.12$$

where μ_N = nuclear magneton

I = nuclear spin (> 0)

g = nuclear g-factor.

Solving this Hamiltonian gives the energy levels of the nucleus as:

$$E_m = (-\mu B/I)m_z = -g\,\mu_N\,Bm_z \qquad -2.13$$

where m_z = magnetic quantum number relative to z-axis

= I, I-1, ..., -I

Thus, the presence of a magnetic field splits an energy level into 2I + 1 non- degenerate, equi-spaced sublevels with a separation of $\mu B/I$.

The origin of the magnetic field at the nucleus may be external or internal. An external field of several Teslas may be applied by a superconducting magnet. Internal magnetic fields arise from coupling between the nucleus and unpaired s-electrons, from the magnetic orbital moment, and from the dipole interaction of the spin moment of the electrons with the nucleus. The first cause is generally the most important in determining the magnitude of the internal field. Internal magnetic fields can be as large as 100 T.

2.1.3d Combined quadrupole and magnetic splitting

In the preceding sections, the quadrupole and magnetic hyperfine interactions were treated as being separate events. However, they can combine to produce a more complicated Mossbauer spectrum. The Hamiltonian

describing this situation is the sum of the separate Hamiltonians for the quadrupole and magnetic interactions

i.e. $H = H_o + H_q + H_m$ -2.14

where H_o represent the energy of the nuclear state in the absence of quadrupole and magnetic hyperfine coupling. H has no general solution but Kundig (1967) and van Dongen Torman et al. (1975) gave a range of possible solutions for the Mossbauer transitions in the ^{57}Fe nucleus (i.e. I = 3/2 -> I = 1/2). There are eight possible transitions and these are shown in the energy level diagram in Fig 2.5.

In most instances of combined quadrupole and magnetic hyperfine interactions, the former is much weaker than the latter. Under this condition, the quadrupole interaction can be treated as a small perturbation on the magnetic hyperfine interaction. The result is a shift in the energy levels of the magnetic hyperfine splitting, and this depends upon the angle between the EFG and the magnetic field. The most obvious manifestation in the Mossbauer spectrum, arising from a small quadrupole perturbation, is that there is no longer a symmetry about the centroid of the resonant lines (Fig 2.6).

However, when the EFG is comparable to the magnetic hyperfine interaction (as in the Fe^{2+} ion), eight

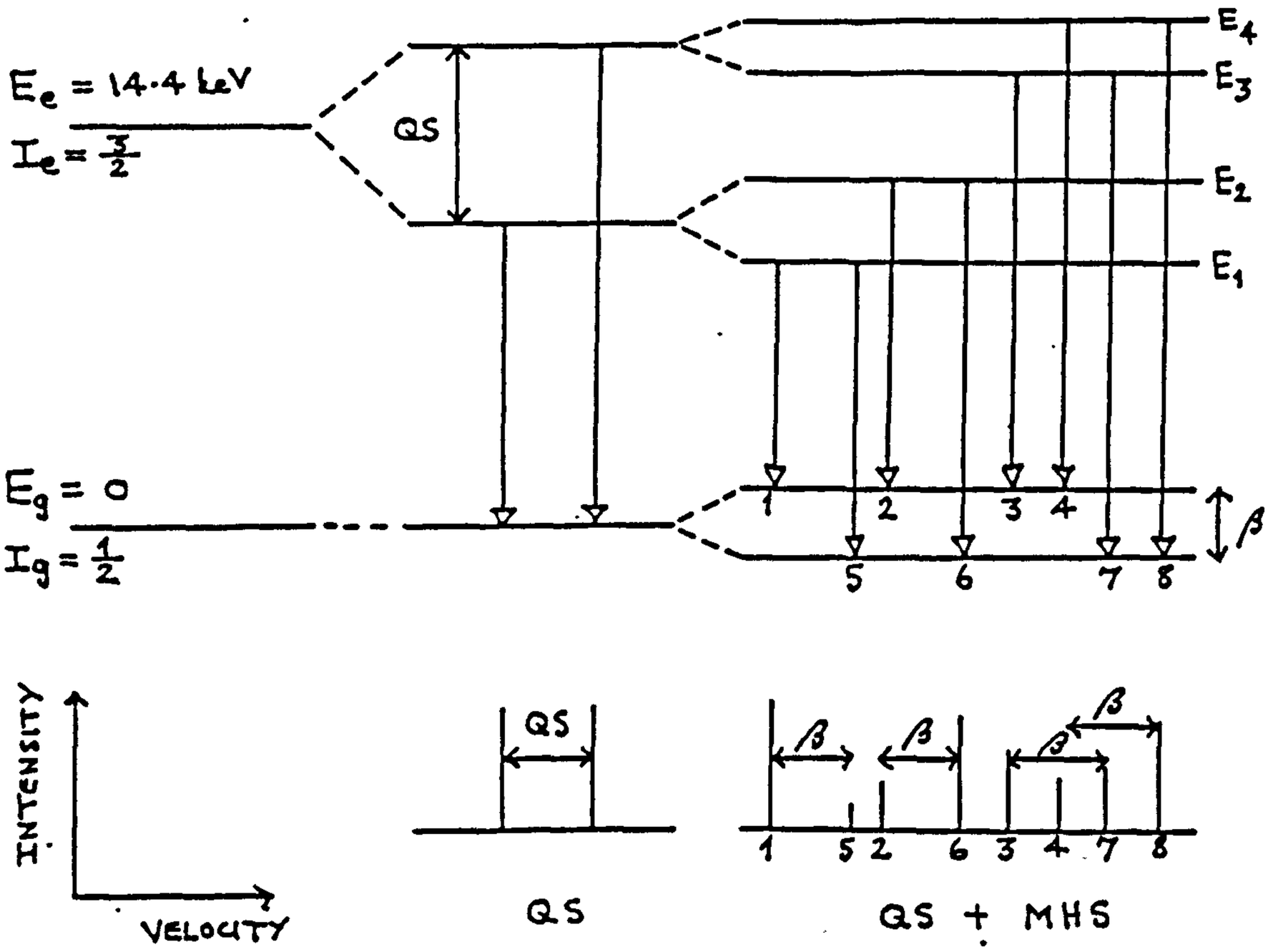

Fig 2.5 Energy levels of ^{57}Fe for combined quadrupole and magnetic hyperfine interactions.
(after van Dongen Torman et al., 1975)

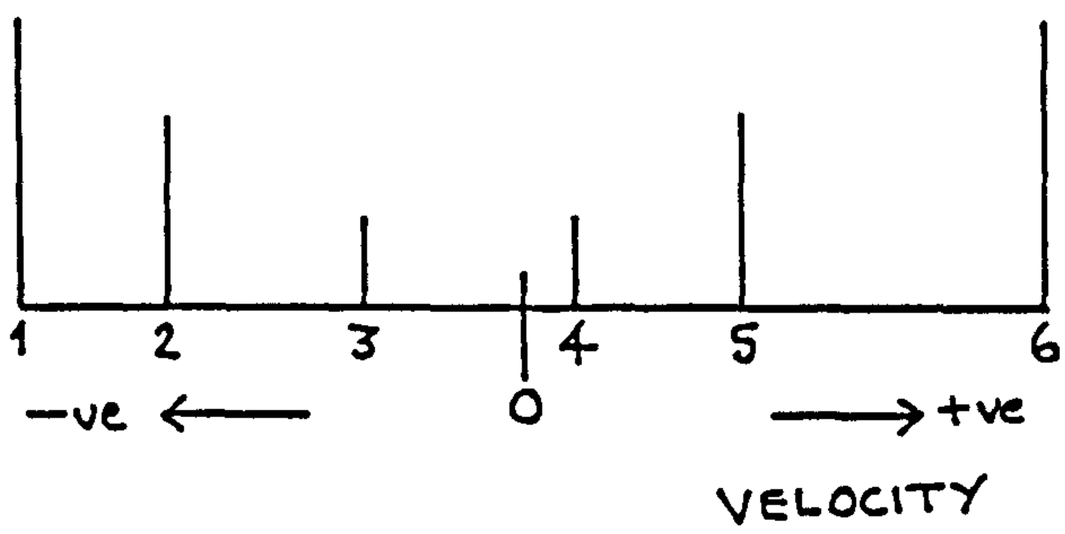

Fig 2.6 Asymmetric resonant lines due to a small quadrupole perturbation on the MHS.

lines are produced. The intensity of the lines depend on the orientation of the magnetic axis and EFG to the γ-ray. The probability of each transition can be predicted by computer averaging over all angles for randomly orientated powder.

2.1.4 ^{57}Fe Mossbauer spectroscopy

Iron-57 Mossbauer spectroscopy makes use of the 14.41 keV γ-transition in ^{57}Fe. The source for γ-rays of this energy is provided by the radionuclide, ^{57}Co. The decay scheme for ^{57}Co is shown in Fig 2.7.

2.1.5 Mossbauer spectroscopy and iron oxides

2.1.5a Mossbauer parameters

The Mossbauer parameters readily obtainable from observed spectra are (i) isomer shift, (ii) lineshape (intensity and halfwidth), (iii) relative line intensities, (iv) quadrupole splitting and (v) magnetic hyperfine splitting. The magnitude of each parameter will usually depend upon the temperature at which the spectrum is recorded.

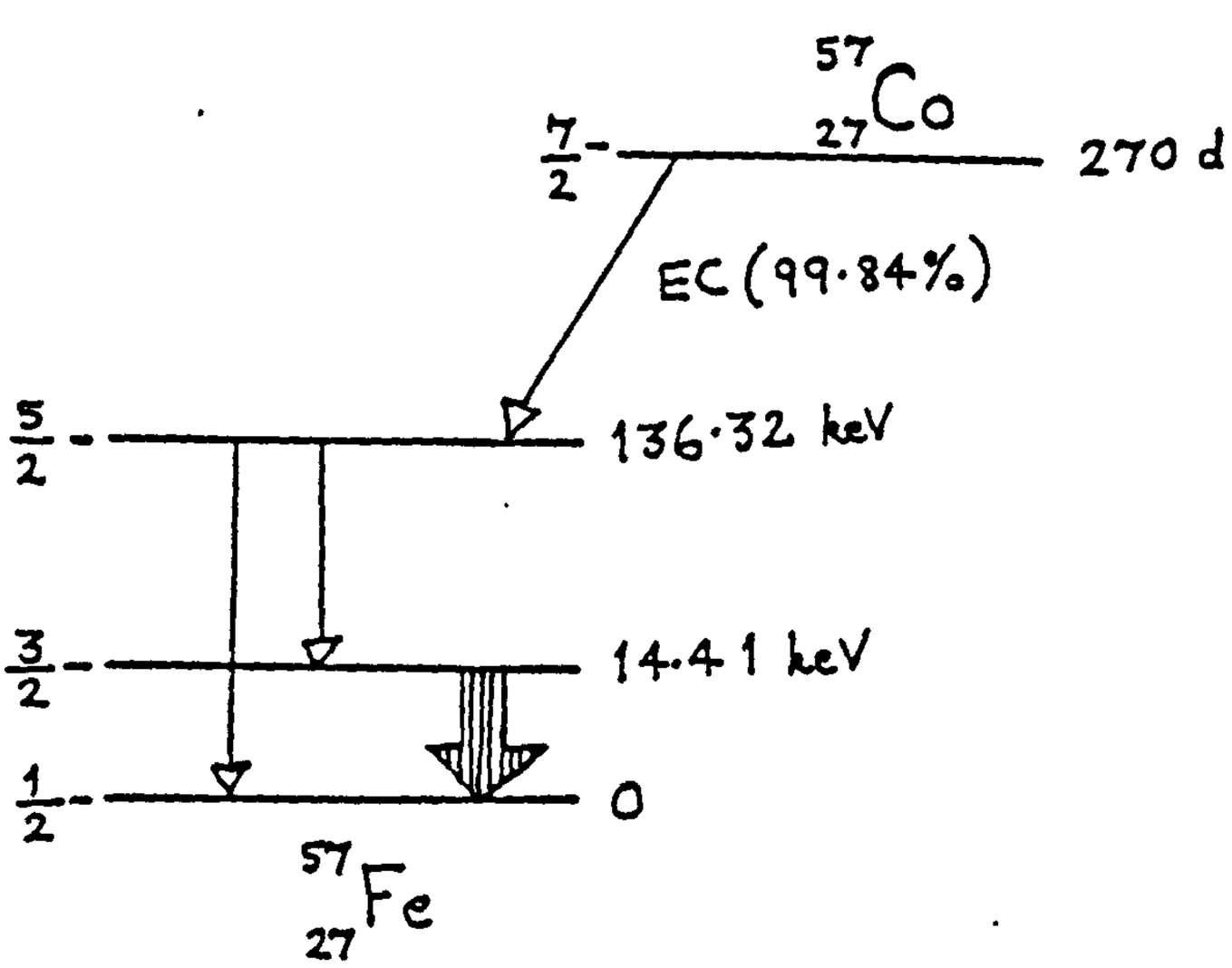

Fig 2.7 Decay scheme for ^{57}Co showing the 14.41 keV transition.

2.1.5b Advantages

1. Non-destructive - samples are usually fully recoverable.

2. Specific to ^{57}Fe nuclide - no cross-interference from other nuclide can ever arise since they will have absorption energies in a different energy region. However, the presence of other nuclide may affect the chemical environment around the ^{57}Fe atom, and may be observed as a subtle change in the Mossbauer spectrum.

3. Little or no sample preparation, although there must be a minimum of ~ 5 mg for an adequate data acquisition rate. Powdered samples are normally used. However, wet samples can be utilised (even at room temperature) providing Brownian motion does not interfere significantly to prevent resonant absorption.

4. Samples can be frozen at 77 K or lower to prevent oxidation from taking place.

5. The oxidation state of iron present in iron oxides can be determined from both the isomer shift and the quadrupole splitting. Most Fe(III) components in iron oxides have IS's in the range 0.3-0.7 mms^{-1} (relative to Fe metal) for measurements taken at room

temperature (RT) and 77 K. By contrast, Fe(II) components have IS's of ca. 1.1-1.5 mms^{-1}, which reflects the difference in the s-electron density around the Fe nucleus.

Similarly, because of the greater distortion in charge distribution in the Fe(II) cation, Fe(II) components normally have much greater QSs than Fe(III) components (2.0-3.2 mms^{-1} compared to 0.4-0.8 mms^{-1}).

6. Fe(II)/Fe(III) ratios can be determined from the quadrupole splitting.

7. The presence of similar lattice sites can be shown up by asymmetric lineshapes.

8. Magnetic ordering is given by the magnetic hyperfine splitting. A few Fe(III) oxides are paramagnetic down to 77 K while others are magnetically ordered at RT. Fe(II) components do not normally order magnetically until ~ 4 K or less. If the quadrupole field is small (or non-existent), the size of the internal magnetic field can be calculated from the separation of the outer pair of lines. If an oxide has more than one magnatic lattice, then this will show up on the Mb spectrum. By taking Mb spectra for a range of temperature, it is possible to determine the Neel point for a given iron oxide.

9. If the quadrupole interaction is comparable to the magnetic hyperfine interaction, then it is possible to obtain information regarding the relationship between the direction of the EFG tensor and that of the magnetic field. However, unique solutions are available only for single crystals.

2.1.5c Main disadvantages and limitations

1. Only the local environment around the Fe atom can be determined - i.e. short-range ordering can be deduced but not the bulk ordering.

2. Many Fe(III) oxides derived from quite different preparations and treatments have similar Mb parameters, indicating that their immediate chemical environment is closely related. Therefore, differentiating between these oxides is difficult.

4. Fine particle sizes cause relaxation effects, leading to the collapse of magnetic hyperfine fields and to line broadening in a Mb spectrum. This makes identification of samples difficult or impossible.

5. Thick samples can cause broadening of linewidth, leading to problems in curvefitting of the Mb spectrum.

6. Because of long counting times, samples which are extremely unstable to oxidation cannot always be prevented from deteriorating at RT. This results in a more complicated spectrum caused by the presence of the degradation products.

2.2 X-ray diffraction

X-ray diffraction is the primary method for structural determination and identification of solids. In the present work, X-ray diffraction has been used solely for the identification of iron oxide samples. The method chosen for this purpose was the step-scanning technique using powdered samples.

The d-spacing, d, is calculated from the measured peak angle, θ, using the familiar Bragg equation:

$$d = \lambda/(2\sin\theta) \qquad -2.15$$

where λ is the wavelength of X-ray used. For iron, the most suitable X-rays are Cu K_α X-rays and λ was taken as 1.54199 A.

2.2.1 Usefulness and limitations

The use of XRD by the powder method for identifying iron oxides works very well for samples which are crystalline and stable to oxidation (providing the Fe content by weight is at least 5%). However, many iron oxides, whether synthetic or natural, are poorly crystalline or have structural disorder and so do not give good X-ray

diffractograms. Peaks are either weak or missing and/or broadened. Also the iron fluorescent X-rays tend to give a high background with Cu K_{α} radiation. This may make it virtually impossible to identify the type of iron oxide under analysis. Even for fairly crystalline iron oxides, identification may prove difficult if certain characteristic lines are missing. For example, if the basal d-spacing is missing, then identification of Fe(III) oxides is uncertain because many of the other lines are similar from one oxide to another.

In the case of natural iron oxides, samples are usually mixtures of one or more different iron oxides, and contaminated by foreign material such as quartz, micas and other silicates. The X-ray diffractogram may thus be too complex for meaningful analysis. The problem of impurities is overcome to a certain extent by differential X-ray analysis, where diffractograms are obtained for both untreated and treated samples (the Fe content is removed) and then compared (Mehra & Jackson, 1960; Pawluk, 1972; Schwertmann & Taylor, 1977). Low percentage Fe in natural samples (such as lithogeneous particles with iron coatings) also result in weak peaks and line broadening.

Iron oxides, such as the Green Rusts, which are very unstable in air (complete oxidation occurring in ~ 0.5-3 h) present great problems because the material changes as

the diffractogram is being taken. This generally results in an irregular background, jagged and broadened peaks, and lines missing towards the end of an X-ray scan. In fact, the angle of scan is restricted to the time taken for a sample to oxidise completely. Also, as the powder technique was employed, samples had to be dried beforehand (e.g. vacuum-drying), which meant that they were partially oxidised even before they were used for XRD.

The d-spacings for some iron oxides are shown in Table 2.2. Only the basal line plus the next seven strongest lines are given.

OXIDE	d-SPACINGS (Å)								ASTM CARD OR REFERENCE
Haematite (α-Fe_2O_3)	3.66	2.69	2.51	2.20	1.84	1.69	1.48	1.45	13-534
Maghemite (γ-Fe_2O_3)	5.90	2.95	2.52	2.08	1.61	1.48			4-0755
Goethite (α-FeOOH)	4.97	4.18	3.36	2.69	2.58	2.48	2.44	2.25	3-024
Akageneite (β-FeOOH)	7.40	5.25	3.31	2.62	2.54	2.34	2.29	2.10	13-157
Lepidocrocite (γ-FeOOH)	6.26	3.29	2.47	2.36	2.09	1.94	1.85	1.73	8-98
δ-FeOOH	4.61	2.55	2.26	1.69	1.47	1.27	1.22	1.10	13-87
Magnetite (Fe_3O_4)	4.85	2.97	2.53	2.10	1.71	1.61	1.48	1.33	11-614
Cl Green Rust I	8.02	4.01	2.70	2.41	2.04	1.81	1.60	1.57	13-88
$\{Fe_x^{2+} Fe_y^{3+} (O,OH,Cl)_9\}$									
CO_3 Green Rust I	7.50	3.76	2.67	2.46	2.34	1.96	1.74	1.58	(a)
$\{Fe_x^{2+} Fe_y^{3+} (O,OH,CO_3)_9\}$									
SO_4 Green Rust II	10.92	5.48	3.65	2.75	2.66	2.46	2.20	1.94	13-92
$\{Fe_x^{2+} Fe_y^{3+} (O,OH, SO_4)_9\}$									

(a) McGill, I.R., McEnaney, B. and Smith, D.C. (1976) Nature 259, 200-201

TABLE 2.2 X-ray d-spacings for iron oxides.

2.3 Infrared spectroscopy

The molecules in chemical compounds vibrate mainly at frequencies in the infrared region. They can thus be made to absorb and scatter infrared radiation. The vibrational modes in any molecule or group of molecules are quantised and determined by the nature of the bonding. An infrared spectrum is a record of absorption versus frequency or more usually wavenumber ($1/\lambda$). Hence the infrared spectrum of any substance will give a characteristic absorption pattern which will reflect on the bonding in the structure.

Infrared spectroscopy is not a primary structural technique (such as XRD), but can be used to identify a particular phase once calibration against a good set of standards has been obtained. In the case of iron oxides, an IR spectrum gives a measure of the molecular environment around an Fe atom. It can be sensitive to the Fe-O bond and to the structural environment of hydrous components (e.g. OH bending and stretching).

2.3.1 Usefulness and limitations

Infrared spectroscopy is useful as a supporting technique for identifying and characterising iron oxides. For a well-crystalline iron oxide, there is a distinctive set of IR absorption peaks in the 1000-200 cm^{-1} range, due to OH bending, which can be used to distinguish one oxide from another. The method is simple and little time is consumed in sample preparation. It can be used to show up the presence of adsorbed anions, such as NO_3^- or SO_4^{2-}. Because samples are dispersed in KBr and pressed into a disk under high pressure, it appears that oxidation of unstable oxides is prevented to some extent. For instance, the yellowish-green disks made for the Green Rust samples were still fairly green on examination a few months later, indicating that any change had occurred slowly (cf. XRD where some Green Rust samples change from a green to orange colour after a few hours).

If samples are non-crystalline, then IRS is severely limited. Good crystalline solids give sharp and distinctive vibrational modes whereas, for poorly crystalline material, the vibrational modes are reduced by the various types of disorder. Many iron oxides, particularly natural ones, are amorphous and so do not give a good characteristic IR pattern. The result is that the various forms give very similar spectra. In addition, as in XRD, natural iron oxides can be composed of one or

more phases, including foreign matter, which complicates the IR spectrum.

2.4 Surface area measurements

2.4.1 Gas adsorption

When a solid is exposed to a gas, it will adsorb some gas molecules onto its surface. This arises because of both physical and chemical attraction between the surface of the solid and the gas molecules. Physical adsorption is due to van der Waals-type forces and is reversible. Chemical adsorption or chemisorption is the result of true chemical binding of the gas molecules at specific sites on the surface. The strength of the interaction in chemical adsorption is much greater than in physical adsorption, and it is usually irreversible. Physical adsorption is normally the process used in surface area measurements. Comprehensive reviews on the subject of gas adsorption by solids and its practical applications have been published by Gregg & Sing (1982) and Lowell (1979).

The amount of gas adsorbed onto the surface of a solid depends upon the pressure of gas, P, absolute temperature, T, and the interaction potential, E, between the gas and surface.

i.e. $X = f(P, T, E)$ -2.15

where X is the amount of gas adsorbed (normally expressed

in g adsorbed per g of solid). If the temperature is fixed, then equation 2.16 becomes:

$$X = f(P, E) \qquad -2.17$$

The quantity X can be measured by several methods, of which gravimetric N_2 gas adsorption at 77 K is the one used in this thesis. A plot of X against the equilibrium pressure, P, at constant T, is referred to as the adsorption isotherm of a given gas-solid interface. Because the interaction potential, E, varies from interface to interface, there are a variety of adsorption isotherms. However, the majority of adsorption isotherms may be classified broadly into five classes (Fig 2.8). This classification was originally devised by Brunauer, Deming, Deming and Teller (BDDT, 1940), although it is more commonly known as the Brunauer, Emmett and Teller (BET, 1938) classification.

From the adsorption isotherm, it is possible to calculate the surface area of a given solid. To do this, the monolayer capacity of the solid must be first calculated. The monolayer capacity is defined as the amount of gas required to completely cover the surface of a solid with a single layer of molecules. One of the earliest and still most widely used theories for determining the monolayer capacity is that of Brunauer, Emmett and Teller. The BET theory is a multilayer adsorption theory

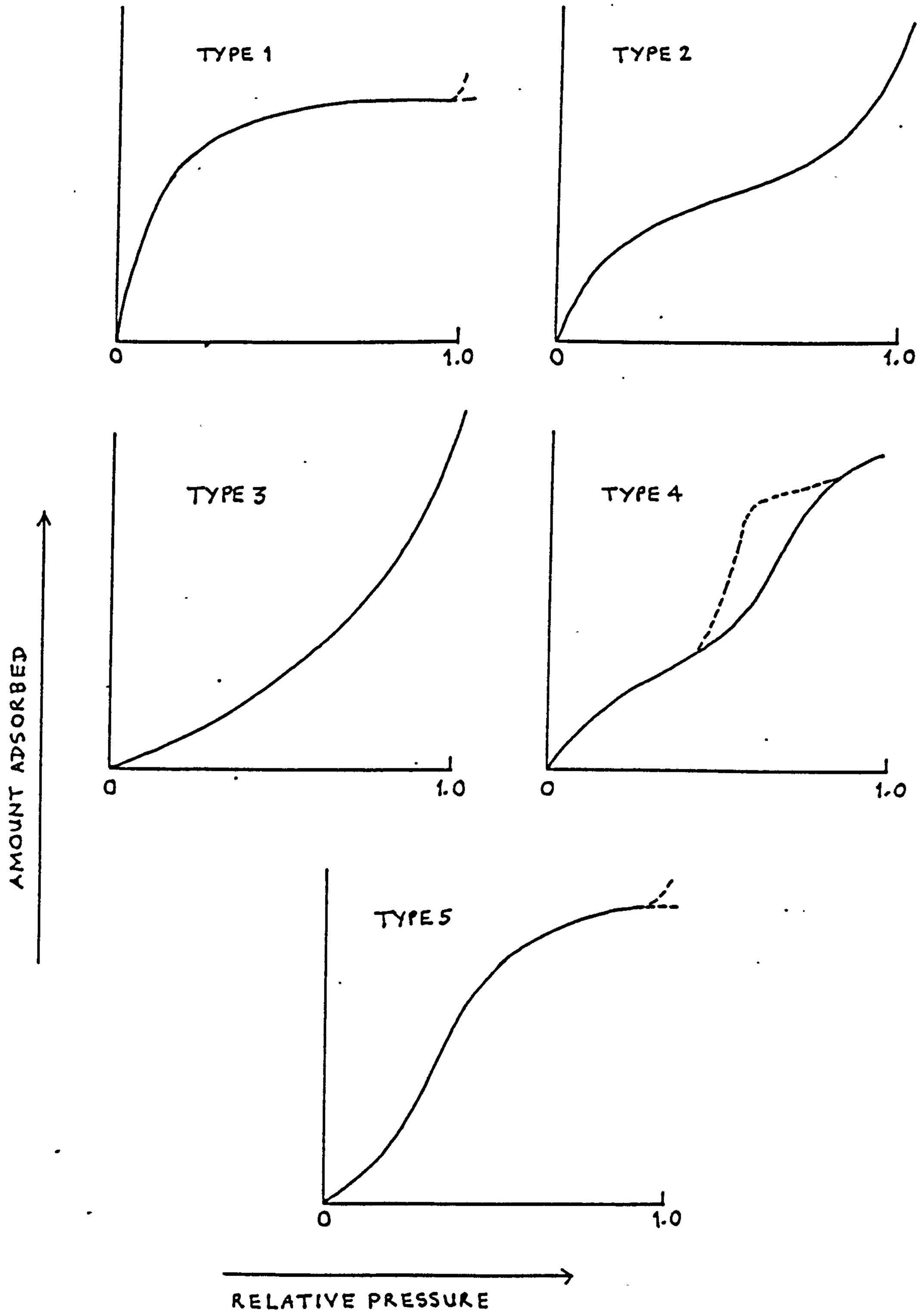

Fig 2.8 The five types of adsorption isotherm in the BET classification.

devised to account for the many different types of adsorption isotherms. It may be simplified for the monolayer case, giving an equation from which the monolayer capacity can be determined:

$$P/(X(P_o-P)) = 1/CX_m + (C-1)/CX_m(P/P_o) \qquad -2.18$$

where P = equilibrium pressure of gas

P_o = saturated vapour pressure of gas at temperature T

X = mass of gas adsorbed per unit mass of solid

X_m = monolayer capacity (same units as X)

C = a constant, which determines shape of derived adsorption isotherm.

The BET constant C is given by:

$$C = \exp\{(E_1-E_L)/RT\} \qquad -2.19$$

where E_1 = heat of adsorption of 1st layer

E_L = latent heat of condensation of gas and is approximately the heats of adsorption of the 2nd and higher layers.

Equation 2.18 effectively accounts for the different types of adsorption isotherms, especially in the low relative pressure region ($0 < P/P_o \leq 0.3$).

If $P/X(P_o-P)$ is plotted against the relative pressure, P/P_o, for values in the range $0.05 \leq P/P_o \leq 0.35$, a straight line graph is obtained for most adsorption isotherms. The monolayer capacity, X_m, can be calculated from the slope and intercept of this plot

i.e. $1/X_m = \text{slope} + \text{intercept}$ -2.20

The specific surface area, S, in $m^2.g^{-1}$ can then be calculated from:

$$S = X_m.A \qquad -2.21$$

where A = area in m^2 occupied by 1g of gas in the completed monolayer.

(For N_2, A = 3485 $m^2.g^{-1}$ at 77 K.)

The BET theory is most useful for determining surface areas from types 2 and 4 isotherms, which are the commoner types and which were applicable to most of the materials in this study.

2.4.2 Porosity

Adsorption isotherms are usually obtained by measuring the amount of gas adsorbed onto a solid as a function of pressure at constant temperature. Experimentally, this is usually divided into two parts. The first part consists of measurements with increasing pressure so that the amount of gas adsorbed increases. In the second part, the pressure is progressively decreased so that some of the gas is desorbed. If a solid is non-porous, then two sets of readings should coincide (within experimental error) as in type II isotherms. However, many solids are porous, resulting in type IV isotherms which show hysteresis (see Fig 2.8). Here the desorption curve (dotted line) lies above the adsorption curve at relative pressures between ~ 0.3-0.95. Type IV adsorption isotherms result from capillary condensation within the pore structure of a solid. The shape of the hysteresis loop depends upon the distribution of pore sizes and the shape of the pores. Average pore size can be estimated by application of the Kelvin equation which relates the relative pressure at which capillary condensation occurs to the size of pores. In the absence of specific knowledge of pore geometry, the shape of the pores is assumed to be cylindrical, in which case the Kelvin equation is given as:

$$\ln(P/P_o) = -2VG/rRT \qquad -2.22$$

where P = equilibrium vapour pressure of gas in pore

P_o = saturated vapour pressure of gas at temperature T

r = radius of cylindrical pore

V = molar volume of liquified gas

G = surface tension of liquified gas

R = universal gas constant.

For nitrogen at 77 K, equation 2.22 can be written as:

$$r = 4.15/\log(P_o/P) \qquad -2.23$$

A correction in r, the "Kelvin radius", must be made since the pore will normally have a layer of adsorbed gas already present before capillary condensation occurs. In other words,

$$r_p = r + t \qquad -2.24$$

where r_p = true pore radius

t = thickness of adsorbed layer.

The value of t may be obtained from the following formula:

$$t = 3.54[5/\ln(P_o/P)]^{(1/3)} \qquad -2.25$$

The start and end of a hysteresis loop in a type IV

adsorption isotherm usually determines the range in pore size. Pore size as governed by its diameter, d, is classified by International Union of Pure and Applied Chemistry, and this classification is given in Table 2.3.

2.4.3 Usefulness and limitations

Surface area measurements by the gravimetric BET N_2 adsorption method cannot be used to identify iron oxides. It can only provide information on surface areas and porosity, and must be used in conjunction with other techniques so that a fuller characterisation of the iron oxides can be obtained.Surface area can also indicate whether an oxide is Fe(II)- or Fe(III)-derived. The former category tend to have smaller surface areas (40-120 $m^2.g^{-1}$ compared to 150-400 $m^2.g^{-1}$), although there is a degree of overlap between the two groups. Small surface areas tend to indicate good crystallinity, while large surface areas tend to indicate a more amorphous and active surface. For unstable materials, the surface area may be affected by the process of oxidation, although work on the sulphate GRs suggest that this does not happen.

Information on the porosity of samples can be obtained from the hysteresis loop of a type IV adsorption isotherm. At best, this can give only an estimation of

the pore size distribution and an idea of the pore shape.

Surface area measurements on natural samples are complicated by the presence of more than one iron oxide phase and, also, by impurities. Thus care must be taken in their interpretation.

Despite some of the limitations, surface area measurements, when taken in conjunction with the other analytical techniques can provide useful information on iron oxides.

Pore type	Pore diameter, d
Micropores	d < 20 A
Mesopores	20 A ≤ d ≤ 500 A
Macropores	d > 500 A

Table 2.3 IUPAC pore size classification

CHAPTER 3:

MOSSBAUER AND OTHER RELEVANT STUDIES OF IRON OXIDES

In this chapter, a survey of previous Mossbauer and other relevant studies relating to the characterisation of iron oxides is presented. Such a survey can only be selective and not all encompassing, and so much literature has been ignored or not mentioned. Most of the work in this chapter deals in the main with the physical properties of iron oxides rather than their chemical behaviour. For instance, the adsorption of ions onto the surfaces of iron oxides has been left out entirely while mechanisms of formation have been briefly mentioned. In respect of analytical techniques, the emphasis has been on MbS since this is the most interesting and versatile technique for the characterisation of iron oxides (this is particularly true if the oxide shows a magnetically-split spectrum).

It is to be noted that most of the studies mentioned in the survey are concerned with Fe(III) oxides.This is to be expected since Fe(III) oxides are the most stable and wide-ranging type. In addition, studies of naturally-occurring iron oxides have been largely left out because characterisation by physical properties is best considered from studies on synthetic samples, which are relatively pure and prepared under controlled

conditions.

A review of early Mossbauer work on synthetic iron oxides is given by Greenwood and Gibb (1971), while a more up-to-date summary which includes natural iron oxides is given by Bowen (1979). Morup et al. (1980) gives useful information on the magnetic properties of iron oxides with particular attention to relaxation effects.

3.1 Haematite (α-Fe_2O_3)

The first reported Mossbauer spectrum of α-Fe_2O_3 was by Kistner and Sunyar (1960), who thereby recorded the first chemical isomer shift and electric quadrupole hyperfine interactions to be observed by this technique. The room temperature spectrum displayed the six-line magnetic hyperfine splitting characteristic of haematite with a field strength of 51.5 T.

A detailed study of powdered α-Fe_2O_3 was made by van der Woude (1966), who measured the temperature dependence of the three principal Mossbauer parameters. The Neel temperature, T_N, was determined to be 956 K, and the value for H_{eff} extrapolated to T = 0 K was 54.4 T. The Mossbauer spectra obtained show the magnetic phase change of haematite, due to spin flipping, as the temperature goes from below T_M, the Morin transition temperature (~ 260 K), to above T_N. The sign of the quadrupole perturbation is reversed when going from below T_M to above T_M. This reversal in sign at the Morin transition is shown more clearly by the temperature variation of the quadrupole interaction. The earlier work of Ono & Ito (1962) has shown that the spin flipping is not a continuous process over the transition region but rather that the magnetic axis of

each Fe atom flips instantaneously from 0 to 90 with increase in temperature. In the material as a whole the process takes place over a finite temperature range because of inhomogeneities in the magnetic domains.

Ultra-fine particles of α-Fe_2O_3 exhibit the phenomenon of superparamagnetism due to a decreasing relaxation time with decreasing particle size. Superparamagnetism can be regarded as a motional narrowing due to the rapid relaxation of antiferromagnetic spins compared with the nuclear Larmor precession ($\sim 10^{-8}$ s for ^{57}Fe). This produces a partial or complete collapse of the MHS and a broadening of lines in the Mossbauer spectrum. The superparamagnetic behaviour of ultrafine α-Fe_2O_3 particles was shown by Nakamura et al. (1964); indeed this was the first observation of the phenomenon in any material by Mossbauer spectroscopy. The Mossbauer spectra of a sample of α-Fe_2O_3, whose particle size was about 50 A in diameter, were obtained at 300 K and 120 K. The spectrum at 120 K shows the magnetically split six-line spectrum expected of α-Fe_2O_3, but at 300 K (which is well below T_N) the spectrum consists only of the two-lines (i.e. a doublet) which was more characteristic of paramagnetic materials. Both this work and that of Bando et al. (1965) shows that the Morin transition temperature is lowered by decreasing particle size.

The magnetic properties of small particles of α-Fe_2O_3 supported on a high-area silica have been investigated by Kundig et al. (1965). A variation of the Mossbauer spectra with average particle size was observed. For particle size of $\leq$ 135 A, the Mossbauer spectrum at RT shows only the two lines due to the quadrupole interaction i.e. their behaviour is suoerparamagnetic. As the particle size increases, the magnetic hyperfine interaction gradually appears as six peaks in the spectrum, until around 180 A this almost completely swamps the quadrupole lines. At this order of particle size, the spectrum almost corresponds to the six-line spectrum of bulk α-Fe_2O_3 particles of 135 A size or less with decreasing temperature. At 440 K, the Mossbauer spectrum shows only the paramagnetic doublet due to the quadrupole interaction but as the temperature was decreased to 12 K, the magnetic hyperfine splitting becomes dominant. The results also showed that no Morin transition occurs for small size particles of 180 A and below down to a temperature of at least 10 K. However, this may be partly governed by the nature of the supporting substrate.

Using the characteristic behaviour of superparamagnetic particles of α-Fe_2O_3, Ganges et al. (1973) have made a Mossbauer study of small particles of iron oxides in soils taken from the Attica region of Greece. They

have concluded that superparamagnetism was responsible for the lack of magnetic hyperfine structure in most of the spectra obtained at RT for clay fractions of various soils. Secondly, the free iron oxide in the C horizon of one of the soils was mostly in the form of ultrafine particles of haematite.

Other Mossbauer studies of α-Fe_2O_3 include one by Srivastava & Sharma (1972) on the magnetic dilution of haematite and its effect on the Morin transition temperature. (Magnetic dilution has a similar effect to superparamagnetism in that the magnitude of the hyperfine field is reduced and line broadening occurs i.e. it is a relaxation phenomenon.) They have shown that T_M decreases in a nonlinear rapid fashion with increasing magnetic dilution of the α-Fe_2O_3 lattice. The magnetic dilution was carried out by introducing α-Al_2O_3 into haematite to form $(1-x)Fe_2O_3$-xAl_2O_3 systems. Work of a similar nature on the Morin transition temperature has also been carried out by Povitskii et al. (1976b). Using haematite doped with a small amount (x) of chromium, forming a $(Fe_{1-x}Cr_x)_2O_3$ system ($0.005 \leq x \leq 0.02$), they have shown that the Morin temperature decreased with increasing x, and hence can be a criterion in indicating the perfection of crystal structure of haematite.

Particle size also affects IR spectra as shown in a study of powdered haematite by Rendon & Serna (1981). Haematites formed by heating goethite in the range 250-600 K have significantly different IR spectra from those formed at 700-950 K. The differenceswere correlated with variation in the size and shape of the particles.

3.2 Maghemite (γ-Fe_2O_3)

In a Mossbauer study, the magnetic hyperfine structure of maghemite was shown tc consist of two fields by Armstrong et al. (1966). The magnitude of the fields, which are due to the A (tetrahedral) and B (octahedral) sublattices, were found to be 48.8 and 49.9 T at RT, respectively. Normally, the two fields would not be resolved in a Mossbauer spectrum but Armstrong et al. (1966) applied an external field of 1.7 T to separate them.

The X-ray diffraction work of Bernal et al. (1959) has shown that four types of γ-Fe_2O_3 can be distinguished as a result of different modes of formation. Three of them belong to the cubic system, while the other belongs to the tetragonal system. They have been differentiated according to the strengths of the non-magnetite (superlattice) lines present in the XRD pattern.

The structural inter-relationship between γ-FeOOH and γ-Fe_2O_3, between Fe_3O_4 and γ-Fe_2O_3, and between γ-Fe_2O_3 and α-Fe_2O_3 have been studied extensively using XRD by Bernal et al. (1957), Dasgupta (1961) and Mackay (1960). The solid phase transformations γ-FeOOH $\xrightarrow{HEATING}$ γ-Fe_2O_3 and Fe_3O_4 $\xrightarrow{OXIDATION}$

γ-Fe_2O_3 were shown to be topotactic i.e. rearrangement of atoms without altering the basic crystal lattice. The transformation γ-Fe_2O_3 $\xrightarrow{HEATING}$ α-Fe_2O_3 was shown to be epitactic because the latter appears as an intergrowth on the crystal face of the spinel.

The occurrence of maghemite in soils has been partly attributed to the conversion of lepidocrocite (γ-FeOOH) or limonite (mainly α-FeOOH) to γ-Fe_2O_3 on heating in air in the presence of organic matter (van der Marel, 1951). Work by Taylor & Schwertmann (1974) in a synthesis study indicated that a Green Rust phase was a necessary precursor in the formation of maghemite under conditions approaching those in soils. Maghemite formation was favoured by slow oxidation and probably via magnetite.

3.3 Goethite (α-FeOOH)

The early Mossbauer studies of Takada et al. (1964) and Rossiter & Hodgson (1965) showed that goethite had a magnetic hyperfine splitting up to RT. This fact coupled with magnetic susceptibility measurements showed goethite to be antiferromagnetic. The paramagnetic Neel temperature was estimated to be about 400 K. The size of the hyperfine field was found to be approximately 36 T at RT and 52 T at 77 K.

Other early Mossbauer data on goethite gave evidence for two hyperfine patterns which it was claimed had a different temperature dependence, and ordered at 340 K and 370 K, respectively (Hrynkiewicz & Kulgawczuk, 1963; Hrynkiewicz et al., 1965). This implies the existence of two internal fields and thus of four magnetic sublattices. However, the work of Takada et al.(1964) and Rossiter & Hodgson (1965), mentioned above, do not support this assumption. To clear up these discrepancies, Dezsi & Fodor (1966) made Mossbauer measurements on a single synthetic and several natural samples of goethite. They showed that the differences in the earlier results could be explained by the presence of water in some of the goethite used. Of the five goethite samples studied, two were found to contain excess water and these gave clear evidence of two hyperfine fields. The other three

samples were stoichiometric α-FeOOH and gave single hyperfine patterns. Dezsi & Fodor (1966) also determined T_N to be 367 k.

In a more recent work on goethites containing excess water molecules, Gendler et al. (1976) have found that T_N for so-called "hydrogoethites" (α-FeOOH.nH_2O) was a function of the number of water molecules present. The Neel temperature was found to fluctuate around 383 ± 5 K on increasing the water content to 9-10 mole %, and then falls sharply on increasing the water content further.

The definitive work on the magnetic structure of goethite was carried out by Forsyth et al. (1968) in a Mossbauer and neutron diffraction study of powdered synthetic α-FeOOH. A value of 403 K was found for T_N. The magnitude of the internal field at RT was determined to be 38.4 T, while at 77 K it was 50.4 T. As indicated by the neutron diffraction results, there is both ferromagnetic and antiferromagnetic coupling between the iron atoms. The Neel temperature will correspond to the point where the weaker of these breaks down, and the residual order above T_N gives a reduced susceptibility compared with that expected for completely disordered S = 5/2 spin states. No evidence was found for the existence of more than one hyperfine field in the temperature range between 4.2 K and RT.The direction of

the electron spin was shown to be parallel to the C-axis of the crystal structure. This last fact was supported by the work done on oriented particles of powdered α-FeOOH by Yamamoto et al. (1968).

The occurrence of superparamagnetism in ultrafine particles of α-FeOOH has been shown by van der Kraan & van Loef (1966) and Shinjo (1966). The former workers used three different particle size distributions: normal (> 2000 A) and two samples labelled A and B (both < 200 A). The particle size in sample B was smaller than in sample A. Mossbauer spectra of the three distributions were taken at 295 and 77 K. The spectra showed that at 295 K, the finest particles (sample B) display only the quadrupole-split doublet, and so was superparamagnetic. Even at 77 K, there was evidence of the collapsing of the magnetic hyperfine field. The spectrum of sample A shows this to a lesser extent, but the spectrum of normal α-FeOOH particles shows only a slight broadening at 295 K. It seems from this kind of study that the onset of superparamagnetic behaviour in goethite occurs in relatively large particles (~ 500 A), which is several times greater than for haematite, where such a behaviour occurs in particle size of ~ 100 A or less.

The isomorphous substitution of Fe by Al in α-FeOOH has been shown to occur quite commonly in soil goethites by Norrish & Taylor (1961) in an XRD study. Magnetic

dilution of the Fe content in synthetic goethite by Al substitution has been studied by Golden et al. (1979), Goodman & Lewis (1981), and Murad & Schwertmann (1983) using Mossbauer spectroscopy. The degree of magnetic relaxation, as indicated by the reduction in the size of the hyperfine field and line broadening, was shown to increase with Al substitution. The effect was more drastic at RT than at 77 K, showing that Al substitution had lowered the magnetic-ordering temperature. At RT total collapse of the hyperfine field was observed for Al substitution in the range 8-13 mole %. The same amount of substitution at 77 K did not produce a total collapse but only a relaxed hyperfine splitting. However, the work of Goodman & Lewis (1981) has indicated that total collapse could occur at 77 K given sufficient Al substitution. This would make it difficult even to distinguish between Al-substituted goethite and lepidocrocite (γ-FeOOH) in soil samples on the basis of their Mossbauer spectra (lepidocrocite is paramagnetic down to 73 K). The more likely confusion would occur between Al-substituted goethite and akaganeite (β-FeOOH), the latter being paramagnetic at RT. Murad & Schwertmann (1983) have shown that crystallinity affects the degree of relaxation caused by Al substitution. Generally, good crystallinity reduces the effect of magnetic relaxation. In addition, particle size effects come into play because it decreases as the amount of Al substitution increases.

The effects of Al substitution and/or small particle size have been used to explain the Mossbauer spectra of natural goethites (Bowen & Weed, 1981; Govaert et al., 1976a & b).In an XRD study, Fitzpatrick & Schwertmann (1982) has shown that the degree of Al substitution and crystallinity of natural goethites reflect the type of pedogenic environment in which they were formed, and so serve as an indicator of soil-forming processes.

3.4 Akaganeite (β-FeOOH)

Magnetic susceptibility measurements by Creer (1962) and Mossbauer spectra by Takada et al. (1964), Rossiter & Hodgson (1965), and Dezsi et al. (1967) showed that β-FeOOH was antiferromagnetic below the Neel temperature of 295 K. The Mossbauer spectrum at RT shows only the paramagnetic doublet due to the quadrupole interaction while at 77 K it shows the 6-line pattern due to the magnetic interaction. The work of Dezsi et al. (1967) indicates that β-FeOOH was paramagnetic from 295 to 670 K, at which point it decomposes to haematite (α-Fe_2O_3). The value of H_{eff} (T = 0 K) was calculated to be 47.5 T. This agrees well with the value of 47 T at 77 K obtained by Rossiter & Hodgson (1965). A Mossbauer study of β-FeOOH using oriented particles by Yamamoto et al. (1968) showed that the antiferromagnetic spin direction was parallel to the C-axis of the crystal.

The thermal conversion of β-FeOOH to haematite has been studied by Vlasov et al. (1970b,1972) using MbS, XRD and electron microscopy. Mossbauer spectra were taken as a function of temperature and show clearly the breakdown of β-FeOOH to haematite. This transformation takes place in the temperature range 523-565 K, which was lower than that indicated by Dezsi et al. (1967).

In a Mossbauer study of small particles of β-FeOOH, Voznyuk & Dubinin (1973) obtained spectra at 80 K for particle sizes of 500, 1250 and 5000 A. The spectra were superpositions of two components: one due to the paramagnetic doublet and the other due to the 6-line MHS. The contribution of the paramagnetic component increases with decreasing particle size. However, the magnitude of the hyperfine field remained unchanged, and thus this behaviour cannot be explained by superparamagnetism. Voznyuk & Dubinin (1973) have suggested that, for very small particles, the Neel temperature falls sharply at the surface, so that at 80 K the surface layer of each particle was paramagnetic. They estimated that the Mossbauer spectra obtained could be explained if the particles have paramagnetic surface layers 7-8 A thick.

In many of the Mossbauer works mentioned above, a single doublet was fitted to the QS at RT. The values were in the range 0.6-0.7 mms^{-1}. However, in more recent work, Chambaere et al. (1978) and Murad (1979) fitted two doublets to the spectrum at RT. The doublets were virtually symmetric about the centre of each other, and had values of 0.55 mms^{-1} (inner) and 0.95 mms^{-1} (outer). Both Chambaere et al. (1978) and Murad (1979) were satisfied that their samples of β-FeOOH were pure (as shown by XRD, electron microscopy and IRS), so that the complex nature of the quadrupole splitting is an intrinsic property of the material. Chambaere et al.

(1978) showed that the existence of two discrete EFG's in β-FeOOH was due to the presence of Cl- anions in the lattice, which somehow induced two differently distorted Fe sites. They further suggested that, since F^- anions also gave the same values of QS, the distortion was of an electrical nature rather than a geometrical one, since the Cl^- anion is much larger than the F^- anion. Murad found by colorimetry that his samples of akaganeite contained on average 7.27 % by weight of chlorine.

Mossbauer evidence for the presence of akaganeite in New Zealand soils was given by Logan et al. (1976). However, this has since been refuted by Childs & Johnston (1980).

3.5 Lepidocrocite (γ-FeOOH)

The Mossbauer spectra taken by Takada et al. (1964) and Rossiter & Hodgson (1965) showed that lepidocrocite was paramagnetic down to at least 77 K. Johnson (1969) took Mb spectra below liquid N_2 temperatures, and showed that lepidocrocite was an antiferromagnet with a Neel temperature of 73 K. At liquid He temperature (4.2 K), the 6-line spectra due to the nuclear Zeeman splitting can be seen very sharply. The transition to a magnetically-ordered state occurred over a 10 K range for both synthetic and natural samples. The effective magnetic field at the Fe nucleus at 4.2 K was found to be 46.0 T. The low value of the Neel temperature (which is much lower than that of α-FeOOH) can be explained by the weak hydrogen bonding between the layers of iron octahedra. Johnson (1969) further showed by applying an external magnetic field to a single crystal of γ-FeOOH, that the Fe(III) magnetic moments are collinear in the antiferromagnetic state, with the alignment along the C-axis.

The Mossbauer spectra of thin layers of γ-FeOOH (down to 10 A) were taken by Minkova & Schunck (1975) using the conversion electron technique. The results revealed an increase in the quadrupole splitting with a decrease of layer thickness. The values of the quadrupole splitting

may also be considered as experimental proof of the increase of the EFG in the vicinity of the crystal lattice surface.

Lepidocrocite is found less frequently in soils than goethite and haematite, and is often associated with goethite. Its occurrence in soils is indicative of hydromorphic conditions, being commonly found in gleys and pseudogleys (Schwertmann & Taylor, 1977). The occurrence of lepidocrocite in some British soils has been studied by Brown (1953). Chukhrov et al. (1973) has given a detailed account of the conditions under which lepidocrocite may be formed in nature. A study of some of the conditions under which lepidocrocite was formed in synthetic systems has been done by Schwertmann & Thalmann (1976).

As mentioned in section 3.2, lepidocrocite dehydrates on heating to maghemite. In nature, this transformation may be carried out in reduction-oxidation processes, such as those found in peaty soils. Van der Marel (1951) has investigated the conversion of lepidocrocite to maghemite in the peaty soils of Groningen and Drenthe in the Netherlands. The transformation of lepidocrocite to goethite under solution has been studied by Schwertmann & Taylor (1972) in order to obtain a clearer understanding of the conditions and mechanism of transformation.

3.6 Delta Fe(III) oxyhydroxide (δ-FeOOH) and feroxyhite (δ'-FeOOH)

Until about 1977, only one form of δ-Fe(III) oxyhydroxide was known, namely, δ-FeOOH. Then in 1977, Chukhrov et al. presented electron diffraction and Mossbauer data, demonstrating the existence of two forms of δ-Fe(III) oxyhydroxide in the laboratory: ferrimagnetic, ordered δ-FeOOH, and the practically non-magnetic, slightly ordered δ'-FeOOH. As mentioned in section 1.2.2b, Chukhrov et al. (1977) show that δ- and δ'-FeOOH have basically the same structure, and differ only in the population by Fe of the octahedral sites. In δ'-FeOOH, the distribution of Fe was ordered in the octahedral sites but non-uniform in the lattice as a whole. For δ-FeOOH, the Fe distribution was random in the sites but uniform throughout the structure.

On the basis of their experimental work, Chukhrov et al. (1977) suggested that the formation of δ'-FeOOH in nature was quite possible. They then duly identified natural δ'-FeOOH in iron-manganese nodules from the bottom of the Pacific Ocean, Baltic, White, and Kara seas, and also in gleyed soils. The samples were in the form of yellowish-brown deposits. The name "feroxyhite" was then proposed for the new-found mineral. The extreme conditions (relative to natural) under which δ'-FeOOH was

produced in the laboratory meant that its genesis in the natural environment was very unlikely.

Despite the work of Chukhrov et al. (1977), there has been little interest in feroxyhite so far. An exception was the work of Carlson & Schwertmann (1980) which undertook to elucidate the genesis of feroxyhite in nature. Feroxyhite was identified by XRD in some rusty precipitates from Finland. The Mossbauer spectra at 4.2 K for these natural samples gave the usual 6-line Zeeman pattern. The magnitude of the internal magnetic field at 4.2 K was found to be ~ 51 T. The paramagnetic Neel temperature was not determined.

Ferrimagnetic δ-FeOOH has been studied more extensively. It was originally identified by XRD as "δ-Fe_2O_3" by Glemser & Gwinner (1939) but later shown to be δ-FeOOH by Francome & Rooksby (1959) and Bernal et al. (1959). From the intensities of the x-ray lines, Francome & Rooksby (1959) showed it likely that 80% of the Fe was distributed randomly in the octahedral sites, with the remaining 20% distributed randomly in the tetrahadral sites. However, this was not a fixed distribution but varied from sample to sample. The two workers also studied the thermal decomposition of δ-FeOOH and found that it partly converted to goethite on heating to ca. 423 K. On heating to about 513 K, both the goethite and the remaining δ-FeOOH converted to

haematite.

The Mossbauer spectrum of δ-FeOOH taken at 77 K by Rossiter & Hodgson (1965) gives a 6-line pattern and showed only a single magnetic field. The magnitude of this field was ~ 53 T. However, a more in-depth study by Dezsi et al. (1967) indicated the presence of two internal magnetic fields which corresponded to the octahedral and tetrahedral sites. The values of these fields were 52.5 and 50.5 T at 80 K, respectively, and the intensity ratio as evaluated from the Mossbauer spectrum was 60:40. Dezsi et al. (1967) also interpreted the results of annealing as conversion first to goethite at ~ 400 K and then to haematite at ~ 510 K, thus confirming the work of Francome & Rooksby (1959). Other thermal studies of δ-FeOOH by MbS, XRD, electron microscopy and differential thermal analysis do not show the transition to goethite before conversion to haematite (Loseva & Murashko, 1972; Povitskii et al., 1976a; Vlasov et al., 1970a&b). Indeed Loseva & Muashko (1972) and Povitskii et al. (1976a) has suggested that δ-FeOOH converts to "δ-Fe_2O_3" before transformation to haematite. Vlasov et al. (1970a) gives the conversion temperature to haematite as ~ 500 K, which agrees well with Dezsi et al. (1967).

In the Mossbauer work of Dezsi et al. (1967), the spectrum of δ-FeOOH at RT showed an MHS which was

virtually the same at 77 K. The Curie or Neel temperature must therefore be greater than RT. Indeed T_N was estimated at ~ 455 K using the outer octahedral field. However, because δ-FeOOH starts to convert at ~ 400-420 K, the Neel temperature has no useful meaning here.

Superparamagnetism was shown to occur in fine particles of δ-FeOOH by Vlasov et al. (1970a) in their thermal conversion study of δ-FeOOH to α-Fe_2O_3. The RT Mb spectrum consisted of a broad doublet which, on application of an external field of 2.1 T, split into a 6-line pattern. Povitskii et al. (1976a) studied the thermal conversion of superparamagnetic particles of δ-FeOOH using an external field of 2.0 T.

We end this section by commenting on the evidence presented by Chukhrov et al. (1977) for distinguishing between δ- and δ'-FeOOH. They have said that the difference is due to the population by Fe of the octahedral sites, and the distribution of the Fe in the lattice as a whole. The evidence for the difference was from the electron diffraction patterns: the absence of certain lines in δ'-FeOOH was explained by disorder in the crystal lattice. However, the Mb spectra does not give this distinction but only shows the absence of magnetic ordering for δ'-FeOOH down to 77 K. Since the samples of δ'-FeOOH were of finer particles than the samples of δ-FeOOH, the absence of an MHS at 77 K could

be accounted for by superparamagnetic behaviour. Thus the difference between δ- and δ'-FeOOH may not be a true one but rather one of different grades of the same oxide. Particle size could account for the absence of certain reflections in the electron diffraction patterns of δ'-FeOOH.

3.7 Ferrihydrite ($5Fe_2O_3.9H_2O$)

The first distinct XRD patterns for hydrous Fe(III) oxides were obtained by van der Giessen (1966) and independently by Towe & Bradley (1967) for material precipitated by the hydrolysis of Fe(III) nitrate solutions. Hydrous Fe(III) oxides have a gel-like nature when first precipitated and were previously thought to be amorphous. They were often referred to as "amorphous ferric oxides" or "ferric gels". The XRD patterns obtained by van der Giessen (1966) and Towe & Bradley (1967) were very similar. However, the former author proposed a cubic structure for the material while the latter workers suggested a defect haematite structure. Chukhrov et al. (1972) studied a naturally-occurring hydrous Fe(III) oxide which gave five broad x-ray and electron diffraction lines, corresponding to the strongest x-ray lines of the aforementioned synthetic samples. The name ferrihydrite was proposed for this naturally-occurring oxide, which had a bulk composition of $5Fe_2O_3.9H_2O$, and the defect haematite structure proposed by Towe & Bradley (1967) was accepted as a tentative structure. Essentially the structure is that of haematite except that some of the O atoms are replaced by OH^- and H_2O groups, and less Fe occurs in the octahedral sites. This leads to a lower Fe/O ratio and the absence of the two strongest lines of

haematite (i.e. 3.67 A and 2.69 A).

From electron micrographs, van der Giessen (1966) found that the particles constituting his oxide gel was about 30 A in diameter. Magnetic susceptibility measurements suggested that the material was antiferromagnetic with a superparamagnetic behaviour. Mossbauer spectra down to 140 K only showed a quadrupole doublet. Van der Giessen et al. (1968) also studied the freezing behaviour of Fe(III) oxide gels. The peak height of the quadrupole doublet was shown to vary with temperature. From this, information on the constitution of the gel can be obtained. It was concluded that the gel consisted of a network of small particles (< 200 A) interlaced with pores containing water.

Using IRS, Russell (1979) gave evidence for structural OH groups in ferrihydrite. It was proposed that the OH groups in ferrihydrite are about half as numerous as those in akaganeite (β-FeOOH), and that they may occur in environments similar to those in this mineral. He further suggested that the chemical formula of ferrihydrite should be amended to $Fe_2O_3.2FeOOH.2.6H_2O$ to take account of the structural OH groups.

The first Mb study of ferrihydrite itself (as opposed to "amorphous Fe(III) hydroxides", etc.) was made by Murad & Schwertmann (1980). The results show that there was

magnetic ordering at 4 K, with a wide distribution of hyperfine fields and a maximum field size of ~ 50 T. The RT spectrum required two Lorentzian doublets to fit the experimental data properly.

The thermal conversion of Fe(III) gel to α-Fe_2O_3 by annealing has been studied by Srivastava & Singh (1974) using MbS, and by Kauffman & Hazel (1975) and Saraswat et al. (1979) using MbS and other techniques. The transformation to α-Fe_2O_3 starts around 520-540 K and is virtually complete at 623 K. The transformation of ferrihydrite to haematite by ageing in aqueous solution at 92 °C has been studied in detail by Johnston & Lewis (1983). It was found that haematite was formed after a relatively short time of ageing for the concentrations of Fe used (0.06 M). The haematite was detectable by XRD after only 10 minutes and by MbS after 30 minutes. The crystallinity of the samples improved with increasing ageing.

Naturally-occurring ferrihydrite has been studied extensively by Chukhrov et al. (1972, 1976). It was established that ferrihydrite is a typical mineral of geologically recent precipitates. Ferrihydrite was found as deposits in cold iron springs (5-10 °C with pH near 7) in different parts of the USSR. Its formation was caused by rapid oxidation in connection with the metabolic activity of iron bacteria. Ferrihydrite was

also found in mines, precipitated from solutions percolating through sulphide ores and containing divalent iron. Schwertmann & Fischer (1973) also studied ferrihydrite from deposits in drainage ditches and from sediments produced by Fe containing spring waters. In their work, Chukhrov et al. (1972) termed poorly-crystalline ferrihydrite, showing only two distinct x-ray and electron diffraction lines (2.5 and 1.5 A), as protoferrihydrite.

3.8 Magnetite (Fe_3O_4)

Mossbauer studies on magnetite have been concerned in the main with the electron hopping process and its magnetic properties below and above the Verwey transition temperature (T_v=119 K). Evidence for electron hopping between the Fe(II) and Fe(III) cations in the octahedral B sites has been given by Bauminger et al. (1961), Ito et al. (1963) and Banerjee et al. (1967). At 77 K, where the Fe(II) and Fe(III) states are discrete and no electron hopping occurs, two partially resolved hyperfine patterns with fields of 50.3 and 48.0 T were observed. The 50.3 T field corresponded to the Fe(III) cations in both A and B sites which are very similar. The other field was due to the B site Fe(II) cations, as indicated also by its relatively large QS. At RT, there were fields of 49.1 and 45.3 T corresponding to A site Fe(III) cations and to the B site (Fe(II) and Fe(III)) cations, respectively. The latter field was the averaged spectrum arising from electron hopping between the Fe(II) and Fe(III) cations in the B sublattice. By applying an external field of 12 T, Kundig & Hargrove (1969) obtained a better resolution of the two hyperfine fields at RT, and also established that the tetrahedral A site spins aligned antiparallel and the B sites parallel to the applied field.

In a more recent Mb study of slightly doped magnetite, Boekema et al. (1976) showed the occurrence of spin and charge oscillation in the B sublattice. The magnetite samples were doped with impurity atoms at the B site of the inverse spinel structure. The general formula of the samples was $M_xFe_{3-x}O_4$ with M = Li, Ni, Al, V, Cr, Ti, Sn and Mo, and x = 0.05 and 0.10. The broadened B site linewidth was interpreted in terms of a classical charge oscillation model, which describes the electron response in narrow bands.

In a Mb and XRD study of the original samples of the magnetite series, Fe_3O_4-γFe_2O_3, of G. Hagg, evidence for vacancy distribution at the tetrahedral A sites as well as the octahedral B sites in non-stoichiometric magnetite was given by Annersten & Hafner (1973). Furthermore, broadening of the B site linewidth in the Mb spectra indicated that the relaxation times of the hopping electrons at constant temperature increases as the deviation from the stoichiometric ratio increases.

The effect of particle size on the electric and magnetic properties of magnetite have been studied quite extensively by MbS. Ultrafine particles of magnetite exhibit the phenomenon of superparamagnetism at RT (McNab et al., 1968). Magnetic relaxation starts to occur for particle sizes of 150 A, and a complete collapse of the

hyperfine spectrum results for particles of 100 A diameter.

Krupyanskii & Suzdalev (1974) has shown that a metal-insulator transition occurs for microcrystalline particles of Fe_3O_4 (size between 200 and 4000 A) as the particle size decreases. The Verwey transition temperature was found to increase with decreasing particle size. Also, magnetisation measurements showed that, for particles in the range 200-300 A, the order in the insulating state was different from the Verwey order in bulk material.

Lipka et al. (1977) have demonstrated the usefulness of the Mossbauer technique for studying the properties of microcrystals. In their study, using microcrystals of Fe_3O_4, they have shown that it is possible to determine the particle volume and the magnetic anistrophy energy constant K. In addition, the question of magnetically "dead layers " on the surface of microcrystal can be easily answered by MbS. For Fe_3O_4 embedded in acetone and oleic acid, it was shown that this does not exist.

3.9 Green Rusts

Most of the work done on Green Rusts arose from corrosion studies of iron and steel. Only very recently has there been interest in Green Rusts in terms of their probable role as intermediaries in the formation of iron oxides in the natural environment. There have been very few Mb studies of the Green Rusts.

The crystal structures of the Green Rusts were characterised in the XRD work of Bernal et al. (1959). As already mentioned in section 1.2.3b, two slightly different types of Green Rusts are recognised: Green Rust I (GRI) with a basal d-spacing of 7.5-8.0 A, produced from Fe(II) solutions containing Cl^-, Br^- or SO_4^{2-} anions, and Green Rust II (GRII) with a basal d-spacing of 10.6-10.9 A, originating from $FeSO_4$ solutions only.

In a Mb study of the corrosion products of iron in aqueous solutions of ammonium nitrate, Gancedo et al. (1976) synthesised GRI and II, and obtained RT spectra of both materials. Both spectra show the existence of an Fe(II) and an Fe(III) component. The Fe(II) doublet has parameters of IS = 1.22 mms^{-1} (with respect to Fe metal) and QS = 2.30 mms^{-1} for GRI, and IS = 1.19 mms^{-1} and QS = 2.37 mms^{-1} for GRII. Thus the

two Green Rusts were very similar from the viewpoint of MbS. They differ only in the ratio Fe(II)/Fe(III), being 1.88 for GRI and 2.63 for GRII. A green precipitate formed in the early stages (4-8 h) of the corrosion experiments was found to have a RT spectrum very similar to the synthetic Green Rusts.

In a study of the corrosion of cast iron in carbonate solutions, McGill et al. (1976) reported the formation of a green rust compound which gave similar XRD lines to GRI, but differing structurally. Brindley & Bish (1976) then pointed out from the XRD data that the compound was likely to be a member of the pyroaurite group, which are carbonate-hydroxides with the formula

$Mg_6M_2^{III}(OH)_{16}CO_3.4H_2O$

where M^{III} = Fe, Al or Cr. Indeed, this was suggested earlier by Taylor (1973) for the Green Rusts proper and, although not all Green Rusts are carbonates, they are now recognised as belonging to the pyroaurite group. A detailed analysis of the crystal structure of pyroaurite has been presented by Allmann (1968).

Green Rusts have also been studied from the viewpoint of formation in solutions. Using UV spectrophotometry and chemical analysis, Misawa et al. (1973 & 1974) made a study of the Fe(II)-Fe(III) intermediate green complex formed by aerial oxidation of neutral and slightly alkaline $FeSO_4$ solutions. This complex was shown to

be a precursor of GRII and named "Green Complex II" (GCII). On this basis, the ratio Fe(II)/Fe(III) in GRII was estimated to be 1.

Taylor (1980) synthesised a Green Rust of the Fe(II)-Fe(III) hydroxycarbonate type by using small amounts of Fe(III) to induce precipitation of Fe(II) from carbonate solutions. The synthesis was carried out under near pedogenic conditions to demonstrate the possible significance of Green Rusts as a precursor of soil iron oxides. It was shown that the carbonate Green Rust (carbonate Fe-GR) was of a very unstable character, and converts on oxidation to other common iron oxides such as ferrihydrite, goethite and lepidocrocite. As an extension to this work, Taylor & McKenzie (1980) produced a series of Fe(II)-Al(III) hydroxy-chlorides, -sulphates and -carbonates. These compounds are analogous to the Green Rusts and therefore belong to the pyroaurite family. As previously mentioned in section 1.2.3b, they have been termed "aluminium Green Rusts" (Al-GRs) in this thesis. The Al-GRs were again very unstable to oxidation, and converted to akaganeite, aluminous ferrihydrite, lepidocrocite and aluminous goethite.

The Mb spectra of carbonate Fe-GR and carbonate Al-GR have been obtained by Murad & Taylor (1984). At 120 K, the compounds were in a paramagnetic state, and the spectra consisted of Fe(II) and Fe(III) components. The

carbonate Fe-GR was fitted with two Fe(II) and two Fe(III) Lorentzian doublets, while the carbonate Al-GR was fitted with two Fe(II) and one Fe(III) doublets. The outer Fe(II) doublet for both types of GR have values of IS = 1.14 mms^{-1} (w.r.t Fe) and QS = 2.8 mms^{-1}.

The results were interpreted in terms of an ordered cation arrangement in the pyroaurite-type structure.

Compound	T (K)	IS v Fe (mms^{-1})	QS (mms^{-1})	MHS (T)	Magnetic transition temp. (K)	Reference
α-Fe_2O_3	298	0.38	-0.24	51.5		Kistner & Sunyar (1964)
	296	0.39	-0.21	51.8		Kundig et al. (1966)
	83		+0.35	54.2		
	RT	0.37			T_N=956	Van der Woude (1966)
	0			54.4		
γ-Fe_2O_3	RT	0.27(A)		48.8		Armstrong et al. (1966)
		0.41(B)		49.9		
α-FeOOH	300	0.55*		36	T_N~400	Takada et al. (1964)
	110	0.70*		52		
	295	0.44		36		Rossiter & Hodgson (1965)
	77	0.69		52		
	RT	0.35	-0.3	38.4	T_N=403	Forsyth et al. (1968)
	77			50.4		
	4.2			50.4		
(natural)	RT	0.41	-0.32	38.1		Govaert et al. (1976a)
β-FeOOH	300	0.45*		0		Takada et al. (1964)
	110	0.45*		49		
	295	0.34	0.62	0		Rossiter & Hodgson (1965)
	77			47		
	RT	0.35	0.70	0	T_N=295	Dezsi et al. (1967)
	0		-0.21	47.5		
	RT	0.39	0.62	0		Voznyuk & Dubinin (1973)
	80	0.48	0.64	48.5		
	295	0.38	0.55	0		Murad (1979)
		0.39	0.95	0		
	4	0.36	0.90	47.3		
		0.35	0.30	47.9		
		0.37	-0.05	48.6		

Unless specified samples referred to are bulk synthetic material

QS = 2E = 1/4{e2Q}{3cos2θ-1} A,B = sites in spinel lattice

* IS relative to unknown source RT = room temperature

Table 3.1 Mossbauer parameters for iron oxides.

Compound	T (K)	IS v Fe (mms^{-1})	QS (mms^{-1})	MHS (T)	Magnetic transition temp. (K)	Reference
γ-FeOOH	300	0.4*		0		Takada et al. (1964)
	110	0.5*		0		
	295	0.39	0.54	0		Rossiter & Hodgson (1965)
	77	0.53	0.62	0		
	RT	0.30	0.55	0	T_N=73	Johnson (1969)
	4.2		<0.1	46.0		
	RT		0.56	0		Minkova & Schunk (1975)
(10 A film)	RT		0.94	0		
δ-FeOOH	77	0.4		53		Rossiter & Hodgson (1965)
	80			50.5(tet) 52.5(oct)		Dezsi et al. (1967)
	RT	0.38	0.48	0		Vlasov et al. (1970)
	83	0.8	0.47	52		
δ'-FeOOH	4			51.3		Carlson & Schwertmann (1980)
$5Fe_2O_3.9H_2O$	291	0.34	0.54	0		Murad & Schwertmann (1980)
		0.33	0.87	0		
	4	0.34	0.06	45.2		
		0.34	0.02	48.2		
		0.34	-0.01	50.5		
("Fe(III) hydroxide")	296	0.37	0.64	0		Srivastava & Singh (1974)
("Fe(III) oxide gel")	RT	0.37	0.60	0		Kauffman & Hazel (1975)

Unless specified samples referred to are bulk synthetic material
QS = $2\varepsilon = 1/4(e2Q)(3\cos^2\theta-1)$ A,B = sites in spinel lattice
* IS relative to unknown source RT = room temperature

Table 3.1 (cont'd) Mossbauer parameters for iron oxides.

Compound	T (K)	IS v Fe (mms^{-1})	QS (mms^{-1})	MHS (T)	Magnetic transition temp. (K)	Reference
Fe_3O_4	300			49.1{Fe^{3+}(A)}		Banerjee et al. (1967)
				45.3{$Fe^{2+,3+}$(B)}		
	77			50.3{Fe^{3+}(A+B)}		
				48.0{Fe^{2+}(B)}		
	295	0.35		48.6{Fe^{3+}(A)}		McNab et al. (1968)
		0.78		46.0{$Fe^{2+,3+}$(B)}		
	4.2	0.50	-0.1	51.1{Fe^{3+}(A+B)}		
		0.92	-0.8	50 {Fe^{2+}(B)}		
GRI	RT	0.49		(Fe^{3+})		Gancedo et al. (1976)
		1.22	2.30	(Fe^{2+})		
GRII	RT	0.49		(Fe^{3+})		"
		1.19	2.37	(Fe^{2+})		
CO_3 GR (GRI)	120	0.36	0.49	(Fe^{3+})		Murad & Taylor (1984)
		0.40	0.95	"		
		1.13	2.23	(Fe^{2+})		
		1.14	2.89	"		

Unless specified samples referred to are bulk synthetic material
QS = $2\varepsilon = 1/4\{e^2Q\}\{3\cos^2\theta-1\}$ A,B = sites in spinel lattice
* IS relative to unknown source RT = room temperature

Table 3.1 (cont'd) Mossbauer parameters for iron oxides.

CHAPTER 4: EXPERIMENTAL PROCEDURES

The experimental work undertaken in this thesis was divided into two parts:

(a) a short study for references purposes of the characteristics of synthetic Fe(III) oxides was carried out using the analytical techniques discussed in Chapter 2. Since Fe(III) oxides are generally well-documented, this part of the experimental work was kept to a minimum. A selection of Fe(III) oxides were synthesised and their properties and behaviour determined using the analytical techniques at hand.

(b) an in-depth study of the metastable Green Rusts, which are probably intermediaries in the formation of Fe(III) oxides such as lepidocrocite, maghemite and akaganeite (Bernal et al., 1959; Misawa et al., 1973; Schwertmann & Thalmann, 1976; Taylor & McKenzie, 1980; Taylor & Schwertmann, 1974 & 1978). To this end, a series of Green Rusts was synthesised and investigated. For comparison, the analogous aluminium Green Rusts (Al-GRs), which may be important in the formation of soil iron oxides, were also synthesised and studied. Because of the instability of both the Green Rusts (or Fe-GRs) and the Al-GRs to oxidation (lifetime in air of the order 5-30

mins. for the Fe-GRs, and 0.5-3 h for the Al-GRs), experimental apparatus was specially adapted to provide an oxygen-free environment for the preparation of these compounds. Preliminary syntheses of Green Rust samples were carried out to test the adequacy of these experimental procedures. These preliminary syntheses show that, despite the inherent handling difficulties, Green Rusts and the related Al-GRs could be produced with consistency. The work on the Fe-GRs forms the main part of this Ph.D. thesis.

4.1 Reagents and glassware

The chemicals used in the experimental work were all of analytical grade (Analar) quality unless otherwise stated. All solutions were prepared fresh unless otherwise stated. The glassware was usually cleaned immediately after use: for vessels holding Fe or Al solutions, this involved washing with conc. HCl before thoroughly rinsing with distilled water. If the iron stains were too difficult to remove initially, then the glassware would be soaked overnight in dilute HCl before cleaning as described above.

4.2 Preparation of Fe(III) oxides

The following Fe(III) oxides were synthesised: haematite, goethite, akaganeite, lepidocrocite, δ-Fe(III) oxyhydroxide and ferrihydrite. A sample of maghemite was obtained from magnetic recording tape material. Several attempts were made to produce feroxyhite but the XRD data proved inconclusive, and so it has not been included here. Also, doubts exist as to whether δ'-FeOOH is really a separate phase from δ-FeOOH (Cuttler, private comm.). Although magnetite is strictly a mixed Fe(II)-Fe(III) oxide, it has been prepared and included here for convenience. The methods used here to make the iron oxide samples are summarised below.

4.2.1 Haematite (α-Fe_2O_3)

Haematite was made by heating a sample of δ-FeOOH to 700 °C in air for 2 h.

4.2.2 Goethite (α-FeOOH)

Several samples of this oxide were synthesised using the method of Brauer (1954). Molar KOH was added to a solution of 0.01 M $FeCl_3$ until the pH reached ~ 11-12. The resultant chocolate-brown precipitate was left

in the original solution to age. At intervals of a few days, samples of the precipitate were taken and washed twice with distilled water and then dried in air at RT. One sample was taken after the precipitate had been aged for approximately 10 months.

4.2.3 Akaganeite (β-FeOOH)

This was prepared by the slow hydrolysis of $FeCl_3$ solution (Weiser et al., 1946). A solution of 0.1 M $FeCl_3$ was heated slowly to 80 °C and kept at this temperature for 2 h. After cooling, the resulting precipitate was separated from the solution by centrifuging. It was washed first by distilled water, then followed by 0.1 M NH_4OH to remove the excess water. The sample was dried at 110 °C for 24 h.

4.2.4 Lepidocrocite (γ-FeOOH)

Lepidocrocite was prepared according to the method of Schwertmann & Taylor (1972). A solution of 0.1 M $FeCl_2$ was taken to pH 7 and maintained at ~ 7 by the addition of 0.1 M NaOH (free from carbonates) using an automatic titrimeter. A dark-green precipitate was produced on addition of the alkali. Oxygen was then bubbled through the suspension. This changed the colour

of the precipitate to orange-brown. Subsequently, the precipitate was washed twice with distilled water and left to dry in air at RT.

4.2.5 δ-Fe(III) oxyhydroxide (δ-FeOOH)

A method based on that of Glemser & Gwinner (1939) was employed to make δ-FeOOH. Excess M KOH was added to a solution of 0.1 M $FeCl_2$ to precipitate most of the iron in the form of $Fe(OH)_2$. The latter was separated from solution by decanting the supernatant and then frozen by liquid N2. It was then placed in a vacuum freeze-drier to be dried overnight. During this drying process, the $Fe(OH)_2$ was oxidised to δ-FeOOH (the original frozen precipitate was dull greenish-white in colour while the dried material was bright reddish-brown and had bulk magnetism). The material was then washed twice with distilled water and dried in air at RT.

4.2.6 Ferrihydrite ($5Fe_2O_3.9H_2O$)

Using the method of Lewis & Schwertmann (1979), two samples of ferrihydrite were prepared as follows:

(i) M KOH was added to a solution of 0.01 M $FeCl_3$ to pH ~ 11.5. The chocolate-brown precipitate

was washed 4 times by centrifuging at 2000g and re-suspension of the sediment in distilled water (at least twice the volume of the original suspension). The precipitate was then dried in an oven at 40 °C.

(ii) repeat of (i) except pH taken to ~ 8 and precipitate dried in open air at ~ 36 °C.

4.2.7 Magnetite (Fe_3O_4)

Magnetite was synthesised by partial precipitation of an $FeCl_2$ solution, followed by slow oxidation in air. A solution of 0.01 M $FeCl_2$ was partially precipitated with 0.1 M NaOH under anoxic conditions. The resulting fine, dark-green suspension was then left to oxidise in air. After 2 days, the colour of the suspension had changed to black. A sample was taken and the precipitate separated by centrifuging. The precipitate was then washed twice with distilled water and dried in air at RT.

4.3 Preparation of Green Rusts

Attempts to synthesise Green Rusts using the method of Bernal~ et al. (1959) were unsuccessful. The main reason was insufficient information given by Bernal et al. (1959). In particular, no detail was given of the need to be very rigorous in keeping oxygen-free conditions. As far as is known in the literature, there are only two methods which describe in detail the preparation of Green Rusts and/or the Al-GRs. One method is by Misawa et al. (1973), the other by Taylor & McKenzie (1980). Other studies have been on the corrosion of iron metal in electrolytic solutions (Dasgupta & MacKay, 1959; Gancedo et al., 1976; McGill et al., 1976). The method described here to synthesise the Green Rusts and the related Al-GRs (section 4.4) was based on that of Taylor & McKenzie (1980). To make the Fe-GRs, Fe(III) hydroxide suspensions were used instead of Al(III) hydroxide suspensions (as in the case of the Al-GRs). The Fe(II) systems studied were $FeSO_4$ and $FeCl_2$.

4.3.1 $FeSO_4$ and $FeCl_2$ systems

Solutions of $FeSO_4$ and $FeCl_2$ were prepared by dissolving the appropriate quantities of $FeSO_4.7H_2O$ and $FeCl_2.4H_2O$,

respectively, in oxygen-free distilled water. The distilled water was deoxygenated beforehand by bubbling through high purity nitrogen ($\geq$ 99.9 N_2) for at least 45 mins. The Fe(II) salt was then added and dissolved under the flow of N_2. The chloride used, $FeCl_2.4H_2O$, was a reagent grade chemical with a purity of at least 96%. Iron analysis using the Ferrozine reagent (Gibbs, 1979) on a spectrophotometer showed that the $FeCl_2$ (4-5 months old at the time of use) consisted of 98% Fe(II) and 2% Fe(III) material. Tests were carried out to see if filtering of the $FeCl_2$ solutions under the experimental conditions would give appreciable differences in the synthesis of the Green Rusts. The results indicated that the filtering made little or no difference to the syntheses. Thus, thereafter filtering of $FeCl_2$ solutions was not performed.

The concentrations of the Fe(II) solutions were generally 0.1 M for both sulphates and chlorides, and the volumes were usually 200 ml. The solutions were made up in a 500 ml three-armed spherical flask of the "Quickfit" type. Nitrogen was passed into the flask through one of the sidearms and bubbled through the solution (see Fig 4.1). The bubbling of the solution not only served to keep the flask oxygen-free but also stirred the solution at a relatively constant rate. The N_2 flow rate was maintained reasonably constant by means of an air-flow

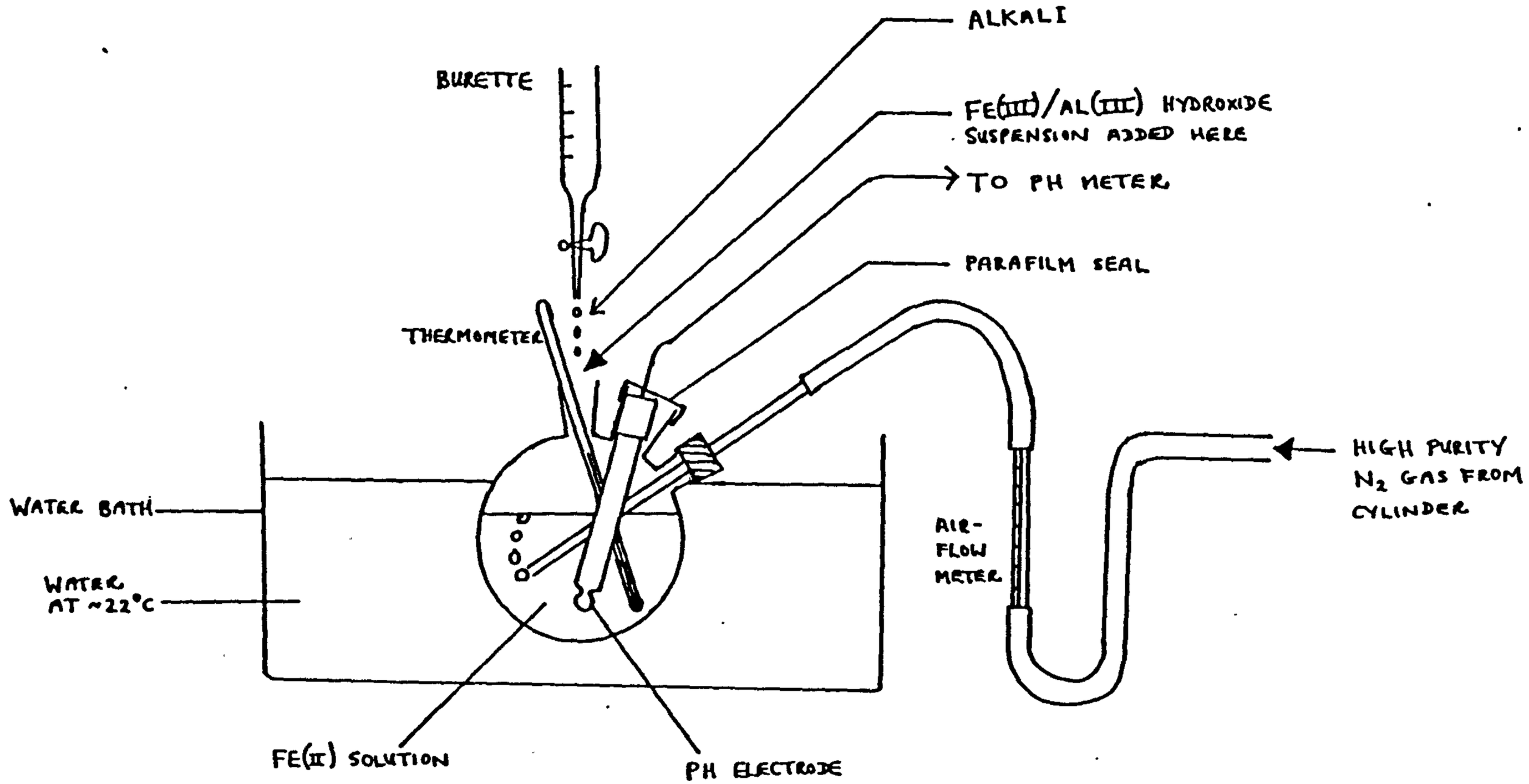

Fig 4.1 Apparatus for the preparation of the Green Rusts and the Al Green Rusts.

meter, and was such that no air could enter into the flask.

A standard combination glass electrode (Kent EIL 1160 series) connected to a PTI-11 portable pH meter was used to measure the pH of the Fe(II) solution. The pH electrode was calibrated with buffer solutions at pH 4 and pH 7, respectively, before the start of each Green Rust synthesis. Fe(III) hydroxide and/or alkali was added through the vertical arm as required. The temperature of the Fe(II) solution was kept constant at 22.0 ± 0.5 °C by a thermostatically-controlled water bath. A glass thermometer was used to record the temperature of the solution.

Fe(III) solutions in the concentration range 0.01-0.4 M were made by dissolving the appropriate amounts of either $FeCl_3.6H_2O$ or $Fe(NO_3)_3.9H_2O$ in oxygen-free distilled water. Most of the Fe(III) solutions were of 50 ml volume. Each solution was stirred magnetically, and kept oxygen-free by a flow of N_2.
A standard Kent EIL 1160 series combination glass electrode, connected to a Kane & May KM 7000 portable pH meter, was used to measure pH. The electrode was calibrated as before. The Fe(III) solution was then taken to approximately pH 7 by adding deoxygenated alkali (0.1 M or M NaOH). The resulting Fe(III) hydroxide suspension was usually dark, reddish-brown in colour.

Separately, the Fe(II) solution in the three-armed flask was taken to about pH 7 by the addition of deoxygenated alkali. The rise in pH (from ~ 3.1 for $FeCl_2$, ~ 3.7 for $FeSO_4$) corresponded to a change in the nature of the solution. It was observed that the latter changed from a light, lime-green ($FeCl_2$) or light, bluish-green ($FeSO_4$) solution to a very fine, dark-green suspension (both $FeCl_2$ and $FeSO_4$), although this depended on the concentration of the alkali. The amount of precipitation was very small (estimated to be 1-2% by weight of the total Fe(II)) and so the concentration of Fe(II) was approximately the initial value. Thus the Fe(II) suspension would still be referred to as an Fe(II) solution. When the pH readings did not vary by more than ± 0.1 units, the Fe(III) hydroxide suspension was added quickly to the Fe(II) solution under the flow of N_2. This gave initially a dark-brown suspension. The pH dropped very sharply and alkali (0.1 M NaOH) was added rapidly to bring the pH up to ~ 7 once more. Thereafter, the pH was maintained around 7 by adding more alkali as required. After a few hours (2-4.5 h), the swirling suspension had assumed a dark-green ($FeCl_2$) or dark, bluish-green ($FeSO_4$) appearance in the majority of cases. By this time, the rate of decrease in pH had slowed down to almost zero. This was taken as an indication that the induced hydrolysis was nearing completion, and no more

alkali was then added. The suspension was then transferred to a separating funnel under the flow of N_2 and left to settle out. A sample of the precipitate was then drawn off under N_2 and centrifuged. The concentrated precipitate was put immediately onto the Mossbauer spectrometer at 77 K without washing or drying. The sample was frozen and kept stable to oxidation by the liquid N_2 used to lower the temperature to 77 K. A 10 ml. sample of the supernatant was acidified with 2 ml of 5 M HCl and retained for determination of the amount of Fe left in solution by AAS. (The samples were stored in a fridge at 2-4 °C until needed.)

Due to the lengthy time involved in the synthesis, the rest of the precipitate in the separating funnel was not utilised immediately, but instead was left overnight sealed under N_2. Subsequently, the aged-overnight material was centrifuged, washed twice with N_2-saturated acetone, and vacuum-dried at RT. The washing was carried out in a two-chamber glove box, flushed out with high purity N_2 initially, and then maintained oxygen-free by a continuous flow of N_2. Prior to the washing, another sample of the wet precipitate was put onto the Mossbauer spectrometer at 77 K. This was for direct comparison with the fresh material put on the Mossbauer spectrometer immediately after synthesis. A 10 ml sample of the supernatant was again

retained for determination of dissolved Fe by AAS. Checks made on the aged-overnight material by Mossbauer spectroscopy showed that there was virtually no difference between washed and unwashed wet precipitate, indicating that the washing procedure did not cause any appreciable alteration in the nature of the precipitate. The washed and dried material was stored in test-tubes, sealed under N_2. These were subsequently used in further MbS work, XRD, IRS and surface area measurements.

4.4 Preparation of Al Green Rusts

As mentioned previously in section 4.3, a method similar to that of Taylor & McKenzie (1980) was used to synthesise the Al-GRs. This was identical to that described in section 4.3 for the preparation of the Fe-GRs, except that Al(III) hydroxide suspension was used instead of Fe(III) hydroxide suspension. Al(III) solutions in the concentration range 0.01-0.1 M were made by dissolving the appropriate amounts of either $AlCl_3$ or $Al_2(SO_4)_3.16H_2O$ in oxygen-free distilled water. The volume of the solutions was normally 200 ml. The Al(III) hydroxide suspensions produced by the addition of deoxygenated alkali were milky-white in colour. Again the Fe(II) systems studied were those of $FeSO_4$ and $FeCl_2$. In adding the Al(III) hydroxide suspension to the Fe(II) solution, the initial drop in pH was also very sharp; although the endpoint of the induced hydrolysis was reached in a shorter time (~ 1-2 h). The colour of the resultant precipitate ranged from greyish-blue to bluish-green. Mossbauer spectra at 77 K were recorded for wet precipitates (unwashed) removed immediately after synthesis (fresh material) and after standing overnight (aged material). Corresponding 10 ml samples of the supernatant were also retained for AAS, stored as before. The remaining precipitate was centrifuged, washed,

vacuum-dried and stored in test-tubes sealed under N_2 as described for the Fe-GRs in section 4.3.

4.5 Practical procedures

4.5.1 Mossbauer spectroscopy

Mossbauer spectra at RT and 77 K were recorded on a standard constant-acceleration spectrometer (Clarke et al., 1967) at Plymouth Polytechnic. Transmission geometry was used and the γ-ray source was ^{57}Co set in a rhodium matrix (supplied by Amersham International). The source strength was initially 25 mCi in 1980 and decreasing to ~ 3 mCi by 1984. The spectra were accumulated overnight in the majority of cases (total time: 15-24 h).

Mossbauer work at 4.2 K on the Green Rusts and the related Al Green Rusts was carried out at AERE Harwell on a constant-acceleration system. Transmission geometry was again used and the gamma source was also ^{57}Co set in rhodium (50 mCi). Most of the samples were made at Plymouth Poltechnic and then taken to Harwell. To prevent oxidation occurring, the synthesised materials were placed immediately in liquid N_2 for storage. The liquid N_2 was contained in a 5 l dewar which was then transported to Harwell. A few samples of Green Rusts were made on site at Harwell.

Samples were placed in a perspex holder, sandwiched

usually between two polythene disks. This was then sealed by cellotape around the outside of the holder. Dried samples were usually 10-25 mg in weight and wet samples were ~ 10-50 mg. In the latter case, some of the samples were fairly thick and only one polythene disk or none at all was used (the cellotape keeping the sample in place).

An Fe foil at RT was used as the reference point for zero velocity for the isomer shift. Spectra were plotted and analysed by a graphics program (which includes interactive curvefitting) on a Prime mainframe computer. The long term stability of the Mossbauer spectrometer at Plymouth Polytechnic over five years operation has been within ± 0.7% (Cuttler, private comm.). The short term stability has been even better (≤ 0.1%).

4.5.2 X-ray diffraction

X-ray diffraction analyses were carried out using an AEI Raymax RX/3D diffractometer. The X-rays were generated by a Cu target using an accelerating voltage of 35-40 kV and a filament current of 10 mA. A nickel filter was used to reduce unwanted K_β radiation. Dry powdered samples were fixed onto microscope cover-slips with the help of a thin layer of silicon grease. The samples were then pressed as flat as possible to minimise orientation effects. The

cover-slips were next mounted on a sample holder and placed vertically in the diffractometer table. Scanning was started at an angle of 5°, then proceeded in steps of 0.1° and stopped at the desired angle. The X-rays were counted for 10 s at each 0.1° step by a scaler-ratemeter. The total counts at the end of the 10 s period was then outputted immediately onto paper tape before proceeding to the next 0.1° step. The data from the total scan was then transferred onto an Apple microcomputer, where it was plotted as an XRD spectrum (i.e. intensity v. angle 2θ). Comparisons with reference data for identification purposes were done using the ASTM powder diffraction file or from other workers.

4.5.3 Infrared spectroscopy

Infrared spectra were obtained on a Perkin-Elmer 1330 grating infrared spectrometer (range 4000 to 200 cm^{-1}). Samples were prepared by dispersing approximately 1 mg of material in about 200 mg of oven-dried KBr. This was thoroughly mixed and ground to a fine powder, and finally pressed to ~ 10 tons per square inch in an evacuated die. This gave a hard, transparent to translucent, coloured disc of about 12.5 mm diameter and thickness 0.5-1.0 mm. The disc was then mounted on a sample holder and placed in the beam of the IR spectrometer.

4.5.4 Surface area measurements

The surface areas of samples were measured by the BET N_2 adsorption method on a vacuum microbalance, designed and constructed for the determination of surface areas within the range 0.2-1000 $m^2.g^{-1}$. (Glasson, 1956). The system used was a C.I. Electronics Microforce Mark 2B balance. The samples were outgassed in vacuo at RT beforehand; their dry weights were in the range 100-250 mg. They were then put in an aluminium bucket which was suspended by a fine glass fibre from one arm of the microbalance. This was enclosed in the vacuum system and immersed in liquid N_2. Nitrogen adsorption at 77 K was recorded from an analogue control unit. The sensitivity ranges used were 0-2.5, 0-10 and 0-100 mg for measurement of nitrogen uptake.

4.5.5 Chemical analyses

Atomic absorption spectroscopy was used to determine the dissolved Fe content in the supernatants left at the end of the synthesis of the Green Rusts and the Al Green Rusts. This was carried out on an Instrumentation Laboratory 151 atomic absorption spectrometer.

A few samples of Green Rusts prepared from $FeSO_4$ solutions were analysed by standard thermogravimetric and titrimetric methods. Total Fe content was determined by calcining portions at 1000 °C for 1-2 h to give a residue of α-Fe_2O_3. The percentage Fe(II) by weight was determined by dissolving a portion of the sample in 6 M HCl and titrating the solution with 0.005 M $Ce(SO_4)_2$. The ferroin indicator used was sufficiently sensitive at this low concentration, but required a blank determination correction of about 0.2-0.3 ml.

The % sulphate by weight was determined by dissolving a portion of the sample in 6 M HCl and adding barium chloride to precipitate the sulphate as $BaSO_4$ for gravimetric determination.

The chemical analysis of the Green Rust samples was useful but it gave only a rough estimate of the composition, particularly the Fe(II):Fe(III) ratio. This was because of the great instability of the GRs to oxidation (lifetime in air of ~ 5-30 mins) which is evident by the rapid colour change (generally, green -> orange-brown). The vacuum-dried material was partially oxidised by the time the drying process was completed (as indicated by its colour and by Mbs). Therefore any further usage of the material would only result in

greater oxidation. For this reason, it was felt that chemical analysis would be limited in its usefulness in the study of the GRs and so was not continued.

CHAPTER 5: RESULTS AND DISCUSSION

5.1 Characterisation of synthetic Fe(III) oxides

The Mossbauer parameters for the synthesised Fe(III) oxides (including magnetite) are given in Table 5.1. These compare well with the values given in Table 3.1 at the end of Chapter 3. In the case of ferrihydrite, two Fe(III) doublets were required to fit the spectrum at 77 K for both samples shown. This is in agreement with Murad & Schwertmann (1980), although they also fitted two Fe(III) doublets at RT. Note also that two Fe(III) doublets were fitted to the spectrum of lepidocrocite at 77K.

Since the Fe(III) oxides produced here are well-documented, Mossbauer parameters are usually sufficient to establish their identity, especially if the samples are fairly crystalline and produced from standard procedures. Also colour and magnetic properties will give supporting evidence. Nevertheless, some XRD spectra were taken of the synthesised oxides for confirmation. The principal d-spacings for some of the synthesised Fe(III) oxides are given in Table 5.2 (cf. Table 2.2 in section 2.2.1).

OXIDE	Temp (K)	IS v Fe (mms^{-1})	QS (mms^{-1})	1/2Γ (mms^{-1})	B (T)
Haematite	RT	0.35	-0.24		51.7
	77	0.44	+0.43		54.0
Maghemite	RT	0.28	+0.01		50.0
Goethite					
(sample 1)	RT	0.36	-0.29		37.8
(sample 2)	RT	0.37	-0.26		36.1
	77	0.43	-0.27		49.2
(sample 3)	RT	0.35	-0.28		36.6
	77	0.45	-0.26		49.0
Akaganeite	77	0.42	-0.06		47.6
Lepidocrocite	RT	0.52	0.59	0.31	0
	77	0.75	0.42	0.35	0
		0.73	1.00	0.35	0
∫-FeOOH	RT	0.34	0.58		0
	77	0.43	-0.14		48.3
Ferrihydrite					
(sample 1)	RT	0.36	0.68	0.29	
	77	0.51	0.63	0.28	
		0.47	1.13	0.30	
(sample 2)	RT	0.35	0.73	0.28	
	77	0.51	0.69	0.25	
		0.52	1.28	0.24	
Magnetite	RT	0.28	-0.11		47.5
	77	0.39	-0.07		50.8

RT = room temperature
(Goethite : sample 1 - aged 10 months
sample 2 - aged 10 days
sample 3 - aged 20 days)

Table 5.1 Mossbauer parameters for Fe(III) oxides.

OXIDE	Principal d-spacings (A)							
Maghemite	3.72	3.40	2.94	2.52	2.08	1.70	1.60	1.47
Goethite (sample 1)	4.19	2.71	2.59	2.46	2.25	2.19	1.72	1.57
Lepidocrocite	6.24	3.30	2.49	1.95	1.73	1.53		
δ-FeOOH	2.54	2.23	1.69B	1.48				

B = broad
(Goethite : sample 1 - aged 10 months)

Table 5.2 XRD data for selected Fe(III) oxides.

Infrared spectra for the types of Fe(III) oxides produced are shown in Fig 5.1, and Table 5.3 gives the absorption peaks and regions corresponding to these spectra. The IR spectrum of a sample of lepidocrocite (P23) supplied by Prof. Schwertmann of the Institute of Soil Science, Freising, W. Germany is also included here because it is a well-crystalline material, and the need is for a good set of reference data.

The IR spectra of the Fe(III) oxides show that there are usually three regions of absorption:

(i) a broad region in the range 3600-2400 cm^{-1}

(ii) a barely perceptible region in the range 1700-1250 cm^{-1}

(iii) a region with many absorption peaks from 1200 cm^{-1} onwards.

Strong absorption occurs in regions (i) and (iii) and this is usually much more intense than the absorption in region (ii). The absorption in region (i) is due to the OH stretching vibrational mode of structural OH groups (Fe-OH groups) and/or molecular water (water of hydration and/or adsorbed water). The absorption in region (ii) (particularly the peak at 1600-1625 cm^{-1}) is due to OH bending (also called deformation) arising from molecular water. Since the intensity of absorption here

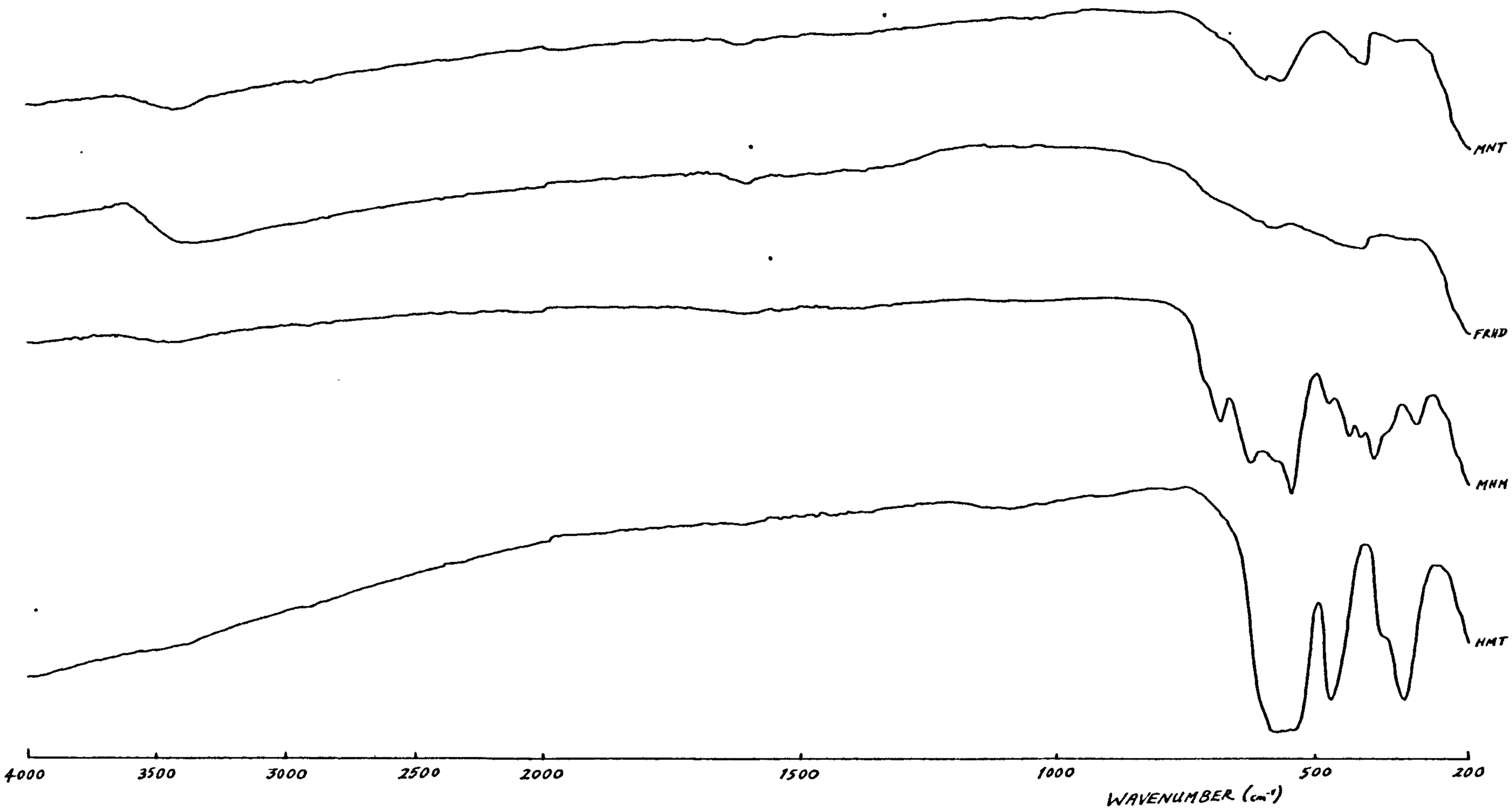

Fig 5.1 IR spectra of Fe(III) oxides.

(HMT = haematite; MHM = maghemite; FRHD = ferrihydrite; MNT = magnetite)

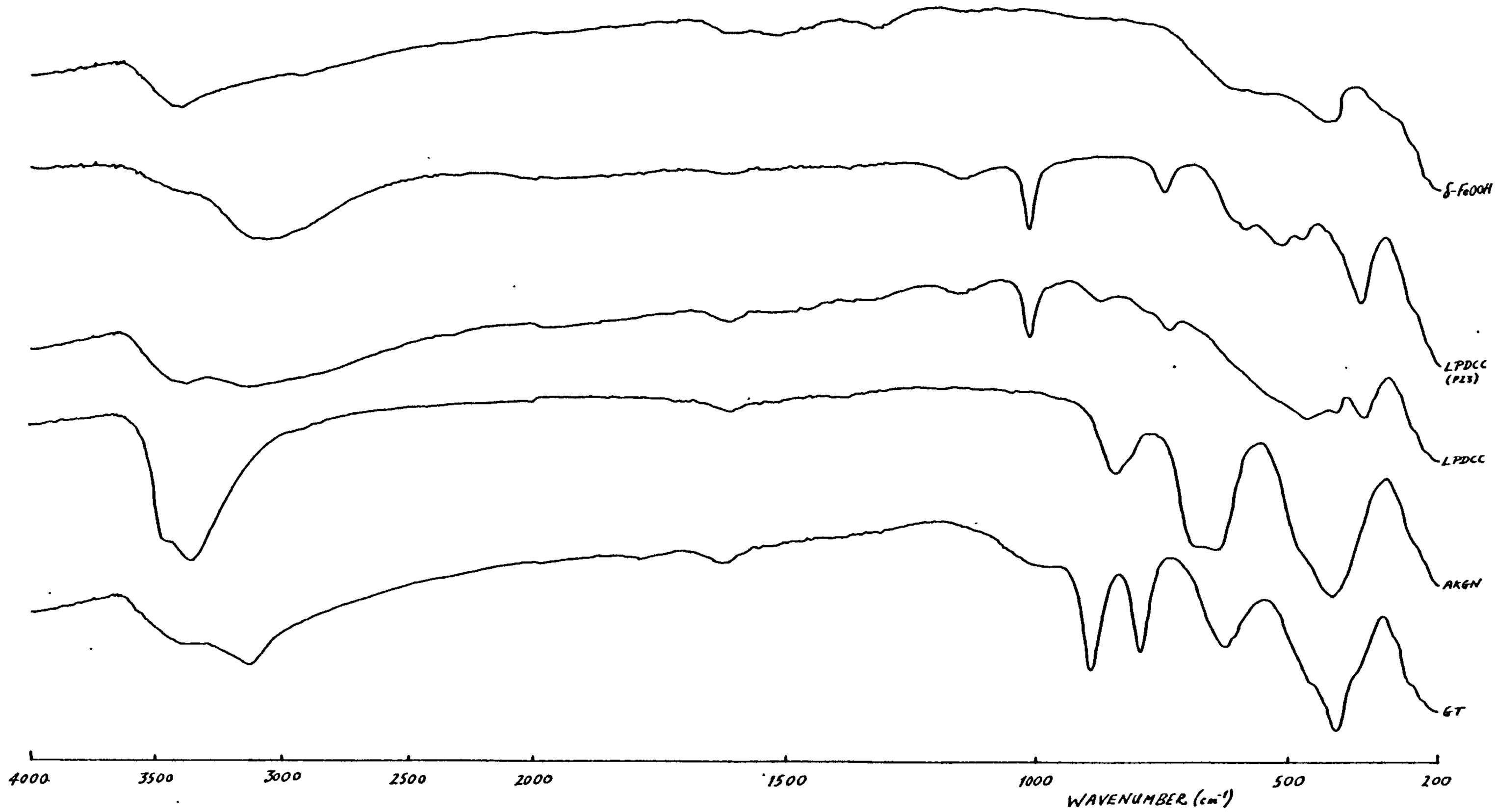

Fig 5.1 (cont'd) IR spectra of Fe(III) oxides.

(GT = goethite; AKGN = akaganeite; LPDCC = lepidocrocite)

Haematite	Maghemite	Ferrihydrite (sample 1)	Magnetite
	Peaks (cm^{-1})		
	3420 ± 40	3365 ± 40	3440 ± 40
		1600 ± 10	1615 ± 10
	720 ± 15		
	687 ± 5		695 ± 20
	627 ± 10		610 ± 10
591 ± 25	577 ± 10	565 ± 20	568 ± 10
550 ± 20	547 ± 5		
475 ± 5	473 ± 5		
	436 ± 5		
	414 ± 5	405 ± 15	406 ± 10
375 ± 10	387 ± 5		
334 ± 5	358 ± 10		340 ± 15
	303 ± 10		
	Regions (cm^{-1})		
4000-2000	3620-3220	3600-2100	3620-2800
		1660-1230	1660-1590
750- 270	780- 270	750- 390	770- 310

Table 5.3 IR absorption peaks and regions of Fe(III) oxides.

Goethite	Akaganeite	Lepidocrocite	Lepidocrocite (P23)	δ-FeOOH
	Peaks (cm^{-1})			
	3450 ± 30	3420 ± 40		3420 ± 30
3350 ± 40	3349 ± 20		3390 ± 60	
3130 ± 20		3130 ± 60	3060 ± 50	
1625 ± 10	1611 ± 15	1620 ± 10		1625 ± 10
				1520 ± 20
		1330 ± 20		1330 ± 15
		1159 ± 15	1147 ± 10	
990 ± 15		1024 ± 5	1017 ± 5	
890 ± 5		885 ± 10		
795 ± 5	842 ± 10			
		750 ± 5	749 ± 5	
	684 ± 15			
630 ± 10	641 ± 15		590 ± 15	590 ± 20
			517 ± 10	
460 ± 20	477 ± 20	473 ± 10	474 ± 10	
405 ± 5	412 ± 15	417 ± 10		425 ± 15
360 ± 15		358 ± 5	358 ± 5	
	Regions (cm^{-1})			
3640-2080	3600-2400	3640-2200	3610-2380	3640-2100
1700-1500	1670-1500	1680-1270		1690-1240
1180- 310	1000- 300	1220- 310	1220- 300	750- 380

Table 5.3 (cont'd) IR absorption peaks and regions of Fe(III) oxides.

is low or non-existent, it would appear that there is hardly any molecular water in the oxides samples, and so the absorption in region (i) must therefore be almost entirely due to the structural OH groups.

The absorption in region (iii) is the most interesting from the viewpoint of the Fe(III) oxides. Here the absorption peaks are caused by the stretching and bending vibrations of Fe-O bonds, and by the bending vibrations of Fe-O-H groups. This gives a characteristic pattern for each type of Fe(III) oxide, and is sufficiently different from one oxide to another to enable a fairly pure and crystalline material to be identified from a set of standards. The exception to this rule is ferrihydrite which by nature is poorly crystalline and so has little or no features in region (iii).

It is to be noted that the IR spectra of the sample of maghemite shown in Fig 5.1 has many closely-spaced peaks in region (iii). These arise from overtones of the main absorption peaks, and probably result because the sample was from recording tape material which has been produced under a rigorous process. If these overtone peaks were absent, then the IR spectra would resemble that of the magnetite produced here. Grimes & Collett (1971) have obtained IR spectra of synthetic maghemite samples which are similar to that of synthetic magnetite. The close resemblance of the IR spectra of maghemite and magnetite

is not surprising since they grade into each other to form a solid solution series of the form Fe_3O_4-γ-Fe_2O_3 (Basta, 1959).

Summarising the IR data, it can be seen from Fig 5.1 that the Fe(III) oxides produced here, with the exception of ferrihydrite and δ-FeOOH, are fairly well-crystalline to crystalline, and so can be used as standards for reference.

5.2 Characterisation of the Green Rusts

The results and analysis for the Green Rusts (i.e. Fe-GRs) are given in terms of each type of Green Rust. This will make the characteristisation more integrated right from the start. The main bulk of data is on the sulphate Green Rusts (abbrev. sulphate GRs or SO_4 GRs) as this was the most intensely studied GR. The main emphasis in terms of analytical techniques is on Mossbauer spectroscopy. X-ray diffraction was used for identification purposes only, and infrared spectroscopy was used as a complementary technique in this respect for confirmation, and where the X-ray data was rendered inappropriate through oxidation. But IRS can also give information on the type of anions present in the samples. Surface area measurements by vacuum microbalance techniques will shed light on the nature of the surface and the porosity of the material. Analysis of the titration and AAS data in the synthesis of the GRs may give an idea of the mechanisms of formation.

5.2.1 The Sulphate Green Rusts

The sulphate GRs were produced from starting or initial Fe(II)/Fe(III) ratios (hereafter denoted as IFFR, standing for initial Fe(II)-Fe(III) ratio; the subscript, I, will denote initial values) ranging from 1 to 40. The majority of the sulphate GRs in these results were synthesised from 0.1 M $FeSO_4$ solutions. In this group, the formation of sulphate GRs seems to be independent of IFFR for the range $1 \leq IFFR \leq 40$. However, sulphate GR formation appears to depend on the initial concentration of $FeSO_4$. For a fixed amount of initial Fe(III) material (5 mmoles), the formation of sulphate GR did not occur for $[Fe(II)]_I < 0.025$ M and IFFR < 1 (see Appendix A and section 5.2.1b). However, for IFFR = 1 and 20 mmoles of initial Fe(III) material, sulphate GR was produced at $[Fe(II)]_I =$ 0.1 M.

When freshly produced, the sulphate GRs had a dark-green (with a slight bluish tinge) colour. On vacuum-drying, the material changed to a dark-green to green colour, depending on the degree of oxidation which always occurred in spite of the precautions taken to prevent this from happening. In air, the sulphate GR samples oxidised rapidly to an orangey-brown colour in ~ 5-30 mins. Hence the need for rapid analysis.

The materials synthesised from the $FeSO_4$ system are summarised in Tables 5.4 and 5.5.

Sample	IFFR	<Fe(III)> (mmole)	pH maintained
GR20	1	20	7.1 ± 0.2
GR5	4	5	7.1 ± 0.2
GR1	5	5	7.0 ± 0.3
GR2	5	5	7.1 ± 0.2
GR13	10	2	7.1 ± 0.2
GR14	20	1	7.1 ± 0.2
GR15	20	1	7.1 ± 0.2
GR16	40	0.5	7.1 ± 0.2
GR21	40	0.5	7.1 ± 0.2

IFFR = initial Fe(II)-Fe(III) ratio
< > = amount of

Table 5.4 Sample identities for sulphate GRs derived from 0.1 M $FeSO_4$.

Sample	IFFR	$[Fe(II)]_i$ (M)	<Fe(III)> (mmole)	pH maintained
S21-3-83	0.4	0.01	5	7.0 ± 0.1
S23-3-83	1	0.025	5	7.0 ± 0.1
GR3	2	0.05	5	7.0 ± 0.2
GR4	2	0.05	5	7.0 ± 0.1
S7-2-83	5	0.1	5	(6.9->6.2)

Table 5.5 Sample identities for sulphate GRs and non-GRs derived from ≤ 0.1 M $FeSO_4$.

5.2.1a Titration and AAS data

The consumption of alkali after the addition of the Fe(III) hydroxide suspension (hereafter referred to as Fe(III) gel for brevity) to the $FeSO_4$ solution at pH 7 was very rapid initially but gradually slowed down until equilibrium was reached after a few hours (typical curves are shown in Fig 5.2). The estimated equilibrium times ranged from 2 to 6 hours depending on the IFFR. The quantity of alkali used was greater for smaller IFFRs i.e. for larger amounts of Fe(III) material at constant $[FeSO_4]_I$. Some of the synthesis experiments were stopped before equilibrium was reached but the samples produced still gave the characteristic XRD pattern of sulphate GRs.

The data showing the alkali consumption (extrapolated to equilibrium where necessary) after the addition of Fe(III) gel to the $FeSO_4$ solution is given in Table 5.6 for the 0.1 M $FeSO_4$ system.

A ln-ln plot of total amount of NaOH used (or $\langle NaOH \rangle_t$, where < > denotes quantity in terms of mass units) against IFFR (Fig 5.3) gives a straight line relationship between the two parameters. A linear least-squares fit of the points gives a gradient of -1.02 and an intercept of 24.8 mmoles (at ln (IFFR) = 0). Thus the equation of the best line is:

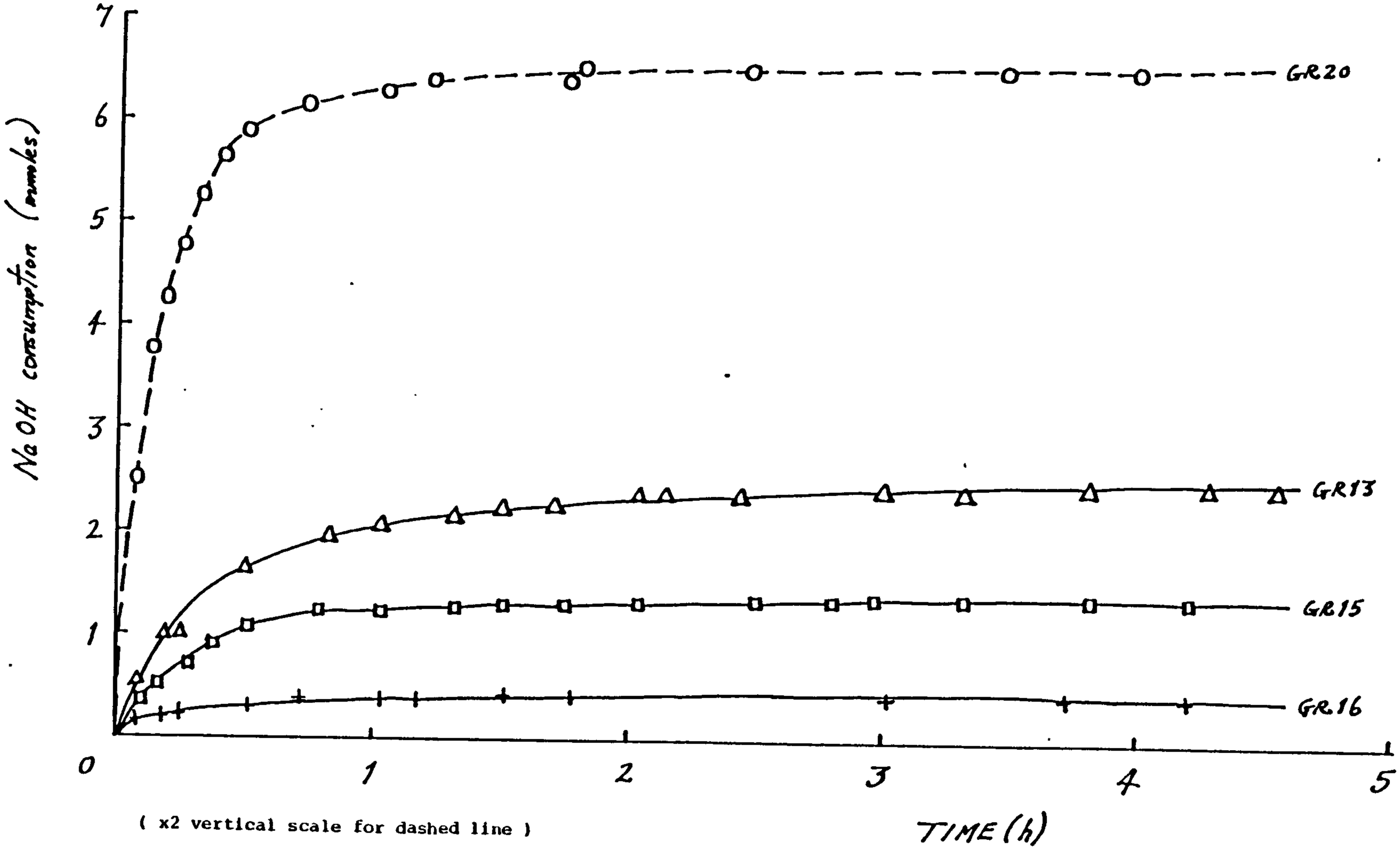

Fig 5.2 NaOH consumption v. time for typical sulphate GR samples derived from 0.1 M $FeSO_4$.

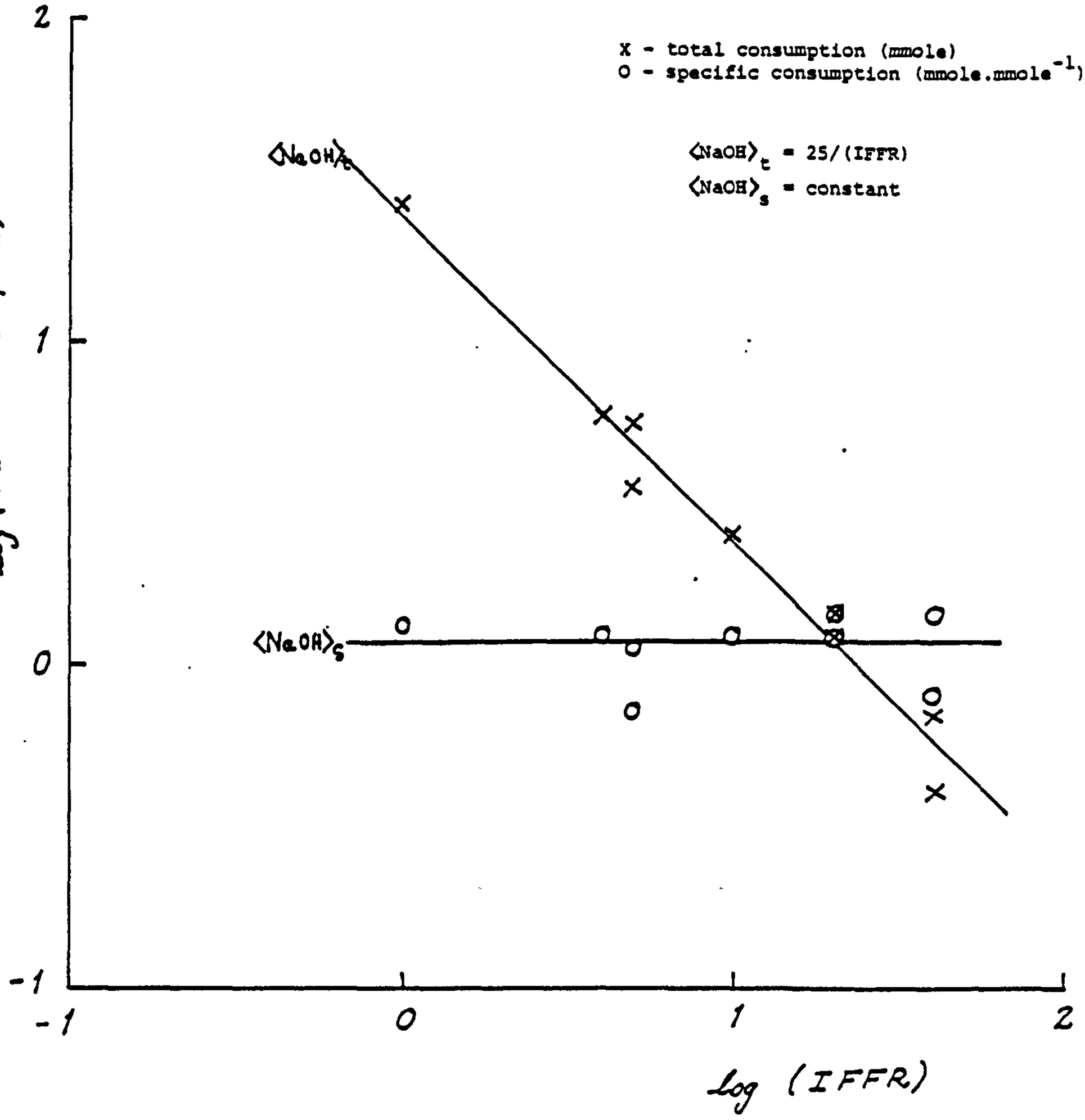

Fig 5.3 NaOH consumption v. IFFR for sulphate GRs derived from 0.1 M $FeSO_4$.

Sample ID	IFFR	⟨Fe(III)⟩ (mmole)	$\langle NaOH \rangle_t$ (mmole)	$\langle NaOH \rangle_s$ (mmole.mmole^{-1})	Estimated eqm. time (h)
GR20	1	20	26.00 ± 0.05	1.3	2.5 - 3
GR5	4	5	5.8 ± 0.2	1.2	3
GR1	5	5	5.5 ± 0.3	1.1	5.5 - 6
GR2	5	5	3.5 ± 0.2	0.7	4.5 - 5
GR13	10	2	2.50 ± 0.05	1.2	4 - 4.5
GR14	20	1	1.20 ± 0.05	1.2	3.5
GR15	20	1	1.40 ± 0.05	1.4	3.5
GR16	40	0.5	0.40 ± 0.05	0.8	3
GR21	40	0.5	0.70 ± 0.05	1.4	3

IFFR = Initial Fe(II)-Fe(III) ratio
⟨ ⟩ = amount of (t = total; s = specific)

Table 5.6 Alkali consumption for sulphate GRs derived from 0.1 M $FeSO_4$.

Sample ID	IFFR	⟨Fe(III)⟩ (mmole)	$\langle Fe(II) \rangle_t$ (mmole)	$\langle Fe(II) \rangle_s$ (mmole.mmole^{-1})
GR20	1	20	19.5	0.98
GR1	5	5	15.8	3.17
GR2	5	5	15.2	3.04
GR13	10	2	10.2	5.11
GR14	20	1	9.9	9.86
GR15	20	1	10.5	10.50
GR16	40	0.5	9.7	19.44
GR21	40	0.5	9.2	18.44

Table 5.7 Fe(II) uptake for sulphate GRs derived from 0.1 M $FeSO_4$.

$$\ln \langle NaOH \rangle_t = -1.02 \ln (IFFR) + 3.21 \qquad -5.1a$$

$$\rightarrow \quad \langle NaOH \rangle_t = 24.8\ (IFFR)^{-1.02} \qquad -5.1b$$

$$\text{or} \quad \langle NaOH \rangle_t \sim 25/IFFR \qquad -5.1c$$

Thus high alkali consumption occurs at low IFFRs and vice versa. This is because low IFFRs imply a large amount of reacting Fe(III) material ($[FeSO_4]_I$ being constant). In fact, a ln-ln plot of $\langle NaOH \rangle_t$ v. $\langle Fe(III) \rangle$, the amount of Fe(III) material added, gives a linear relationship between the two parameters (Fig 5.4). A least-square fit of the points gives the equation of best fit as:

$$\ln \langle NaOH \rangle_t = 0.99 \ln \langle Fe(III) \rangle + 0.12 \qquad -5.2a$$

$$\rightarrow \quad \langle NaOH \rangle_t = 1.13\ \langle Fe(III) \rangle^{0.99} \qquad -5.2b$$

$$\text{or} \quad \langle NaOH \rangle_t \sim 1.1\ \langle Fe(III) \rangle \qquad -5.2c$$

This shows that the alkali consumption increases almost linearly with $\langle Fe(III) \rangle$. The specific alkali consumption [mmole NaOH used per mmole Fe(III) added], $\langle NaOH \rangle_s$, appears to be independent of both the IFFR and $\langle Fe(III) \rangle$ (Figs 5.3-5.4). If alkali consumption is directly concerned with sulphate GR formation, then this fact supports the assertion that sulphate GR formation is independent of both IFFR and $\langle Fe(III) \rangle$ for the 0.1 M $FeSO_4$ system. However, the rate of sulphate GR formation is probably influenced by IFFR and/or

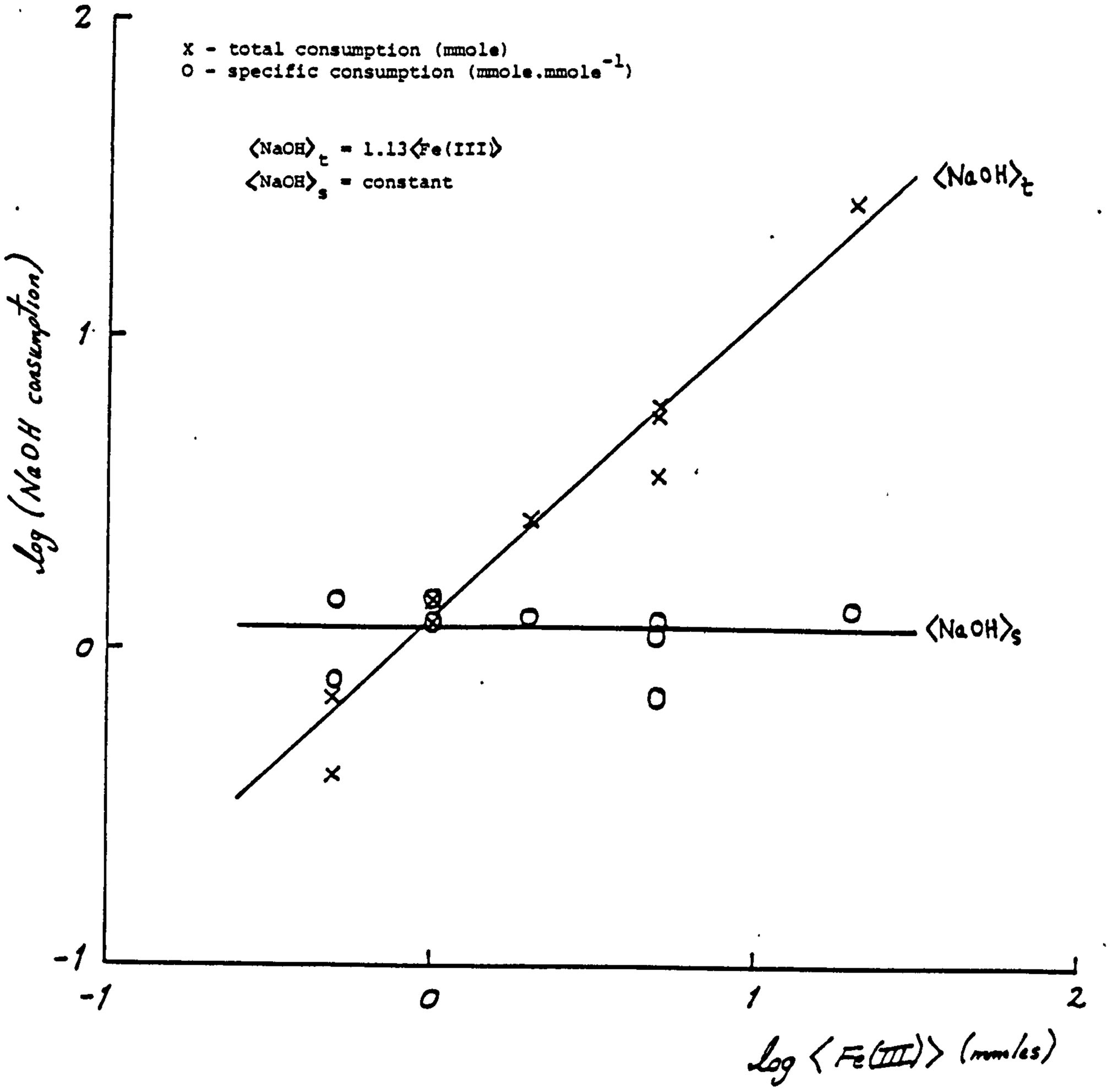

Fig 5.4 NaOH consumption v. <Fe(III)> for sulphate GRs derived from 0.1 M $FeSO_4$.

<Fe(III)>, as indicated by the plots in Fig 5.2.

Atomic absorption spectroscopy of the 10 ml samples of supernatant obtained at the end of each synthesis experiment (see section 4.3.1) gives the amount of dissolved Fe left in solution. By implication and assuming all the Fe in solution to be in the II state, this would give the uptake of Fe(II) by the Fe(III) gel during the course of the sulphate GR synthesis. The data for the uptake of Fe(II) by the Fe(III) gel during the synthesis of the sulphate GR is given in Table 5.7 for $[FeSO_4]_I$ = 0.1 M.

A ln-ln plot of total Fe(II) uptake (or $\langle Fe(II)\rangle_t$) v. IFFR (Fig 5.5) shows that, at 22.0 °C (the temperature at which the synthesis was conducted), the amount of Fe(II) material taken up by the Fe(III) gel seems to decrease with IFFR. This is because high values of IFFR imply small amounts of Fe(III) material used ($[FeSO_4]_I$ = a constant), and so the total Fe(II) uptake is less. A linear least-squares fit of the data gives the following equation:

$$\ln \langle Fe(II)\rangle_t = -0.21 \ln (IFFR) + 2.99 \qquad -5.3a$$

$$\rightarrow \quad \langle Fe(II)\rangle_t = 19.97\ (IFFR)^{-0.21} \qquad -5.3b$$

The relationship between $\langle Fe(II)\rangle_t$ and <Fe(III)> is shown in Fig 5.7, where ln $\langle Fe(II)\rangle_t$ is plotted

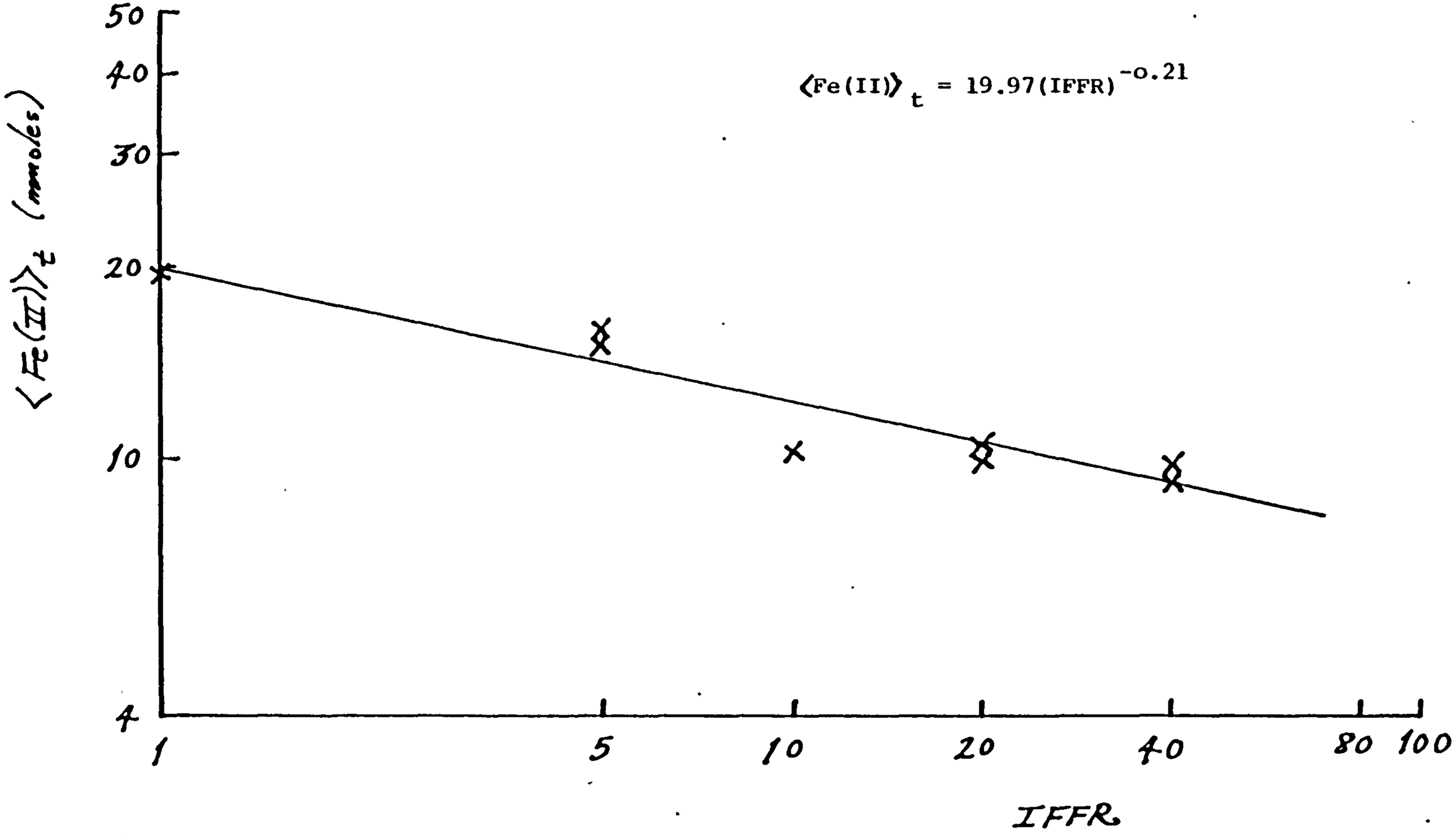

Fig 5.5 $\langle Fe(II) \rangle_t$ v. IFFR for sulphate GRs derived from 0.1 M $FeSO_4$.

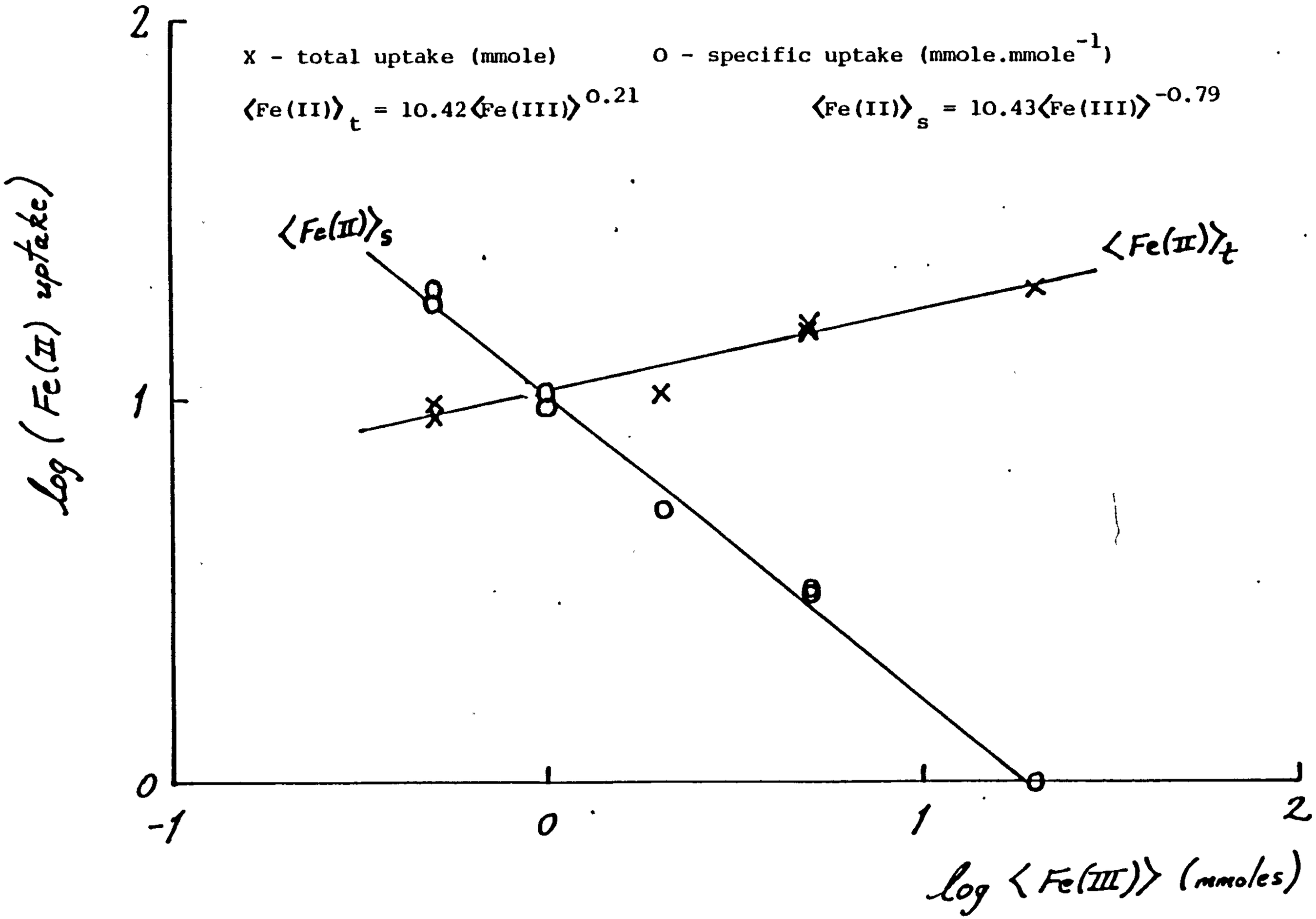

Fig 5.7 Fe(II) uptake v. <Fe(III)> for sulphate GRs derived from 0.1 M $FeSO_4$.

against ln <Fe(III)> and demonstrates clearly that $\langle Fe(II)\rangle_t$ increases with <Fe(III)>. The equation of the best line for the points is:

$$\langle Fe(II)\rangle_t = 10.42\ \langle Fe(III)\rangle^{0.21} \qquad -5.4$$

and this is virtually the inverse of equation 5.3b, which is as expected.

When the specific Fe(II) uptake or $\langle Fe(II)\rangle_s$ (mmole Fe(II) taken up per mmole Fe(III) added) is plotted against IFFR (Fig 5.6), a linear relationship is obtained showing that the specific Fe(II) uptake increases with IFFR. This is because, at high values of IFFR, unit mass of Fe(III) gel have more Fe(II) cations to uptake than at low IFFR. A least-squares fit of the points gives the gradient of the line as 0.46 $mmole.mmole^{-1}$ and the intercept as 0.75 $mmole.mmole^{-1}$

i.e. $$\langle Fe(II)\rangle_s = 0.46\ (IFFR) + 0.75 \qquad -5.5$$

A ln-ln plot of $\langle Fe(II)\rangle_s$ v. <Fe(III)> also results in a straight line with the equation of best fit as:

$$\langle Fe(II)\rangle_s = 10.43\ \langle Fe(III)\rangle^{-0.79} \qquad -5.6$$

Up to this point, no mention has been made of the process of Fe(II) uptake. The uptake is presumbly due to an

adsorption process since Fe(III) gel is known to have a large surface area and hence an active surface (see Appendix A). A Freundlich isothermal plot of the AAS data seems to confirm this view (Fig 5.8). This plot is based on the Freundlich equation for the adsorption of gases by solids but which can be applied equally to the adsorption of solute from solution by a solid:

$$x/m = k\, C^{1/n} \qquad -5.7a$$

$$\rightarrow \ln (x/m) = (1/n) \ln C + \ln k \qquad -5.7b$$

where x = amount of solute adsorbed by solid

m = mass of solid

C = equilibrium concentration of solution

k, n = constants

The Freundlich equation is entirely empirical in nature and, if it applies, a plot of ln (x/m) v. ln C would give a straight line. The data for the Freundlich isothermal plot in Fig 5.8 is given in Table 5.8.

Fig 5.8 shows that apart from one point (2, 0.98) the plot is a straight line. If this point is ignored then a least-squares fit of the points gives the slope as 4.70 and the intercept as 7.15 i.e. $1/n = 4.70$ and $\ln k = 7.15$ or $k = 1.414 \times 10^{7}$. Thus the Freundlich equation for the Fe(II) adsorption in the range 3.5×10^{-3} M < $[FeSO_4]_{eqm}$ < 5.5×10^{-3} M is:

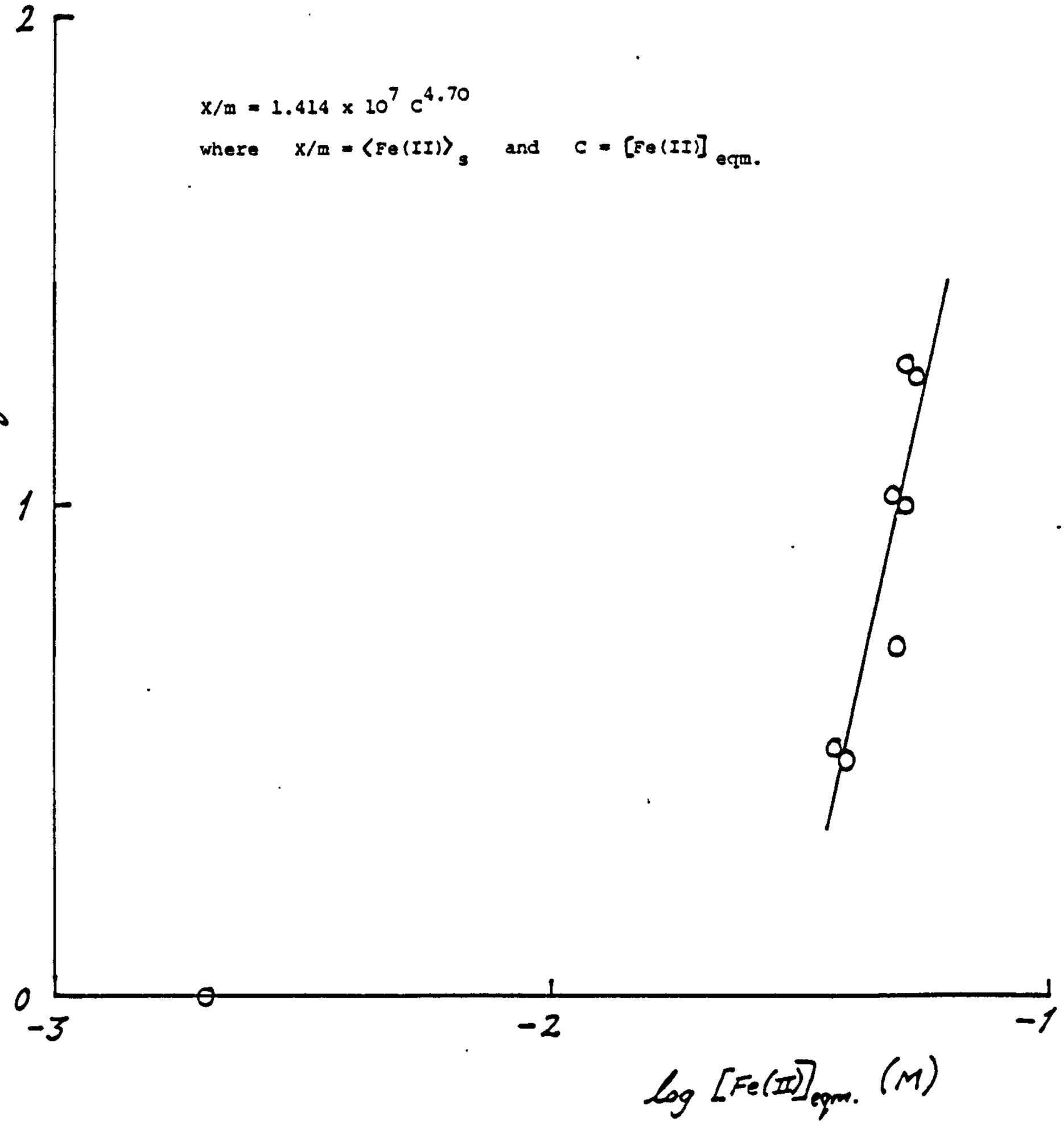

Fig 5.8 Freundlich isotherm for sulphate GRs derived from 0.1 M $FeSO_4$.

Sample	$[FeSO_4]_{eqm}$ (M, $\times 10^{-3}$)	$\langle Fe(II) \rangle_e$ ($g.g^{-1}$)
GR20	2	0.98
GR1	37	3.17
GR2	39	3.04
GR13	49	5.11
GR14	51	9.86
GR15	48	10.50
GR16	51	19.44
GR21	54	18.44

Table 5.8 AAS data for Freundlich isotherm for sulphate GRs derived from 0.1 M $FeSO_4$.

$$x/m = 1.414 \times 10^{7}\, C^{4.70} \qquad -5.8$$

Another isotherm which can be applied to adsorption from solution is the Langmuir isotherm. This is based on the assumption that adsorption is confined to one layer of molecules i.e. a monolayer. The Langmuir equation is given by:

$$C/(x/m) = C/(x/m)_{max} + (1/a)(x/m)_{max} \qquad -5.9$$

where x, m & C are the same as before

a = constant related to bonding energy

$(x/m)_{max}$ = monolayer capacity

If the Langmuir isotherm applies, then a plot of C/(x/m) v. C would give a straight line. However, this has been done for the AAS data at hand and no trends seem to come from it (not shown here).

5.2.1b X-ray diffraction

X-ray diffractograms of all the material produced from the sulphate GR synthesis experiments were taken using the vacuum-dried samples which were stored under N_2. As noted in the introduction to section 5.2.1, the sulphate GRs were usually partially oxidised by vacuum-drying, and became more oxidised by the end of the XRD scan which took 1.5-2.5 h (in the case of the chloride GRs, oxidation was almost complete in every instance). The oxidation was evident by the change in colour from dark-green/green to lime-green/orangey-green/orange over the period of scan. Despite this problem, the sulphate GRs were stable long enough for very good diffractograms to be obtained for the majority of the samples. Typical XRD patterns for sulphate GRs synthesised from 0.1 M $FeSO_4$ are shown in Fig 5.9. The X-ray lines are very well-resolved and intense in most of the diffractograms, and indicates well-crystalline material.

The X-ray d-spacings of the sulphate GRs synthesised from 0.1 M $FeSO_4$ are given in Table 5.9. The data shows that the d-spacings are consistent with those given by Bernal et al. (1959) for the sulphate GRII which they studied, along with lines consistent with that of the strongest low-angle reflections of goethite (see Table 5.10). The goethite lines are indicated by square

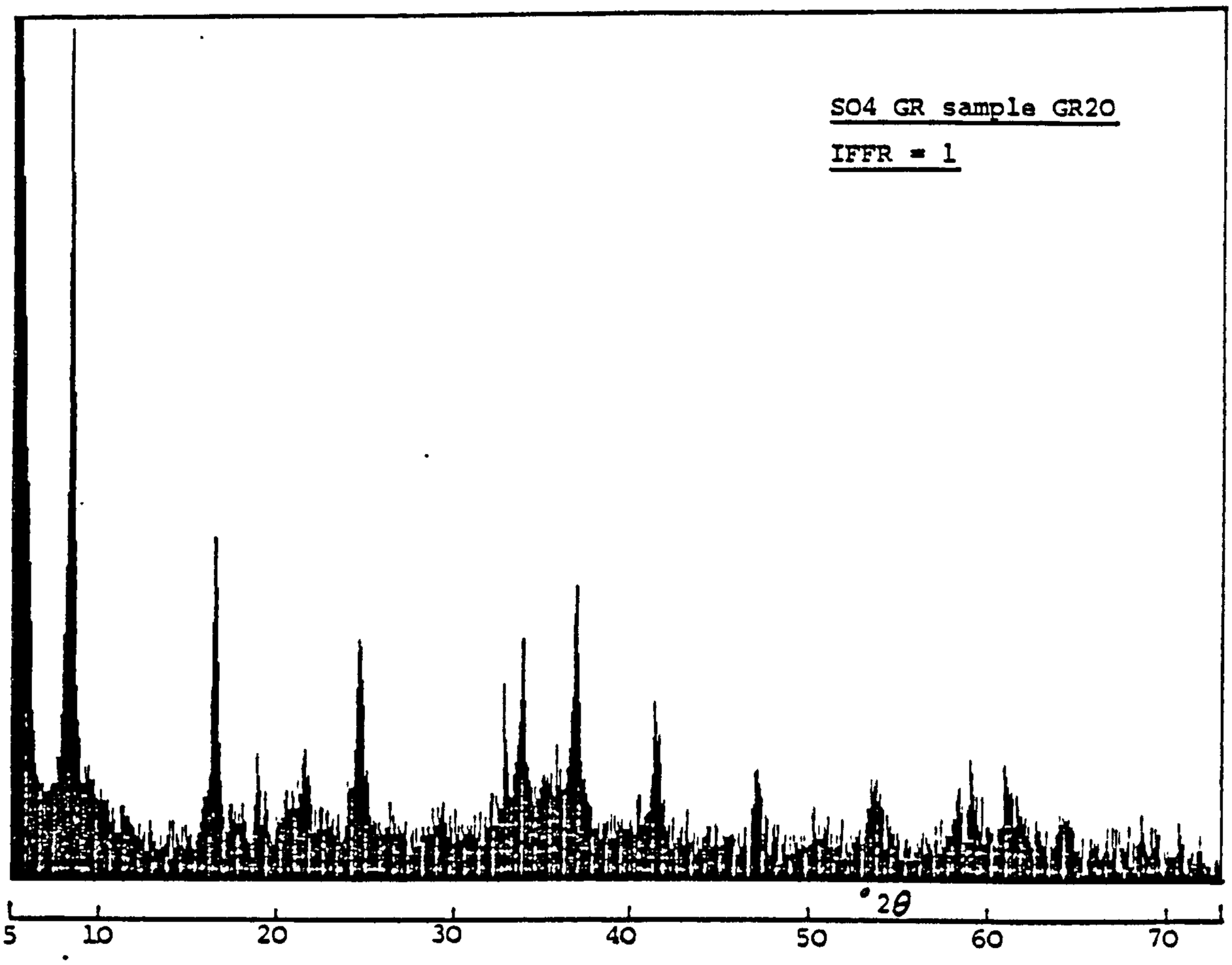

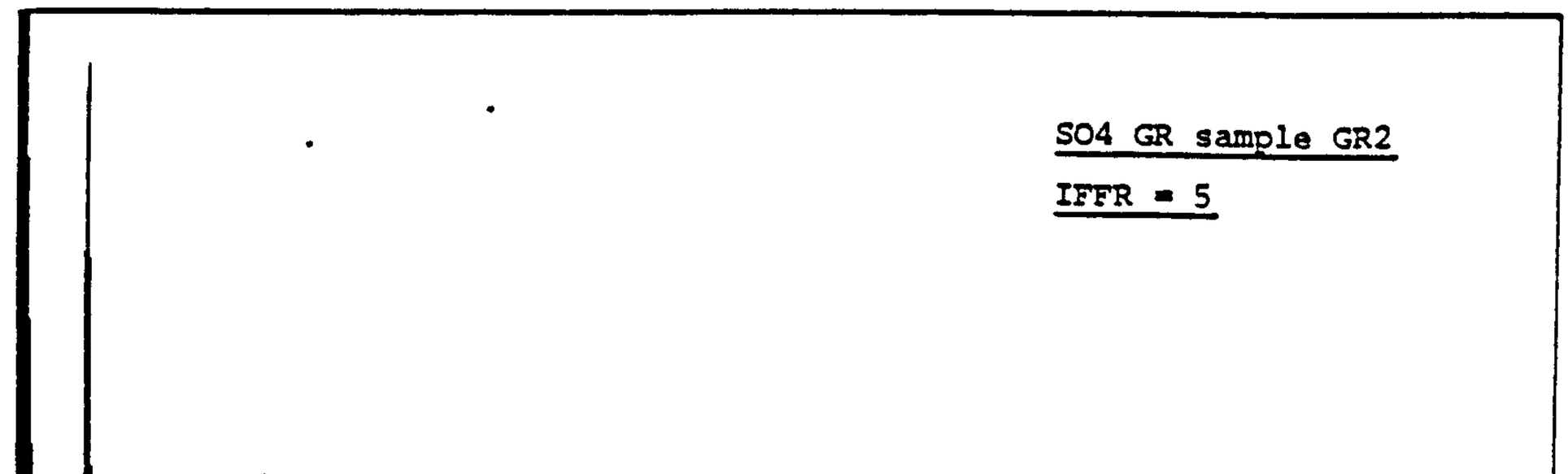

Fig 5.9 Typical X-ray diffractograms of sulphate GRs derived from 0.1 M $FeSO_4$.

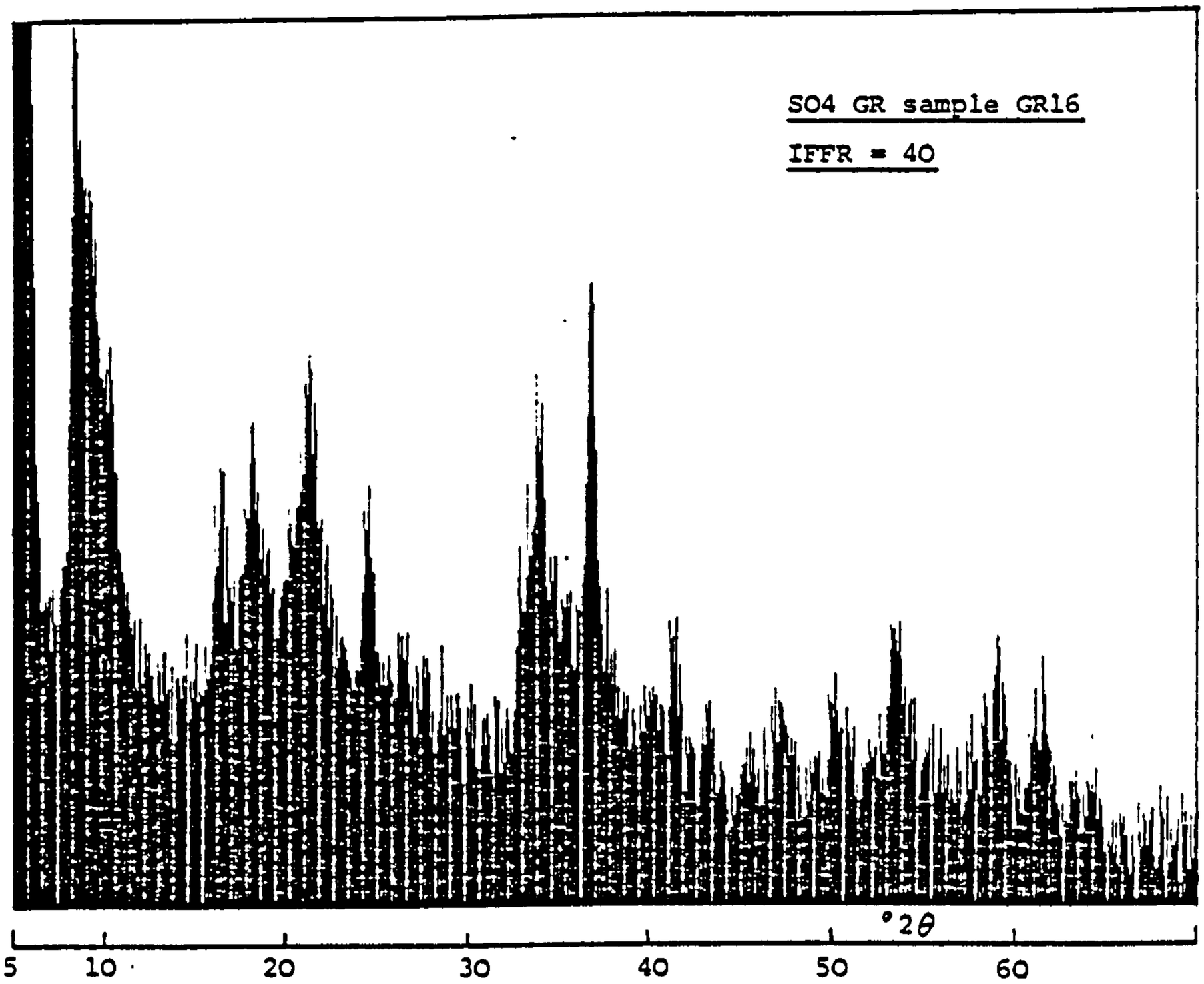

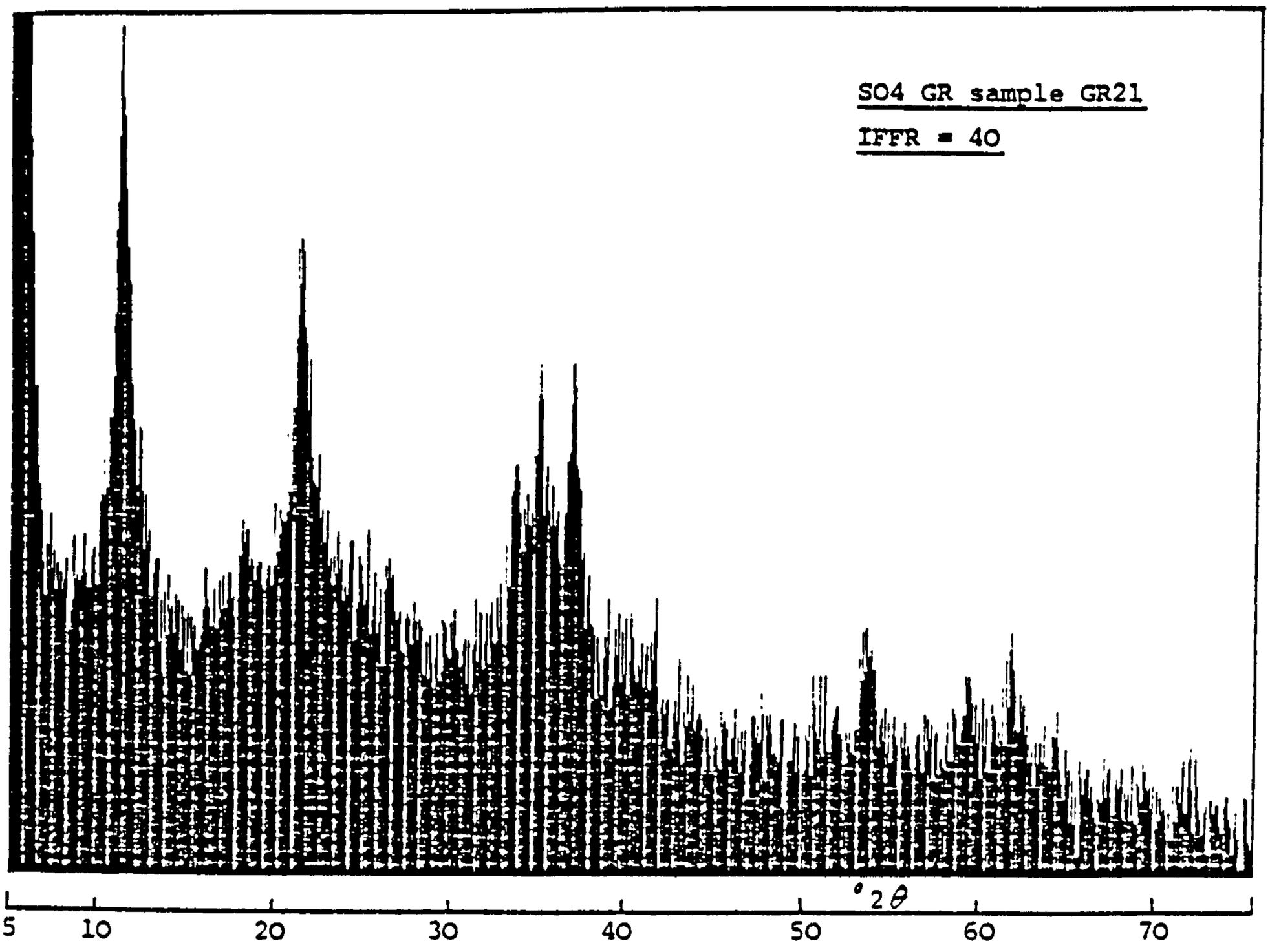

Fig 5.9 (cont'd) Typical X-ray diffractograms of sulphate GRs derived from 0.1 M $FeSO_4$.

Sample = GR20 IFFR = 1		Sample = GR1 IFFR = 5		Sample = GR2 IFFR = 5		Sample = GR13 IFFR = 10	
d-spacing (A)	Int	d-spacing (A)	Int	d-spacing (A)	Int	d-spacing (A)	Int
10.78	100	10.92	100	10.78	100	10.78	100
						8.85	40
5.41	38	5.47	50	5.44	52	5.44	38
[4.72]	[12]	[4.88]	[12]	[4.85]	[13]		
[4.13]	[10]	[4.17]	[11]	[4.17]	[19]	[4.15]	[40]
3.16	24	3.65	39	3.63	35	3.63	30
2.731	15	2.747	19	2.739	15		
2.660	21	2.668	31	2.660	28	2.683	37
		[2.578]	[6]	[2.578]	[10]	[2.578]	[27]
2.443	29	2.455	45	2.455	52	2.449	56
				[2.243]	[6(?)]		
2.186	18	2.191	25	2.191	24	2.181	28
1.934	10	1.941	18	1.937	24		
1.710	9	1.716	16	1.713	17		
1.583	6			1.583	9		
1.566	9	1.568	12	1.571	13		
1.521	10	1.524	12	1.519	13		
[1.451]	[4]			[1.453]	[6]		

[ ] = Indicate lines due to goethite

Table 5.9 X-ray d-spacings of sulphate GRs derived from 0.1 M $FeSO_4$.

Sample = GR14 IFFR = 20		Sample = GR15 IFFR = 20		Sample = GR16 IFFR = 20		Sample = GR21 IFFR = 40	
d-spacing (A)	Int	d-spacing (A)	Int	d-spacing (A)	Int	d-spacing (A)	Int
10.65	100	10.78	100	10.65	100		
8.85	57	8.85	54				
				8.52	49		
						7.90	100
5.41	57	5.47	43	5.44	29		
				[4.90]	[39]	[4.85]	[12]
[4.17]	[57]	[4.19]	[22]	[4.19]	[51]	[4.15]	[57]
3.65	38	3.65	23	3.63	32		
						[3.38]	[10]
2.660	45	2.668	21	2.652	52	2.683	25
						[2.578]	[44]
2.449	61	2.455	24	2.449	65	2.443	48
2.186	33			2.181	22		
				1.930	16		
				[1.821]	[14(B)]		
				1.719	23	1.716	17
				1.568	25	1.563	6
				1.517	25(B)	1.506	18
						[1.315(?)]	[10]

Table 5.9 (cont'd) X-ray d-spacings of sulphate GRs derived from 0.1 M $FeSO_4$.

GOETHITE		SO_4 GREEN RUST I		SO_4 GREEN RUST II	
d-spacing (A)	Int	d-spacing (A)	Int	d-spacing (A)	Int
4.97	60	7.49	100	10.92	100
4.18	100	3.84	80	5.48	80
3.36	60	2.72	60	3.65	80
2.69	70	2.47	60	2.747	40
2.58	55	2.029	40	2.660	60
2.44	80	1.616	40	2.459	60
2.25	60	1.579	40	2.195	60
2.18	60			1.938	60
1.80	50			1.712	20
1.72	70			1.587	20
1.69	50			1.570	20
1.60	50			1.525	20
1.56	65				
1.51	60				
1.45	60				
1.42	50				
1.39	50				
1.36	50				
1.32	60				

N.B. For goethite, only lines with intensity > 40% are shown

Table 5.10 X-ray d-spacings of goethite and sulphate Green Rust I & II.

brackets in Table 5.9. The intensity of the line at 2.45 A is probably the sum of the contributions from the sulphate GR and goethite since they both have reflections at this location. Thus strictly speaking, the material produced should be termed sulphate GR/goethite samples. However, when speaking of sulphate GR samples, it is implied that goethite is also usually present.

In addition to the two sets of X-ray d-spacings, a line at ~ 8.8 A is present in samples GR13-16 where 10 $\leq$ IFFR $\leq$ 40. This line is not given by Bernal et al. (1959) for either sulphate GRI or II nor is it due to any of the other iron oxides. It may be a transition line from sulphate GRI -> sulphate GRII or from sulphate GRII -> partially oxidised sulphate GRII. It may also be due to a metastable phase similar to Fe hydrogen sulphate hydrate [$Fe(SO_4)_3.H_2SO_4.8H_2O$]. The latter has strong lines at d = {9.22, 8.81} A (see ASTM file no. 8-82). However, XRD diffractograms of the partially oxidised GR material shows up lines between 10 and 6 A which were absent initially (see Table 5.13 - samples GR20 & GR1). So this suggest that the line at ~ 8.8 A arose from partial oxidation of the sulphate GR during vacuum-drying, and not from a reaction between the Fe(II) cations and Fe(III) gel (which incorporated SO_4^{2-} anions) during GR synthesis. The question is why does this line not appear in every instance since all the samples were treated in a similar fashion? Also

it seems to occur only in high values of IFFR (> 5) and, in the case of sample GR21 (IFFR = 40), the basal line occurs at 7.90 A which suggests that the sample may be degraded sulphate GRI material. A possible answer to the origin of the X-ray line at ~ 8.8 A is given in the conclusions chapter.

For comparison with the sulphate GR synthesised from 0.1 M $FeSO_4$, the X-ray d-spacings of two samples of sulphate GR produced from 0.05 M $FeSO_4$ are shown in Table 5.11. The X-ray diffractograms for the samples are shown in Fig 5.10. For both samples, IFFR = 2 and <Fe(III)> = 5 mmoles. Since IFFR changes with $[FeSO_4]_I$, direct comparison is between these samples and samples GR1 & GR2, where <Fe(III)> is also = 5 mmoles. The XRD trace in Fig 5.10 show very well-defined lines indicating good crystalline material. Table 5.11 indicate clearly that there are more goethite lines than in the sulphate GR samples produced from 0.1 M $FeSO_4$, and implies that the ratio sulphate GR/goethite has decreased. Strictly speaking then, the two samples should (again) be termed sulphate GR/goethite mixtures. Again the line at ~ 8.8 A appears, although IFFR is low (= 2).

The information presented in Table 5.11 suggests that the ratio sulphate GR/goethite decreases with decreasing $[FeSO_4]_I$. To further substantiate this view,

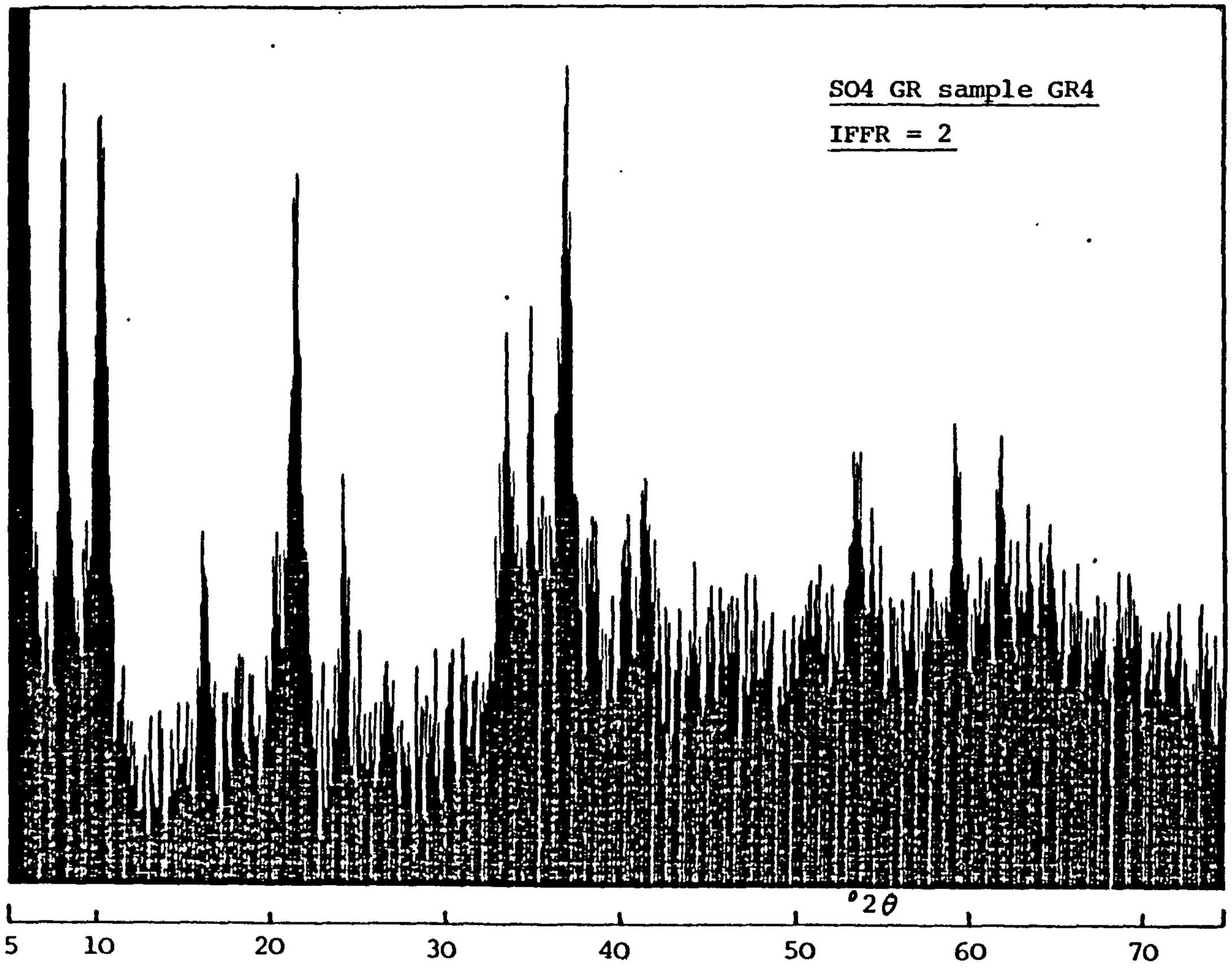

Fig 5.10 X-ray diffractogram of sulphate GR sample derived from 0.05 M $FeSO_4$.

Sample = GR3 IFFR = 2		Sample = GR4 IFFR = 2	
d-spacing (A)	Int	d-spacing (A)	Int
10.92	100	10.92	100
8.85	10	8.67	94
5.51	38	5.54	40
[4.90]	[8]	[4.90]	[15]
[4.70]	[8]	[4.38]	[24]
[4.15]	[52]	[4.13]	[99]
3.68	30	3.69	47
[3.35]	[9]	[3.35]	[16]
2.731	12	2.960	17
2.675	26	2.675	58
[2.571]	[23]	[2.571]	[57]
2.443	51	2.436	98
		2.350	[24]
[2.233]	[9]	[2.243]	24
2.186	14	2.186	32
1.945	8	1.961	10(B)
		[1.797]	[15]
1.719	19	1.716	32
		[1.690]	[26]
[1.561]	[16]	[1.563]	[35]
[1.508]	[9]	[1.504]	[28]
[1.451]	[10]	[1.447]	[16]
		[1.361]	[14]

[ ] = Indicates lines due to goethite

Table 5.11 X-ray d-spacings of sulphate GRs derived from 0.05 M $FeSO_4$.

the X-ray traces and corresponding d-spacings for two samples produced from $[FeSO_4]_I$ = {0.025, 0.01 } M are given in Fig 5.11 and Table 5.12, respectively. The <Fe(III)> was kept constant at 5 mmoles so that IFFR = {0.4, 1}, respectively. As shown in Table 5.12, there is virtually no lines associated definitely with sulphate GR. This plus the X-ray traces in Fig 5.11 show that the samples are well-crystalline goethite. This statement must be qualified since the X-ray data was obtained for the dried material. In section 5.2.1e, the Mossbauer spectrum of sample S23-3-83 (IFFR = 1) indicate the presence of small amounts of sulphate GR, along with the goethite, for the undried, fresh precipitate.

Included in Table 5.12 is the X-ray d-spacing for a non-GR sample produced from 0.1 M $FeSO_4$ without the addition of alkali to maintain pH at 7 (mentioned in section 5.2.1a). This sample (S7-2-83) can be directly compared to samples GR1 & 2 since IFFR = 5 and <Fe(III)> = 5 mmoles. The XRD data shows that the material is well-crystalline goethite (see also Fig 5.11), and indicates that alkali was required for sulphate GR formation.

When oxidised in the dry state, the sulphate GRs changed colour from dark-green/green to orangy-yellow. This orangy-yellow colour was taken to indicate that complete (or virtually complete) oxidation has occurred for any

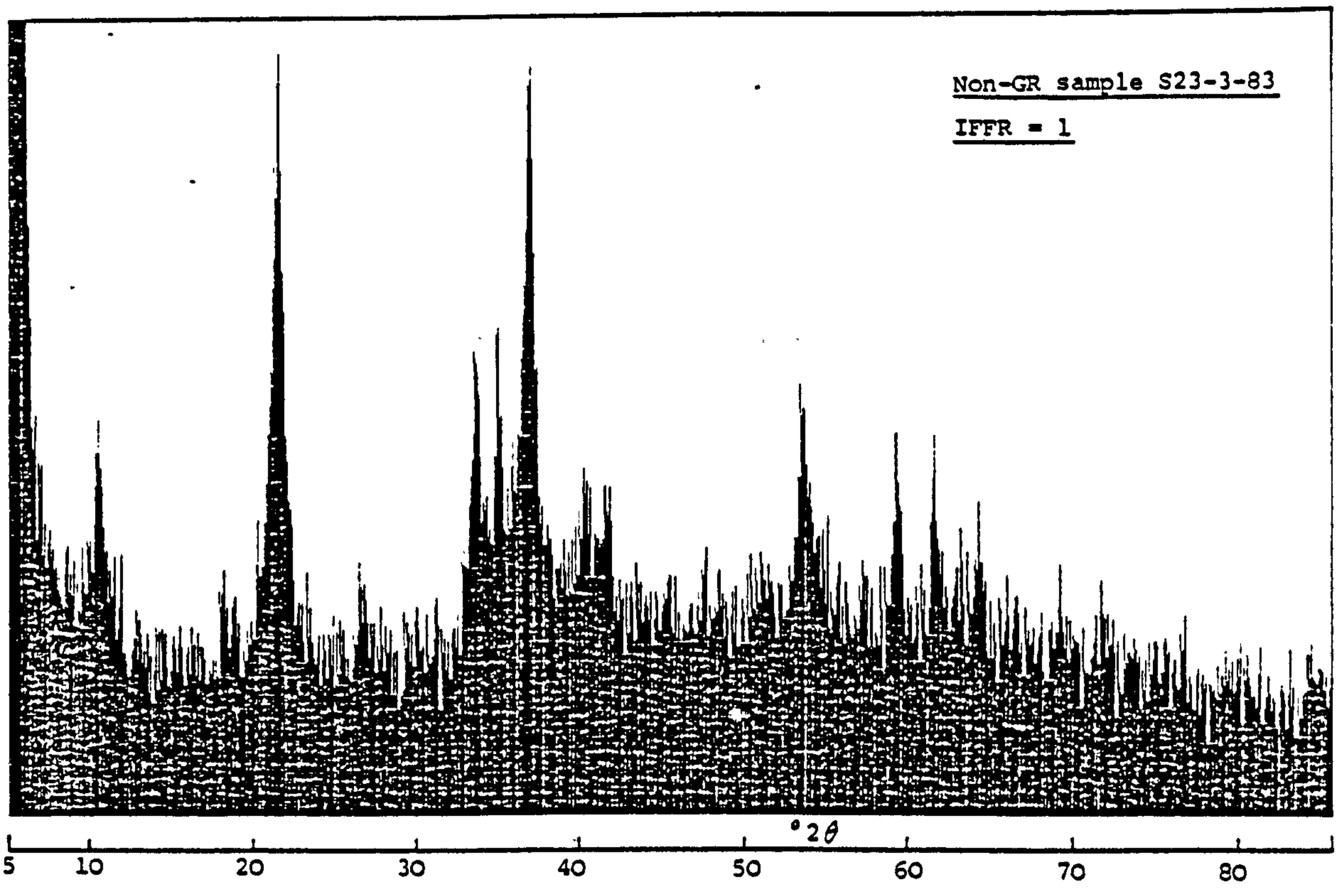

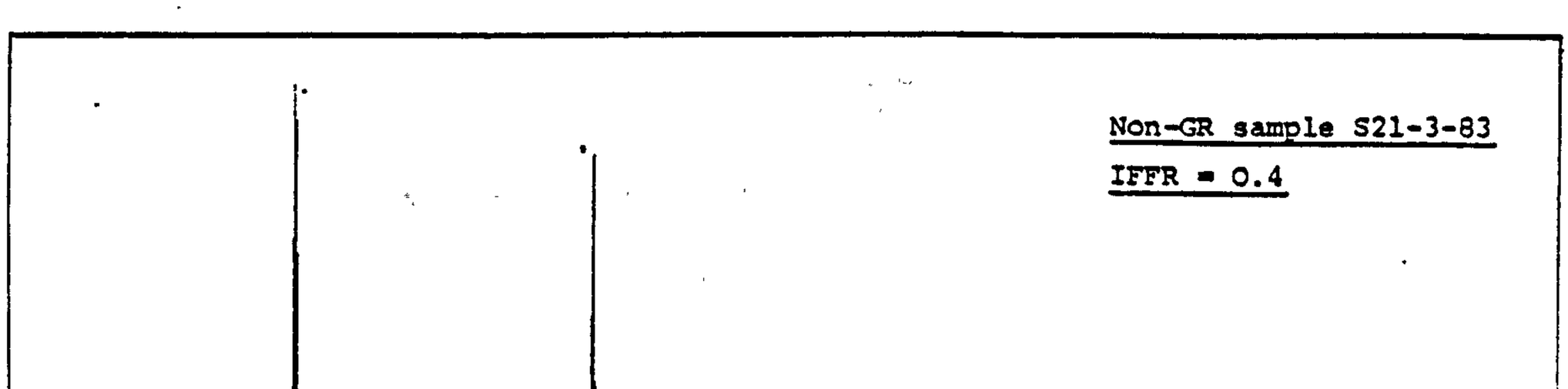

Fig 5.11 X-ray diffractograms of non-GRs derived from ≤ 0.1 M $FeSO_4$.

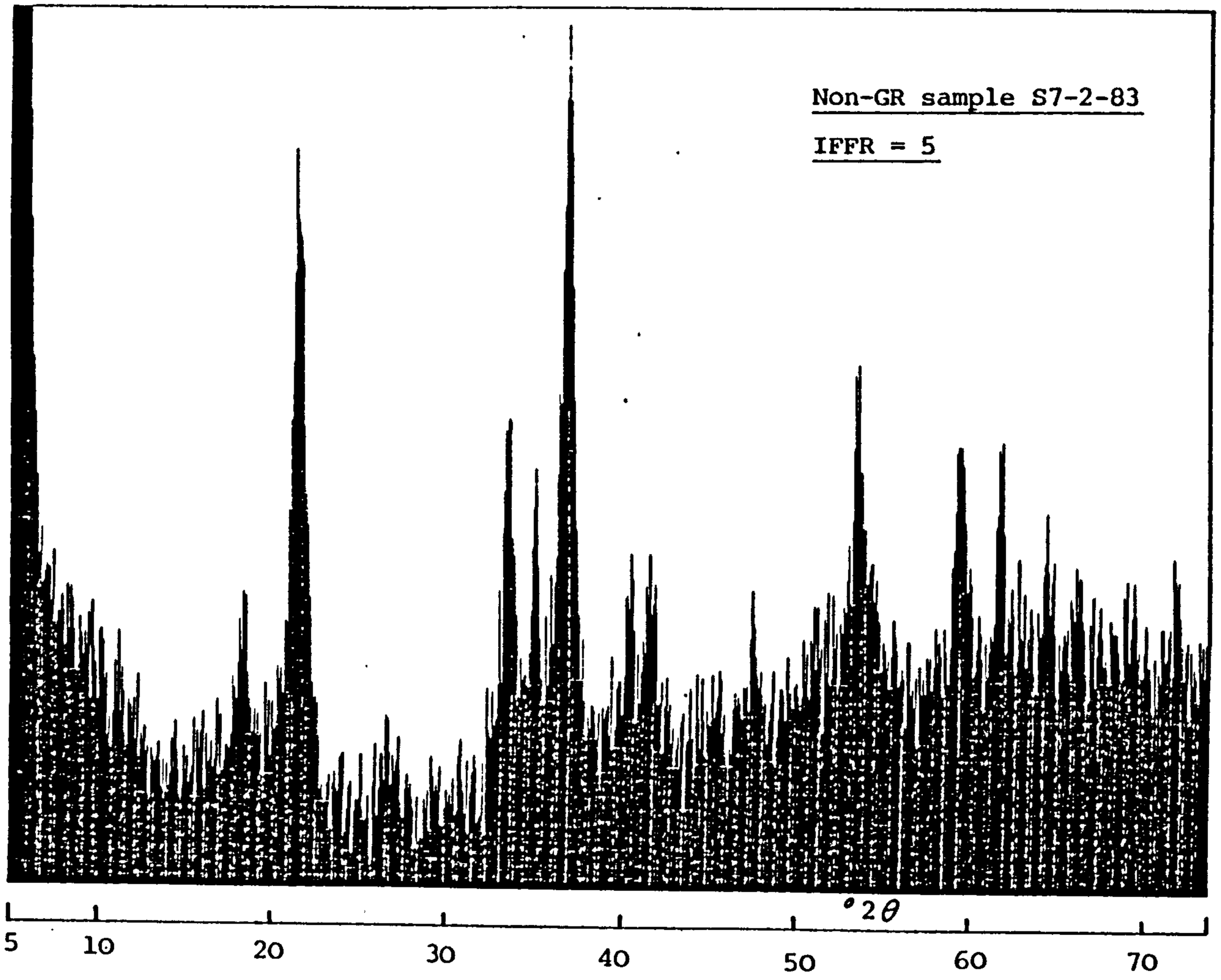

Fig 5.11 (cont'd) X-ray diffractograms of non-GRs derived from ≤ 0.1 M $FeSO_4$.

Sample = S21-3-83 IFFR = 0.4		Sample = S23-3-83 IFFR = 1		Sample = S7-2-83* IFFR = 5	
d-spacing (A)	Int	d-spacing (A)	Int	d-spacing (A)	Int
		8.43	35		
4.90	14	4.88	14	4.85	23
4.13	100	4.12	100	4.15	90
3.35	11	3.35	16	3.35	17
2.876	5				
2.675	38	2.668	42	2.675	50
2.571	28	2.564	43	2.557	42
2.436	88	2.436	83	2.436	100
2.243	17	2.238	22	2.238	23
2.176	22	2.171	22	2.171	23
2.002	9				
1.914	10			1.914	19
1.794	8				
1.716	40	1.713	38	1.710	44
1.687	11				
1.598	9				
1.559	29	1.559	33	1.556	34
1.508	24	1.506	31	1.504	32
1.451	14	1.449	19	1.447	18
				1.414	13
1.353	9			1.354	11
1.315	11			1.313	14

*No alkali added to maintain pH at 7

Table 5.12 X-ray d-spacings of non-GRs derived from ≤ 0.1 M $FeSO_4$.

sample of sulphate GR. It was with this criterion that X-ray diffractograms were taken for the oxidised material corresponding to the original sulphate GR sample. Table 5.13 gives the X-ray d-spacings for the oxidised material corresponding to the samples in Table 5.9. The XRD trace for an oxidised sample is shown in Fig 5.12. Virtually all the lines can be associated with goethite. The exceptions are the lines at d > 6 A. Although sample GR1 seems to be completely oxidised from its colour, the XRD pattern shows that traces of unoxidised sulphate GR still remain.

The X-ray lines at 6 < d < 10 A are due to degraded sulphate GR material, and is consistent with the oxidation of Fe(II) to the smaller Fe(III) cation. However, in the case of the sulphate GRs with lines originally at d ~ 8.8 A (samples GR13-15), there seems to be a two-way movement in this region. One movement concerns the lines at ~ 10.8 A going towards lower values while the other concerns the lines at ~ 8.8 A moving slightly upwards. This results in lines at d = {9.03, 9.21, 9.12} A for the oxidised material. In the case of sample GR21, which may be degraded sulphate GRI material, the line originally at 7.90 A has shifted slightly up to 8.12 A. If the assumption that sample GR21 is degraded sulphate GRI is correct, then the oxidation of the sample has caused the basal line at 7.90 A to move right up through the sulphate GRII phase (d -> 10.8 A), and then

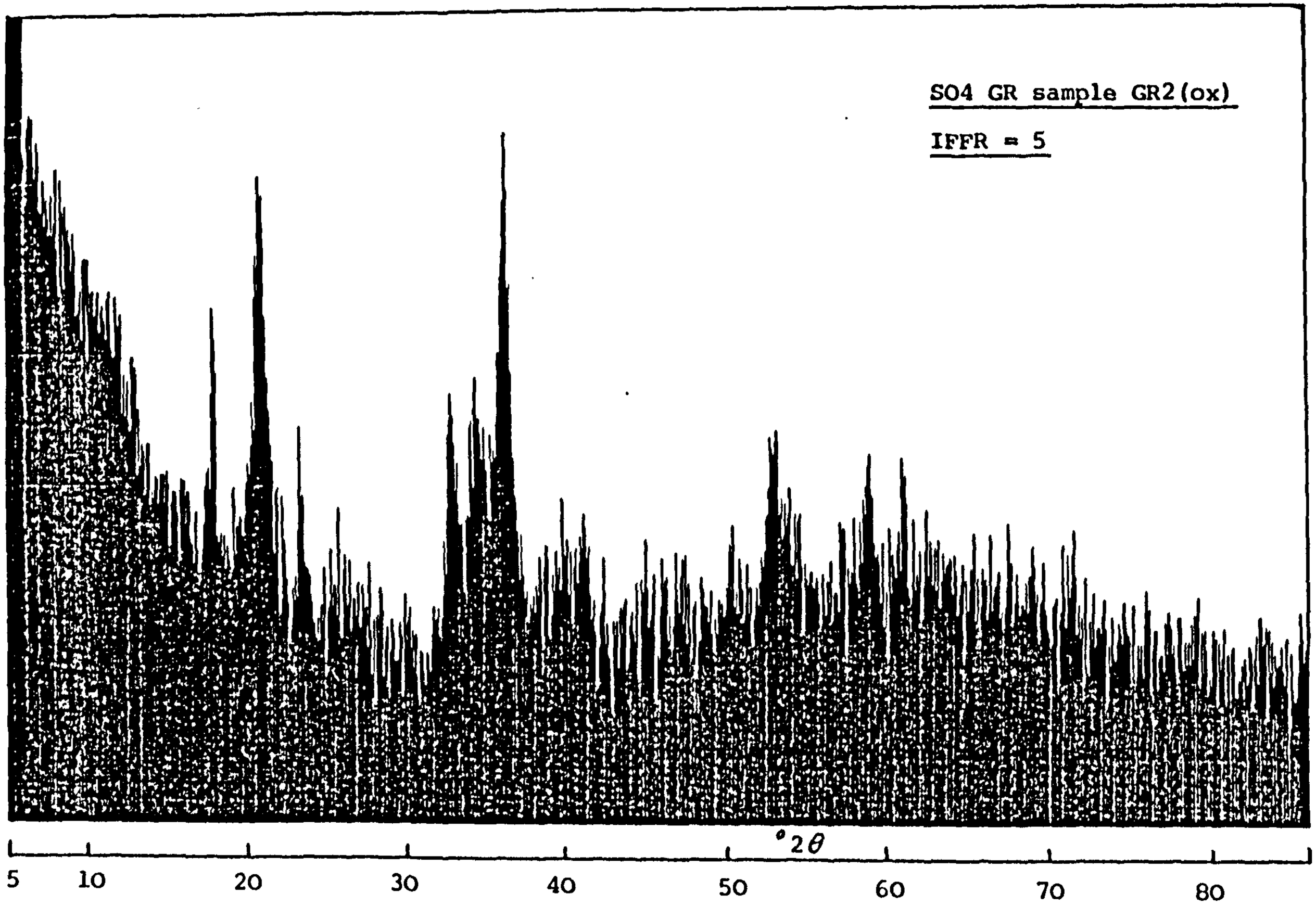

Fig 5.12 X-ray diffractogram of an oxidised sulphate GR sample derived from 0.1 M $FeSO_4$.

Sample = GR20 IFFR = 1		Sample = GR21 IFFR = 5		Sample = GR2 IFFR = 5		Sample = GR13 IFFR = 10	
d-spacing (A)	Int.	d-spacing (A)	Int.	d-spacing (A)	Int.	d-spacing (A)	Int.
		10.78	85				
9.51	42						
						9.03	55
		7.70	45(B)				
		5.41	45				
		4.85	44	4.85	56	4.93	20
		4.53	28				
4.17	92	4.13	73	4.17	89	4.15	100
		3.66	23(?)	3.71	43		
2.683	48	2.660	60	2.691	51	2.683	46
2.571	72	2.564	49	2.571	52	2.564	37
2.443	100	2.449	100	2.449	100	2.443	98
		2.186	35	2.176	27	2.186	24
1.722	27	1.713	32	1.716	36		
		1.559	26	1.556	30		
		1.510	26(B)	1.508	26		
				1.312	22(?)		

Table 5.13 X-ray d-spacings of oxidised sulphate GRs derived from 0.1 M $FeSO_4$.

Sample = GR14 IFFR = 20		Sample = GR15 IFFR = 20		Sample = GR21 IFFR = 40	
d-spacing (A)	Int.	d-spacing (A)	Int.	d-spacing (A)	Int.
9.21	57	9.12	100		
				8.12	100
4.9o	27				
4.15	100	4.17	97	4.15	82
2.691	61	2.683	55	2.691	30
2.571	51	2.571	50	2.571	60
2.449	84	2.449	67	2.449	68
2.176	24(?)			2.191	17

Table 5.13 (cont'd) X-ray d-spacings of oxidised sulphate GRs derived from 0.1 M $FeSO_4$.

back down to the complete oxidised state with the d-spacing at $6 < d < 10$ A (depending on the stability of the original crystal structure).

X-ray diffractograms of the oxidised material of the sulphate GRs produced from 0.05 M $FeSO_4$ (samples GR3 & 4) show a similar behaviour to that above but the dominant reflections can be attributed to goethite.

Ageing of a few samples of sulphate GR have been carried out under non-turbulent conditions. Table 5.14 shows the X-ray d-spacings for two such samples: (i) one aged under anoxic conditions in its own solution for 18 days, (ii) the other aged in its own solution under moderately oxic conditions for ~ 8 months.The corresponding X-ray traces (Fig 5.13) show that the samples were well-crystalline.

It can be seen that sample GR5 is composed entirely of goethite whilst sample GR20 is made up of a mixture of goethite and magnetite. The colour of the aged material of the former sample was brownish-yellow. In the case of sample GR20, the expected conversion to goethite did not materialised, but instead the original dark-green precipitate changed to a black substance which had bulk magnetism. Although the magnetic component has been labelled as magnetite for simplicity, it is most likely to be a mixture of magnetite and maghemite since it very

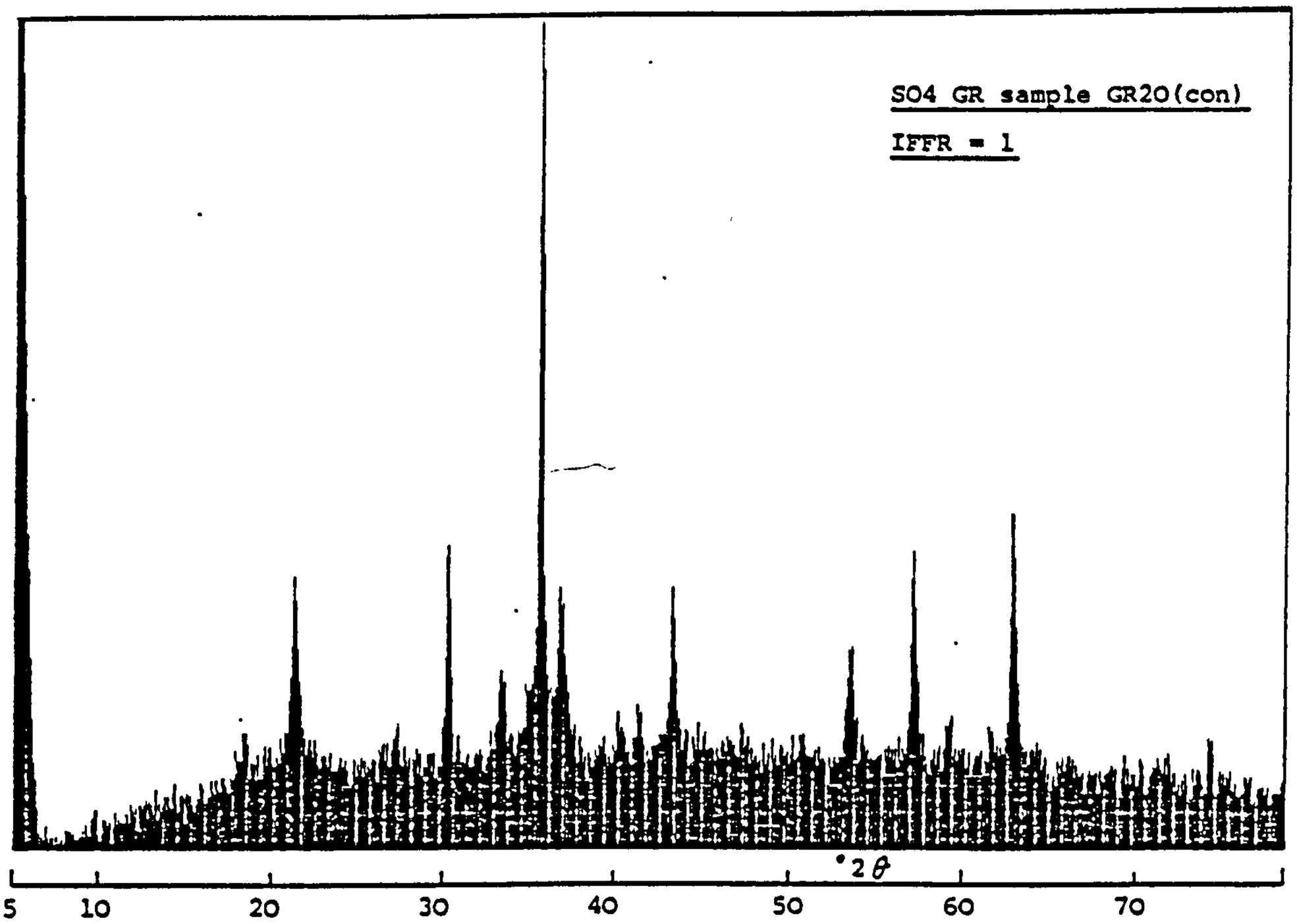

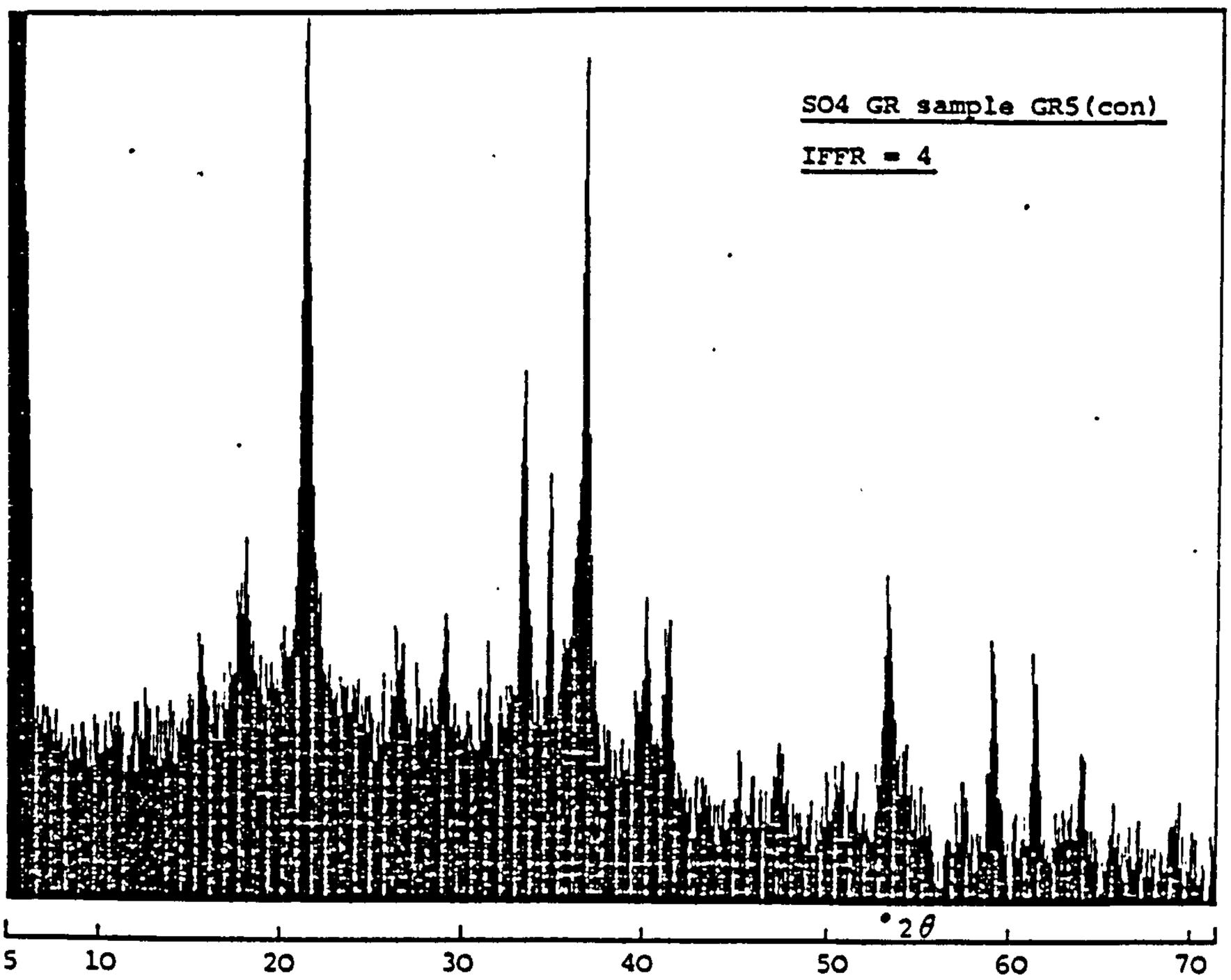

Fig 5.13 X-ray diffractograms of converted sulphate GR samples:
(i) aged under anoxic, non-turbulent conditions
(ii) aged under moderately oxic, non-turbulent conditions.

(i)Sample = GR20 IFFR = 1		(ii)Sample = GR5 IFFR = 5	
d(A)	Int.	d(A)	Int.
		5.68	13
{4.82}	{6}	4.96	23
4.17	26	4.15	100
3.28	6(B)	3.36	17
{2.96}	{31}	3.08	19
		2.849	12
2.691	12	2.699	51
		2.585	37
{2.529}	{100}		
2.449	23	2.449	100
2.243	6	2.249	25
2.191	7	2.186	25
{2.094}	{23}		
		1.918	10
		1.794	9
{1.713}	{16}	1.719	39
{1.613}	{29}		
		1.603	10
1.563	6	1.563	32
1.508	5	1.512	29
{1.480}	{35}		
		1.455	17
		1.359	8
{1.278}	{6}		

{ } = magnetite lines

Table 5.14 X-ray d-spacings of aged sulphate GR samples:
(i) anoxic conditions
(ii) moderately oxic conditions.

difficult to distinguish between the two phases by XRD alone. On this occasion, some of the high angle X-ray lines (d = 2.094, 1.713, 1.613 A) agree more with the XRD pattern of magnetite (see ASTM file no. 11-614), and so the magnetic component is more a magnetite phase than a maghemite phase. The line at 3.28 A for sample GR20 may be due to lepidocrocite.

The Mossbauer data in section 5.2.1e will show that the aged-overnight precipitate of sample GR20 already had goethite as one component (sulphate GR being the other). Thus the magnetic component must have been derived from the sulphate GR phase. This is not the usual pathway of transformation for sulphate GR under anoxic conditions. However, oxygen may have leaked into the system, resulting in the partial oxidation and subsequent conversion of the sulphate GR to magnetite (Bernal et al., 1959; Misawa et al., 1974). The probability of conversion would be increased by the high level of Fe(III) material (20 mmoles) used in the synthesis of sample GR20.

5.2.1c Infrared Spectroscopy

Infrared spectra of sulphate GR samples taken by the pressed disc method seem to preserved the material i.e. reduce the rate of oxidation. The freshly prepared disc was dark-green/green in colour and the disc (kept under a dry atmosphere) only gradually became a lighter, more yellowy colour, after many months.

Typical IR spectra of the sulphate GRs synthesised from 0.1 M $FeSO_4$ are shown in Fig 5.14. The IR absorption peaks and regions are given in Table 5.15. As seen from the IR spectra, there are basically three main areas of absorption, similar to those of the Fe(III) oxides (section 5.1):

(i) a broad region in the range 3700-2400 cm^{-1} due to OH stretching vibrations of structural OH groups and/or molecular water (water of hydration and/or adsorbed water).

(ii) a smaller region in the range 1740-1460 cm^{-1} due to OH bending (deformation) vibrations of molecular water.

(iii) a region with many peaks from 1300 cm^{-1} onwards arising from the stretching and bending vibrations of Fe-O bonds, the bending vibrations of Fe-O-OH groups and the contribution from sulphate groups. The latter seems to be the fundamental difference between

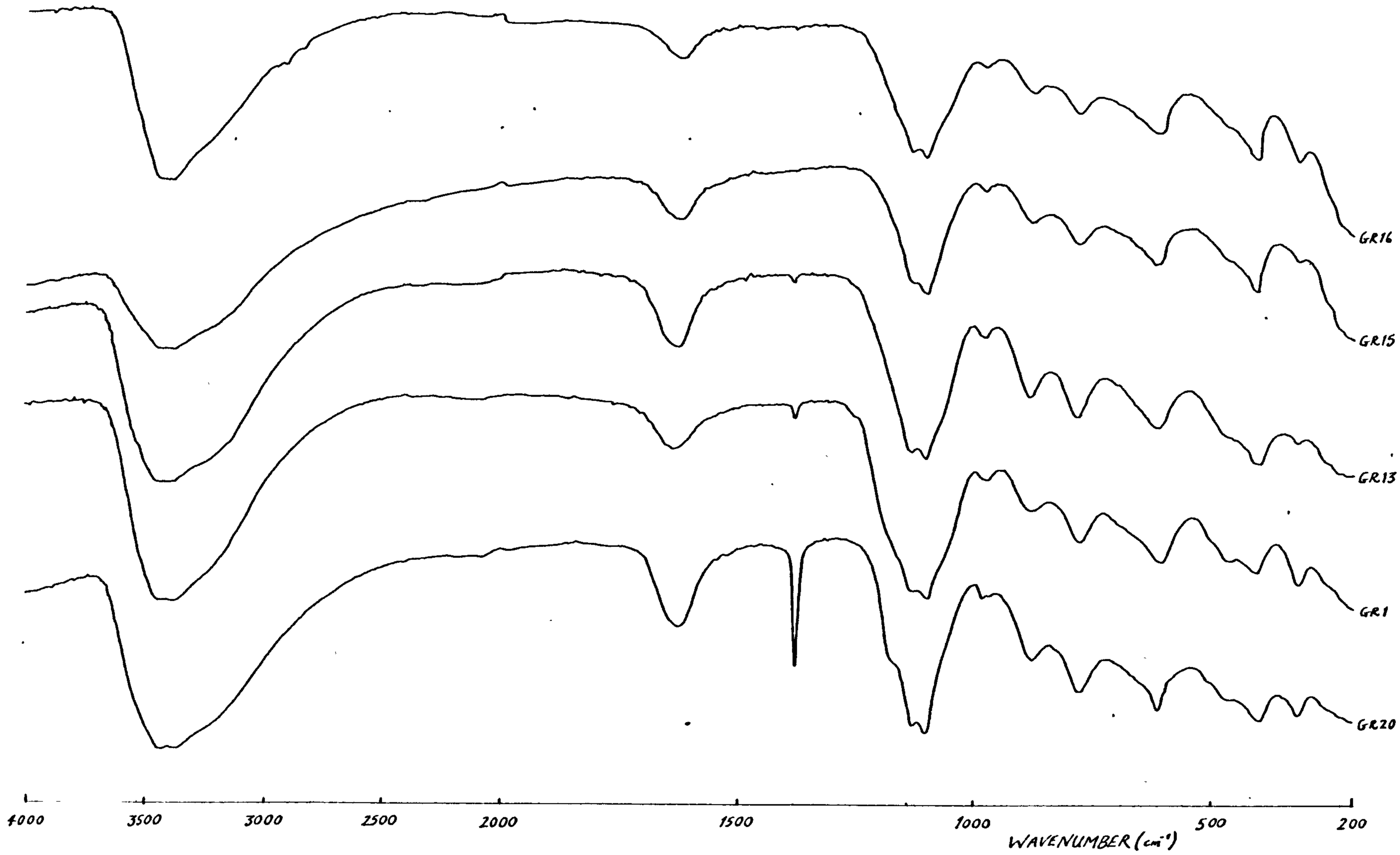

Fig 5.14 Typical IR spectra of sulphate GRs derived from 0.1 M $FeSO_4$.

Sample = GR20 IFFR = 1	Sample = GR1 IFFR = 5	Sample = GR2 IFFR = 5	Sample = GR13 IFFR = 10	Sample = GR14 IFFR = 20	Sample = GR15 IFFR = 20	Sample = GR16 IFFR = 40	Sample = GR21 IFFR = 40
			Peaks (cm^{-1})				
3410 ± 30	3410 ± 30	3410 ± 30	3410 ± 30	3410 ± 30	3420 ± 30	3405 ± 20	3360 ± 40
3220 ± 60	3220 ± 60	3220 ± 50	3240 ± 60	3230 ± 60	3210 ± 60	3210 ± 60	3210 ± 60
1625 ± 5	1634 ± 10	1638 ± 10	1628 ± 10	1630 ± 10	1625 ± 10	1620 ± 10	1620 ± 10
1376 ± 5	1378 ± 5	1377 ± 5	1377 ± 5	1382 ± 5			
1172 ± 10	1178 ± 15	1176 ± 20					
1130 ± 5	1131 ± 10	1131 ± 5	1134 ± 5	1135 ± 10	1131 ± 5	1130 ± 5	
1100 ± 5	1100 ± 5	1098 ± 5	1103 ± 5	1103 ± 5	1099 ± 5	1100 ± 5	1100 ± 10
980 ± 5	976 ± 5	977 ± 5	978 ± 5	981 ± 5	977 ± 5	974 ± 5	975 ± 5
880 ± 5	882 ± 5	886 ± 5	886 ± 5	888 ± 5	881 ± 5	879 ± 5	880 ± 5
779 ± 5	779 ± 5	784 ± 5	786 ± 5	788 ± 5	781 ± 5	779 ± 5	785 ± 5
610 ± 5	608 ± 5	610 ± 10	612 ± 10	617 ± 10	613 ± 5	608 ± 10	615 ± 10
465 ± 10	466 ± 10	461 ± 10	461 ± 15	460 ± 20			
400 ± 5	405 ± 5	396 ± 10	401 ± 5	407 ± 5	405 ± 5	400 ± 5	400 ± 5
314 ± 5	314 ± 5	314 ± 5	315 ± 5	320 ± 5	314 ± 5	310 ± 5	
			Regions (cm^{-1})				
3700-2400	3700-2500	3700-2400	3700-2500	3700-2500	3700-2500	3680-2500	3680-2560
1740-1480	1760-1460	1740-1490	1770-1480	1760-1480	1740-1500	1750-1500	1760-1500
1270- 290	1280- 290	1280- 290	1290- 300	1280- 300	1270- 300	1280- 290	1270- 330

Table 5.15 IR absorption peaks and regions of sulphate GRs derived from 0.1 M $FeSO_4$.

the Fe(III) oxides and the sulphate GRs.

In addition to the three main regions of IR absorption, there is often a very sharp absorption peak at 1378 cm^{-1}. This is due to NO_3^- anions which is derived from the Fe(III) gel used in the sulphate GR synthesis process. Generally, the Fe(III) gel was prepared from Fe(III) nitrate and the NO_3^- anions then becomes incorporated onto the gel by adsorption. These NO_3^- anions are probably not vital in sulphate GR formation since washed Fe(III) gel derived from Fe(III) chloride also produce sulphate GR (samples GR15 & 16). The IR spectra of an Fe(III) gel produced from $Fe(NO_3)_3$ and one made from $FeCl_3$ (both washed twice with distilled water) are compared with $Fe(NO_3)_3.9H_2O$ in Fig 5.15. Note the sharp NO_3^- peak at 1380 cm^{-1} for the gel derived from $Fe(NO_3)_3$ which is absent in the gel derived from $FeCl_3$. The absorption peaks and regions of these gels and $Fe(NO_3)_3.9H_2O$ are listed in Table 5.16.

The main regions of absorption by sulphate groups occurs in the range 1280-950 cm^{-1} with peaks at 1131, 1100 and 977 cm^{-1}, and sometimes a higher wavenumber peak at ~ 1175 cm^{-1}. There are also two other peaks at 610 and 314 cm^{-1} which are associated with the sulphate groups. The presence of sulphate absorption

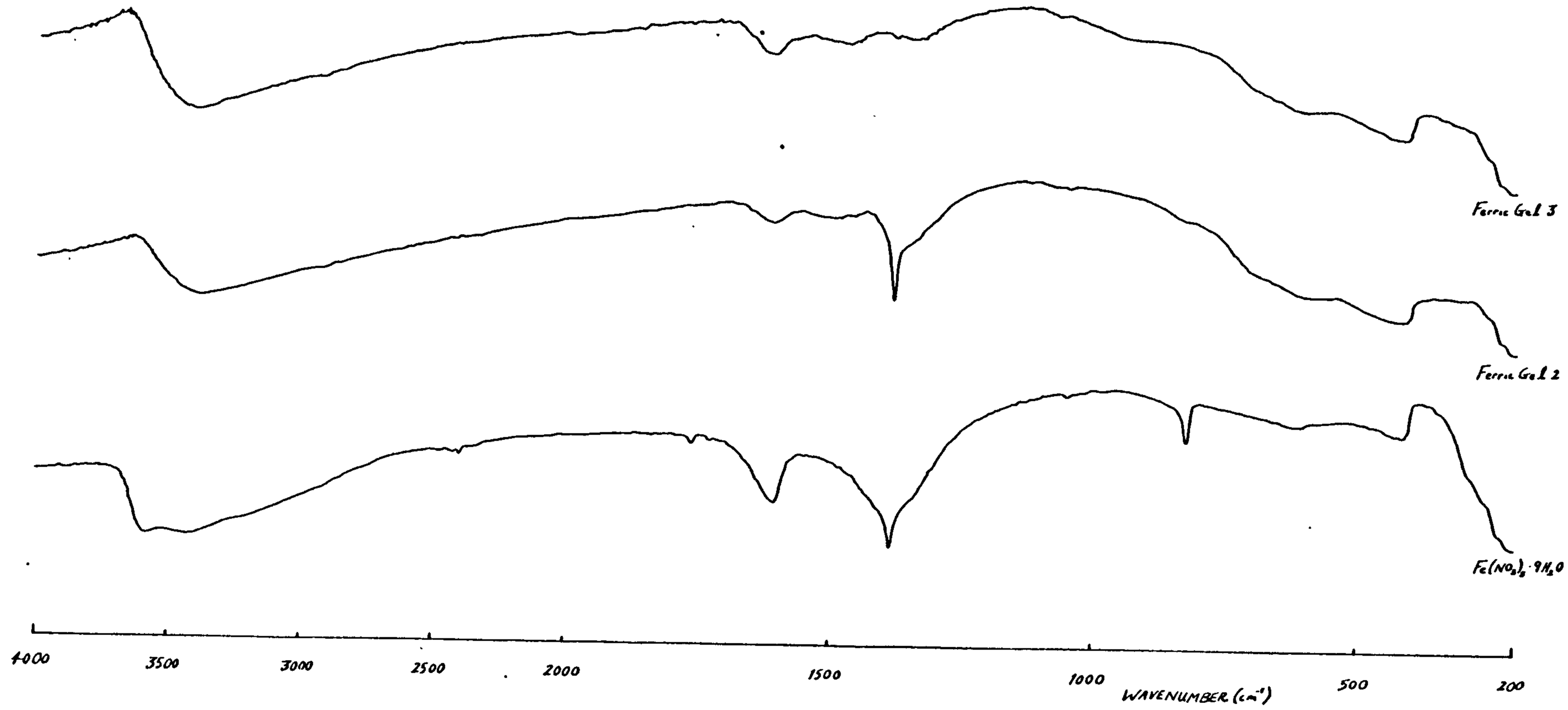

Fig 5.15 Comparison of IR spectra of Fe(III) gels produced from $Fe(NO_3)_3$ and $FeCl_2$ with that of $Fe(NO_3)_3.9H_2O$.
(Ferric gel 2 - made from $Fe(NO_3)_3.9H_2O$
Ferric gel 3 - made from $FeCl_3.6H_2O$)

$Fe(NO_3)_3.9H_2O$	Fe(III) gel 2	Fe(III) gel 3
	Peaks (cm^{-1})	
3570 ± 15		
3410 ± 30	3380 ± 30	3400 ± 30
1758 ± 5		
1605 ± 10	1610 ± 10	1618 ± 10
	1490 ± 20	1470 ± 20
1385 ± 5	1380 ± 5	
1332 ± 20	1335 ± 20	1345 ± 20
		930 ± 25
820 ± 5		
	685 ± 20	680 ± 20
610 ± 20	595 ± 20	610 ± 20
410 ± 15	425 ± 20	420 ± 20
	Regions (cm^{-1})	
3700-2550	3620-1770	3660-1800
1790-1120	1690-1180	1680-1200
910- 390	900- 390	1050- 390

Table 5.16 IR absorption peaks and regions of $Fe(NO_3)_3.9H_2O$ and two Fe(III) gels. (Fe(III) gel 2 - made from $Fe(NO_3)_3.9H_2O$ Fe(III) gel 3 - made from $FeCl_3.6H_2O$.)

peaks in the IR spectra confirms the chemical analyses of the sulphate GR samples in Appendix A. The other IR peaks below 950 cm^{-1} can be attributed to goethite. The absorption peaks ascribed to sulphate groups in the sulphate GRs can be compared with those in $FeSO_4.7H_2O$ and basic $FeSO_4$. (Fig 5.16 and Table 5.17). The latter was made by the partial precipitation of a solution of $FeSO_4$ and has the general chemical formula of $Fe(OH)_2.xFeSO_4$, where x = a variable. The IR spectra of basic $FeSO_4$ is, in fact, very similar to those of the sulphate GRs except that it has no goethite peaks.

It is interesting to note that non-GR samples such as samples S7-2-83 & S23-3-83 made from $FeSO_4$ also show IR absorption peaks due to sulphate groups. (Fig 5.17 and Table 5.18). In the case of sample S7-2-83, where no extra alkali was added to maintain pH at 7 after the addition of the Fe(III) gel to the $FeSO_4$ solution, the SO_4^{2-} anions must have adsorbed onto the gel surface. This would suggest that sulphate groups become incorporated into the GR structure by initial adsorption onto the gel surface, followed by presumbly penetration into the lattice or rearrangement. Appendix A shows that the %sulphate decreases with decreasing $[FeSO_4]_i$ ($\langle Fe(III) \rangle$ being constant).

The IR spectra of some of the sulphate GR oxidised in air

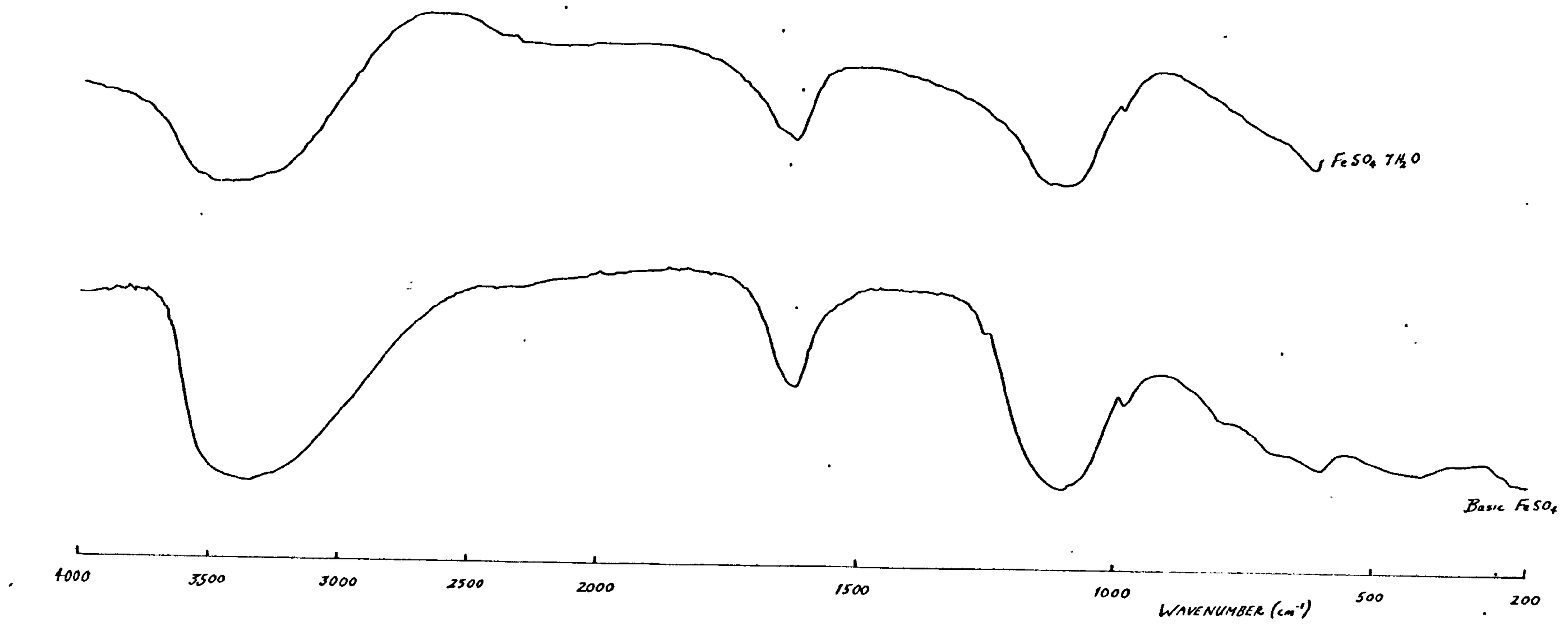

Fig 5.16 IR spectra of $FeSO_4.7H_2O$ and basic $FeSO_4$.

$FeSO_4 \cdot 7H_2O$*	Basic $FeSO_4$
Peaks (cm^{-1})	
3460 ± 80	
3300 ± 80	3360 ± 60
1655 ± 20	
1612 ± 10	1625 ± 10
	1255 ± 5
1106 ± 30	1100 ± 15
988 ± 5	980 ± 5
	785 ± 15
	680 ± 15
615 ± 5	600 ± 10
	410 ± 15
Regions (cm^{-1})	
4000-2700	3730-2480
1900-1540	1750-1480
1450- 600	1310- 350

* Spectra only extend down to 600 cm^{-1} (from 4000 cm^{-1})

Table 5.17 IR absorption peaks and regions of $FeSO_4 \cdot 7H_2O$ and basic $FeSO_4$.

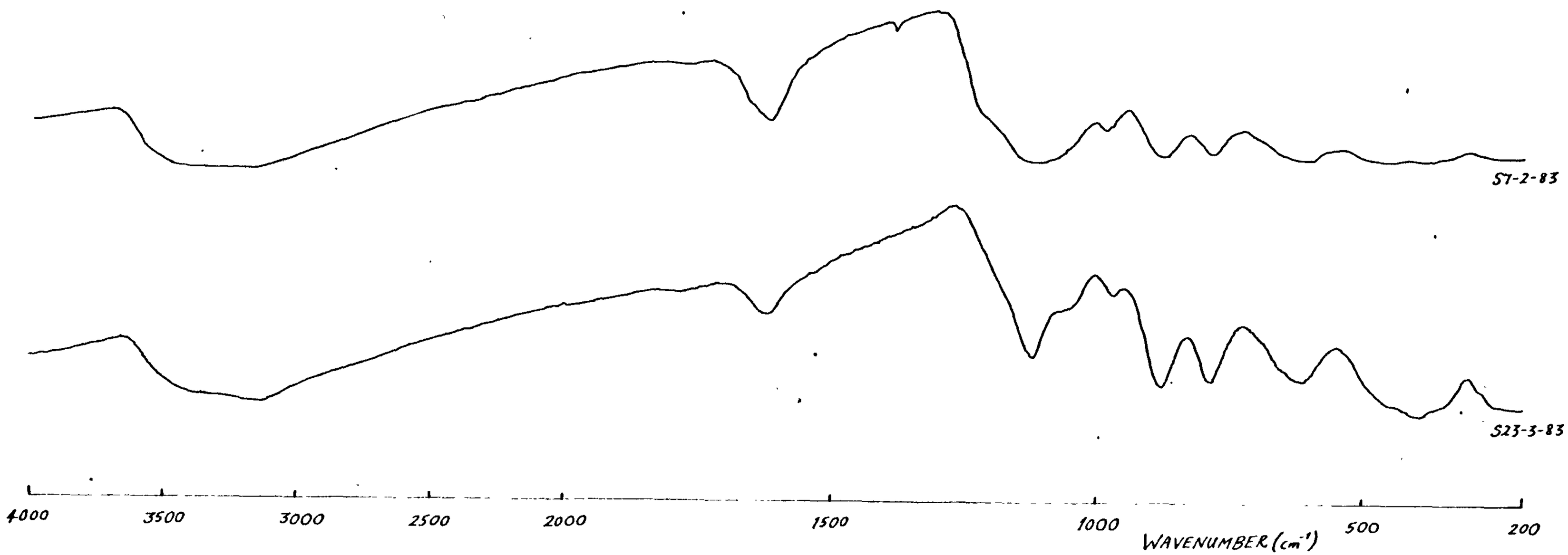

Fig 5.17 IR spectra of non-GRs derived from $\leq$ 0.1 M $FeSO_4$.

Sample = S7-2-83 * IFFR = 5	Sample = S23-3-83 IFFR = 1
Peaks (cm^{-1})	
3370 ± 60	3380 ± 80
3150 ± 60	3200 ± 80
1625 ± 10	1615 ± 10
	1380 ± 5
	1205 ± 15
1120 ± 5	1115 ± 20
1055 ± 10	
970 ± 5	982 ± 5
880 ± 5	877 ± 10
786 ± 5	782 ± 10
615 ± 10	603 ± 20
455 ± 15	
395 ± 10	
345 ± 15	
Regions (cm^{-1})	
3640-2000	3700-1900
1690-1490	1720-1470
1270- 310	1290- 310

*pH not maintained after addition of Fe(III) Hydroxide suspension

Table 5.18 IR absorption peaks and regions of non-GR samples derived from ≤ 0.1 M $FeSO_4$.

are shown in Fig 5.18, and Table 5.19 gives the corresponding IR absorption peaks and regions. It can be seen that the intensity of absorption for the four samples shown have been reduced considerably (see Fig 5.14 also), particularly in the 3700-2500 cm^{-1} (OH stretch) and 1300-950 cm^{-1} (sulphate vibrations) regions. This means a decrease in the crystallinity of the samples. The absorption peaks in the sulphate region are better resolved with an extra peak at 1020 cm^{-1} . The latter coincides with one of the peaks of lepidocrocite but it is very unlikely that the peak is the result of this oxide. The better sulphate region indicates that the vibrational modes of the sulphate groups have increased wavelength separation, and therefore suggests a disordering of the material. It also indicates that the sulphate groups are probably an integral part of the material (either belonging exclusively to the GR phase or part of both GR and goethite phase), since otherwise the vibrational modes would not be so affected (e.g. if it was a pure adsorbed species). The decrease in crystallinity of the material is also suggested by the slight downward shift in wavenumber of the majority of the peaks down to ~ 600 cm^{-1}. This means a change to slower vibrational modes and hence less ordering of the lattice. The downward shift is at the most 1.5% at any given wavenumber. All this evidence for a decrease in crystallinity is not surprising since oxidation

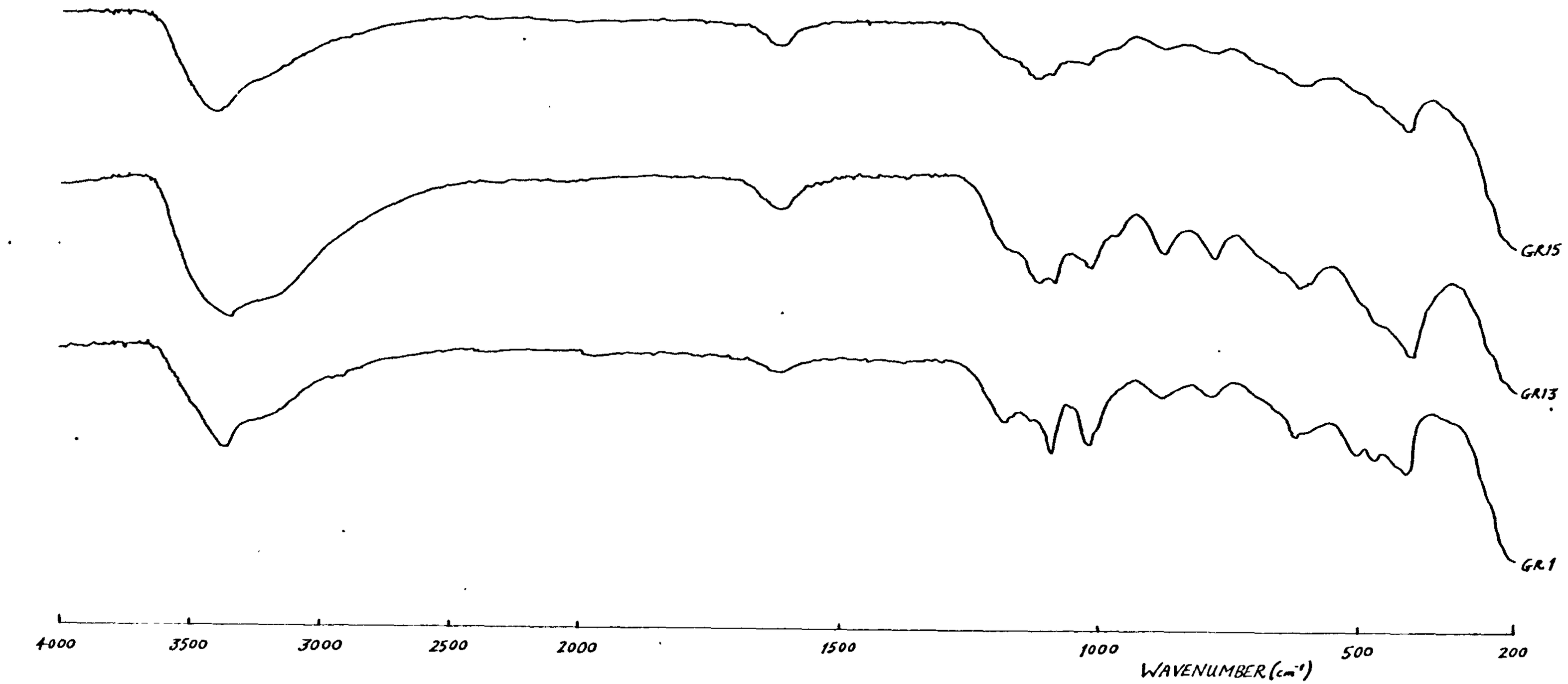

Fig 5.18 Typical IR spectra of oxidised sulphate GR samples derived from 0.1 M $FeSO_4$.

Sample = GR1 IFFR = 5	Sample = GR13 IFFR = 10	Sample = GR14 IFFR = 20	Sample = GR15 IFFR = 20
	Peaks (cm^{-1})		
3370 ± 20	3360 ± 40	3380 ± 20	3400 ± 40
3210 ± 40	3200 ± 40	3200 ± 40	3190 ± 50
(2955 ± 10)			
(2915 ± 10)			
(2850 ± 15)			
1620 ± 10	1618 ± 10	1615 ± 10	1615 ± 10
1182 ± 10	1180 ± 10	1180 ± 10	1180 ± 15
	1120 ± 10	1120 ± 5	1118 ± 10
1091 ± 5	1091 ± 5	1090 ± 5	1089 ± 5
1020 ± 5	1021 ± 5	1020 ± 5	1022 ± 10
	970 ± 5	970 ± 10	969 ± 10
882 ± 10	882 ± 5	880 ± 5	875 ± 10
785 ± 10	782 ± 5	782 ± 5	782 ± 10
	650 ± 15(?)		
625 ± 5	618 ± 10	615 ± 10	605 ± 10
505 ± 10	497 ± 10	494 ± 10	495 ± 10
473 ± 5	465 ± 10	463 ± 10	462 ± 10
410 ± 5	403 ± 5	403 ± 5	404 ± 5
	Regions (cm^{-1})		
3640-2500	3660-2500	3640-2540	3680-2580
1710-1550	1700-1520	1690-1550	1700-1560
1280- 370	1280- 330	1280- 350	1280- 370

( ) = hydrocarbon pump oil contaminant

Table 5.19 IR absorption peaks and regions of oxidised sulphate GR samples derived from 0.1 M $FeSO_4$.

invariably affects the crystal lattice. In addition, the IR spectra seems to show that the crystallinity of the samples decreases as IFFR increases.

It is to be noted that the NO^{3-} absorption peak at ~ 1380 cm^{-1} is now totally absent in the spectra shown in Fig 5.18. This suggests that the NO^{3-} groups are not an integrated part of the structure, and probably formed a volatile adsorption layer.

The IR spectra of the converted sulphate GR samples, mentioned in the previous section (5.2.1b), are shown in Fig 5.19. The corresponding absorption peaks and regions are given in Table 5.20. The spectrum of the aged sample of GR20 (aged in solution under anoxic, non-turbulent conditions) is essentially that of magnetite (see Fig 5.1 also) with goethite peaks at 889 and 792 cm^{-1}. Also, besides the small NO^{3-} peak at 1385 cm^{-1}, there is still some absorption in the sulphate region (~ 1220-1030 cm^{-1}). The aged sample of GR5 (aged in solution under moderately oxic, non-turbulent conditions) is a fairly crystalline goethite, again with absorption in the sulphate region.

The IR data presented so far show that the fundamental difference between pure goethites (and indeed Fe(III) oxides) and sulphate GRs is the presence of sulphate groups in the latter. There are also more water and OH

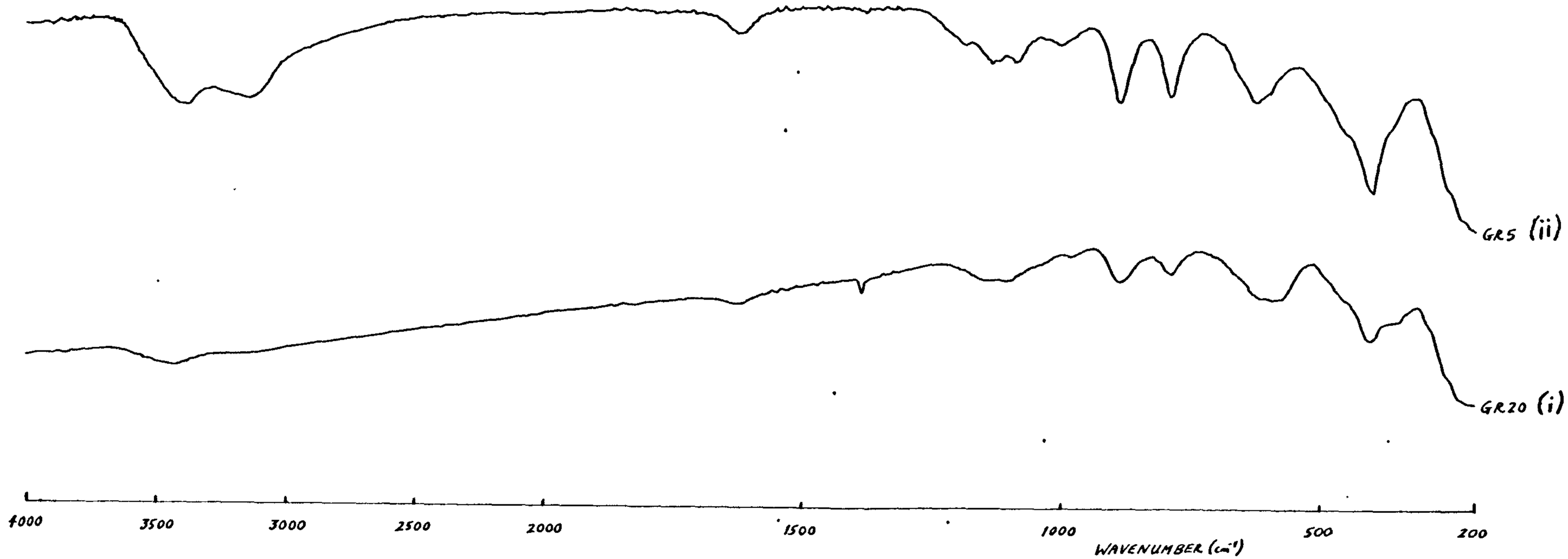

Fig 5.19 IR spectra of converted sulphate GR samples:
(i) aged under anoxic, non-turbulent conditions
(ii) aged under moderately oxic, non-turbulent conditions.

(i)Sample = GR20 IFFR = 1	(ii) Sample = GR5 IFFR = 4
Peaks (cm^{-1})	
3430 ± 40	3390 ± 30
	3140 ± 40
1625 ± 10	1618 ± 10
1385 ± 5	
	1197 ± 10
1145 ± 15	1130 ± 10
1104 ± 15	1084 ± 10
982 ± 10	998 ± 10
889 ± 5	884 ± 5
792 ± 5	788 ± 5
595 ± 15	620 ± 15
455 ± 15	448 ± 15
404 ± 10	398 ± 10
Regions (cm^{-1})	
3640-2300	3640-2460
1650- 310	1710-1550
	1270- 320

Table 5.20 IR absorption peaks and regions of aged sulphate GR samples:
(i) anoxic conditions
(ii) moderately oxic conditions.

groups in sulphate GRs. The IR data also indicate that the sulphate groups form an integral part of the GR structure since it is still present after oxidation and after ageing in solution. However, there remains the question as to whether the goethite and sulphate GR are separate phases or part of the same overall crystal structure.

5.2.1d Surface Area Measurements

The surface areas, as determined from linear BET plots, for the sulphate GRs synthesised from 0.1 M $FeSO_4$ are given in Table 5.21. Representative N_2 adsorption isotherms for the sulphate GR samples are shown in Fig 5.20. These are adsorption isotherms typical of Fe(II)-derived material rather than Fe(III)-derived material (Crosby, 1982; Crosby et al., 1983; Appendix A). The isotherms are all of Type IV which show hysteresis.

The surface areas of the sulphate GR samples are in the range 43-64 $m^2.g^{-1}$ which is low for iron oxides. Precipitates derived from Fe(III) material have surface areas in the range 159-234 $m^2.g^{-1}$ while those obtained from Fe(II) material are usually lower, being in the range 97-121 $m^2.g^{-1}$ (Crosby, 1982; Crosby et al., 1983). The work in this thesis support this view (see Appendix A). A well-crystalline goethite (Fig 1, Appendix A) was found to have an area of 148.7 $m^2.g^{-1}$ whilst two hydrous Fe oxides made from Fe(II) sources (basic Fe(II) salts) have areas of 64-76 $m^2.g^{-1}$. Also, surface area measurements of the dried, freshly-produced Fe(III) gel used in the synthesis experiments gave results of the order 370-378 $m^2.g^{-1}$ which is extremely high. These samples gave Type I isotherms with hysteresis loops (Fig 5.21)and therefore are indicative of microporous materials. Thus

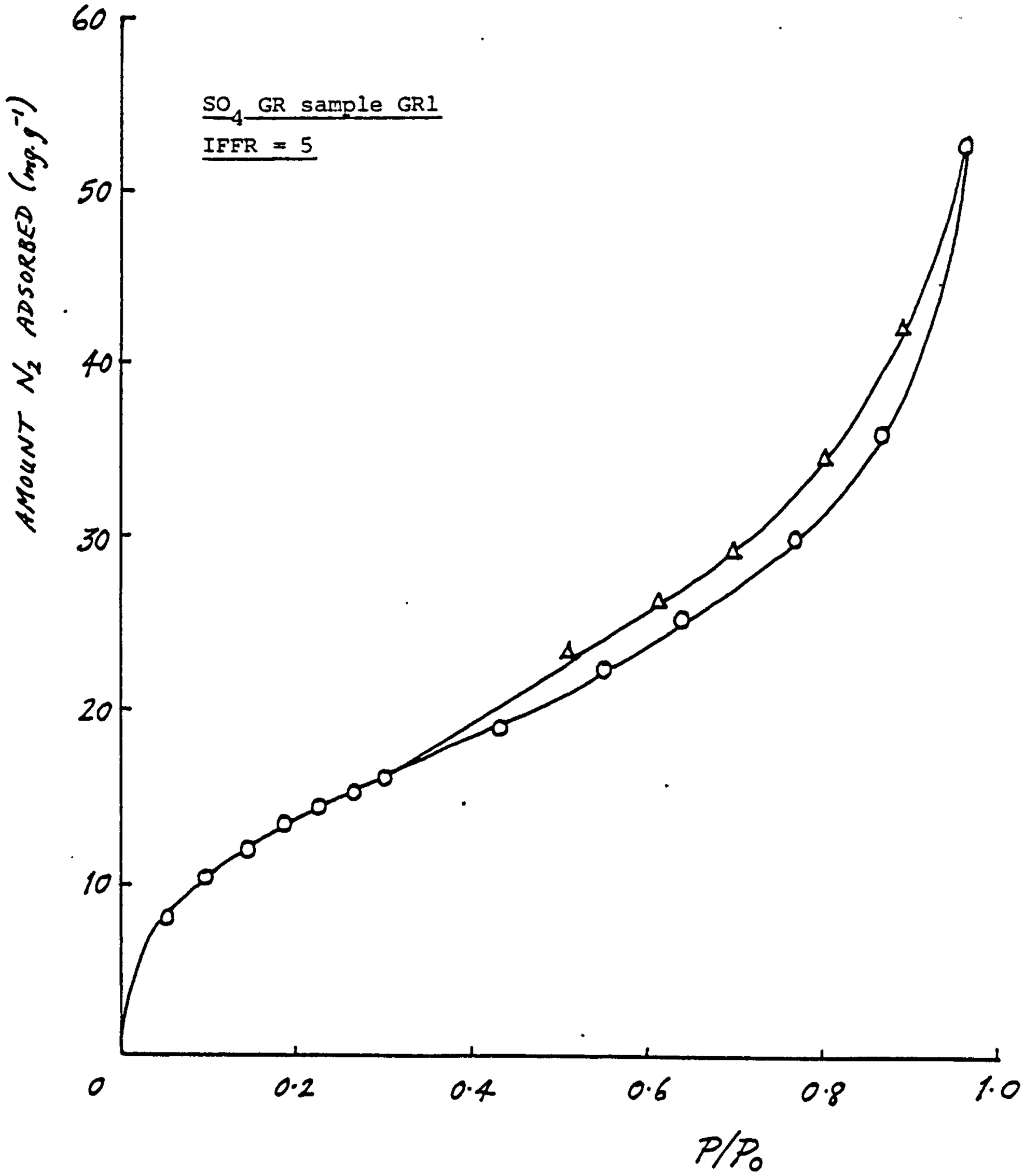

Fig 5.20 Typical N_2 adsorption isotherms of sulphate GRs derived from 0.1 M $FeSO_4$.

(O - adsorption Δ - desorption)

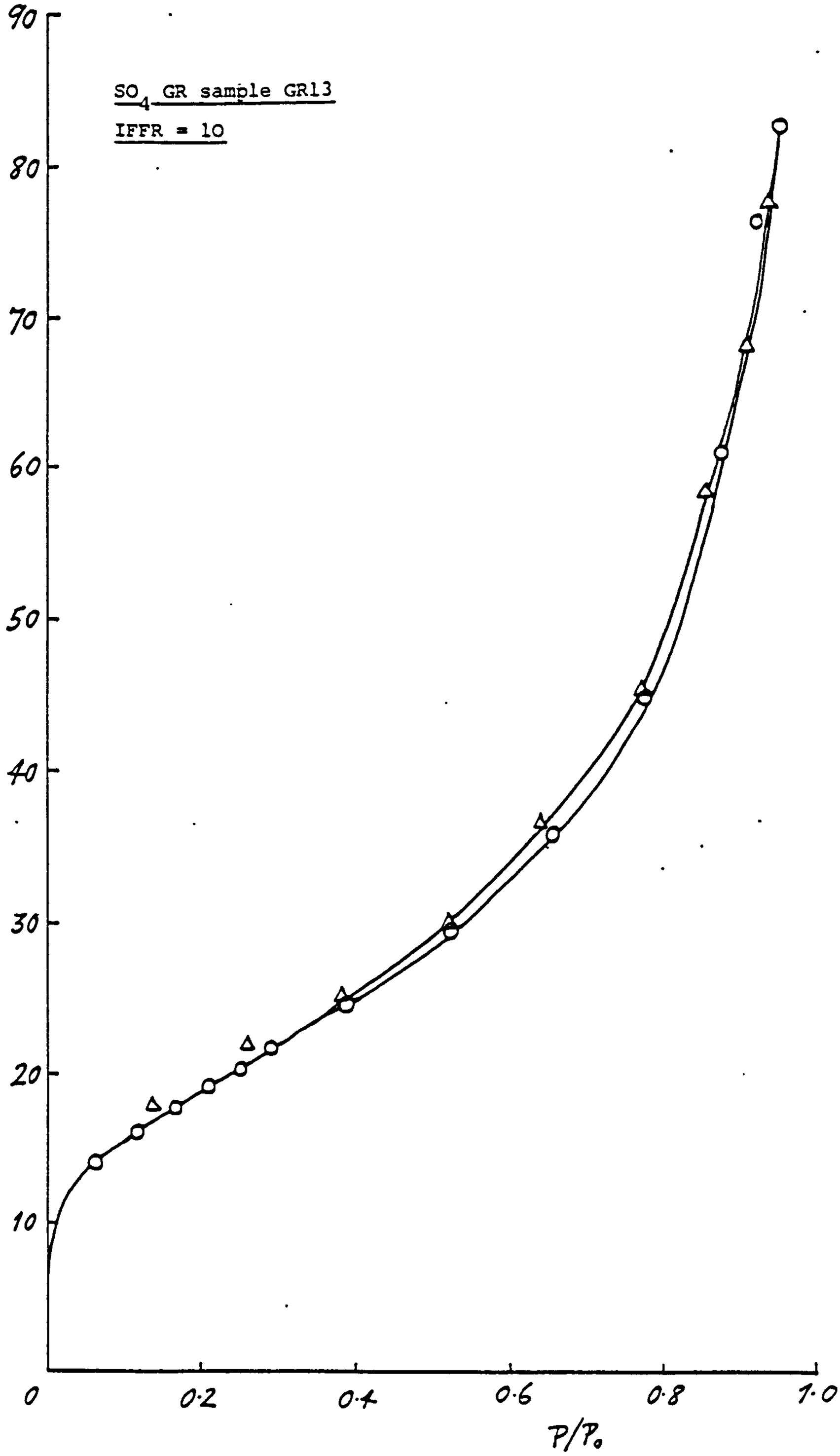

Fig 5.20 (cont'd) Typical N_2 adsorption isotherms of sulphate GRs derived from 0.1 M $FeSO_4$.

(O - adsorption Δ - desorption)

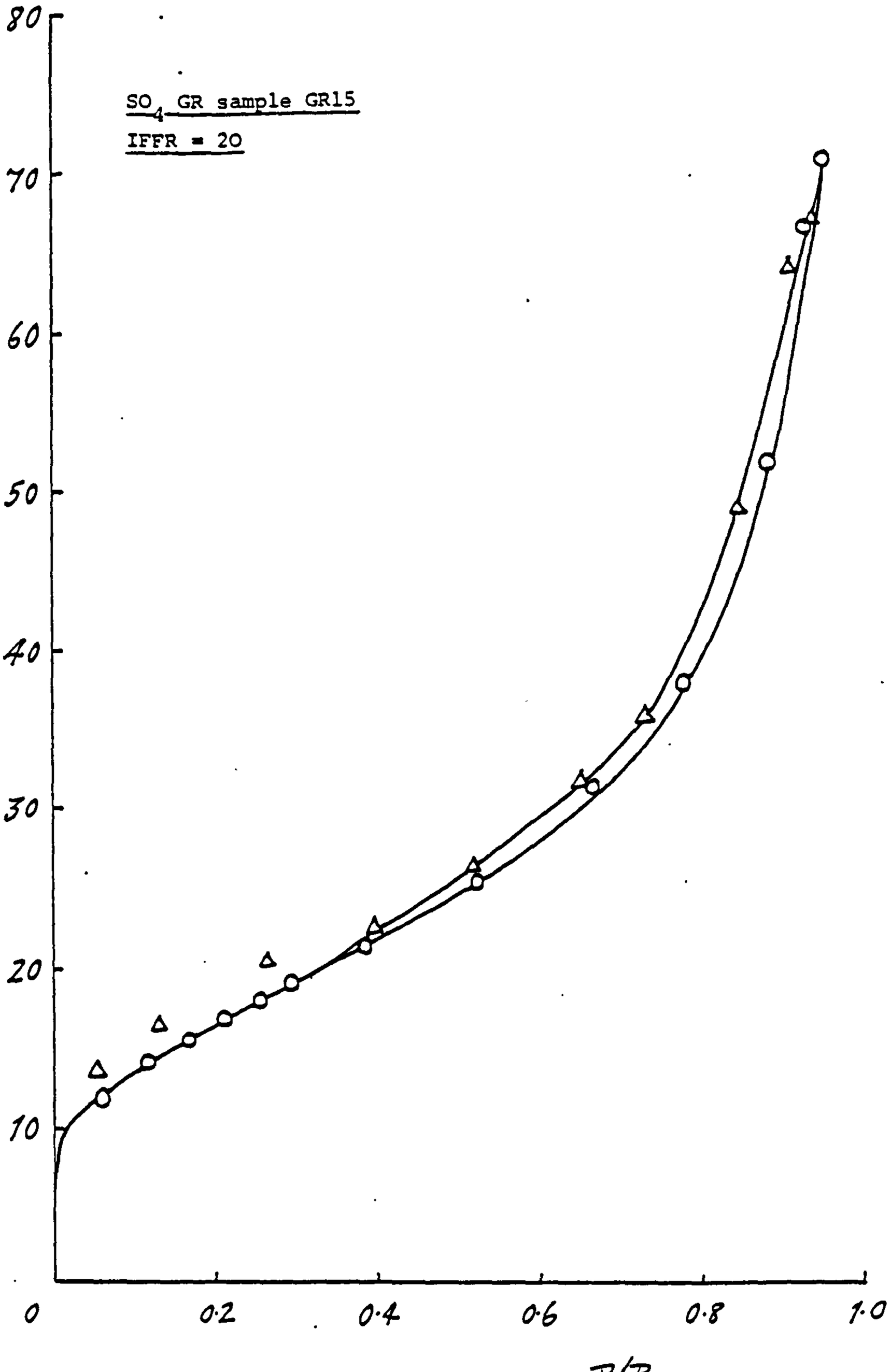

Fig 5.20 (cont'd) Typical N_2 adsorption isotherms of sulphate GRs derived from 0.1 M $FeSO_4$.

(O - adsorption Δ - desorption)

Sample	IFFR	<Fe(III)> (mmole)	Surface Area ($m^2.g^{-1}$)
GR20	1	20	42.7
GR1	5	5	43.7
GR2	5	5	43.0
GR13	10	2	55.3
GR14	20	1	63.6
GR15	20	1	49.2
GR21	40	0.5	55.5

<Fe(III)> = amount of Fe(III) gel

Table 5.21 Surface areas of sulphate GRs derived from 0.1 M $FeSO_4$.

Sample	IFFR	$[FeSO_4]_I$ (M)	Surface Area ($m^2.g^{-1}$)
GR3	2	0.05	51.7
GR4	2	0.05	55.2
S23-3-83	1	0.025	98.3
S21-3-83	0.4	0.01	92.6

<Fe(III)> = 5 mmoles

Table 5.22 Surface areas of sulphate GRs and non-GRs derived from < 0.1 M $FeSO_4$.

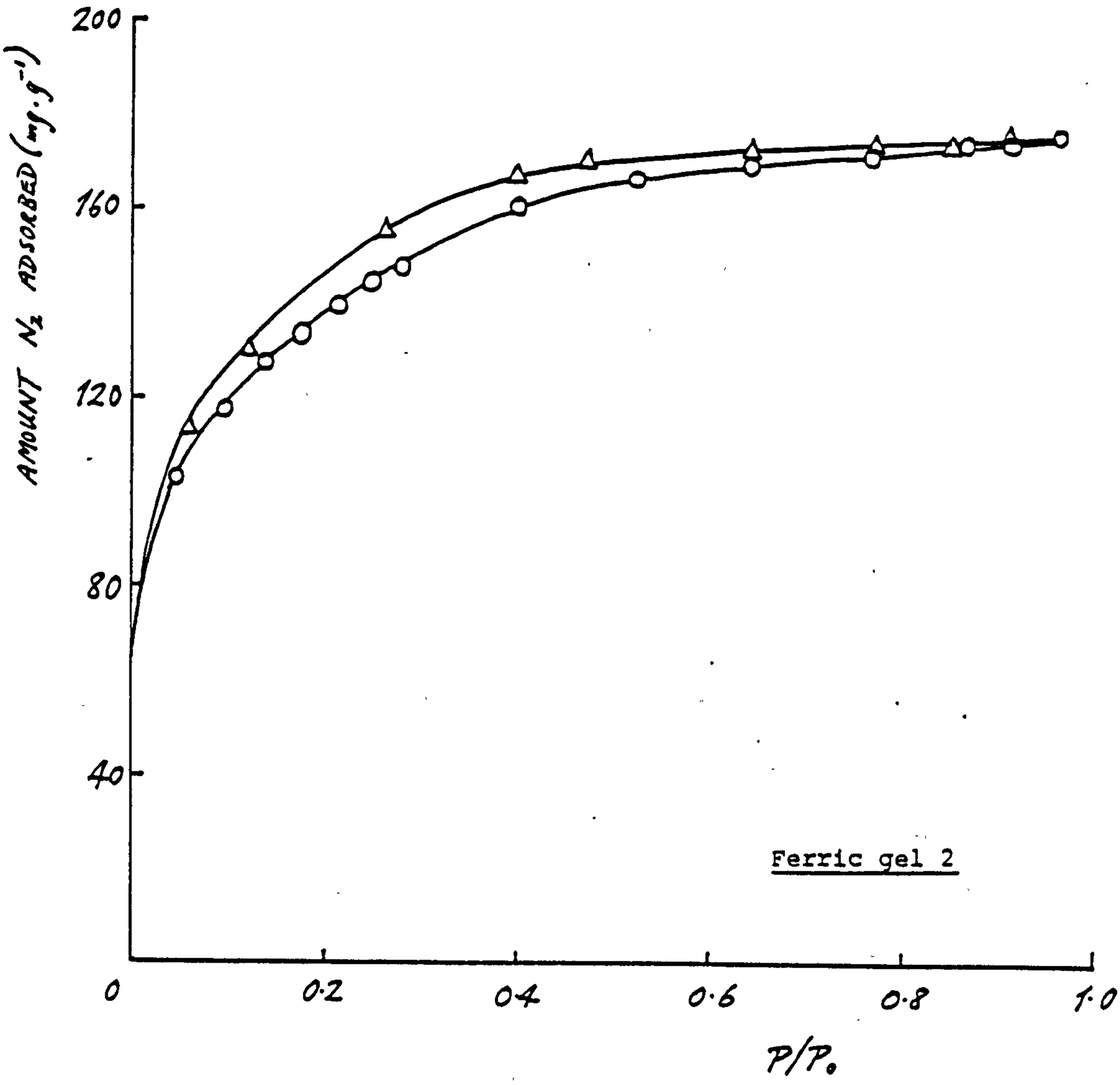

Fig 5.21 N_2 adsorption isotherm of Fe(III) gel sample. (Ferric gel 2 - made from $Fe(NO_3)_3.9H_2O$)

(O - adsorption Δ - desorption)

the fact that the sulphate GR samples have considerably lower surface areas than what would be expected from corresponding mixtures of Fe(II)- and Fe(III)-derived oxides, suggests that the samples are markedly different from those of the materials from which they have been produced, as confirmed by XRD. It is to be noted also that the shape of the adsorption isotherms for the sulphate GRs is similar to that for the aforementioned goethite. The difference is in the degree of N_2 adsorption.

The work in Appendix A show that if <Fe(III)> is kept constant, then the surface area apparently increases with decreasing $[FeSO_4]_I$. Table 5.22 gives the surface area for the non-GR samples synthesised from varying $[FeSO_4]_I$. the samples termed "Green Rust B", "green rust A" and "green rust B" in Appendix A are, respectively, samples GR4, S23-3-83 and S21-3-83 in Table 5.22. The increase in surface area can be explained if it is assumed that adsorption of Fe^{2+} cations (and SO_4^{2-} anions) reduces available surface sites. Thus at low $[FeSO_4]_I$, there are less ions in solution and so less ions are adsorbed. Therefore, there are more surface sites left unused and results in a larger surface area. The corroborating evidence can be seen in Appendix B where $<Fe(II)>_{aq}$ decreases with decreasing $[FeSO_4]_I$.

The existence of a hysteresis loop for the Type IV isotherms shows that the samples are porous. The pore size distributions for the Type IV materials, as estimated from the hysteresis closure points and using equation 2.23, are given in Table 5.23. The lower closure points on half of the samples cannot be determined because the desorption points at the low relative pressure end have long equilibrium times, and thus the hysteresis loop does not close experimentally. This is probably caused by microporosity in the material which makes the desorption process difficult.

It can be seen from Table 5.23 that the pore sizes in the sulphate GR samples are in the mesopore range (20-500 A diameter) with some samples having micropores (< 20 A diameter) as well. The shape of the hysteresis loop conforms most closely to type B in the de Boer classification (de Boer, 1958). This type of hysteresis is associated with either slit-shaped pores or the space between parallel plates.

Sample	IFFR	Hysteresis Closure P/P_o (approx.)	Pore Size Range, d (A)
GR20	1	0.30 - 0.90	30 - 200
GR1	5	0.30 - 0.95	30 - 400
GR2	5	* - 0.85	* - 140
GR13	10	0.35 - 0.95	30 - 400
GR14	20	* - 0.95	* - 400
GR15	20	0.30 - 0.95	30 - 400
GR21	40	* - 0.95	* - 400

* indicates that lower limit cannot be determined

Table 5.23 Pore size distributions for sulphate GRs derived from 0.1 M $FeSO_4$.

5.2.1e Mossbauer Spectroscopy

Before discussing the various aspects of the Mossbauer data, a reminder of the different types of Mb samples is given here. First, there is the unwashed, wet, freshly-produced sulphate GR material which was put immediately onto the Mb spectrometer at 77 K. Second, there is the precipitate left to stand overnight (because of time considerations) and so has aged somewhat. Samples of this aged overnight (or simply aged) material was put on the Mb spectrometer at 77 K in the wet state (usually unwashed). The rest of the aged material was washed and vacuum-dried, and used subsequently for the Mb spectrometer and the other analyses. The samples prepared for the 4.2 K work at AERE Harwell were usually fresh precipitates (unwashed) which were stored in liquid N_2. Thus there are basically three types of Mb samples: (i) wet, fresh material (ii) wet, aged material and (iii) dried, aged material. The previous sections (XRD, IRS and surface area measurements) have dealt with the last category, so there will probably be some subtle differences between some of the Mb analysis and the other analytical techniques.

1) Sulphate GRs synthesised from 0.1 M $FeSO_4$

(i) 77 K data

The Mb parameters at 77 K for the wet, fresh material of sulphate GRs derived from 0.1 M $FeSO_4$ are given in Table 5.24. Typical spectra at 77 K of the wet, fresh precipitates are shown in Fig 5.22. It can be seen that, in general, the spectra are composed of three components:

(i) an Fe(III) quadrupole doublet

(ii) an Fe(II) quadrupole doublet and

(iii) an Fe(III) magnetic hyperfine splitting (MHS) with a small quadrupole interaction.

The exception to this is sample GR20 (IFFR = 1) which has virtually no Fe(III) MHS. The rest of the samples have a substantial magnetic component which vary from sample to sample. In addition, a few spectra show the presence of an extra Fe(II) quadrupole doublet which is probably due to $FeSO_4$ (e.g. sample GR16 where IS = 1.51 mms^{-1} and QS = 3.40 mms^{-1} for this $FeSO_4$-type doublet).

The Fe(II) and Fe(III) quadrupole doublets have values of IS and QS which are invariant over the whole range of IFFR investigated. The Fe(II) doublet has an IS of 1.26 $\pm$ 0.10 mms^{-1} (relative to Fe) and a QS of 2.93 $\pm$ 0.05

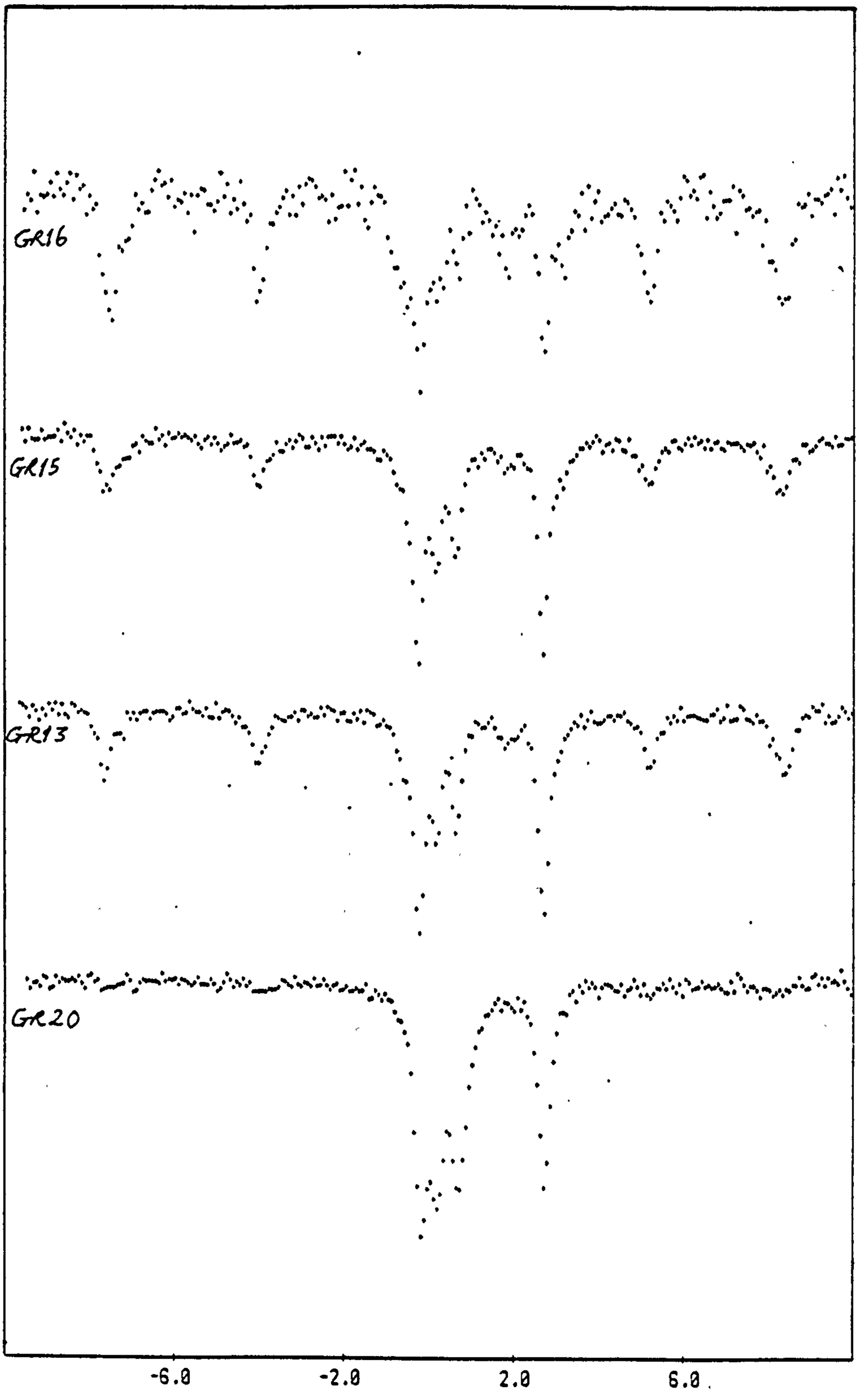

Fig 5.22 Typical 77 K Mb spectra of the wet, fresh precipitate of sulphate GRs derived from 0.1 M $FeSO_4$.

Sample	IFFR	Fe(II) doublet			Fe(III) doublet			MHS			FFR
		δ	Δ	$\frac{1}{2}\Gamma$	δ	Δ	$\frac{1}{2}\Gamma$	δ	Δ	B	
GR20	1	1.28	2.90	0.15	0.45	0.50	0.20				0.88
GR5	4	1.26	2.93	0.14	0.44	0.47	0.14	0.47	-0.24	49.6	1.86
GR1	5	1.26	2.90	0.20	0.46	0.48	0.19	0.44	-0.30	48.6	1.78
GR2	5	1.26	2.91	0.19	0.46	0.45	0.18	0.48	-0.23	49.3	2.34
GR13	10	1.26	2.93	0.16	0.43	0.46	0.13	0.46	-0.22	49.6	2.51
GR14	20	1.26	2.96	0.14	0.44	0.43	0.15	0.47	-0.24	49.7	2.14
GR15	20	1.24	2.94	0.14	0.45	0.42	0.14	0.47	-0.23	49.2	2.03
GR16	40	1.26	2.94	0.15	0.48	0.48	0.14	0.51	-0.17	49.0	2.41
GR21	40	1.27	2.94	0.18	0.45	0.45	0.16	0.49	-0.23	49.3	2.33
Mean		1.26	2.93	0.16	0.45	0.46	0.16	0.47	-0.23	49.3	

FFR = Fe(II)-Fe(III) ratio
All Mb parameters in mms^{-1} except B (T)

Table 5.24 77 K Mb parameters for the wet, fresh precipitate of sulphate GRs derived from 0.1 M $FeSO_4$.

mms^{-1}, while the Fe(III) doublet has IS = 0.45 ± 0.10 mms^{-1} and QS = 0.46 ± 0.05 mms^{-1}. These values are very similar to the quadrupole components of basic $FeSO_4$ samples which have parameters of: (i) Fe(II) doublet:- IS = 1.24 ± 0.10 mms^{-1}, QS = 2.92 ± 0.05 mms^{-1}; and (ii) Fe(III) doublet:- IS = 0.43 ± 0.10 mms^{-1}, QS = 0.47 ± 0.05 mms^{-1}. [Basic $FeSO_4$ has a chemical formula of $Fe(OH)_2.xFeSO_4$, where x = a variable (Glasson, private comm.).] There is normally no MHS present in the Mb spectra of basic $FeSO_4$ samples (see Fig 5.23 for a typical 77 K spectrum). The similarity between the sulphate GRs and basic $FeSO_4$ is not altogether surprising since , in essence, the GR synthesis process is a modification of the process of precipitation of basic $FeSO_4$. The Fe(III) gel was added at pH 7 before the onset of large-scale precipitation of basic $FeSO_4$ (which occurs at pH > 7.5). Since the sulphate GRs are more stable than the basic $FeSO_4$ precipitates, this means that the Fe(III) gel acts as a surface to stabilise the precipitated Fe(II). Also, since the basic $FeSO_4$ do not have any MHS, then the magnetic component in the sulphate GRs must originate from the Fe(III) gel.

The Fe(II)/Fe(III) ratio (or FFR) of the two main quadrupole components varies from 0.88 to 2.51, but there is no correlation with IFFR. The magnetic phase had a

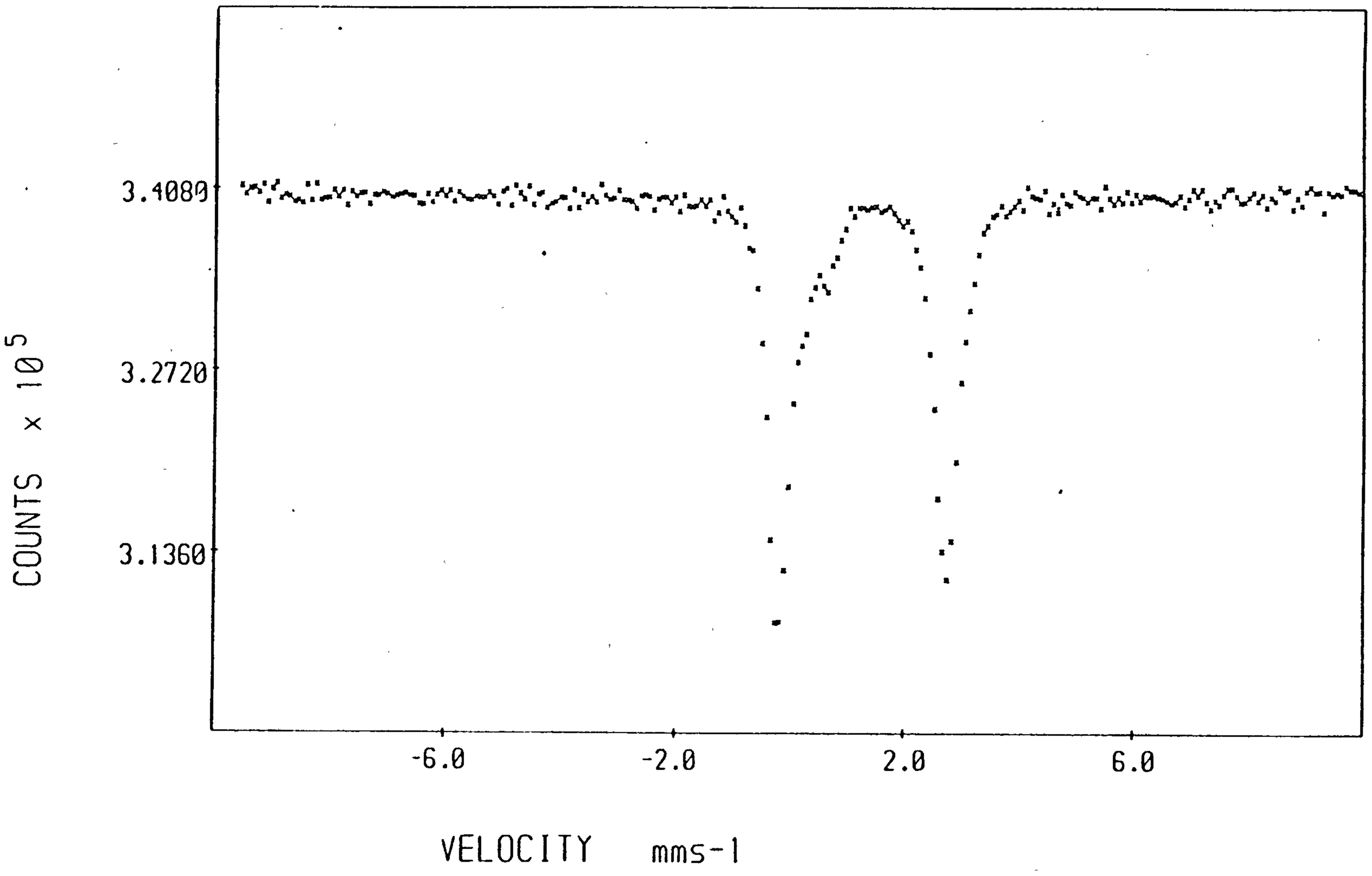

Fig 5.23 77 K Mb spectrum of a basic $FeSO_4$ sample.

magnetic field of B = 48.6–49.7 T and a small quadrupole perturbation of -0.23 ± 0.10 mms^{-1}. These parameters are very similar to those for goethite (see Tables 3.1 & 5.1). Since XRD and IRS show that the dried, aged material consisted of both sulphate GR and goethite phases, it is reasonable to assume that the quadrupole components arise from the sulphate GR phase and the MHS originate from the goethite phase.The relative sharpness and symmetry of the lines of the quadrupole doublets and those of the MHS (in most spectra) indicate that the components arise from fairly ordered material.

While the IS and QS for the paramagnetic Fe(II) and Fe(III) components are constant over the range of IFFR studied, the same cannot be said of the FFR or the MHS. These vary from sample to sample and there is no correlation with IFFR. This is probably because the variables involved in each synthesis experiment (e.g. initial temperature and pH of solutions, ionic concentration, time taken, purity of Fe(II) salts, total amount of alkali added, agitation rate, etc.) are many and so the end-products will differ from synthesis to synthesis. However, it appears on the whole that the amount of magnetic component (as determined by the intensity of the Mb lines) relative to the Fe(II) and Fe(III) quadrupole components, increases with IFFR. One of the factors affecting the quantity of magnetic component is probably the time taken for the syntheses.

For example, samples GR2 & GR5 were produced in relatively short synthesis experiments (~ 1.5-2.8 h), and have relatively large amounts of the magnetic component which does not fit in with the trend.

The Fe(III) quadrupole component in the sulphate GR can be reasonably assumed to have arisen from the starting Fe(III) gel material. Now while wet, freshly-produced Fe(III) gel has a similar IS at 77 K (0.45 mms^{-1}) to that of the Fe(III) component, the QS is slightly higher at ~ 0.7 mms^{-1} (compared to 0.46 mms^{-1}). This is the value normally associated with amorphous Fe(III) oxides (see Table 5.1 and Bowen, 1979). The halfwidth ($1/2\Gamma$) is also slightly larger, being 0.22 mms^{-1} for the gel compared to 0.16 mms^{-1} for the Fe(III) doublet in the GR. This suggests that the Fe(III) gel has been modified during the course of sulphate GR synthesis, and implies that it has been incorporated into some kind of structure. The modification of the Fe(III) gel is not surprising since Fe^{2+} (and SO_4^{2-}) ions were adsorbed onto the gel surface, and so would alter the EFG around the Fe^{3+} cations in the gel. As mentioned previously, the XRD data in conjunction with the MbS data implies that the Fe(III) gel must be a part of the sulphate GR phase, and further support is given by the surface area measurements (section 5.2.1d), which showed that the sulphate GR has a low surface area (43-64 $m^2.g^{-1}$) whereas Fe(III) gel has a large surface

area (~ 380 $m^2.g^{-1}$). In addition, the 77 K Mb spectrum of the wet, fresh precipitate of sample S7-2-83 (Fig 5.24) show that when Fe(III) gel was added to a 0.1 M solution of $FeSO_4$, under the same conditions used in the sulphate GR synthesis but without pH maintenance, only crystalline goethite was produced (confirmed by XRD - see section 5.2.1b). Similar results were obtained by Chukhrov et al. (1972) who established that, under the influence of Fe(II) anions at pH < 7, ferrihydrite transformed into goethite. In sample S7-2-83, the pH of the $FeSO_4$ solution was always less $\leq$ 7. With pH maintenance, sulphate GR was produced and the Fe(III) doublet was present in the spectrum along with the Fe(III) MHS. Thus the paramagnetic Fe(III) must be a part of the GR structure since it would otherwise convert to goethite, and hence not show up in the Mb spectrum. The spectrum in Fig 5.24 also shows the presence of an Fe(II) component. This must be surface-adsorbed Fe(II) since amorphous Fe(III) oxides and goethite are known to adsorb metal cations (Chukhrov et al., 1972; Forbes et al., 1974 & 1976; Schwertmann & Taylor, 1977)

On ageing overnight, the behaviour of the magnetic component in the wet precipitate seems to depend on IFFR. At IFFR $\leq$ 5, the amount of goethite increases on ageing overnight and seems to be more crystalline (sharper; more intense MHS with a slightly increased field magnitude - Fig 5.25. Indeed for sample GR20 (IFFR = 1), the increase

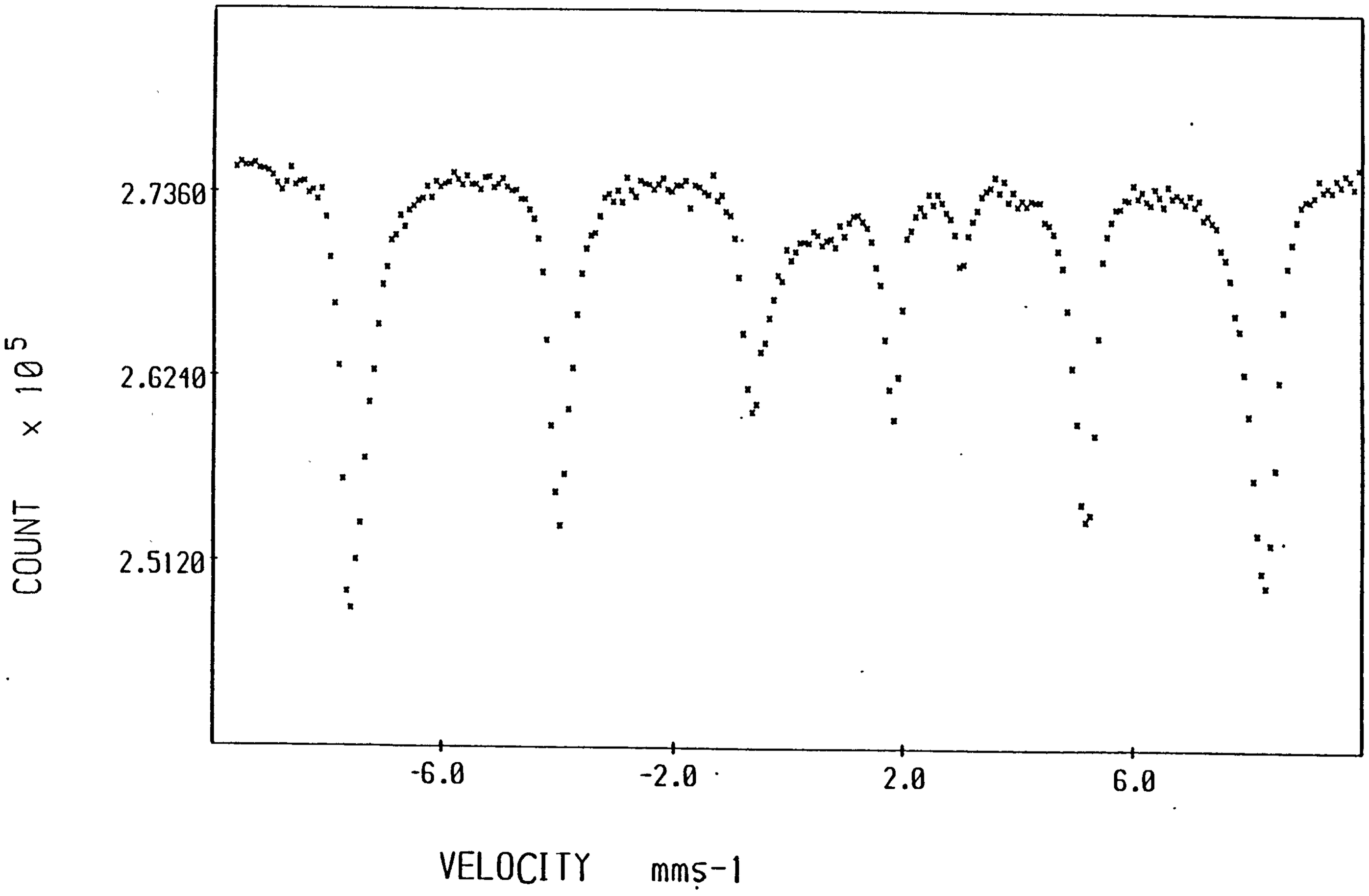

Fig 5.24 77 K Mb spectrum of the wet, fresh precipitate of non-GR sample S7-2-83.

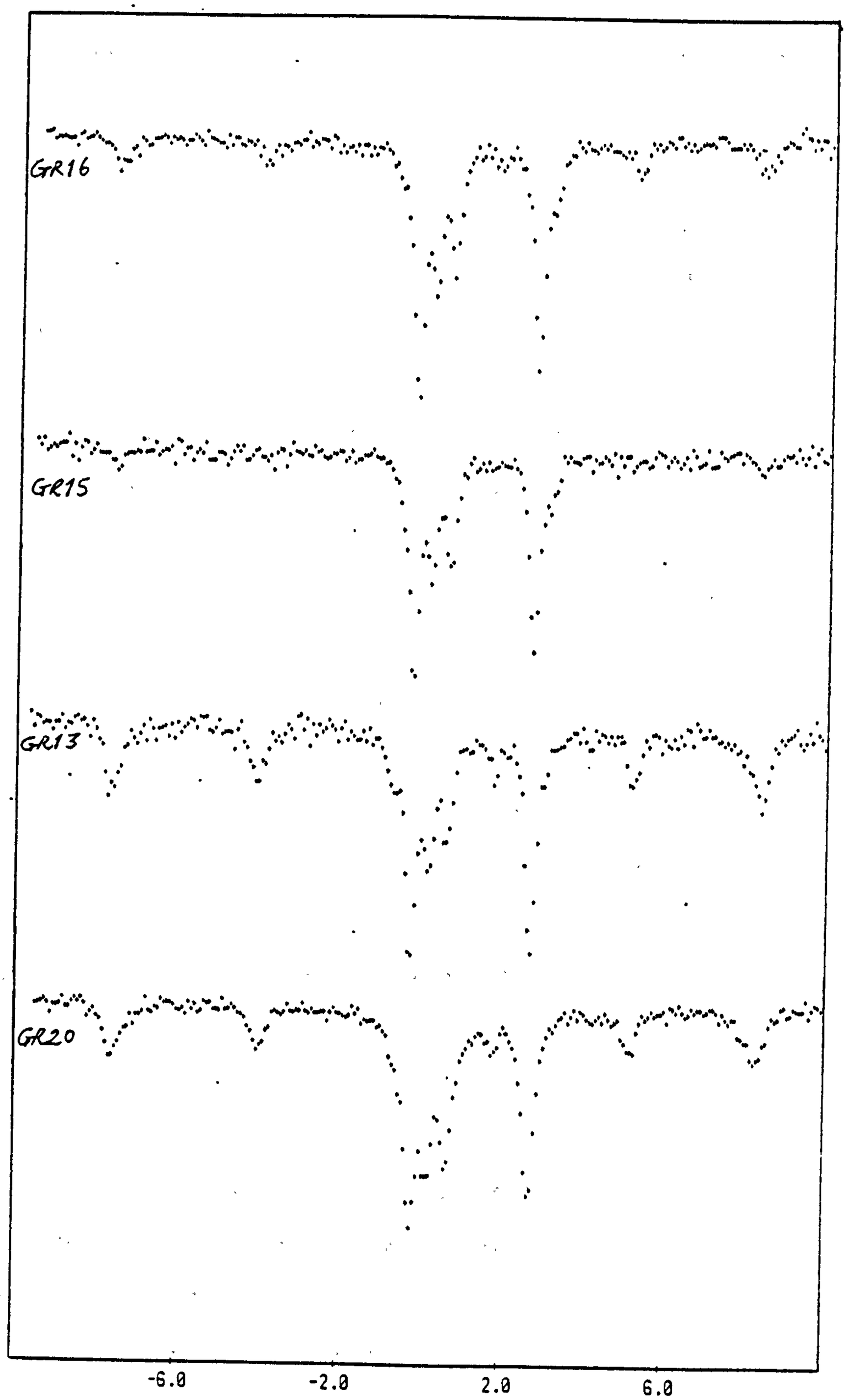

Fig 5.25 Typical 77 K Mb spectra of the wet, aged precipitate of sulphate GRs derived from 0.1 M $FeSO_4$.

is dramatic since there is virtually no trace of a magnetic component in the fresh material. At IFFR $\geq$ 10, the behaviour is reversed i.e. the amount of goethite decreases on ageing overnight. The decrease is most significant in samples GR15 & GR16, and indeed in sample GR15, the decrease is almost down to zero. A similar behaviour also occurs for the FFR. At IFFR $\leq$ 5, the FFR increases on ageing overnight, while at IFFR $\geq$ 10, the FFR decreases (Table 5.25). (Although the direct evidence in the range 1 $\leq$ IFFR $\leq$ 5 is scant, nevertheless the previous statements are valid because the dried, aged material for sample GR1 (IFFR = 5) show an increase in both the magnetic component and the FFR (1.78 -> 1.94).) This behaviour parallels that of the MHS and is therefore connected. There is no correlation between the changes in FFR and Fe(II) uptake since the AAS data for the aged overnight samples (not mentioned in section 5.2.1a) do not show this. A discussion of the changes in MHS and FFR is given in the conclusions chapter (Chapter 6).

The 77 K Mb parameters for the wet, aged material of the sulphate GRs derived from 0.1 M $FeSO_4$ are presented in Table 5.26. The IS and QS for the quadrupole doublets remain virtually the same for the wet, aged material [Fe(III) doublet: IS = 0.44 $\pm$ 0.10 mms^{-1}, QS = 0.45 $\pm$ 0.05 mms^{-1}; Fe(II) doublet: IS = 1.25 $\pm$ 0.10 mms^{-1}, QS = 2.94 $\pm$ 0.05 mms^{-1}].

Sample	IFFR	FFR	
		Fresh	Wet, aged
GR20	1	0.88	1.49
GR5	4	1.86	
GR1	5	1.78	
GR2	5	2.34	
GR13	10	2.51	2.21
GR14	20	2.14	2.00
GR15	20	2.03	1.94
GR16	40	2.41	2.23
GR21	40	2.33	

Table 5.25 Comparison of the 77 K FFRs between fresh and aged material for the sulphate GRs derived from 0.1 M $FeSO_4$.

Sample	IFFR	Fe((II) doublet			Fe(III) doublet			MHS			FFR
		δ	Δ	$\frac{1}{2}\Gamma$	δ	Δ	$\frac{1}{2}\Gamma$	δ	Δ	B	
GR20	1	1.27	2.92	0.17	0.45	0.47	0.18	0.49	-0.30	49.2	1.49
GR13	10	1.24	2.94	0.16	0.43	0.43	0.16	0.47	-0.20	49.7	2.21
GR14	20	1.24	2.94	0.14	0.43	0.46	0.15	0.47	-0.29	49.4	2.00
GR15	20	1.24	2.95	0.14	0.42	0.47	0.14				1.94
GR16	40	1.28	2.94	0.15	0.46	0.44	0.14	0.50	-0.21	49.1	2.23
Mean		1.25	2.94	0.15	0.44	0.45	0.15	0.48	-0.25	49.4	

Table 5.26 77 K Mb parameters for the wet, aged precipitate of sulphate GRs derived from 0.1 M $FeSO_4$.

Sample	IFFR	Fe(II) doublet			Fe(III) doublet			MHS			FFR
		δ	Δ	$\frac{1}{2}\Gamma$	δ	Δ	$\frac{1}{2}\Gamma$	δ	Δ	B	
GR20	1	1.26	2.93	0.17	0.44	0.43	0.16	0.49	-0.22	49.2	1.84
GR1	5	1.27	2.93	0.20	0.46	0.50	0.20	0.49	-0.25	49.0	1.94
GR2	5	{1.28	2.87	0.19	0.48	0.61	0.23	0.46	-0.23	49.3	0.90}
GR13	10	{1.24	2.78	0.21	0.43	0.63	0.20	0.45	-0.24	49.5	0.82}
GR14	20	{1.28	2.78	0.18	0.47	0.61	0.18	0.49	-0.27	49.2	0.83}
GR15	20	{1.24	2.83	0.20	0.42	0.61	0.19	0.45	-0.25	48.9	1.00}
GR16	40	{1.28	2.79	0.17	0.46	0.59	0.18	0.51	-0.23	49.1	1.18}
Mean		1.26	2.84	0.19	0.45	0.57	0.19	0.48	-0.24	49.2	

{ } = partially oxidised material

Table 5.27 77 K Mb parameters for the dried, aged precipitate of sulphate GRs derived from 0.1 M $FeSO_4$.

With the drying of the aged precipitate, the magnetic phase was present in all the sulphate GR samples and had increased intensity. Most of the sulphate GR were partially oxidised by the vacuum-drying process, as evident by the decreased FFR values (Table 5.27). While the ISs remain more or less the same, the QS increases for the Fe(III) doublet (0.45 -> 0.61 mms^{-1}) but decreases for the Fe(II) doublet (2.93 -> 2.84 mms^{-1}). This change in the QS is probably due to oxidation rather than the drying process because, on complete oxidation, the Fe(III) QS increases further (-> 0.69 mms^{-1}) and, also, the curvefitting tends to require the use of two Fe(III) doublets (the outer doublet, labelled $Fe(III)_2$, has IS = 0.46 mms^{-1} and QS = 1.09 mms^{-1} :- see Table 5.28). However, it is very difficult to differentiate between the two causes, since it can be argued equally that not all the water was removed on initial vacuum-drying. Indeed, the two processes may be related.

Typical 77 K spectra of the dried sulphate GR samples (not completely oxidised) are shown in Fig 5.26. These have more or less the same pattern as the spectra for the fresh and wet, aged material except for the contribution from the oxidised Fe(II) component which has superimposed itself on the original Fe(III) doublet, resulting in the increased halfwidth (0.15 -> 0.20 mms^{-1}) for the Fe(III) doublet. The magnetic hyperfine peaks show some

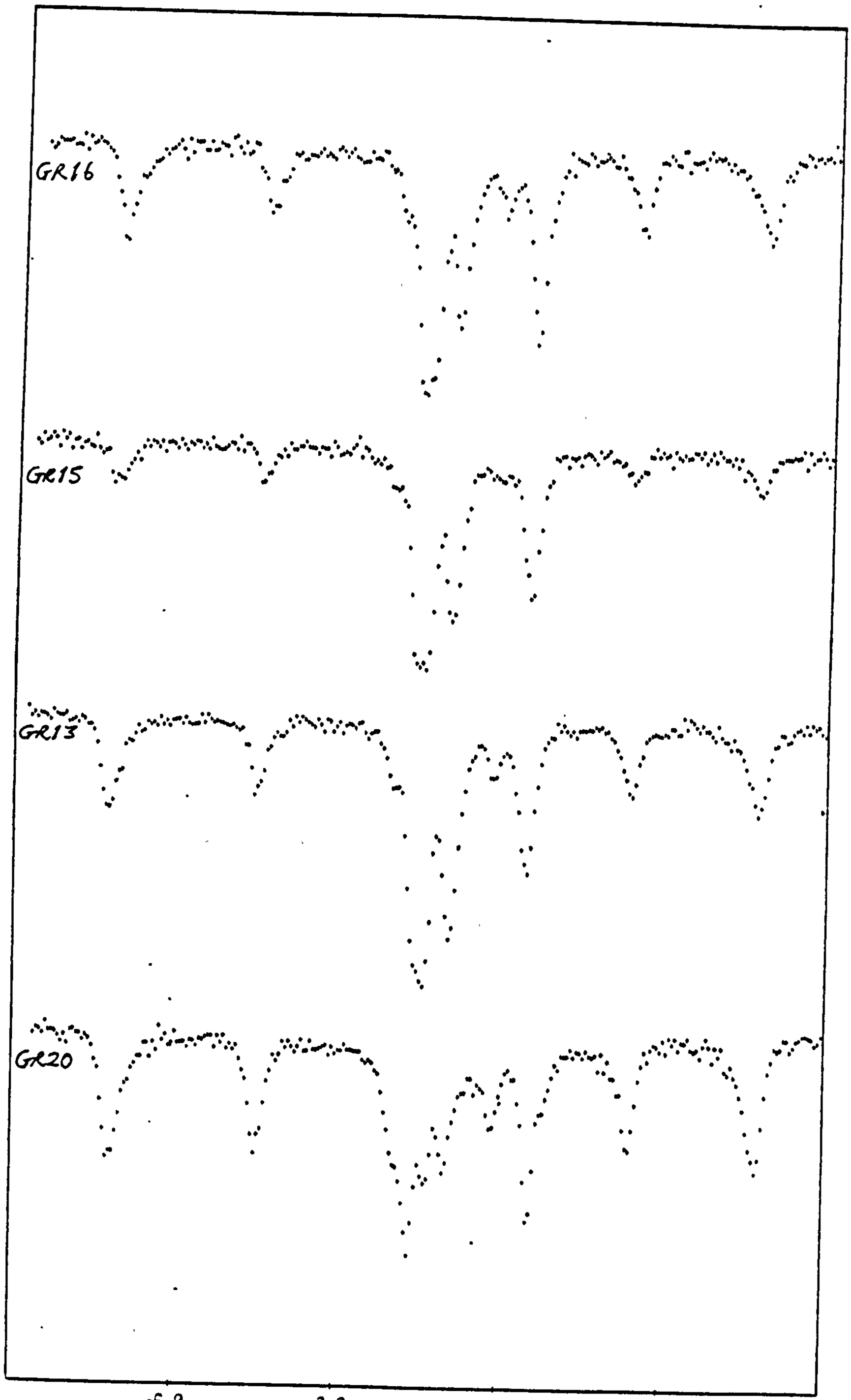

Fig 5.26 Typical 77 K Mb spectra of the dried, aged precipitate of sulphate GRs derived from 0.1 M $FeSO_4$.

Sample	IFFR	$Fe(III)_1$ doublet			$Fe(III)_2$ doublet			MHS		
		δ	Δ	$\frac{1}{2}\Gamma$	δ	Δ	$\frac{1}{2}\Gamma$	δ	Δ	B
GR1	5	0.45	0.70	0.22	0.44	1.08	0.21	0.44	-0.28	48.9
GR2	5	0.42	0.69	0.21				0.48	-0.24	49.3
GR13	10	0.47	0.69	0.20	0.49	1.10	0.21	0.47	-0.25	49.3
Mean		0.45	0.69	0.21	0.46	1.09	0.21	0.46	-0.26	49.2

Table 5.28 77 K Mb parameters for the dried, aged & oxidised precipitate of some sulphate GRs derived from 0.1 M $FeSO_4$.

Sample	IFFR	Fe(II) doublet			Fe(III) doublet			FFR
		δ	Δ	$\frac{1}{2}\Gamma$	δ	Δ	$\frac{1}{2}\Gamma$	
GR1	5	1.17	2.52	0.33	0.35	0.66	0.23	0.42
GR2	5				0.35	0.64	0.20	
GR13	10				0.35	0.66	0.20	
					(0.39	1.09	0.24)	
GR5*	4	1.16	2.60	0.20	0.33	0.50	0.14	2.45
GR14*	20	1.15	2.66	0.20	0.34	0.36	0.20	1.76

* Wet material: GR5-fresh, GR14-aged (others are dried, aged material)
( ) = 2nd Fe(III) doublet, labelled $Fe(III)_2$

Table 5.29 RT Mb parameters for the aged precipitate of some sulphate GRs derived from 0.1 M $FeSO_4$.

asymmetry, indicating that there may be a distribution of fields rather than a single field.

The 77 K Mb spectra of the fully oxidised, dried material usually consist only of the Fe(III) quadrupole doublet(s) and the Fe(III) MHS.

(ii) RT data

Most of the RT Mb spectra were taken using the dried, aged precipitate. These were hampered by the oxidation of the samples during the course of spectrum accumulation, resulting in line distortion and poor statistics for the Fe(II) doublet. Compounding this was the relaxation of the MHS due to small particle size. There were no adequate facilities on the Mb spectrometer to prevent oxidation from occurring. In any case, it seems that, once oxidation has been initiated in the dried material, the oxidation continued until completion, and nothing short of freezing at low temperatures would prevent this from happening. Nevertheless, a few good spectra were obtained for both wet and dried precipitates, from which the Mb parameters were extracted. In fact the best RT spectrum was for a wet, fresh precipitate (sample GR5), and this was taken at AERE Harwell using their much stronger ^{57}Co source. A shorter accumulation time has resulted in better statistics and the strong presence

of the Fe(II) doublet. The fact that the precipitate was wet meant probably that the entire volume of the sample holder was taken up, thus reducing the chances of oxidation. This spectrum is shown in Fig 5.27. Magnetic relaxation is evident in all the samples, showing that the goethite was fine-grained. The RT Mb parameters for some of the sulphate GRs are given in Table 5.29.

The data is somewhat limited, and there seems to be a slight difference between the wet and dried material. However, it can be said that the Fe(III) doublet (inner) has IS = 0.35 ± 0.10 mms^{-1} and QS = 0.65 ± 0.07 mms^{-1} for the dried material. These values are in keeping with amorphous Fe(III) oxides such as ferrihydrite and Fe(III) gels (Table 5.1; Bowen, 1979). The wet material has a similar IS but the QS shows less distortion (reflected in the FFRs as well). The Fe(II) doublet has an IS = 1.16 ± 0.10 mms^{-1} for both dried and wet material but there seems to be a slight difference in the QS (2.63 ± 0.07 mms^{-1} for wet precipitate but 2.52 ± 0.07 mms^{-1} for the dried material). Most of the MHSs cannot be determined except for sample GR2 where IS = 0.38 ± 0.10 mms^{-1}, QS = -0.23 ± 0.10 mms^{-1} and B = 33.7 ± 0.5 T.

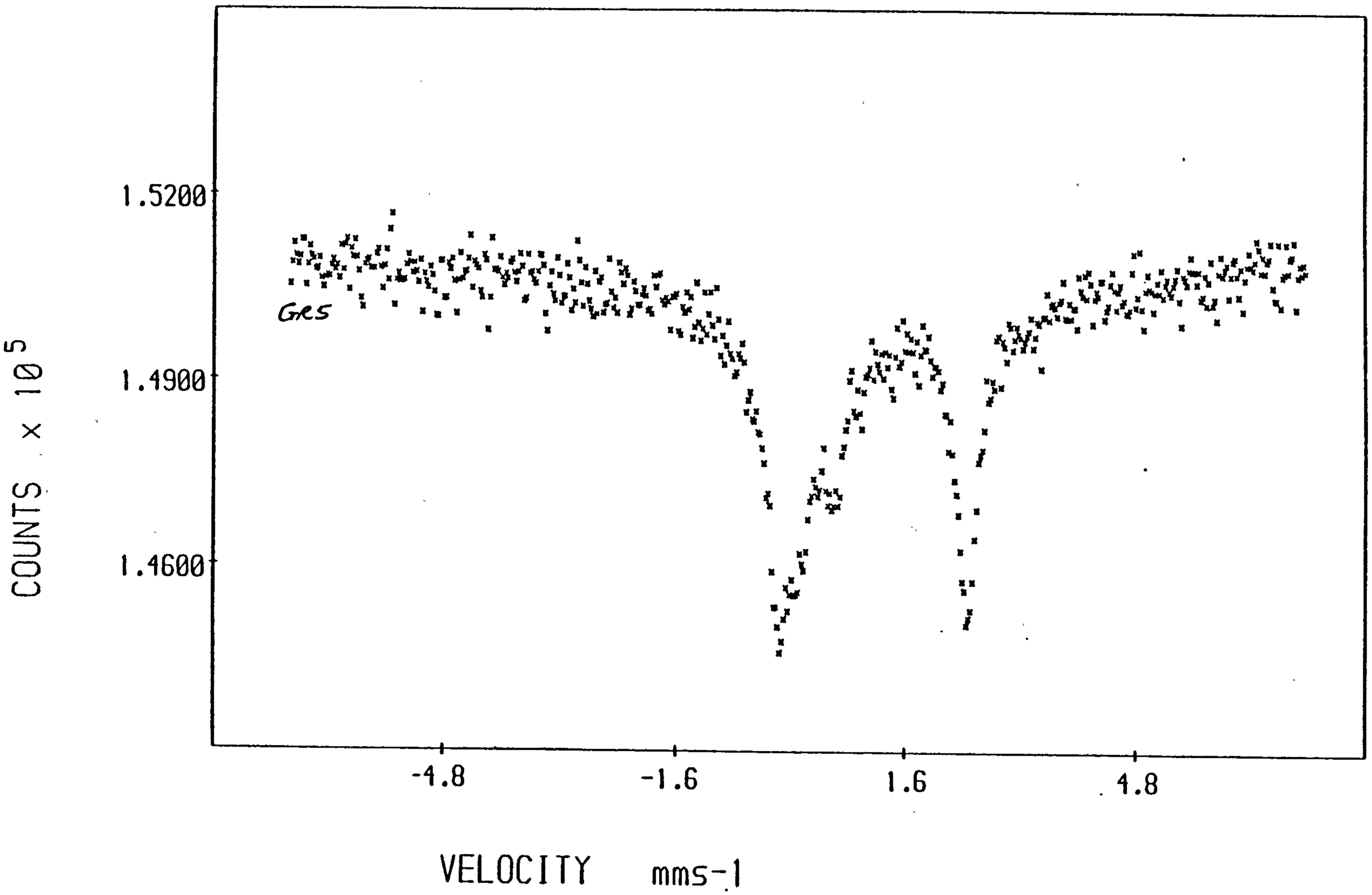

Fig 5.27 RT Mb spectrum of the wet, fresh precipitate of a sulphate GR sample derived from 0.1 M $FeSO_4$.

(iii) 4.2 K data

Mossbauer spectra at 4.2 K were obtained for three samples of sulphate GRs synthesised from 0.1 M $FeSO_4$. The samples used were GR15 (aged overnight) and GR16 (fresh) plus a sample actually made at AERE Harwell. The last sample (designated T6220483) had the following parameters at 77 K: IS = {1.27 (Fe(II)), 0.45 (Fe(III)), 0.47 (MHS)} mms^{-1}, QS = {2.92 (Fe(II)), 0.48 (Fe(III)), -0.25 (MHS)} mms^{-1} (FFR = 2.00) and B = 49.6 T. The raw spectra are shown in Fig 5.28. These are highly complex spectra and consist basically of:

(i) an Fe(III) magnetic hyperfine splitting with a small quadrupole perturbation

(ii) an Fe(II) combined magnetic and quadrupole hyperfine splitting.

The two hyperfine splittings are superimposed on each other, making analysis very difficult. Nevertheless, it has been possible to determine some of the Mb parameters relating to the region of interest i.e. the Fe(II) hyperfine field.

The analysis of the Fe(II) hyperfine field essentially followed the approach of van Dongen Torman et al. (1975). The procedure involved trying to locate four pairs of lines with the same separation from the observed

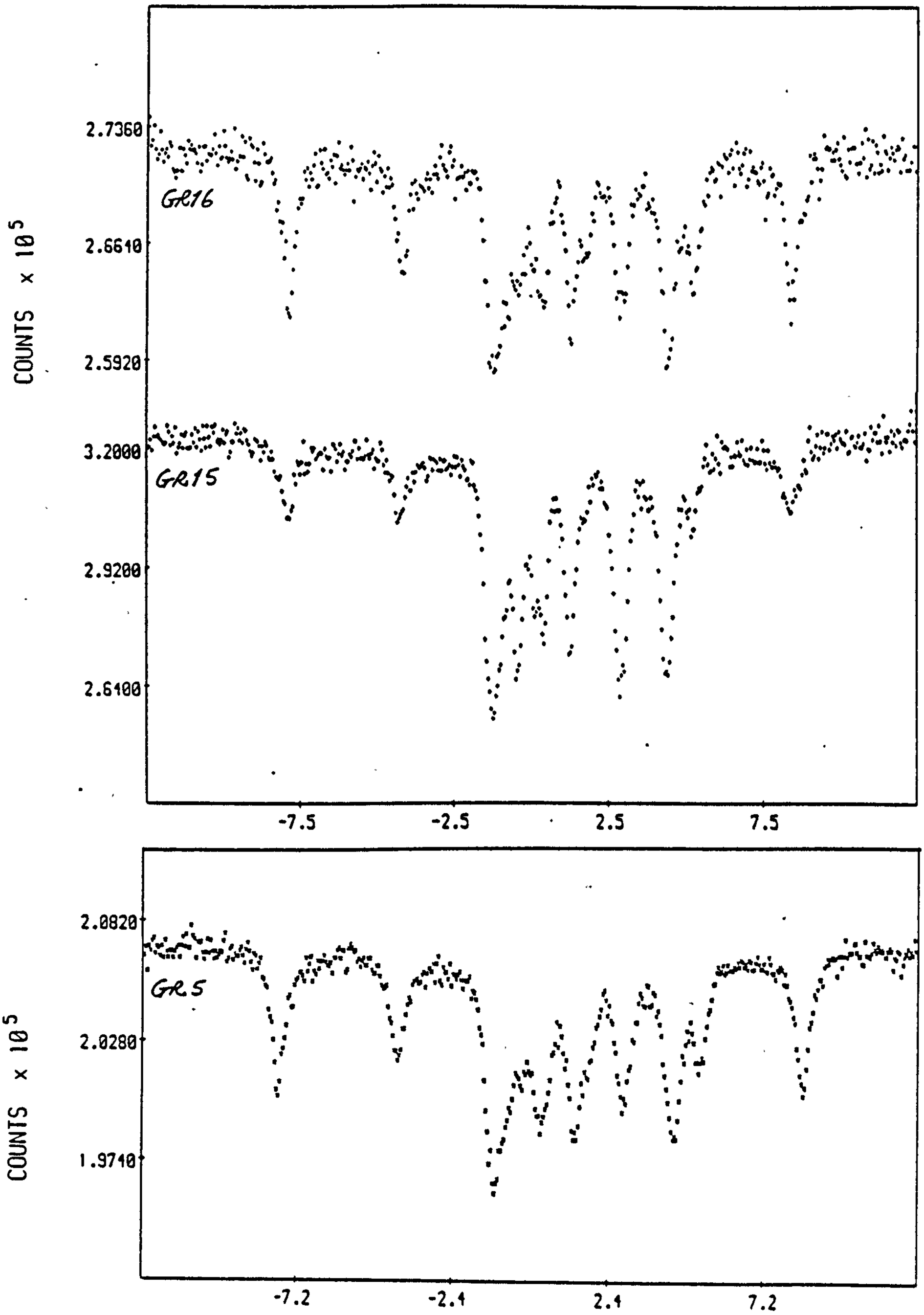

Fig 5.28 4.2 K Mb spectra of sulphate GRs derived from 0.1 M $FeSO_4$.

spectrum. This separation gave the groundstate splitting, β. The spectrum of $Fe(OH)_2$ (pp. 256, Greenwood & Gibb, 1971), which had a similar shape to the observed Fe(II) hyperfine field, was a useful guide in this respect. Once β was determined, the magnetic field, B, can be calculated from:

$$\beta = \mu_g B \qquad -5.10$$

where μ_g = groundstate nuclear magnetic moment.

Since Fe metal was used for calibration, then the magnetic field was actually obtained from:

$$B = (33/3.922).\beta \qquad -5.11$$

where β was in mms^{-1} and B was in teslas (T).

The excited state splitting, α (= μ_e B where μ_e is the excited state nuclear magnetic moment) can be obtained from:

$$\beta / \alpha = 1.747 \qquad -5.12$$

Thus the QS can be determined from:

$$QS = \pm \left(-2 \sum_{i<j}^{4} E_i E_j - 5\alpha^2\right)^{(1/2)} \qquad -5.13$$

where the Es are the energy levels of the excited state.

Finally, the IS can be derived from:

$$IS = 1/8 \sum_{i=1}^{8} \mathcal{E}_i \qquad -5.14$$

where $\mathcal{E}_i$ = transition energies = line positions in mms^{-1}.

In practice, it was very difficult to locate the eight line positions accurately by eye. For the sulphate GR spectra, normally only two pairs of lines were found with any degree of precision (lines 5&6 and lines 7&8 - see Fig 5.29). However, noting the energy level diagram of van Dongen Torman et al. (1975) and the 4.2 K spectrum of $Fe(OH)_2$, it was assumed that lines 1&2, 2&4 formed two closely overlapping doublets, and that lines 6&7, although weak, were close together forming a broad peak (in reality this peak was complicated by the superposition of an Fe(II) doublet). Following this criterion, reasonable line positions were obtained which gave values in fair agreement with each other, and also a value for the IS which was in line with the value at 77 K. Approximate values for the excited state energy levels E_1 -> E_4 (in mms^{-1}) were obtained by finding the centre of each pair of lines (i.e. 1&3, 2&4, 5&6 and 7&8) and subtracting the IS:

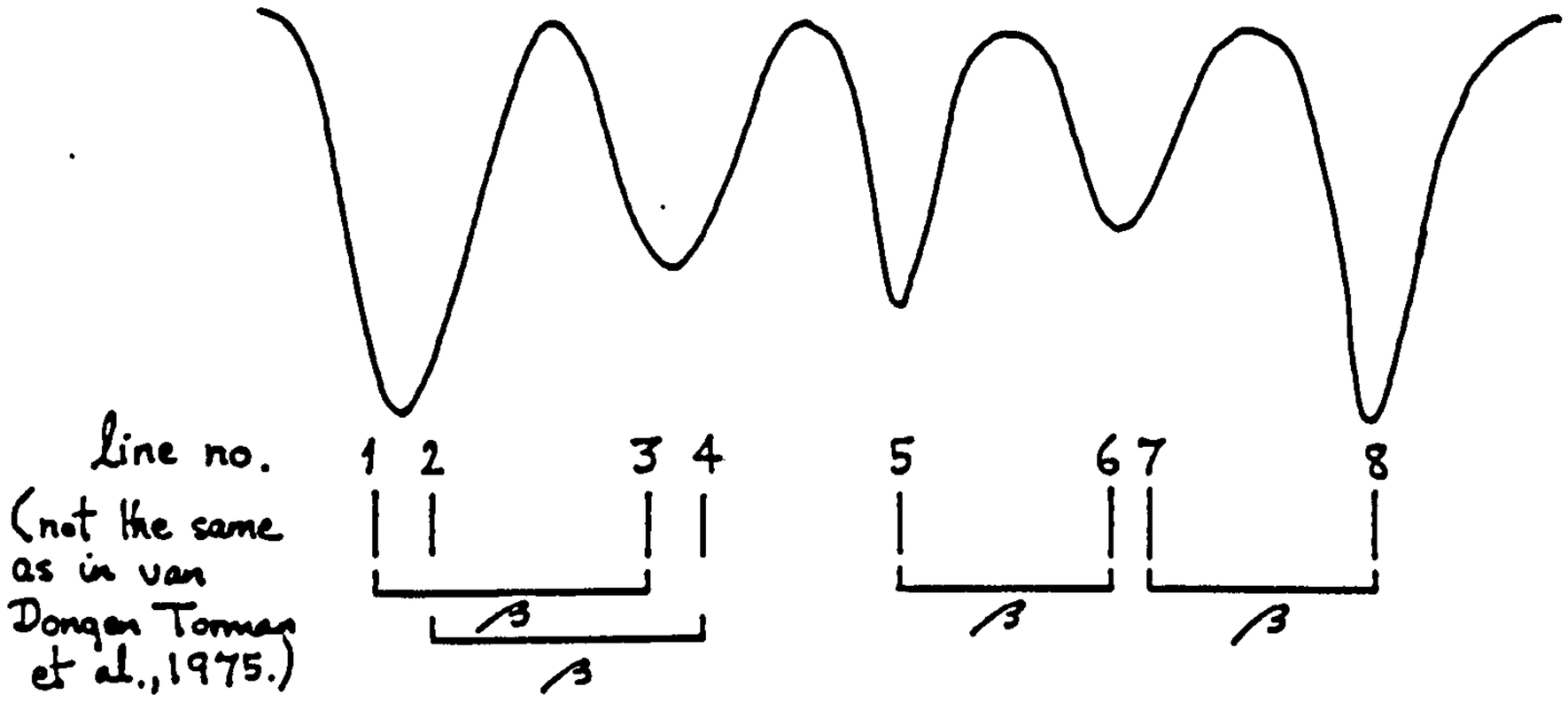

Fig 5.29 Basic Mb lineshape of the Fe(II) hyperfine envelope at 4.2 K for the sulphate GRs.

i.e. E_i = centre of each pair of lines (separation β)

- IS -5.15

Thus $\sum_{i<j}^{4} E_i E_j$ can be determined and hence an approximate value for the QS can be obtained. The latter was found to be in good agreement with the value at 77 K.

In order to refine the eight line positions, the energy levels E_1 -> E_4 were next calculated from the solution to the Hamiltonian (for combined quadrupole and magnetic interactions) by inputting the approximate values for β, IS and QS for given values of η, the asymmetry parameter of the EFG tensor, and θ and ϕ, the angles specifying the direction of B with respect to the EFG. The solution to the Hamiltonian involved the quartic equation:

$$E_i^4 + a_2 E_i^2 + a_1 E_i + a_o = 0 \qquad -5.16$$

with

$$a_2 = -(5/2)\alpha^2 - (1/8)B(1 + \eta^2/3) \qquad -5.16a$$

$$a_1 = (1/2)\alpha^2 B[\sin^2\theta\cos^2\phi(3-\eta) + \sin^2\theta\sin^2\phi(3+\eta) - 2] \qquad -5.16b$$

$$a_o = (9/16)A^4 + [(1/16)B^2(1+\eta^2/3)]^2 - (1/16)\alpha^2\beta^2[4 - 3/2(1+\eta^2/3) - \sin^2\theta\cos^2\phi(3-\eta)(1+\eta) - \sin^2\theta\sin^2\phi(3+\eta)(1-\eta) \qquad -5.16c$$

and where $B = e^2qQ$

The solution to equation 5.19 was carried out by a computer program which used an iterative procedure. Thus, from approximate values of β, IS and QS, a series of E_i values can be obtained for different values of η, 8 and 0. Next the E_i values which were thought to be the most appropriate for a given Fe(II) hyperfine spectrum (ignoring Fe(III) MHS) were selected for curvefitting. The curvefitting was done using a 8-line Lorentzian constrained to the eight transition energy values, E_i, and with relative intensity values taken from the graphs in Kundig's paper (Kundig, 1967). If the curvefitting was not good enough, then another set of E_i values would be tried. Thus by a process of trial and error, reasonably good fits were obtained for the Fe(II) hyperfine envelope.

The best fits for the sulphate GR samples are shown in Fig 5.30. The Mb parameters corresponding to the fitted spectra are given in Table 5.30. In order to get the reasonably good fits, an Fe(II) doublet also had to be put into the Fe(II) envelope. This doublet has a similar IS and QS to that of $FeSO_4.7H_2O$ which has IS = 1.39 mms^{-1} and QS = 3.38 mms^{-1} at 5 K (Greenwood & Gibb, 1971). As the percentage intensity of this doublet is a significant portion of the Fe(II) hyperfine envelope, then it must be "real". Part of this Fe(II) quadrupole doublet may be due to $FeSO_4$

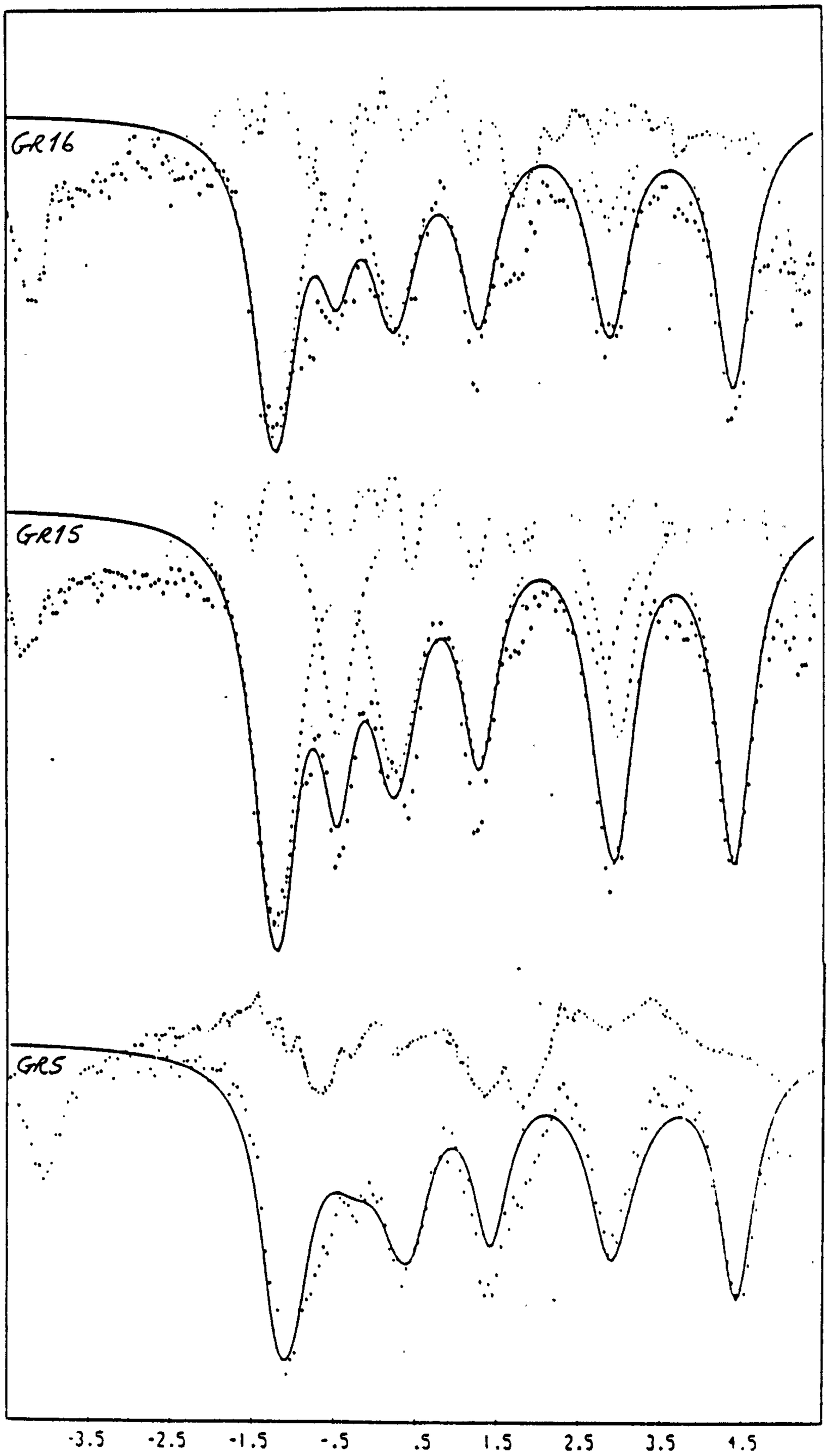

Fig 5.30 Partially-fitted 4.2 K Mb spectra for the sulphate GRs derived from 0.1 M $FeSO_4$.

Sample	Fe(II) Hyperfine Field								Fe(II) Doublet			
	δ	Δ	$\frac{1}{2}\Gamma$	η	θ	ϕ	B	%I	δ	Δ	$\frac{1}{2}\Gamma$	%I
GR5	1.28	-2.94	0.30	0	85	0	12.2	86	1.35	3.20	0.35	14
GR15	1.30	-2.94	0.27	0.2	90	90	12.5	75	1.38	3.43	0.30	25
GR16	1.30	-2.94	0.25	0.2	90	90	12.5	74	1.36	3.38	0.50	26

All parameters in mms^{-1} except η (dimensionless), θ and ϕ (°) and B(T).
The % intensity (%I) refers only to the Fe(II) components.

Table 5.30 4.2 K Mb parameters for the Fe(II) hyperfine envelope of the sulphate GRs derived from 0.1 M $FeSO_4$.

Sample	Fe(III) MHS		
	IS(mms^{-1})	QS(mms^{-1})	B(T)
GR5	0.47	-0.20	50.1
GR15	0.47	-0.20	50.7
GR16	0.47	-0.20	50.4

Table 5.31 4.2 K Mb parameters for the Fe(III) MHS of sulphate GR samples.

co-ordinated sites since the latter also shows up at 77 K for some of the samples. However, the main contribution to this quadrupole doublet is probably due to relaxation of the Fe(II) hyperfine field which produces a doublet at velocity positions of ~ -0.3 mms^{-1} and ~ 3.0 mms^{-1} (Cuttler, private comm.).

As seen from Table 5.30, the Fe(II) hyperfine field has virtually the same values of IS and QS as that of the main Fe(II) quadrupole doublet at 77 K. Since the latter has given rise to the Fe(II) hyperfine field at 4.2 K, then it is obvious that magnetic ordering has occurred in the transition 77 -> 4.2 K. The three sulphate GR samples have similar values of n, θ and B showing that the Fe(II) cations have similar environments. The two important points to note are : the magnitude of the magnetic field, B, is ~ 12.5 $\pm$ 0.5 T, and the direction, θ, of this field with respect to the Vzz component of the EFG tensor is ~ 90° (close to being axially symmetric - η ~ 0).

Further curvefitting of the spectra was carried out to account for the Fe(III) MHS (including minor adjustments for the relative intensities in the Fe(II) hyperfine envelope), and the fits from this are shown in Fig 5.31. The Mb parameters appropriate to the fitted Fe(III) peaks are given in Table 5.31. The Fe(III) MHSs were fitted with a small distribution of fields and so the values in Table 5.31 are mean values. The parameters are consistent

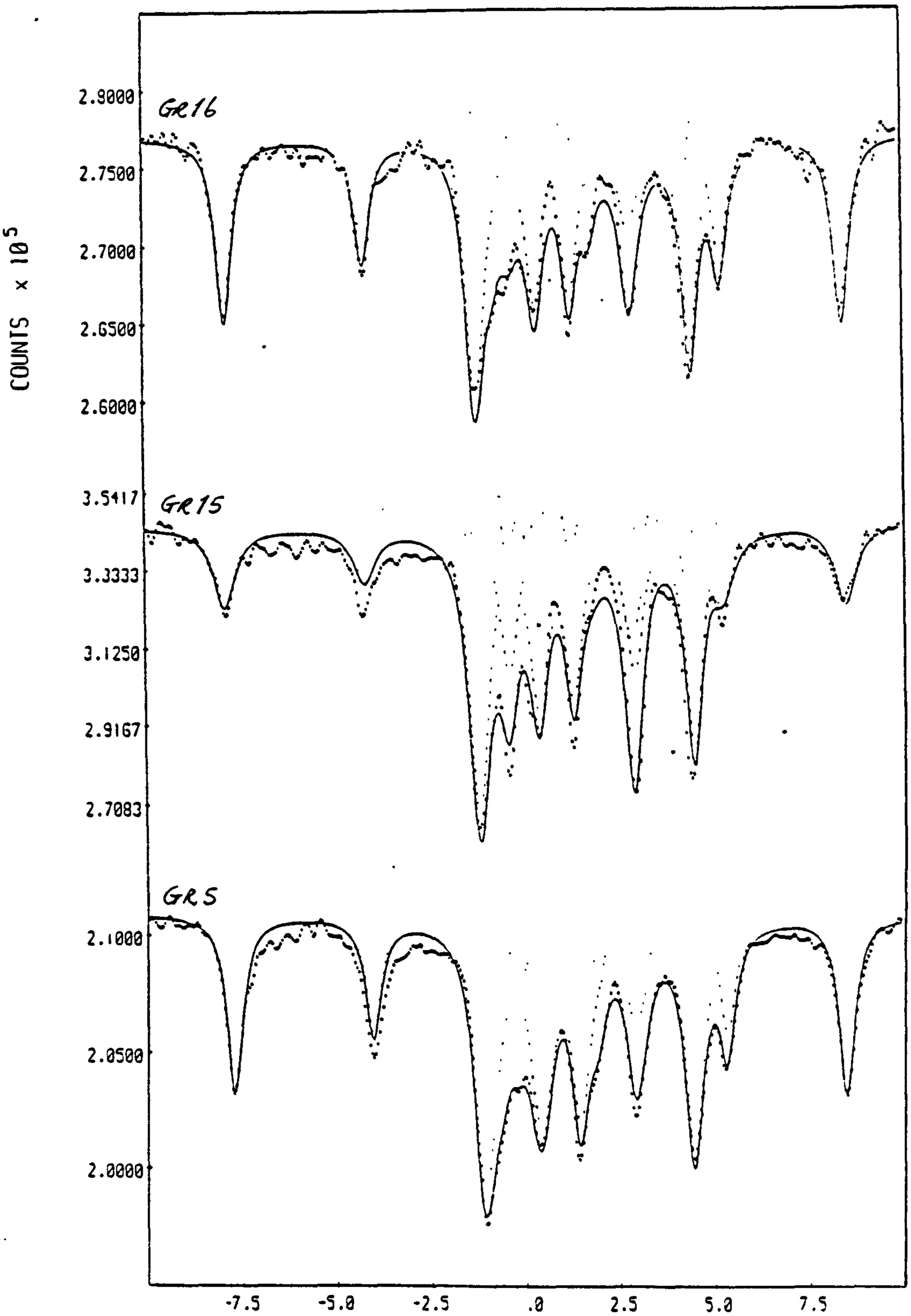

Fig 5.31 Completely-fitted 4.2 K Mb spectra for the sulphate GRs derived from 0.1 M $FeSO_4$.

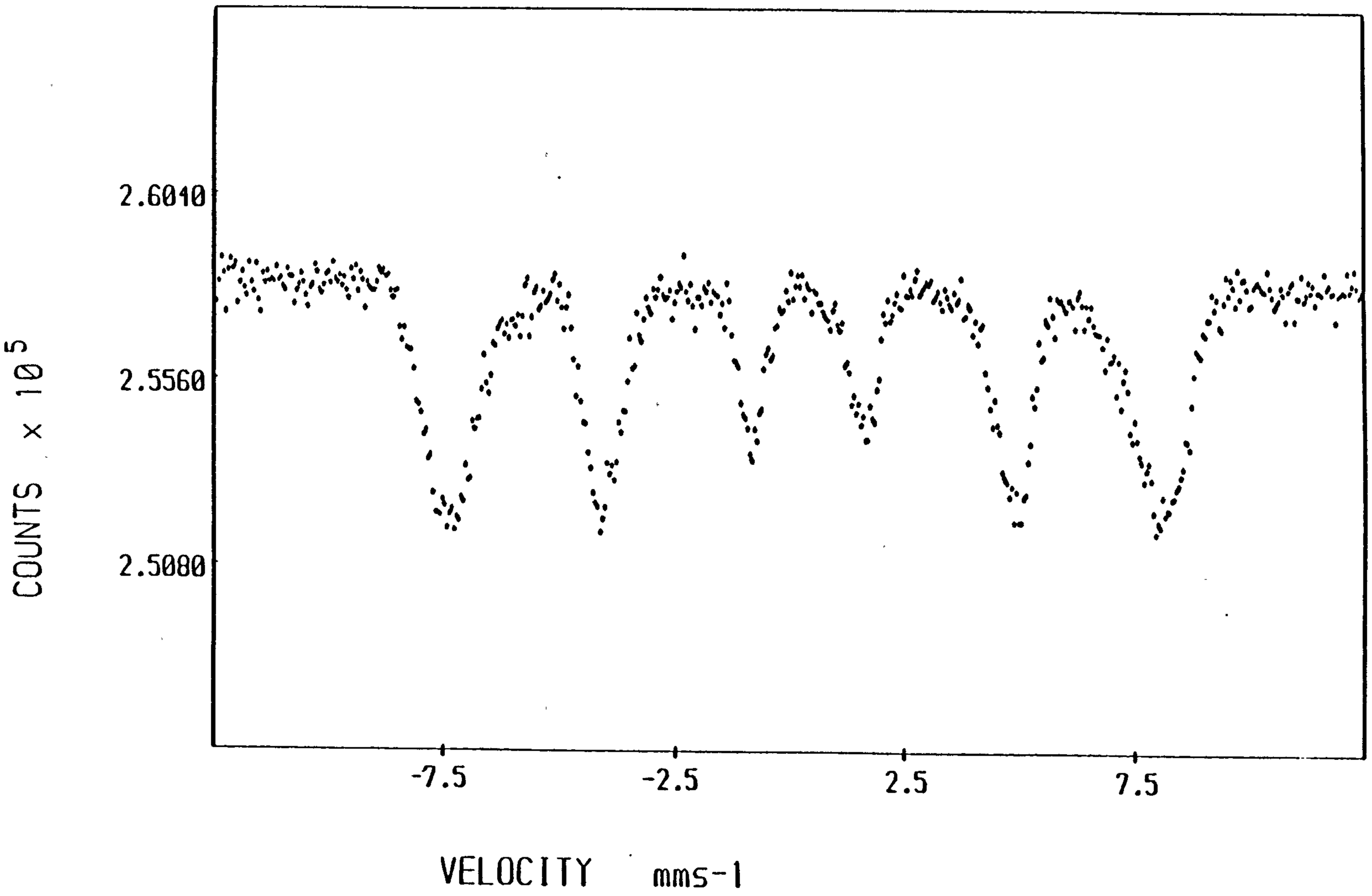

Fig 5.32 4.2 K Mb spectrum of Fe(III) gel sample derived from $FeCl_3.6H_2O$.

with those for goethite which was as expected.

The contributions from all the Fe(III) components must reside in the Fe(III) MHS since the Fe(II) hyperfine envelope appears not to contain any Fe(III) doublet (present in the 77 K spectra). This means that the Fe(III) gel part of the sulphate GR structure has become magnetically ordered at 4.2 K. Fig 5.32 shows the 4.2 K spectrum of the Fe(III) gel used in the sulphate GR synthesis. The spectrum has an MHS, showing that the gel is magnetically order at 4.2 K. However, the degree of ordering is not good since the linewidths are relatively large, indicating a large distribution of fields (IS ~ 0.4 mms^{-1}, QS ~ 0.0 mms^{-1} and B ~ 48 T). In contrast, the Fe(III) hyperfine peaks in the sulphate GRs have relatively small linewidths and are symmetrical, indicating a well-ordered Fe(III) magnetic component. All this evidence implies that the Fe(III) gel and goethite components in the sulphate GRs are in similar sites, and possibly part of the same overall superstructure.

2) <u>Samples synthesised from < 0.1 M $FeSO_4$</u>

The 77 K data for the sulphate GR and non-GR samples produced from $[FeSO_4]_I$ < 0.1 M (described in Appendix A and the previous sections) are presented here. The Mb spectra for the wet, fresh precipitate are shown

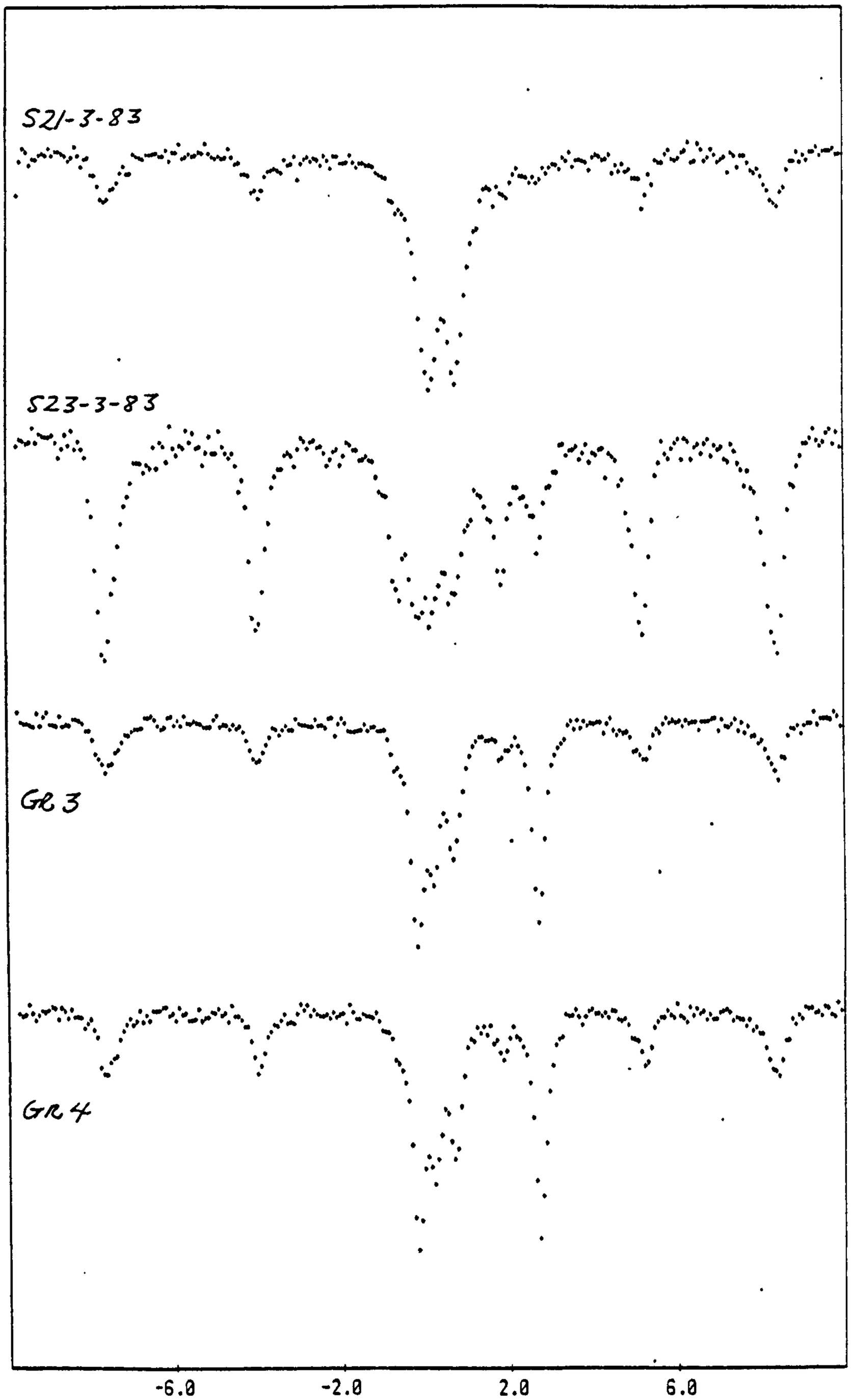

Fig 5.33 77 K Mb spectra of the wet, fresh precipitate of sulphate GRs and non-GRs derived from < 0.1 M $FeSO_4$.

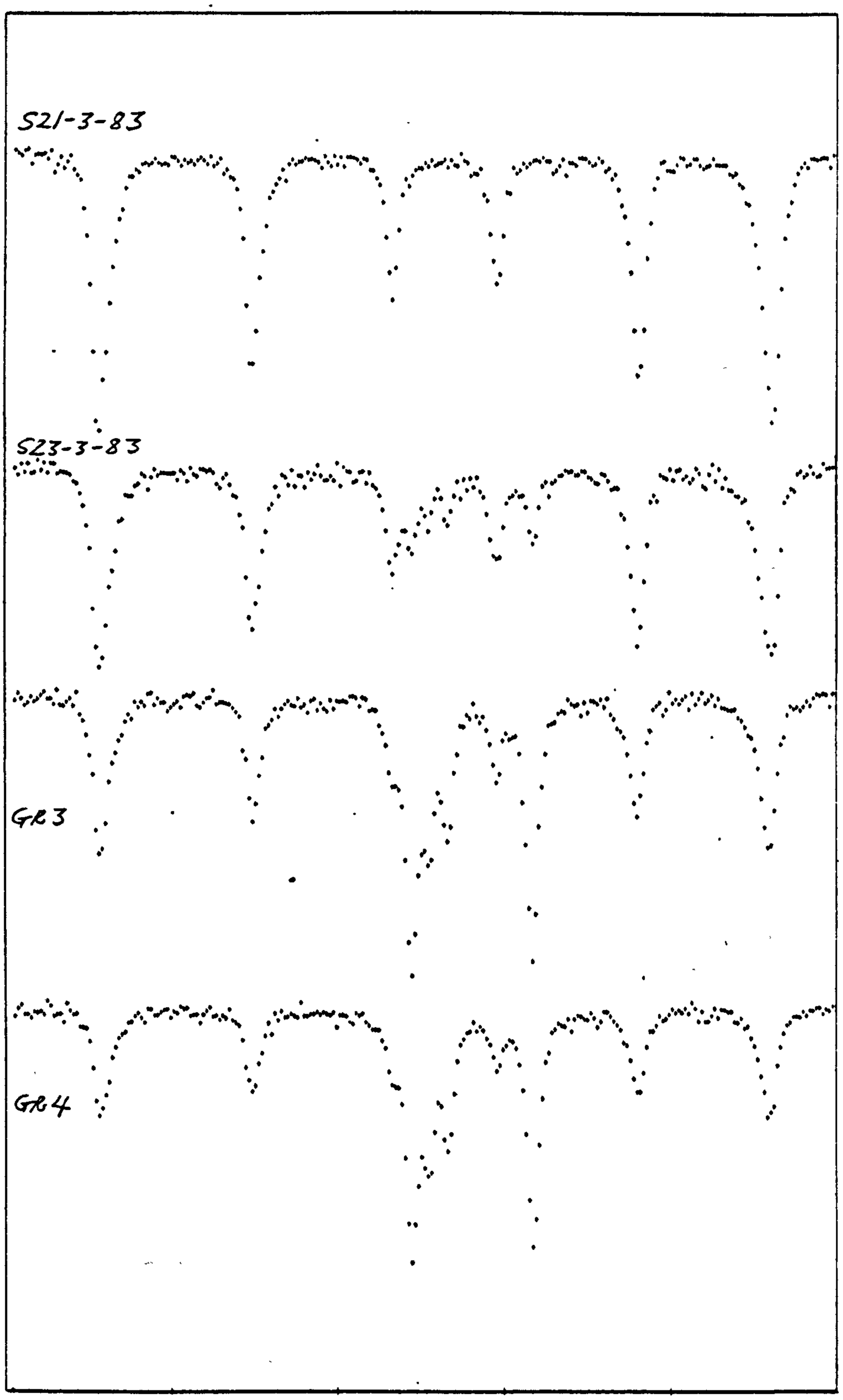

Fig 5.34 77 K Mb spectra of the wet, aged precipitate of sulphate GRs and non-GRs derived from < 0.1 M $FeSO_4$.

Sample	$[FeSO_4]_I$	IFFR	Fe(II) doublet			Fe(III) doublet			MHS			FFR
			δ	$\frac{1}{2}\Gamma$	Δ	δ	$\frac{1}{2}\Gamma$	Δ	δ	Δ	B	
S21-3-83	0.01	0.4				0.44	0.26	0.64	0.51	-0.26	49.7	
S23-3-8-3	0.025	1	1.25	0.21	2.93	0.42	0.24	0.54	0.48	-0.23	49.7	0.77
GR3	0.05	2	1.26	0.16	2.90	0.45	0.17	0.47	0.49	-0.21	49.7	1.69
GR4	0.05	2	1.26	0.16	2.91	0.45	0.16	0.48	0.47	-0.27	49.7	1.81

$\langle Fe(III) \rangle$ = 5 mmoles

Table 5.32 77 K Mb parameters for the wet, fresh precipitate of sulphate GRs and non-GRs derived from $\leq$ 0.1 M $FeSO_4$. (S21-3-83 & S23-3-83 are non-GRs)

Sample	$[FeSO_4]_I$	IFFR	Fe(II) doublet			Fe(III) doublet			MHS			FFR
			δ	$\frac{1}{2}\Gamma$	Δ	δ	$\frac{1}{2}\Gamma$	Δ	δ	Δ	B	
S21-3-83	0.01	0.4	-	-	-	-	-	-	0.47	-0.23	50.1	-
S23-3-83	0.025	1	1.25	0.19	2.93	0.44	(0.11)	0.46	0.47	-0.24	49.9	(2.47)
GR3	0.05	2	1.25	0.16	2.90	0.45	0.16	0.45	0.46	-0.25	49.7	2.19
GR4	0.05	2	1.27	0.16	2.91	0.45	0.16	0.45	0.48	-0.26	49.9	1.96

Fe(III) = 5 mmoles ( ) indicates uncertainty in values

Table 5.33 77 K Mb parameters for the wet, aged precipitate of sulphate GRs and non-GRs derived from $\leq$ 0.1 M $FeSO_4$.

in Fig 5.33 and the corresponding Mb parameters are given in Table 5.32. Similarly, the Mb spectra and parameters for the wet, aged precipitate are given in Fig 5.34 and Table 5.33, respectively.

Looking at both sets of data, it can be seen that there is a progression towards the typical sulphate GR spectra (characteristic of the samples produced from 0.1 M $FeSO_4$) with increasing $[FeSO_4]_I$ (<Fe(III)> being constant at 5 mmoles). There is a point at which the magnetic component is equal to the paramagnetic component (Fe(II) and Fe(III)), and lies in the range .0.025 < $[FeSO_4]_I$ < 0.05 M, or 1 < IFFR < 2.

At $[FeSO_4]_I$ = 0.01 M, there is virtually no sign of any Fe(II) component but, as $[FeSO_4]_I$ increases, the Fe(II) quadrupole doublet becomes more apparent and there is a corresponding change in colour from a muddy, slightly greenish-brown to a more greener brown (i.e. for the end-products). At $[FeSO_4]_I$ = 0.05 M, the colour of the precipitate is green to dark-green, and the paramagnetic components (Fe(II) and Fe(III)) predominates the spectra. The XRD diffractograms show a mixture of sulphate GR and goethite for $[FeSO_4]_I \geq 0.05$ M, while only goethite was present for $[FeSO_4]_I$ < 0.05 M (see section 5.2.1b)

The transition in the Mb spectra is also reflected in the Mb parameters, particularly those of the Fe(III) quadrupole doublet. The QS decreases from 0.64 -> 0.48 mms^{-1} and $1/2\Gamma$ decreases from 0.26 -> 0.16 mms^{-1} (for the fresh precipitate). These changes show that the paramagnetic environment was becoming more stable and ordered, and this was also probably true of the other components. However, what is rather surprising is that the IS and QS for the Fe(II) quadrupole doublet (indicative of GR material) should be invariant with $[FeSO_4]_I$ (although $1/2\Gamma$ decreases from ~ 0.20 -> 0.16 mms^{-1}). This means that any structural changes does not disturb the Fe(II) environment to a any great extent, and so probably involves only the Fe(III) components (both paramagnetic and magnetic Fe(III)). Another way of looking at it is that the Fe(II) component and the Fe(III) gel are not tightly bound together. This is in keeping with the unstable nature of GRs.

The aged overnight material shows a slight increase in crystallinity (B being slightly larger), with an increased amount of magnetic material and an increase in FFR. As mentioned previously, the last two factors are probably linked and will be discussed in the conclusions chapter. The most dramatic change occurs for $[FeSO_4]_I$ = 0.01 M, in which the paramagnetic Fe(III) doublet disappears completely on ageing overnight

to become part of the Fe(III) MHS. This shows the incredibly rapid conversion of the paramagnetic material to goethite. Thus when no sulphate GR component was produced, all the Fe(III) gel seems to convert to thermodynamically-stable goethite (cf. sample S7-2-83).

5.2.2 The Chloride Green Rusts

The sample identities for the chloride GRs and non-GRs produced from the 0.1 M $FeCl_2$ system are given in Tables 5.34 and 5.35, respectively. The synthesis conditions (e.g. pH and $[FeCl_2]_I$) were identical in both groups except for the IFFR. The IFFR obviously determines whether a chloride GR has been formed or not. Looking at the tables, it can be seen that in the 0.1 M $FeCl_2$ system, chloride GRs are produced at IFFR $\geq$ 6. The transition from chloride GRs to non-GRs occur in the range $4 < IFFR < 6$.

The fresh precipitate for the chloride GRs was dark-green in colour and was slightly more unstable than the sulphate GRs in air. On vacuum-drying, the material changed to a green/lime-green colour, although this was not uniform (indicating some partial oxidation of the material). The non-GRs produced from 0.1 M $FeCl_2$ were black in colour and had a high bulk magnetism (shown by bringing a strong magnet close to the suspensions). It was also fine-grained in most cases.

Sample	IFFR	<Fe(III)> (mmole)	pH maintained
GR12	6	3.35	7.0 ± 0.1
GR11	8	2.5	7.0 ± 0.2
GR25	8	2.5	7.0 ± 0.1
GR10	10	2.0	7.0 ± 0.1
GR6	20	1.0	7.1 ± 0.2
GR7	20	1.0	7.1 ± 0.2
GR18	20	1.0	7.0 ± 0.1
GR8	40	0.5	7.1 ± 0.2

< > = amount of

Table 5.34 Sample identities for chloride GRs derived from 0.1 M $FeCl_2$.

Sample	IFFR	<Fe(III)> (mmole)	pH maintained
S14-11-83	1	20	7.1 ± 0.2
S30-3-83	4	5	7.0 ± 0.1
S4-4-83	4	5	7.0 ± 0.1
S6-4-83	4	5	7.0 ± 0.1
S13-6-83	4	5	7.0 ± 0.2

Table 5.35 Sample identities for non-GRs derived from 0.1 M $FeCl_2$.

5.2.2a Titration and AAS data

As with the sulphate GRs, the consumption of alkali for the chloride GR synthesis was very rapid initially but slowed down to equilibrium after a few hours (Fig 5.35). The data showing the alkali consumption at varying IFFRs for the chloride GRs produced from 0.1 M $FeCl_2$ is given in Table 5.36.

The variation in alkali consumption with IFFR is shown by a graph of alkali consumption v. <Fe(III)> as $[FeCl_2]_t$ was constant (plots against IFFR are merely inverses). A ln-ln graph of alkali consumption v. <Fe(III)> shows reverse linear trends for $\langle NaOH\rangle_t$, the total NaOH consumption, and $\langle NaOH\rangle_s$, the specific NaOH consumption (Fig 5.36). The former increases with <Fe(III)> but the latter decreases. Linear least-squares fit of the two trends give the following relationships:

$$\ln \langle NaOH\rangle_t = 0.81 \ln \langle Fe(III)\rangle + 1.11 \qquad -5.17a$$

$$\rightarrow \quad \langle NaOH\rangle_t = 3.04 \langle Fe(III)\rangle^{0.81} \qquad -5.17b$$

$$\ln \langle NaOH\rangle_s = -0.20 \ln \langle Fe(III)\rangle + 1.11 \qquad -5.18a$$

$$\rightarrow \quad \langle NaOH\rangle_s = 3.04 \langle Fe(III)\rangle^{-0.20} \qquad -5.18b$$

The rate of increase in $\langle NaOH\rangle_t$ is thus greater than the rate of decrease in $\langle NaOH\rangle_s$.

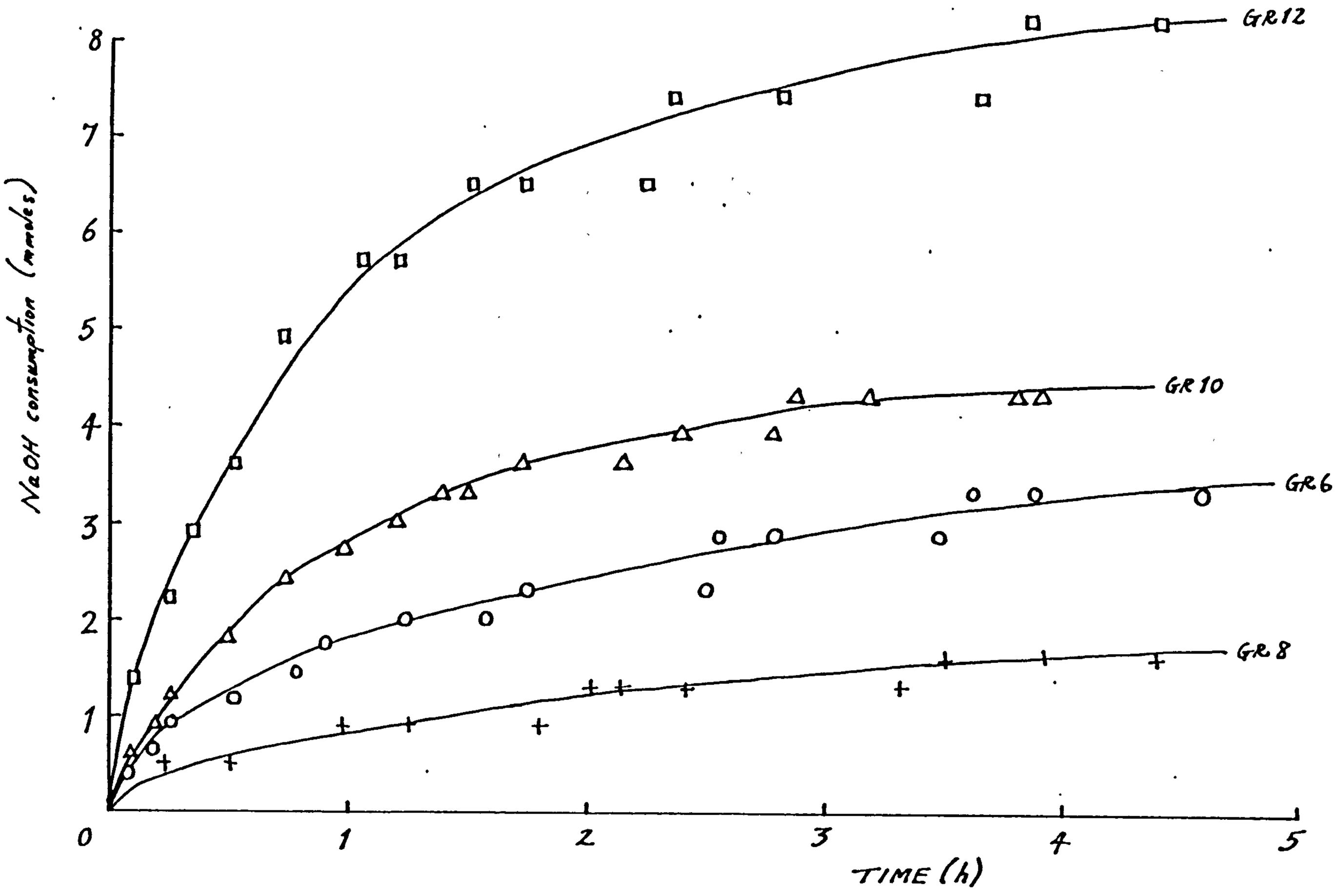

Fig 5.35 NaOH consumption v. time for typical chloride GR samples derived from 0.1 M $FeCl_2$.

Sample	IFFR	⟨Fe(III)⟩ (mmole)	$\langle NaOH \rangle_t$ (mmole)	$\langle NaOH \rangle_s$ (mole $mmole^{-1}$)	Estimated eqm. time (h)
GR12	6	3.35	8.50 ± 0.25	2.5	6
GR11	8	2.5	6.60 ± 0.10	2.6	4
GR25	8	2.5	6.50 ± 0.15	2.6	4.5 - 5
GR10	10	2.0	4.40 ± 0.10	2.2	5
GR6	20	1.0	3.70 ± 0.25	3.7	6
GR7	20	1.0	3.00 ± 0.15	3.0	5 - 5.5
GR18	20	1.0	2.80 ± 0.15	2.8	5
GR8	40	0.5	1.70 ± 0.15	3.4	5.5 - 6

Table 5.36 Alkali consumption for chloride GRs derived from 0.1 M $FeCl_2$.

Sample	IFFR	⟨Fe(III)⟩ (mmole)	$\langle Fe(II) \rangle_t$ (mmole)	$\langle Fe(II) \rangle_s$ (mmole.$mmole^{-1}$)
GR12	6	3.35	12.0	3.6
GR11	8	2.5	11.1	4.4
GR10	10	2	10.6	5.3
GR6	20	1	8.6	8.6
GR7	20	1	8.1	8.1
GR18	20	1	8.3	8.3
GR8	40	0.5	5.8	11.6

Table 5.37 Fe(II) uptake for chloride GRs derived from 0.1 M $FeCl_2$.

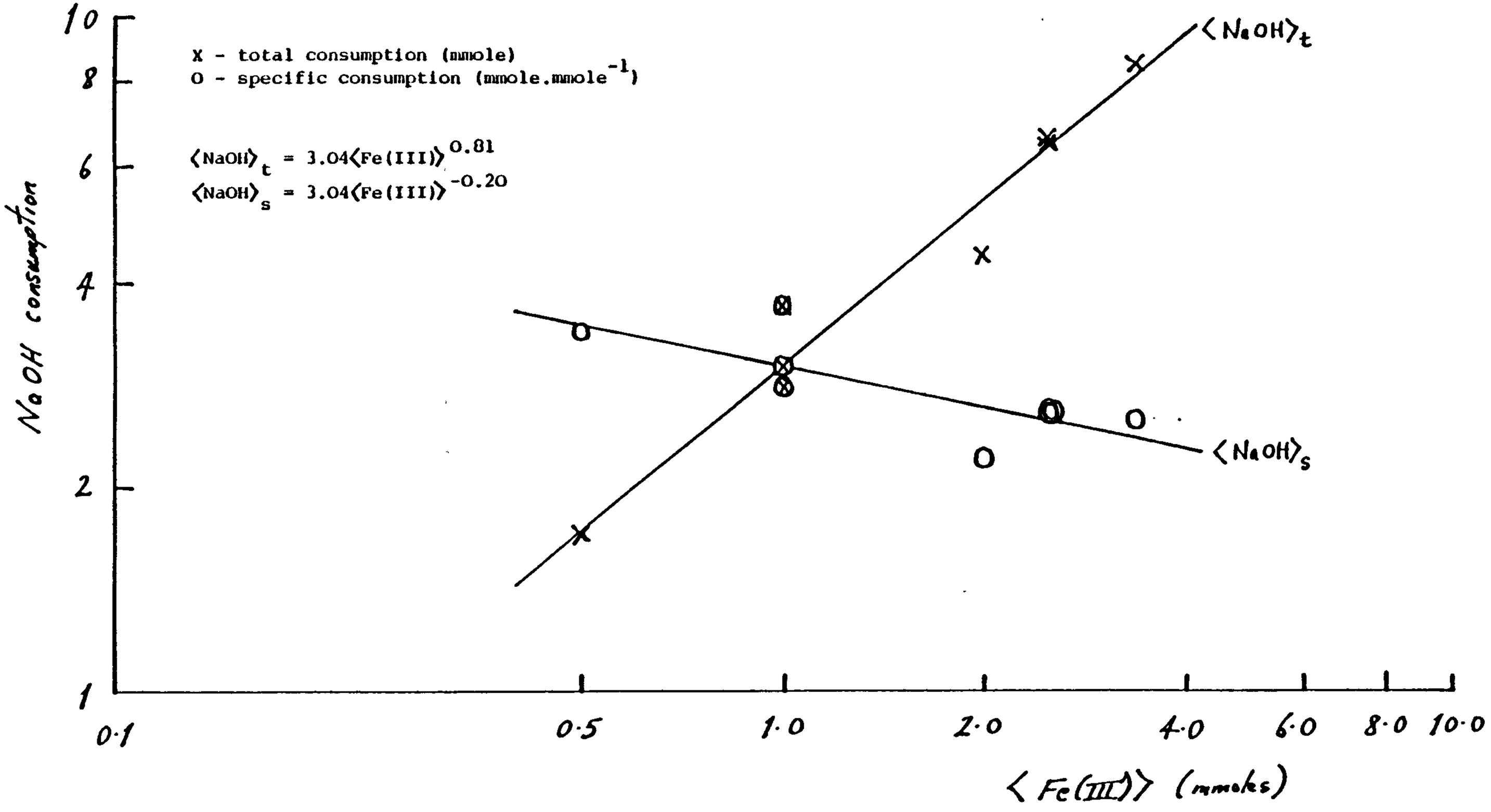

Fig 5.36 NaOH consumption v. <Fe(III)> for chloride GRs derived from 0.1 M $FeCl_2$.

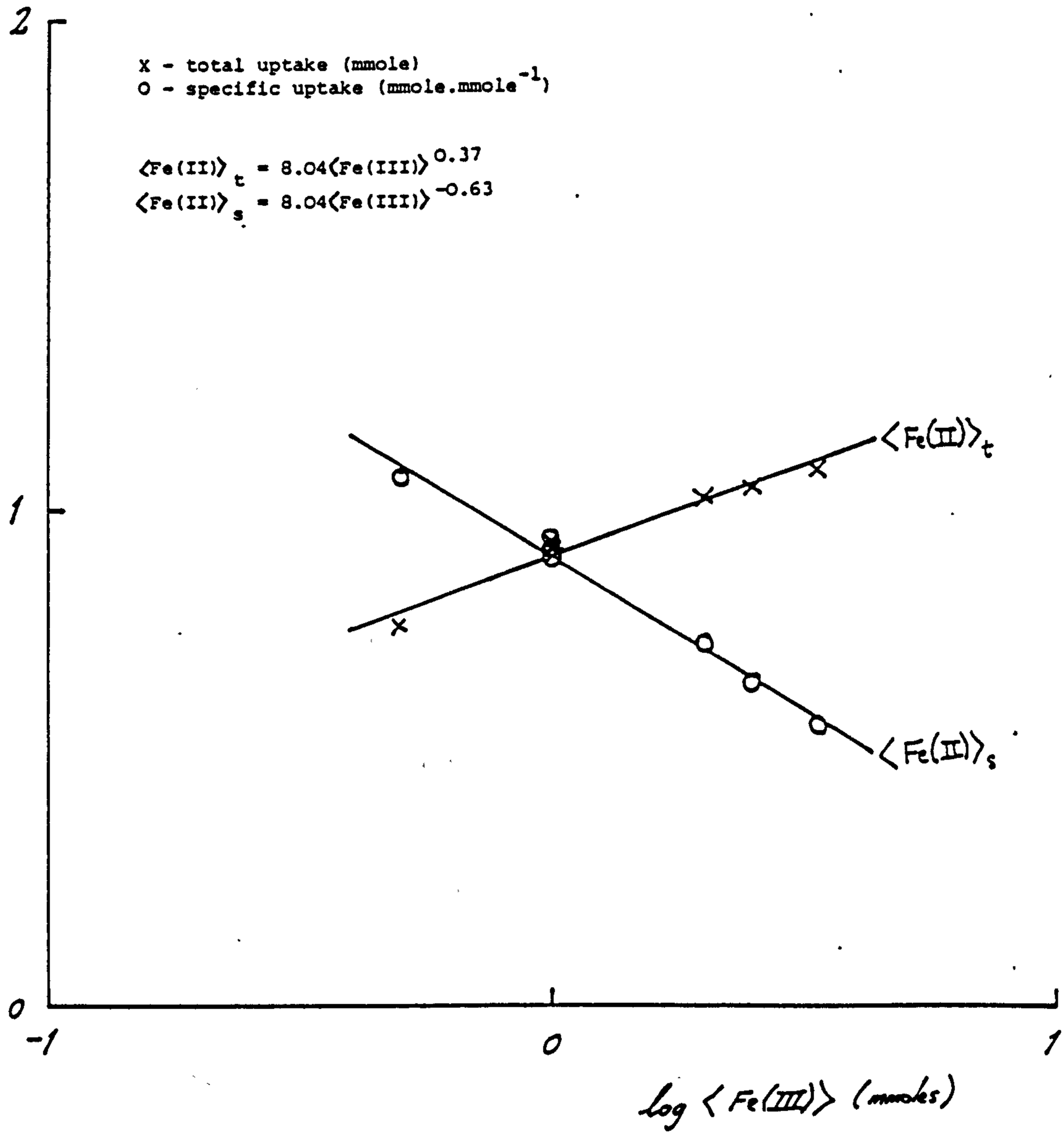

Fig 5.37 Fe(II) uptake v. <Fe(III)> for chloride GRs derived from 0.1 M $FeCl_2$.

The AAS data for Fe(II) uptake during the synthesis of the chloride GRs is given in Table 5.37. A ln-ln graph of Fe(II) uptake v. <Fe(III)> is given in Fig 5.37, and shows reverse linear relationships for $\langle Fe(II)\rangle_t$, the total Fe(II) uptake, and $\langle Fe(II)\rangle_s$, the specific Fe(II) uptake. This behaviour is very similar to that for the NaOH consumption. Linear least-squares fit of the two plots give the following relationships:

$$\ln \langle Fe(II)\rangle_t = 0.37 \ln \langle Fe(III)\rangle + 2.08 \qquad -5.19a$$

$$\rightarrow \quad \langle Fe(II)\rangle_t = 8.04 \langle Fe(III)\rangle^{0.37} \qquad -5.19b$$

$$\ln \langle Fe(II)\rangle_s = -0.63 \ln \langle Fe(III)\rangle + 2.08 \qquad -5.20a$$

$$\rightarrow \quad \langle Fe(II)\rangle_s = 8.04 \langle Fe(III)\rangle^{-0.63} \qquad -5.20b$$

The rate of increase in $\langle Fe(II)\rangle_t$ is less than the rate of decrease in $\langle Fe(II)\rangle_s$ which contrasts with the behaviour of NaOH consumption.

The data for the Freundlich isothermal plot is given in Table 5.38.The plot (Fig 5.38) gives a straight line which means that the process of Fe(II) uptake is adsorption. A least-squares fit of the points gives the best line as:

$$\ln \langle Fe(II)\rangle_s = 2.11 \ln [Fe(II)]_{sqm} + 8.08 \qquad -5.21a$$

$$\rightarrow \quad \langle Fe(II)\rangle_s = 3239 [Fe(II)]_{sqm} \qquad -5.21b$$

Sample	$[Fe(II)]_{eqm}$ ($\dot{M}$, $\times 10^{-3}$)	$\langle Fe(II) \rangle_w$ ($g.g^{-1}$)
GR12	40	3.6
GR11	45	4.4
GR10	47	5.3
GR6	57	8.6
GR7	59	8.1
GR18	59	8.3
GR8	71	11.6

Table 5.38 AAS data for Freundlich isotherm for chloride GRs derived from 0.1 M $FeCl_2$.

$$\langle Fe(II)\rangle_s = 3239\left[Fe(II)\right]^{2.11}_{eqm.}$$

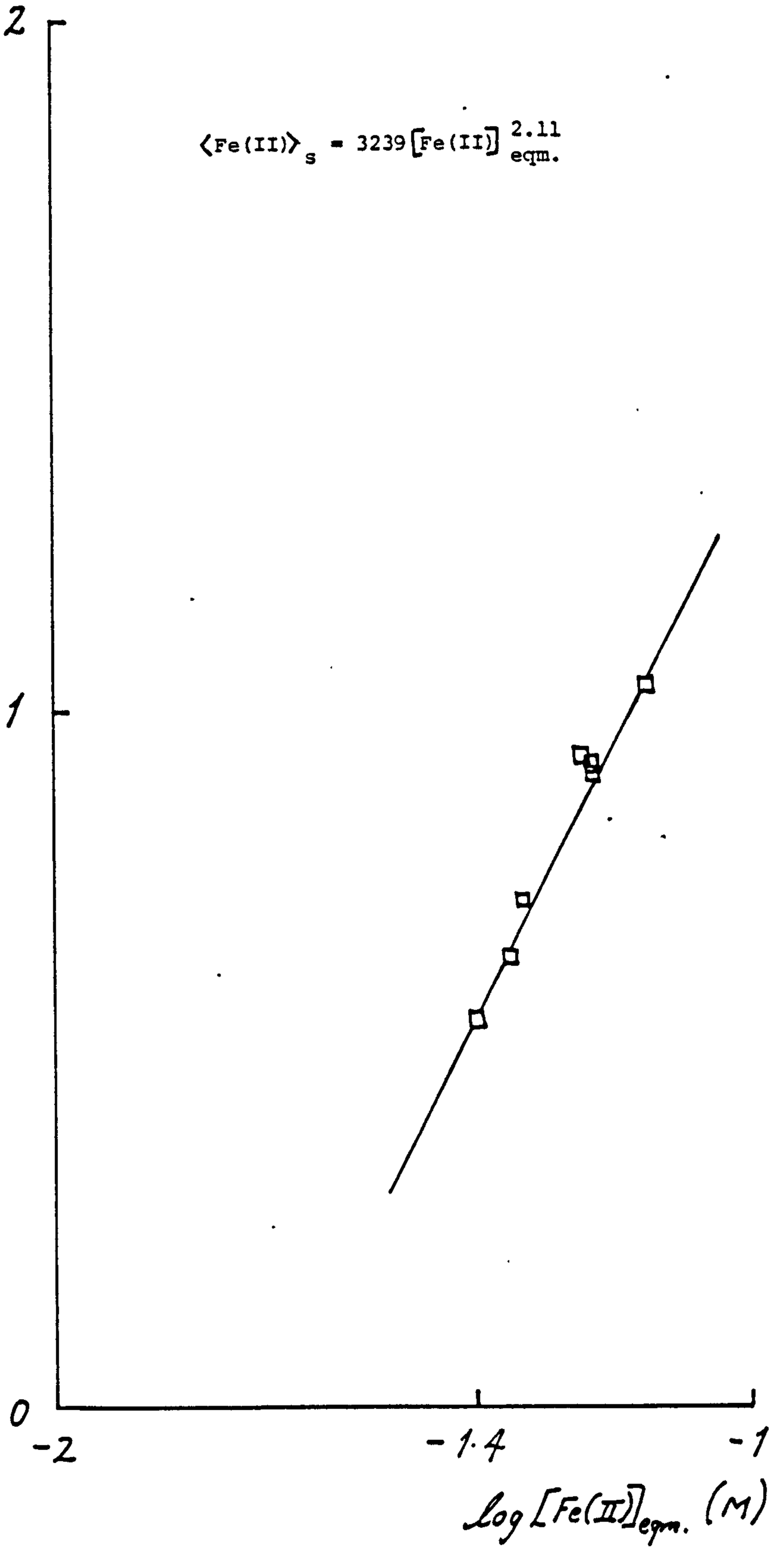

Fig 5.38 Freundlich isotherm for chloride GRs derived from 0.1 M $FeCl_2$.

The gradient of this line is less than that of the corresponding Freundlich plot for the sulphate GRs derived from 0.1 M $FeSO_4$. In other words, the specific Fe(II) uptake by the Fe(III) gel is greater in the 0.1 M $FeSO_4$ system than in the 0.1 M $FeCl_2$ system, and this is confirmed by the plots (Fig 5.7 and Fig 5.37). The difference may be due to the slightly different gel surface resulting from the different Fe(III) source used in the preparation of the gel [for the $FeSO_4$ system, the gel was derived from $Fe(NO_3)_3.4H_2O$ while for the $FeCl_2$ system, the source used was $FeCl_3.6H_2O$].

5.2.2b X-ray Diffraction

As mentioned in section 5.2.1b, the dried chloride GR material was almost completely oxidised at the end of an XRD scan. Thus, unlike the sulphate GRs, the XRD traces obtained for the chloride GRs were usually poor, with badly-resolved and also broad peaks, and usually a high and erratic background (Fig 5.39). In fact the oxidation problem was so bad that the XRD traces obtained were all of the oxidation products. The X-ray d-spacings of the chloride GRs (oxidised) are given in Table 5.39. Except for sample GR11, which was stored under N_2 in a sealed test-tube, the X-ray lines are consistent with that of akaganeite. The XRD patterns shown in Fig 5.39 of the oxidised chloride GRs indicate that the crystallinity was poor to fairly-crystalline. Sample GR11 shows lines of goethite and magnetite/maghemite, and suggests that there was some restructuring and possibly ageing of part of the dried material during storage (the freshly-dried material had the same XRD pattern as the other samples in the table). This solid state transformation of some of the material is similar to that which occurred for the carbonate GR of Taylor (1980) which was stored under vacuum. The other chloride GR samples also partially converted to a magnetic material on storage under N_2. However, the point to note in sample GR11 is the basal line at 7.70 A which is compatible with a chloride GRI basal spacing (see Table 5.40), and similar to the

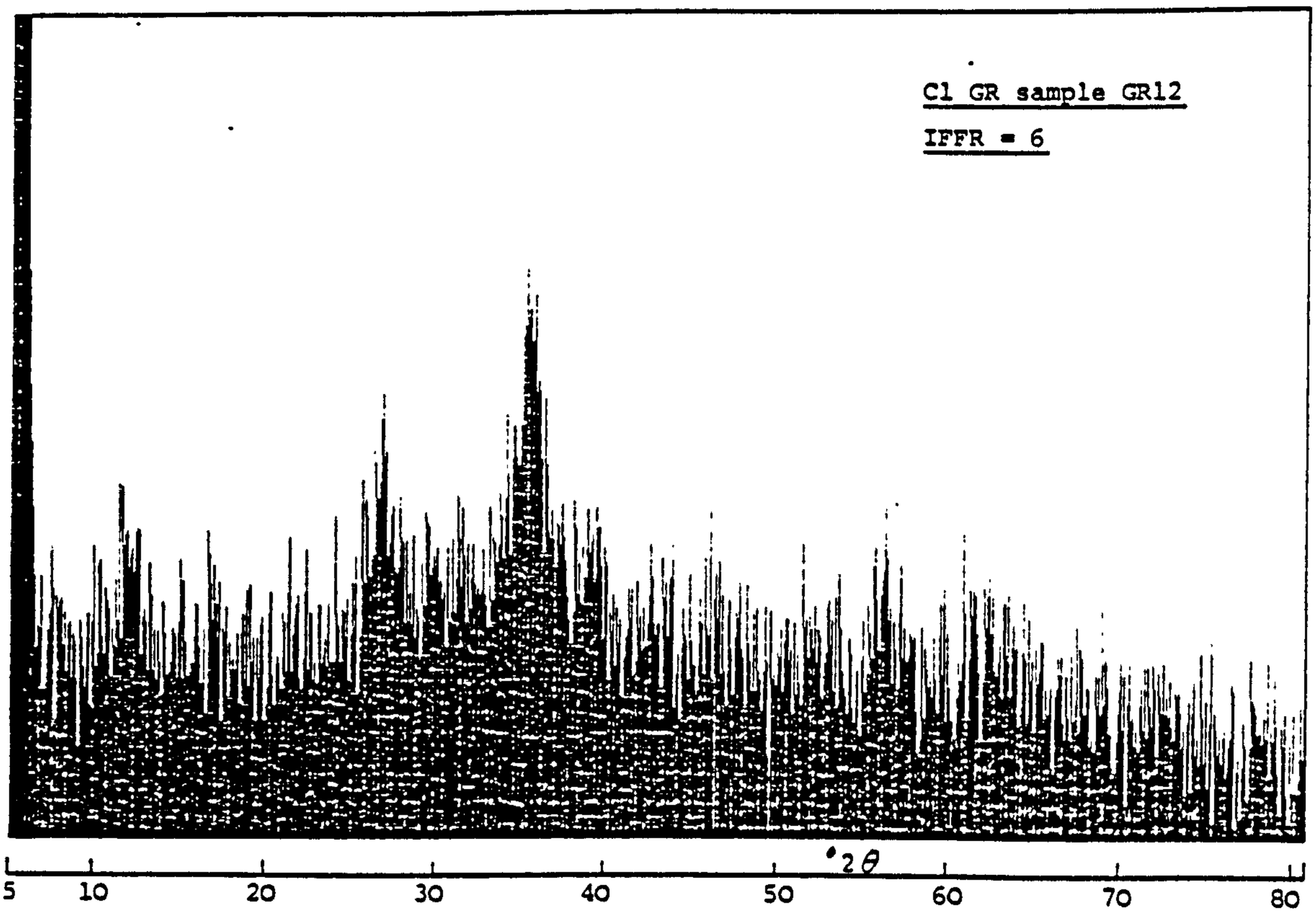

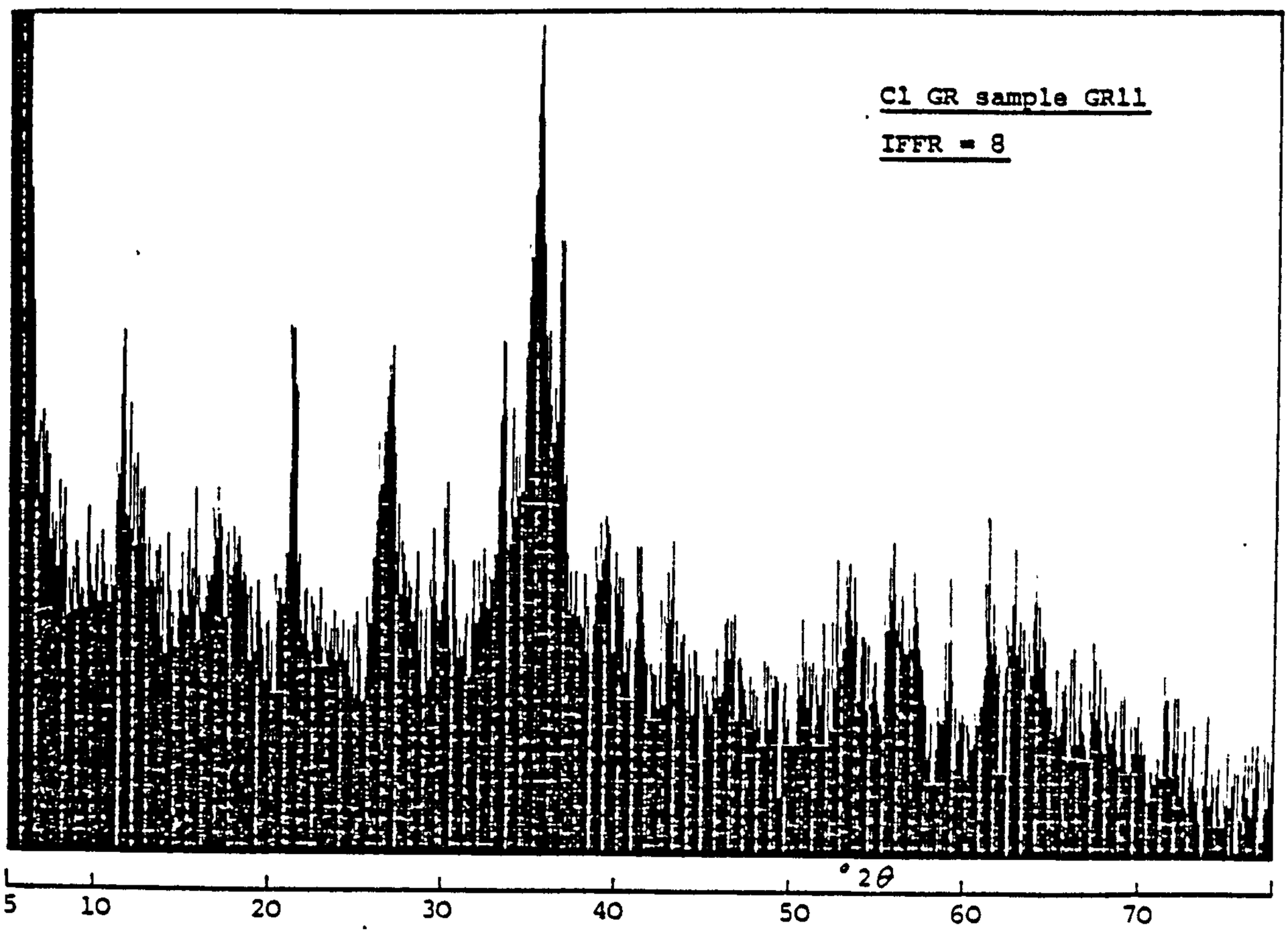

Fig 5.39 Typical X-ray diffractograms of chloride GRs derived from 0.1 M $FeCl_2$. (partially to completely oxidised)

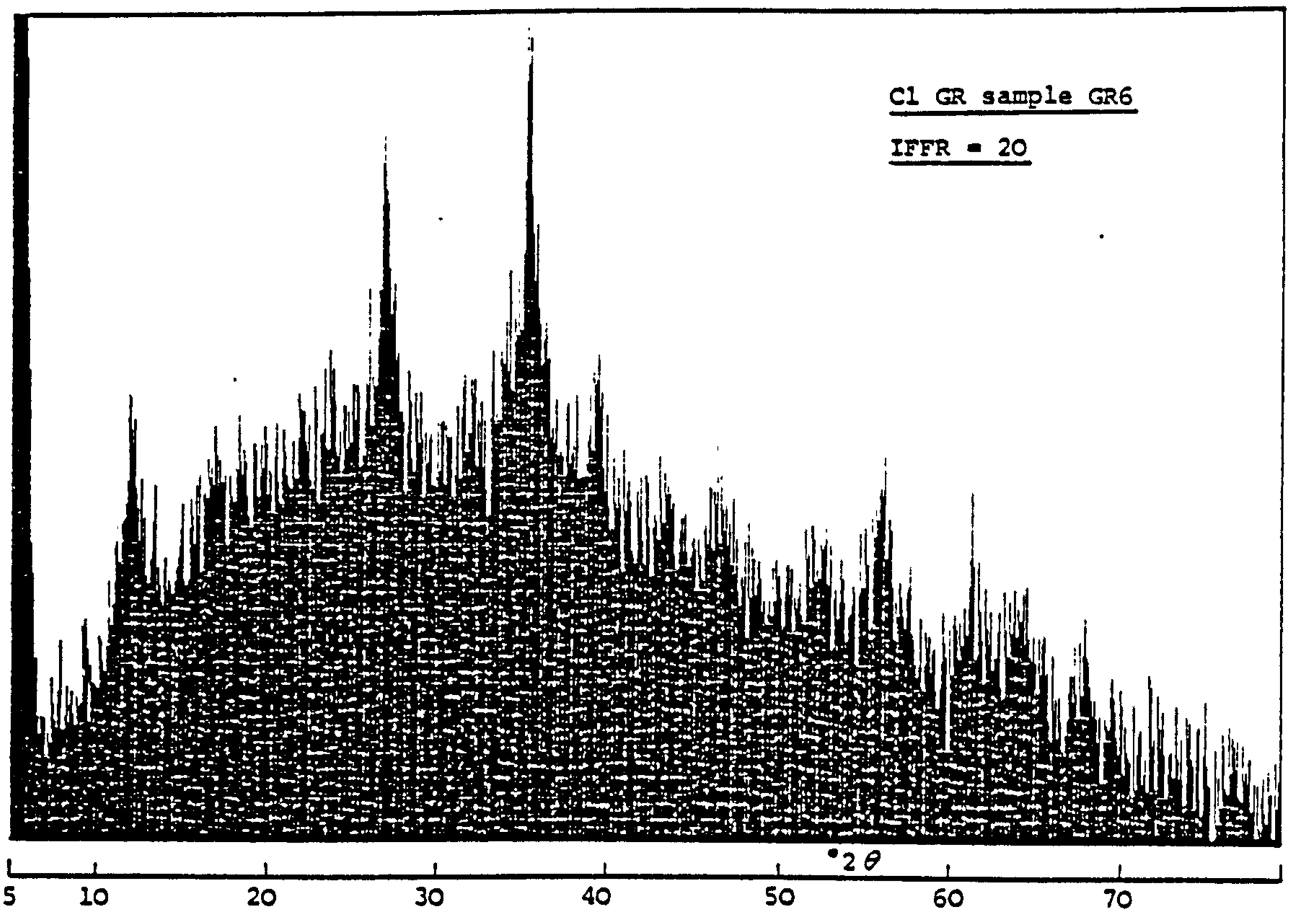

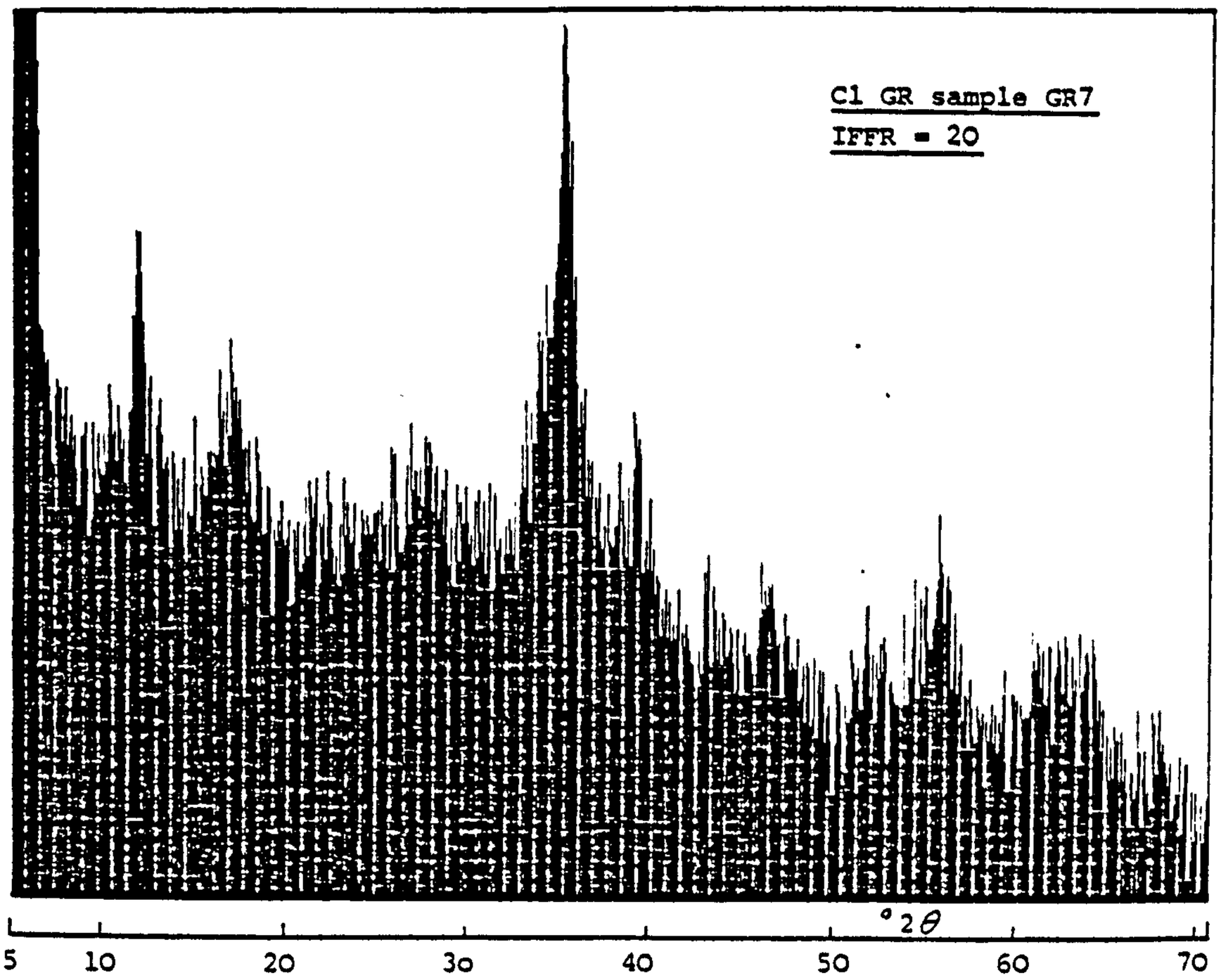

Fig 5.39 (cont'd) Typical X-ray diffractograms of chloride GRs derived from 0.1 M $FeCl_2$. (partially to completely oxidised)

Sample = GR12 IFFR = 6		Sample = GR11 (Stored under N_2) IFFR = 8		Sample = GR10 IFFR = 10		Sample = GR6 IFFR = 20		Sample = GR7 IFFR = 20		Sample = GR8 IFFR = 40	
d-spacing (A)	Int.	d-spacing (A)	Int.	d-spacing (A)	Int.	d-spacing (A)	Int.	d-spacing (A)	Int.	d-spacing (A)	Int.
		{7.70}	45								
7.3	40(B)			7.3	50(VB)	7.38	56	7.44	47	7.44	50
5.2	30(B)	5.19	23(B)	5.3	40(VB)			5.22	38		
		[4.17]	[55]							[4.85]	[41(?)]
3.32	70(B)	3.32	55	3.34	80(VB)	3.32	77	3.22	21(B)	[4.15] 3.36	[38(?)] 60(B)
		(2.98)	(25)								
		[2.683]	[45]								
2.52	100(B)	2.536	100	2.54	100(B)	2.536	100	2.550	100	2.543	100
		[2.443]	[55]								
		2.287	21			2.287	28	2.293	32		
		[2.181]	[20]								
		2.104	20								
		1.949	14	1.94	60(B)	1.953	27	1.957	23(B)		
		1.716	21			1.740	19(B)	1.762	23(B)		
1.63	40(B)	1.648	27			1.637	40	1.645	38	1.648	33(B)
		(1.611)	(23)								
		[1.561]	[23]								
		1.510	27			1.512	23				
		1.480	26								
		1.453	23								
		[1.318]	[16]								

{ } = degraded Cl GRI line [ ] = goethite lines ( ) = maghemite/magnetite lines B = broad VB = very broad

Table 5.39 X-ray d-spacings of chloride GRs derived from 0.1 M $FeCl_2$ (partially & completely oxidised).

Cl Green Rust I		Akaganeite		Maghemite		Magnetite	
d-spacing (A)	Int	d-spacing (A)	Int	d-spacing (A)	Int	d-spacing (A)	Int
8.02	100	7.40	100	5.90	2	4.85	40
4.01	80	5.25	40	4.82	5	2.966	70
2.701	60	3.70	10	4.18	1	2.530	100
2.408	60	3.311	100	3.73	5	2.419	10
2.037	30	2.616	40	3.41	2	2.096	70
1.805	20	2.543	80	2.95	34	1.712	60
1.716	20(B)	2.343	20	2.78	19	1.614	85
1.598	40	2.285	40	2.52	100	1.483	85
1.567	40	2.097	20	2.41	1	1.327	20
1.541	10	2.064	20	2.32	6	1.279	30
1.487	30	1.944	60	2.23	0.5	1.264	10
1.355	10	1.854	10	2.08	24	1.2112	20
1.040	10	1.746	40	1.87	0.5	1.1214	30
		1.719	10	1.70	12	1.0922	60
		1:635	100	1.61	33	1.0489	40
		1.515	40	1.55	0.5		
		1.497	20	1.53	1		
		1.480	20	1.48	53		
		1.459	10	1.43	1		
		1.438	80	1.32	7		
		1.374	40	1.27	11		
				1.26	3		
				1.21	5		
				1.12	7		
				1.09	19		

File No. 13-88	File No. 13-157	File No. 4-0755	File No. 11-614

Table 5.40 X-ray d-spacings of chloride Green Rust I, akaganeite, maghemite and magnetite. (Taken from ASTM powder diffraction file)

basal d-spacing of the chloride Al-GR produced by Taylor & McKenzie (1980). However, this does not really prove conclusively that a GRI was made. In fact, although the term "chloride GR" has been applied to the green precipitate produced here from $FeCl_2$ solutions, strictly speaking there is no real direct XRD evidence to support this supposition. Instead, by analogy with the sulphate GR produced in this study, and by comparison with the previous work of Taylor (1980) and Taylor & Mckenzie (1980), the assumption (and a good one at that) is that under similar conditions, the $FeCl_2$ system would give rise to the corresponding chloride GR compounds. The main indirect evidence is derived from Mossbauer spectroscopy which is considered in section 5.2.2e. However, even from the present XRD data, it can be inferred that a GRI was synthesised. Taylor & McKenzie (1980) showed that they produced chloride Al-GRs, which are the analogous compounds (Fe(II)-Al(III)) to the GRs proper (Fe(II)-Fe(III)). On oxidation the dried material can give rise to akaganeite. Thus by comparison with their results, the evidence presented here would indicate that chloride GRs were produced in this work.

The d-spacings of the non-GRs, produced under similar conditions from 0.1 M $FeCl_2$ but with lower IFFRs, are given in Table 5.41. All the samples shown have lines which are consistent with a magnetite/maghemite phase, with perhaps maghemite being more dominant. The dried

Sample = S14-11-83 IFFR = 1		Sample = S30-3-83 IFFR = 4		Sample = S4-4-83 IFFR = 4		Sample = S6-4-83 IFFR = 4		Sample = S13-6-83 IFFR = 4	
d-spacing (A)	Int.	d-spacing (A)	Int.	d-spacing (A)	Int.	d-spacing (A)	Int.	d-spacing (A)	Int.
4.82	9	4.77	12(B)	4.75	5(B)	4.82	12	4.82	9
		3.12	23						
2.950	21	2.941	29	2.931	24	2.950	27	2.950	27
2.522	100	2.515	100	2.515	100	2.515	100	2.522	100
		2.217	14						
2.094	25	2.090	21	2.085	20	2.085	23	2.090	20
1.704	13	1.707	15	1.698	10	1.707	10	1.707	9
1.611	30	1.608	26	1.608	28	1.611	35	1.616	29
1.480	42	1.478	35	1.478	36	1.478	40	1.482	38
				1.328	5(B)				
		1.278	10	1.275	6(B)	1.275	8(B)		
		1.090	10(B)						

B= Broad

Table 5.41 X-ray d-spacings of non-GRs derived from 0.1 M $FeCl_2$.

samples are black to dark-brown and have a high bulk magnetism. The wet, fresh precipitate was actually black in colour and fine-grained. The Mb spectra will show that for IFFR = 4 the fresh precipitate had a chloride GR pattern in addition to the magnetic splitting, and this disappears on ageing or vacuum-drying. This means that the transition region from chloride GR to non-GR (i.e. magnetite/maghemite) lies in the range $4 \leq IFFR < 6$. The XRD patterns of the non-GRs (Fig 5.40) are generally better than those for the chloride GRs. The peaks are better resolved (sharper and more distinct), and the background is lower and less erratic indicating that the compound was more stable.

It has already been emphasised that the dried chloride GR material oxidises to akaganeite. When oxidised under water, the chloride GR converts to lepidocrocite. This was demonstrated clearly by sample GR18 when some of the initial precipitate was re-suspended in distilled water and left to oxidised and aged for 69 days. The X-ray d-spacings of the converted material are given in Table 5.42 and the corresponding diffractogram shown in Fig 5.41. The intense and well-defined peaks in the X-ray diffractogram show the material to be well-crystalline. The lines given in Table 5.42 match those of lepidocrocite. Thus there appears to be two pathways for the oxidation of the chloride GRs: dry oxidation leads to akaganeite while wet oxidation leads to lepidocrocite.

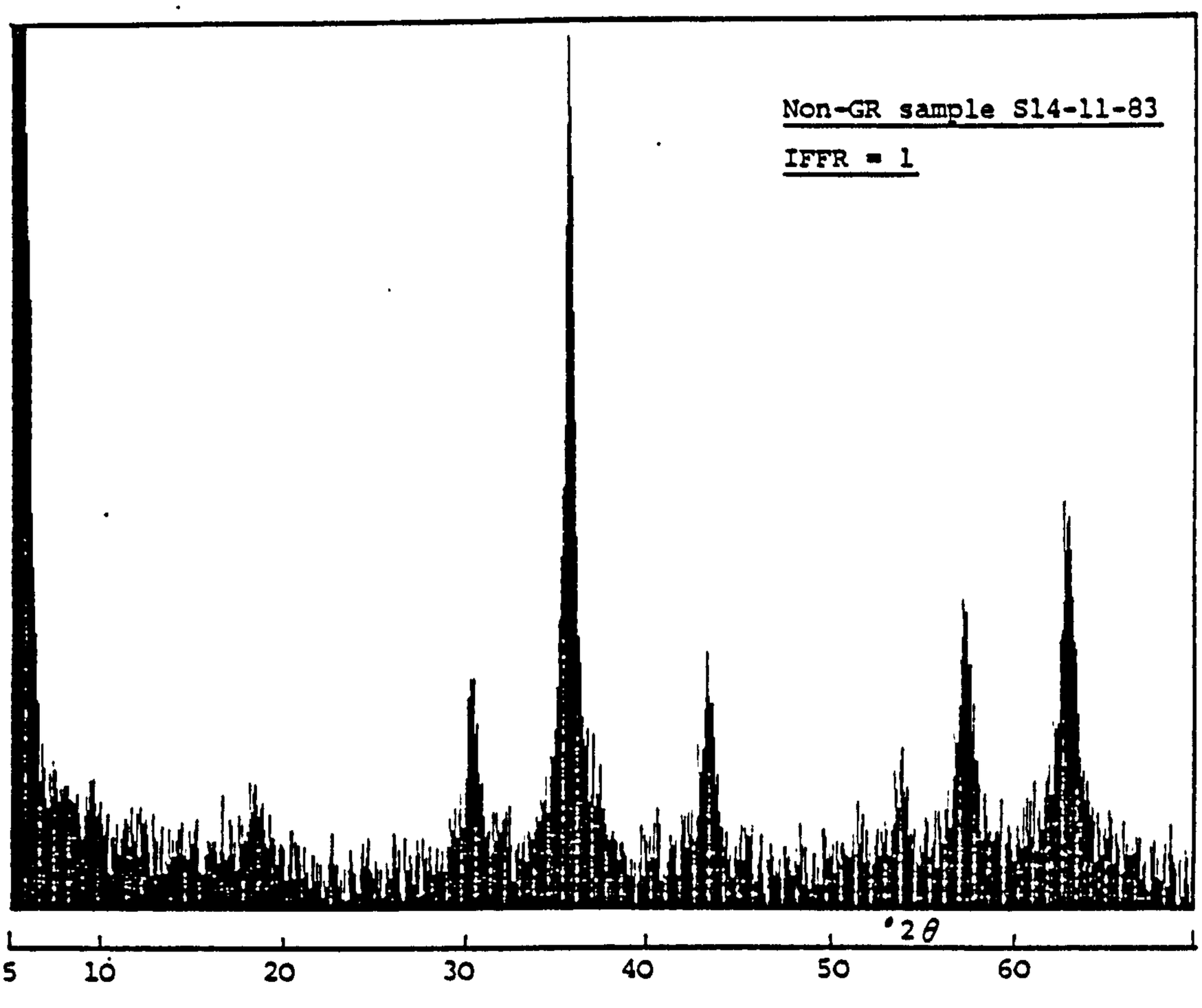

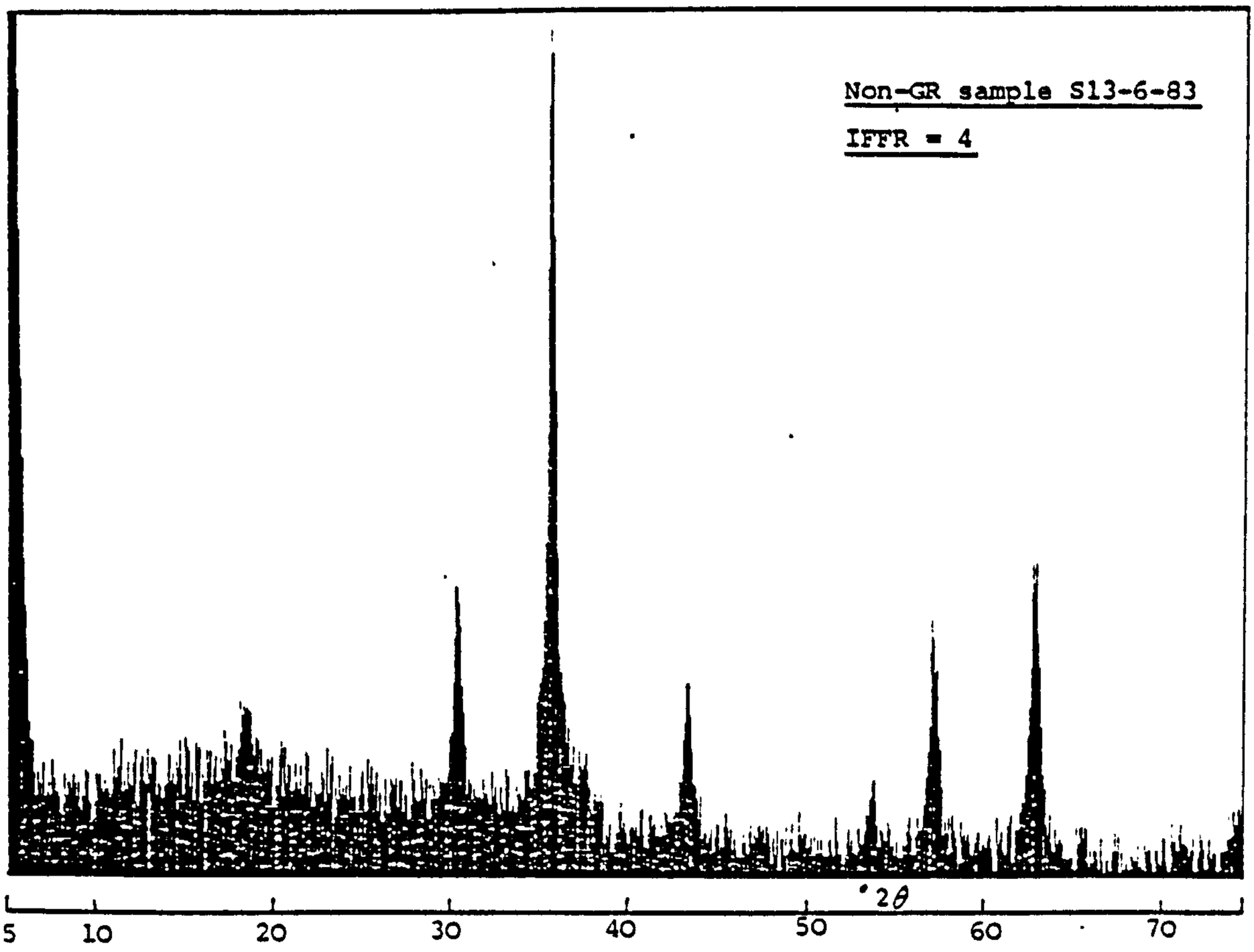

Fig 5.40 Typical X-ray diffractograms of non-GRs derived from 0.1 M $FeCl_2$.

Sample = GR18	
IFFR = 20	
d-spacing(A)	Int.
6.24	93
3.29	93
2.475	100
2.362	23
2.085	12
1.937	69
1.852	10(B)
1.737	31
1.528	28
1.490	12
1.439	14(B)
1.391	10
1.372	15

B = broad

Table 5.42 X-ray d-spacings for converted chloride GR sample (oxidised & aged under water).

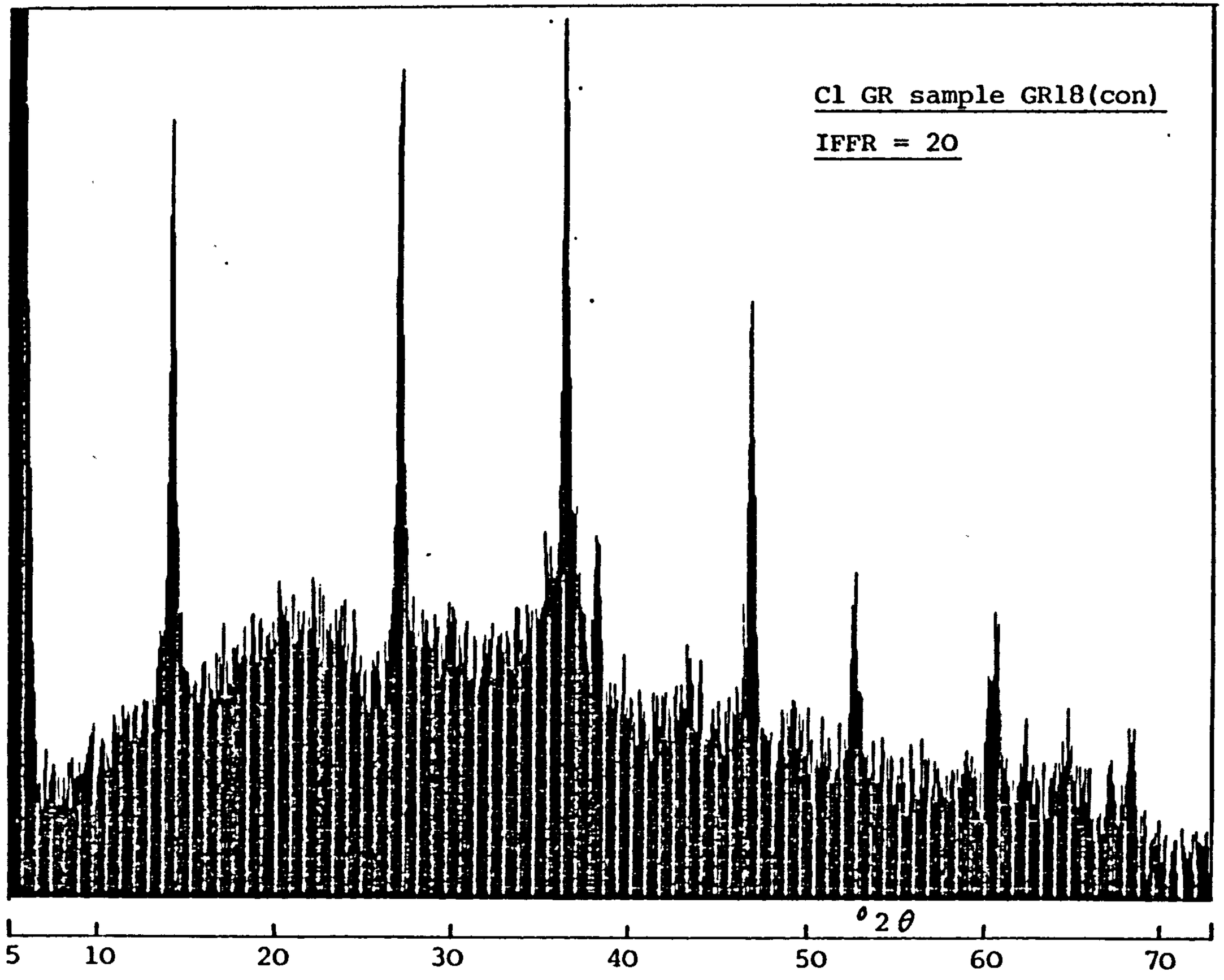

Fig 5.41 X-ray diffractogram of converted chloride GR sample. (aged & oxidised in water)

5.2.2c Infrared spectroscopy

The problem of oxidation for the chloride GRs is less with IR spectroscopy than with XRD because the time involved is much shorter and, also, the pressed disc method preserves the samples to some extent (as already mentioned in section 5.2.1c). Even so, the best IR spectra obtained were of partially oxidised material. The KBr discs themselves were dark-green to green in colour when prepared from freshly vacuum-dried material. Within a few hours, they became greenish-brown to brown in colour.

The IR absorption peaks and regions for partially oxidised (approaching completely oxidised) chloride GRs are given in Table 5.43. Typical spectra are shown in Fig 5.42. As with the sulphate GRs, the IR spectra of the chloride GRs have three main areas of absorption:

(i) a broad region in the range 3660-1830 cm^{-1} due to OH stretching from structural OH groups and/or molecular water.

(ii) a smaller region in the range 1700-1190 cm^{-1} due to OH bending from molecular water and also due to anionic bonds.

(iii) a region from 1000 cm^{-1} onwards arising from the stretching and bending of Fe-O bonds, and the bending of Fe-O-H groups.

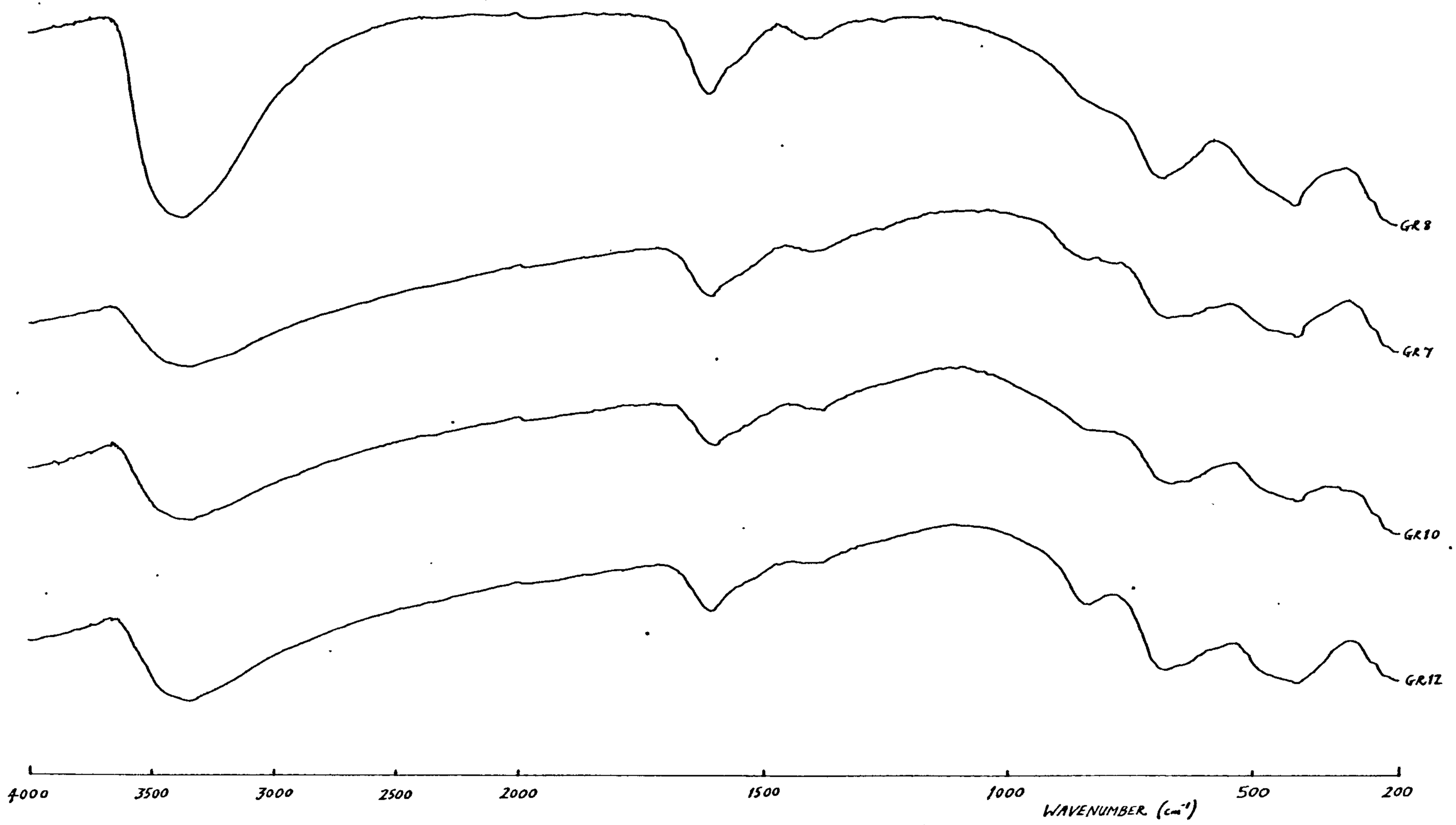

Fig 5.42 Typical IR spectra of chloride GRs derived from 0.1 M $FeCl_{2}$. (partially to completely oxidised)

Sample = GR12 IFFR = 6	Sample = GR11* IFFR = 8	Sample = GR11 IFFR = 8	Sample = 10 IFFR = 10	Sample = GR6 IFFR = 20	Sample = GR7 IFFR = 20	Sample = GR8 IFFR = 40
			Peaks (cm^{-1})			
3350 ± 50	3350 ± 40 3140 ± 60 2945 ± 10 2915 ± 10 2840 ± 10	3360 ± 50	3370 ± 50	3390 ± 60	3380 ± 60 3190 ± 80	3390 ± 40
1610 ± 10	1600 ± 10 1532(?) ± 10 1458(?) ± 10	1610 ± 10	1610 ± 10	1612 ± 10	1610 ± 10	1611 ± 10
1400 ± 20	1415 ± 10 1342 ± 5 880 ± 10	1400 ± 20	1395 ± 20	1415(?) ± 15 1383 ± 5	1390 ± 15	1400 ± 20
840 ± 10	792 ± 5	835 ± 15	825 ± 20	835 ± 30	840 ± 15 790(?) ± 15	830 ± 30
680 ± 10	680 ± 20 620 ± 20	678 ± 10	680 ± 15 630 ± 15	683 ± 10 630 ± 20	680 ± 10 625 ± 15	680 ± 15
480 ± 20		475 ± 20	480 ± 20	480 ± 20	475 ± 20	480 ± 25
412 ± 15	402 ± 10	412 ± 15	410 ± 10	412 ± 10 320 ± 10	405 ± 10	410 ± 10
			Regions (cm^{-1})			
3650-2100	3640-2100	3650-2000	3650-2100	3660-1830	3640-2020	3660-2460
1710-1280	1720-1220	1700-1190	1700-1210	1720-1220	1700-1200	1730-1240
1000- 310	950- 300	1000- 310	980- 350	1000- 290	930- 310	1000- 310

* stored under N_2

Table 5.43 IR absorption peaks and regions of partially oxidised chloride GRs derived from 0.1 M $FeCl_2$.

In general, the chloride GR spectra do not have as many distinct and pronounced peaks as the sulphate GR spectra. This indicates a less ordered and less crystalline material for the chloride GRs. However, this may be due to the deterioration of the material from oxidation. Except for the stored material of sample GR11, the partially oxidised chloride GRs have virtually identical IR spectra. The peaks between 900 cm^{-1} and 450 cm^{-1} indicate the presence of akaganeite (see Table 5.3 and Fig 5.1) which support the XRD evidence. The somewhat squarish peak at ~ 410 cm^{-1} suggests the appearance of a magnetite structure. However, since a magnetite phase does not appear normally in the XRD data for the chloride GRs (whether oxidised or not), it is more likely that the chloride GR and magnetite structures have enough similarity to give a similar IR absorption peak at ~ 410 cm^{-1}. The stored material of sample GR11 also has two extra peaks at 880 and 792 cm^{-1} which is due to the goethite component. The weak but distinctive peak at ~ 2900 and also the ripples around 1500-1300 cm^{-1} for this particular spectrum may be due to hydrocarboons from rotary pump oil contamination, although this is not absolutely certain since it also appears in certain natural iron oxides dried in the open air.

The obvious difference between the sulphate GRs and the chloride GRs is the lack of a characteristic absorption

region associated with chloride bonding for the latter (i.e.assuming that Cl^- anions were incorporated into the GR structure, which from the conversion to akaganeite on oxidation seems to be the case). This rather limits the usefulness of the IR spectrum for characterising the chloride GRs. The weak peak at ~ 1400 cm^{-1} may be ascribed to any bonding associated with Cl^- anions. It is not due to NO_3^- anions since virtually all the Fe(III) gel used was derived from $FeCl_3$. In any case, in the one sample (GR6) which used $Fe(NO_3)_3$, the NO_3^- anions showed up as a fairly sharp peak at a slightly lower wavenumber of 1383 cm^{-1}. A sample of basic $FeCl_2$, made by partially precipitating a solution of $FeCl_2$, also shows absorption at 1400 cm^{-1} (Fig 5.43). [Basic $FeCl_2$ has a chemical formula of $Fe(OH)_2.xFeCl_2$, where x = a variable.] The peak is relatively stronger in basic $FeCl_2$ than in the chloride GRs. If this peak at 1400 cm^{-1} is due to some sort of chloride bonding (say Fe-Cl), then the increased relative absorption in basic $FeCl_2$ is to be expected since the latter has more Cl^- anions in its structure. The IR spectrum of basic $FeCl_2$ is essentially similar to that of the chloride GRs, except for the less well-developed peaks in the 900-450 cm^{-1} region. Basic $FeCl_2$ can thus be thought of as a precursor to the chloride GRs.

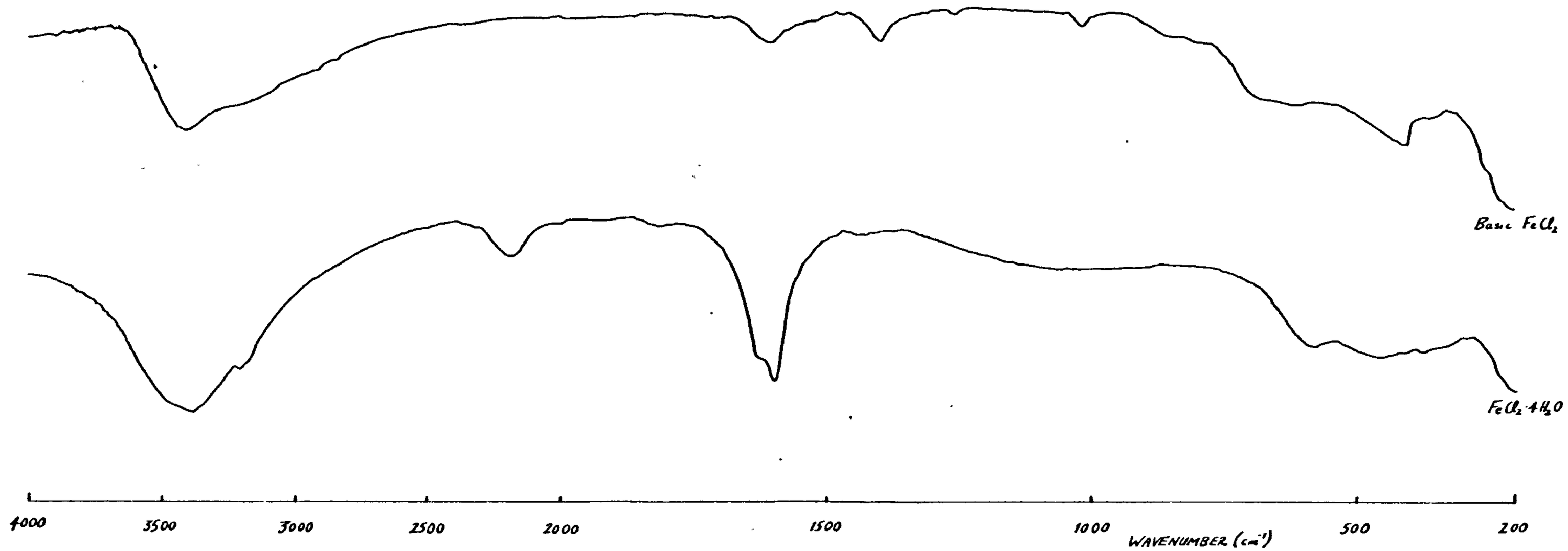

Fig 5.43 IR spectrum of $FeCl_2.4H_2O$ and basic $FeCl_2$.

On complete oxidation, the dried chloride GR material gave essentially the same IR spectrum as before but with more pronounced peaks at 900-450 cm^{-1} due to the increased akaganeite content. The peak at 1610 cm^{-1} is somewhat reduced in intensity, indicating loss of water of crystallisation and/or adsorbed water. The peak at ~ 1400 cm^{-1} is also reduced suggesting that Cl^- anions are volatile (if the peak is associated with chloride bonding).

The main difference between the oxidised chloride GRs and a well-formed akaganeite is the less well-defined peaks from 900 cm^{-1} onwards and inthe 3700-3000 cm^{-1} region. The IR absorption peaks and regions for the completely oxidised chloride GRs are given in Table 5.44 and a few typical spectra are shown in Fig 5.44.

The IR spectra of the non-GR samples synthesised from 0.1 M $FeCl_2$ are virtually identical to that of the magnetite sample shown in Fig 5.1 (see also Table 5.3), which again confirms XRD evidence. The rather steep, rectangular-shaped peak at ~ 410 cm^{-1} is characteristic in all the spectra. The non-GR samples probably has more adsorbed water, resulting in the absorption at ~ 1615 cm^{-1}. Typical spectra are shown in Fig 5.45 and the corresponding absorption peaks and regions are given in Table 5.45.

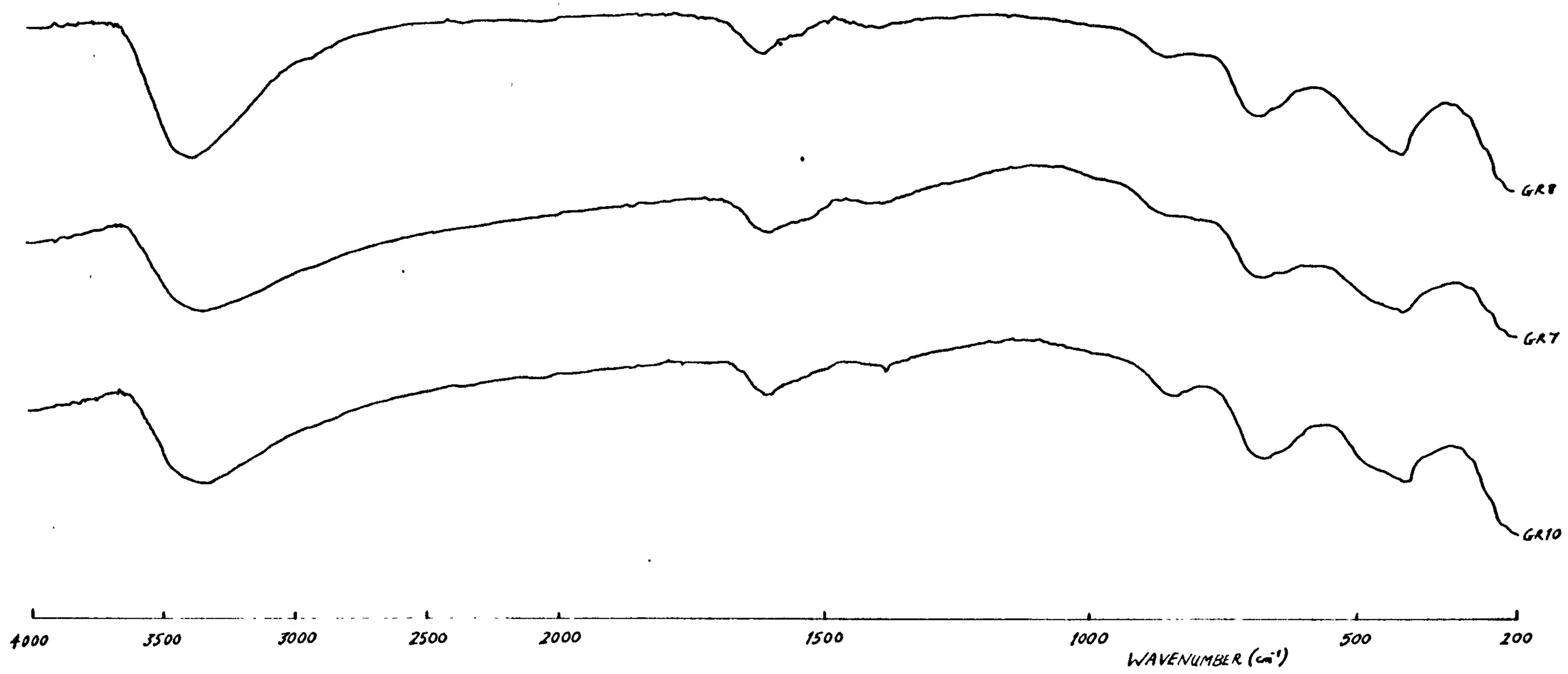

Fig 5.44 Typical IR spectra of completely oxidised chloride GR samples derived from 0.1 M $FeCl_2$.

Sample = GR11	Sample = GR10	Sample = GR6	Sample = GR7	Sample = GR8
IFFR = 8	IFFR = 10	IFFR = 20	IFFR = 20	IFFR = 40
Peaks (cm^{-1})				
3360 ± 40	3370 ± 50	3370 ± 40	3360 ± 50	3390 ± 40
1610 ± 10	1605 ± 10	1610 ± 10	1610 ± 10	1612 ± 10
		1535 ± 20	1530 ± 20	1540 ± 20
1380(?) ± 10	1380 ± 5	1395 ± 15	1390 ± 15	1390 ± 20
845 ± 10	847 ± 10	855 ± 10	850 ± 20	850 ± 10
680 ± 15	680 ± 10	680 ± 15	680 ± 15	680 ± 10
645 ± 15	635 ± 20	635 ± 20	635 ± 20	640 ± 20
480 ± 20	480 ± 20	475 ± 25	485 ± 25	480 ± 20
408 ± 10	410 ± 10	410 ± 10	410 ± 10	412 ± 10
Regions (cm^{-1})				
3640-2180	3660-2180	3640-2200	3640-1900	3660-2500
1700-1250	1680-1230	1700-1300	1690-1200	1730-1290
940- 320	940- 330	940- 320	1040- 340	940- 330

Table 5.44 IR absorption peaks and region of completely oxidised chloride GRs derived from 0.1 M $FeCl_2$.

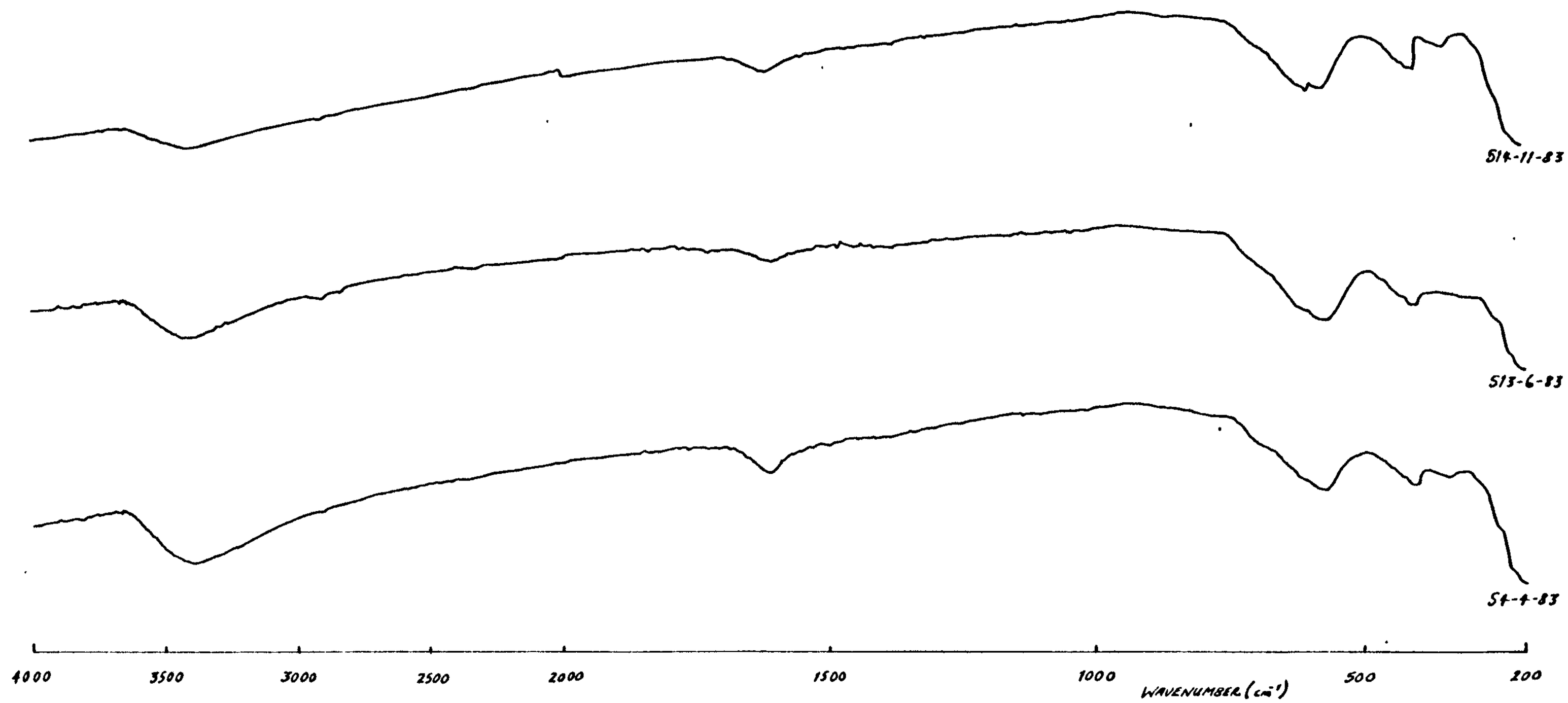

Fig 5.45 Typical IR spectra of non-GRs derived from 0.1 M $FeCl_2$.

Sample = S14-11-83 IFFR = 1	Sample = S30-3-83 IFFR = 4	Sample = S4-4-83 IFFR = 4	Sample = S6-4-83 IFFR = 4	Sample = S13-6-83 IFFR = 4
		Peaks (cm^{-1})		
3410 ± 40	3380 ± 40	3410 ± 40	3420 ± 40	3420 ± 30
1615 ± 10	1625 ± 10	1622 ± 10	1620 ± 10	1610 ± 10
	1400 ± 20			
695(?)± 20	702 ± 20	695 ± 20	700(?)± 20	700 ± 20
625 ± 20	630 ± 20	630 ± 20	630 ± 20	630 ± 20
567 ± 10	585 ± 10	585 ± 10	580 ± 10	580 ± 10
402 ± 10	410 ± 5	410 ± 5	408 ± 5	407 ± 5
350 ± 10	360 ± 10	350 ± 10	352 ± 10	
		Regions (cm^{-1})		
3620-2500	3660-2300	3660-2200	3660-2500	3650-2700
1690-1500	1700-1300	1700-1320	1700-1340	1700-1300
750- 320	760- 320	750- 310	760- 310	760- 390

Table 5.45 IR absorption peaks and regions of non-GRs derived from 0.1 M $FeCl_2$.

The material from sample GR18 which was oxidised and aged under water has an IR spectrum which confirms that lepidocrocite was formed in the process (Fig 5.46). The distinguishing peaks are at 1015, 740 and 355 cm^{-1}.

The structural OH groups seems to be in a slightly different environment to sample P23 (Fig 5.1 and Table 5.3). The IR data for this converted sample from GR18 is given in Table 5.46.

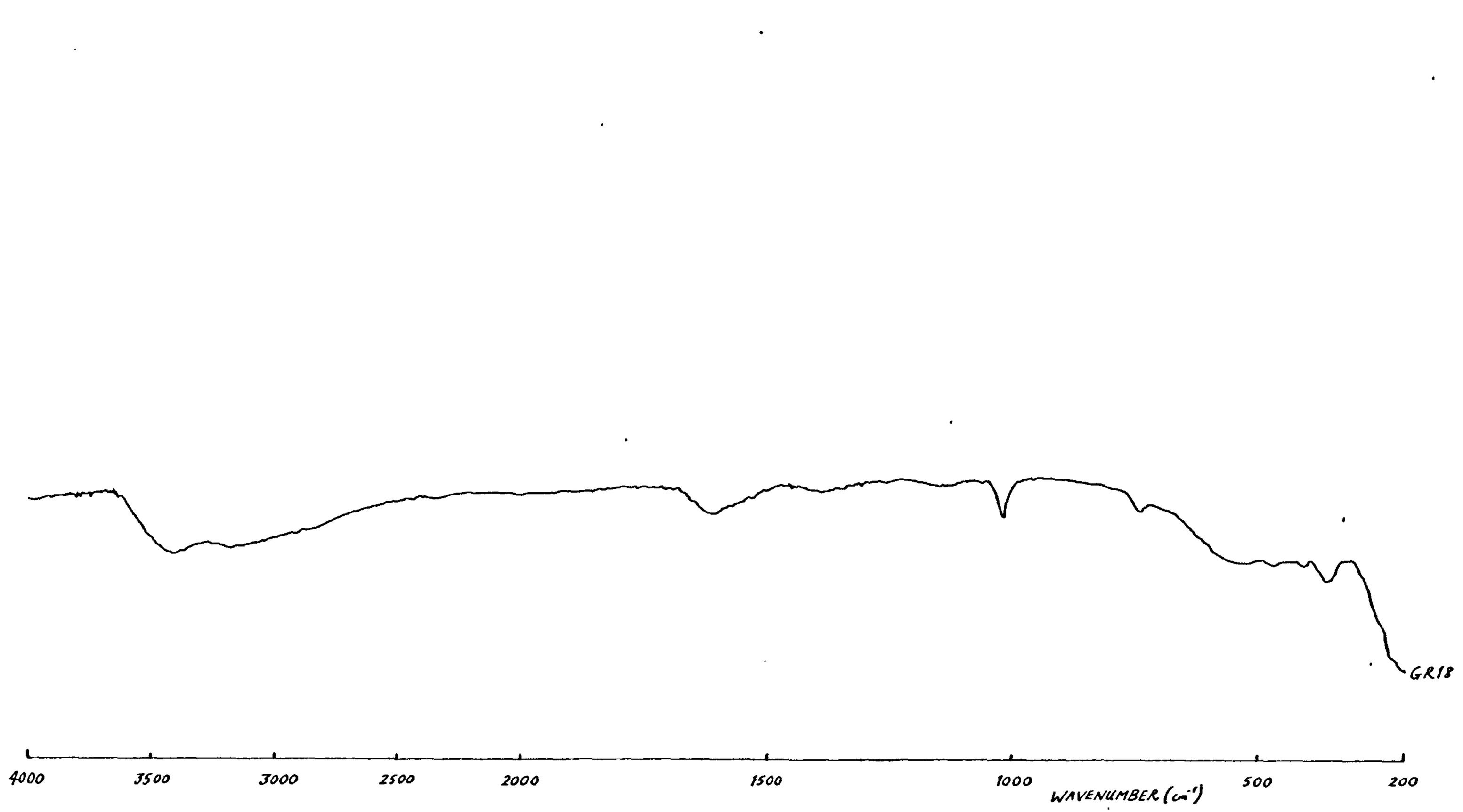

Fig 5.46 IR spectrum of converted chloride GR sample.
(aged & oxidised in water)

Sample = GR18	
IFFR = 10	
Peaks	(cm^{-1})
3410	± 25
3170	± 50
1612	± 10
1385	± 15
1145(?)	± 20
1015	± 5
740	± 10
540	± 20
465	± 10
405	± 10
355	± 10

Table 5.46 IR absorption peaks and regions for converted chloride GR sample (oxidised & aged under water).

5.2.2d Surface area measurements

The surface areas for the chloride GRs and the non-GRs synthesised from 0.1 M $FeCl_2$ are given in Tables 5.47 and 5.48, respectively. Representative N_2 adsorption isotherms of the chloride GRs are shown in Fig 5.47, and a typical adsorption isotherm for the non-GRs is shown in Fig 5.48.

Despite the fact that the samples were located in a vacuum microbalance during measurements, the partially oxidised chloride GRs became completely oxidised by the end of the measurements (~ 2 h to obtain points for the linear BET plot plus another 3-4 h for the complete adsorption isotherm). The surface area values for the chloride GRs are thus applicable to the partially oxidised to completely oxidised material.

It can be seen from Tables 5.47 and 5.48 that for both categories of material, there seems to be no trend in the values of the surface area. For the chloride GRs, this variability may be linked to the oxidation which may lead to changes in the surface. The problem of oxidation might also account for the variability in the non-GR values since magnetite oxidises to maghemite. Also there is no clear distinction between the two groups of material as far as surface area is concerned. What can be said is that the surface area (in the range 60-100

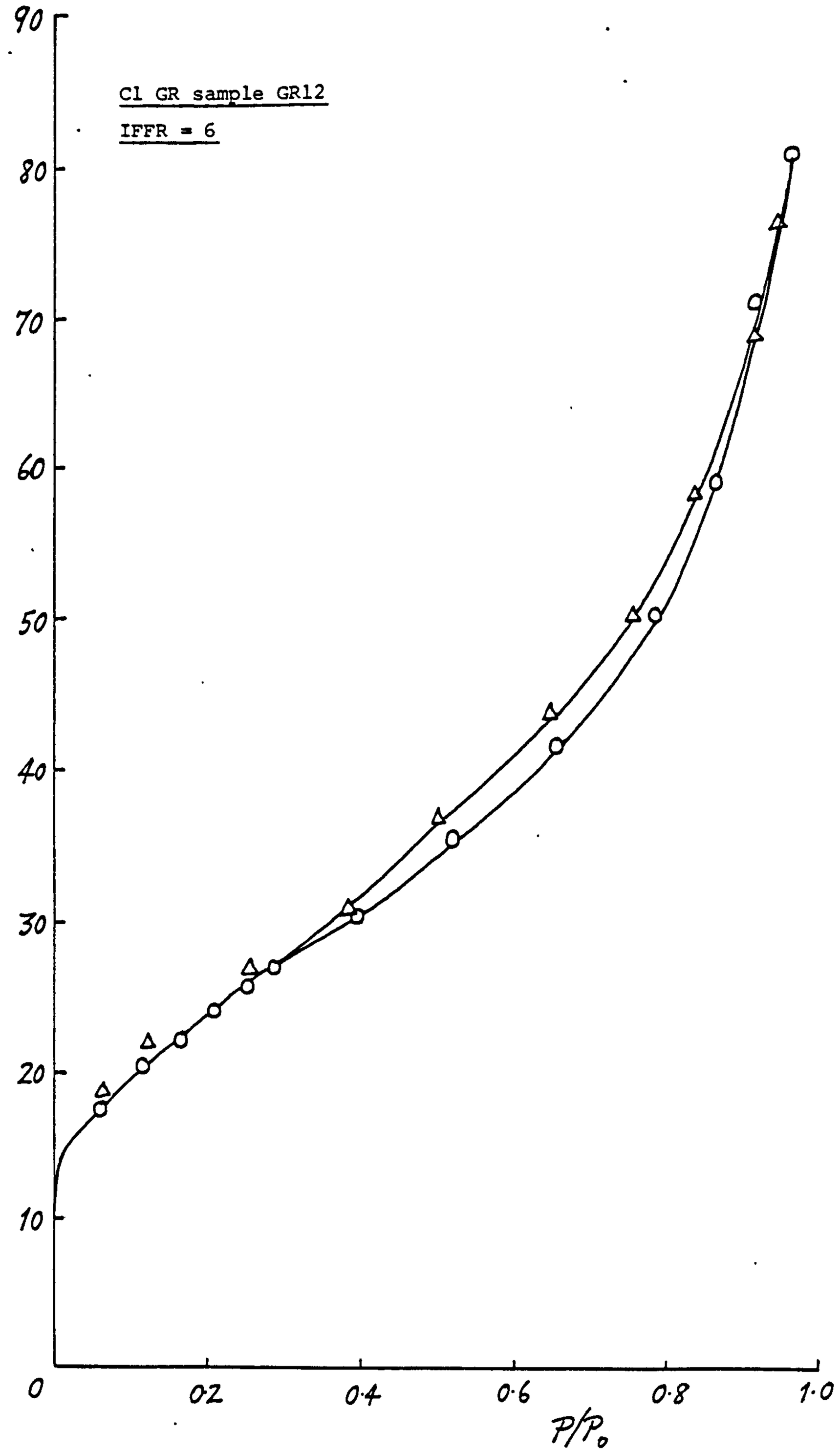

Fig 5.47 Typical N_2 adsorption isotherms of chloride GRs derived from 0.1 M $FeCl_2$. (partially to completely oxidised)

(O - adsorption Δ -desorption)

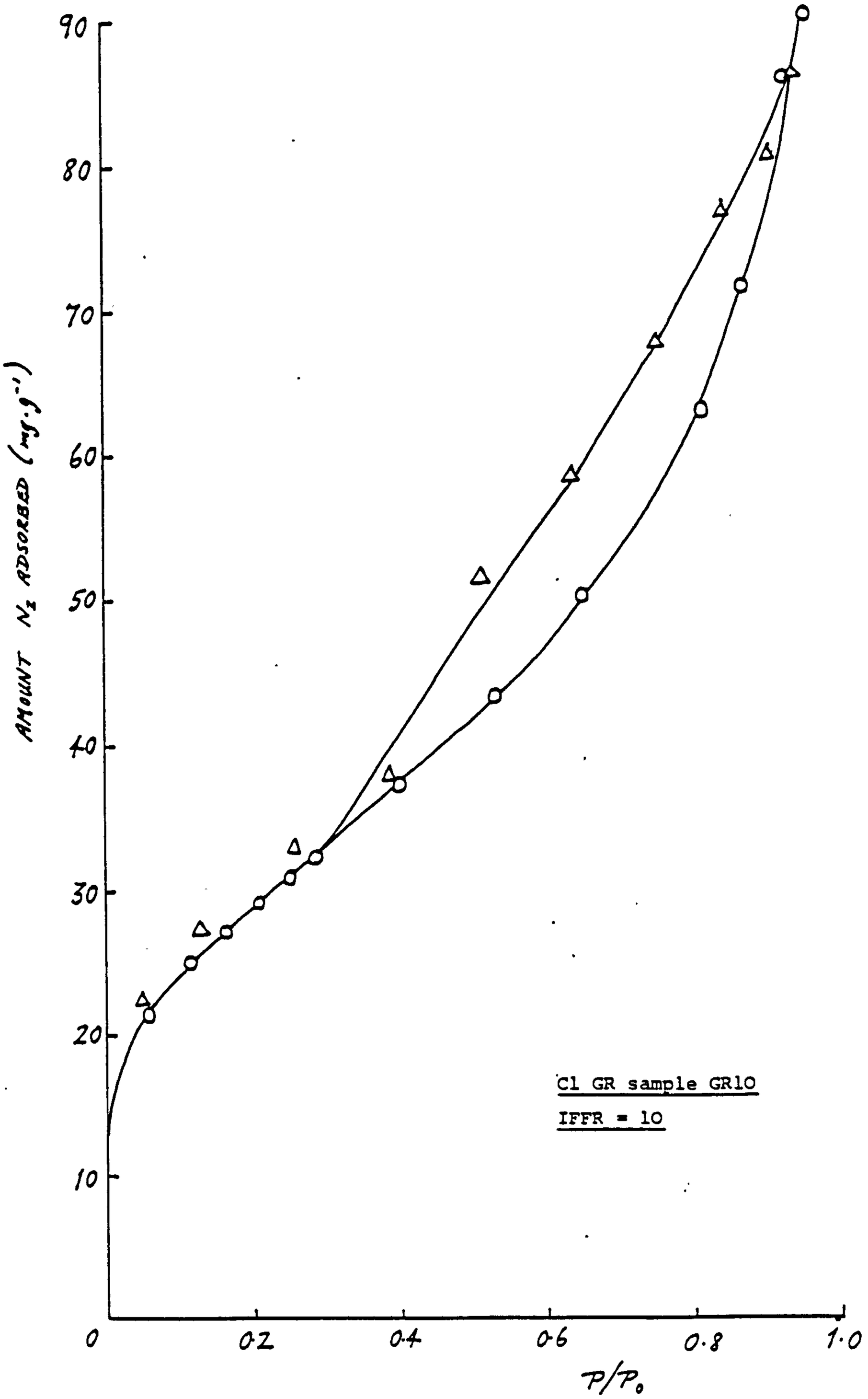

Cl GR sample GR10

IFFR = 10

Fig 5.47 (cont'd) Typical N_2 adsorption isotherms of chloride GRs derived from 0.1 M $FeCl_2$. (partially to completely oxidised)

(O - adsorption Δ - desorption)

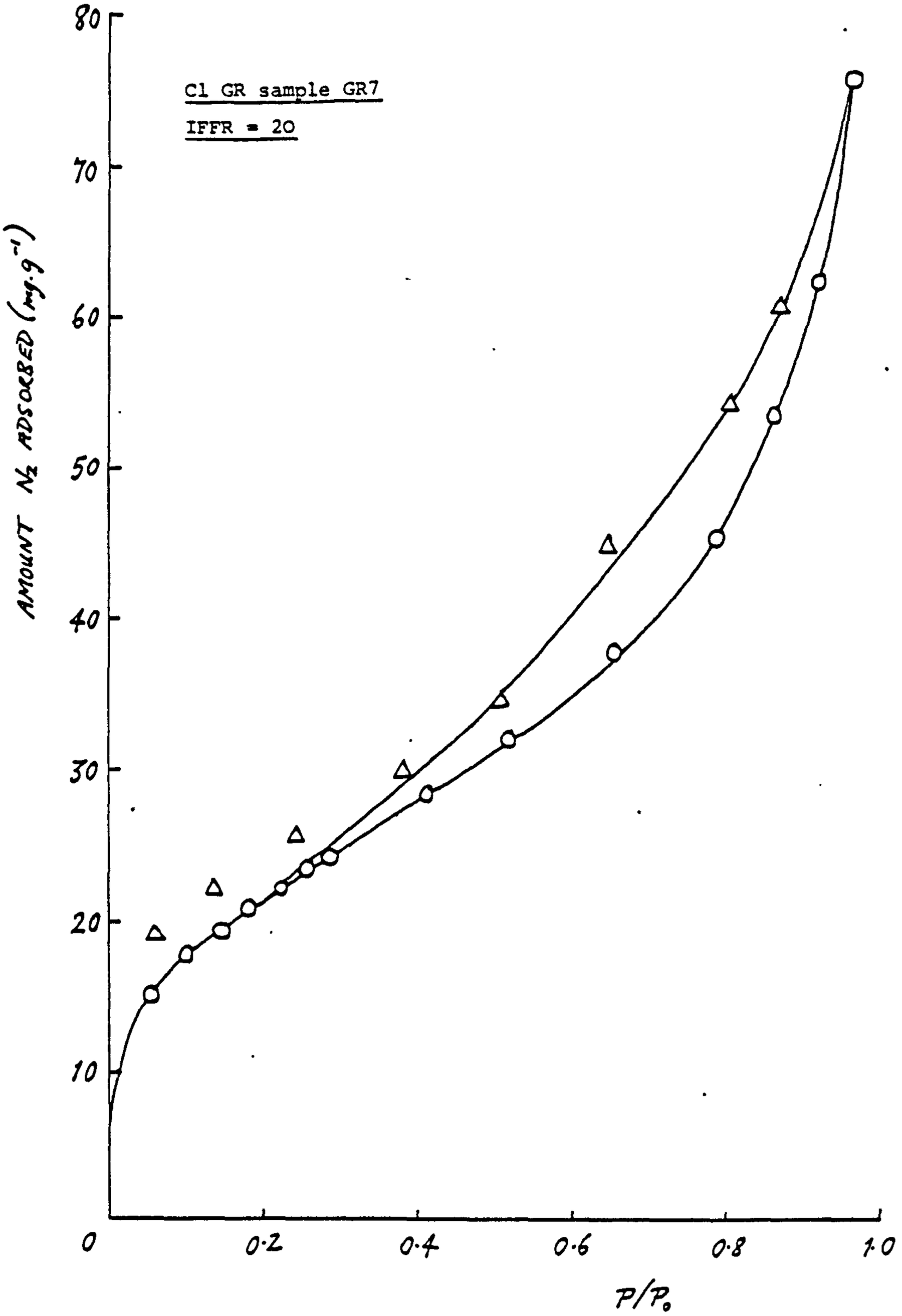

Fig 5.47 (cont'd) Typical N_2 adsorption isotherms of chloride GRs derived from 0.1 M $FeCl_{2-3}$. (partially to completely oxidised)

(O - adsorption △ -desorption)

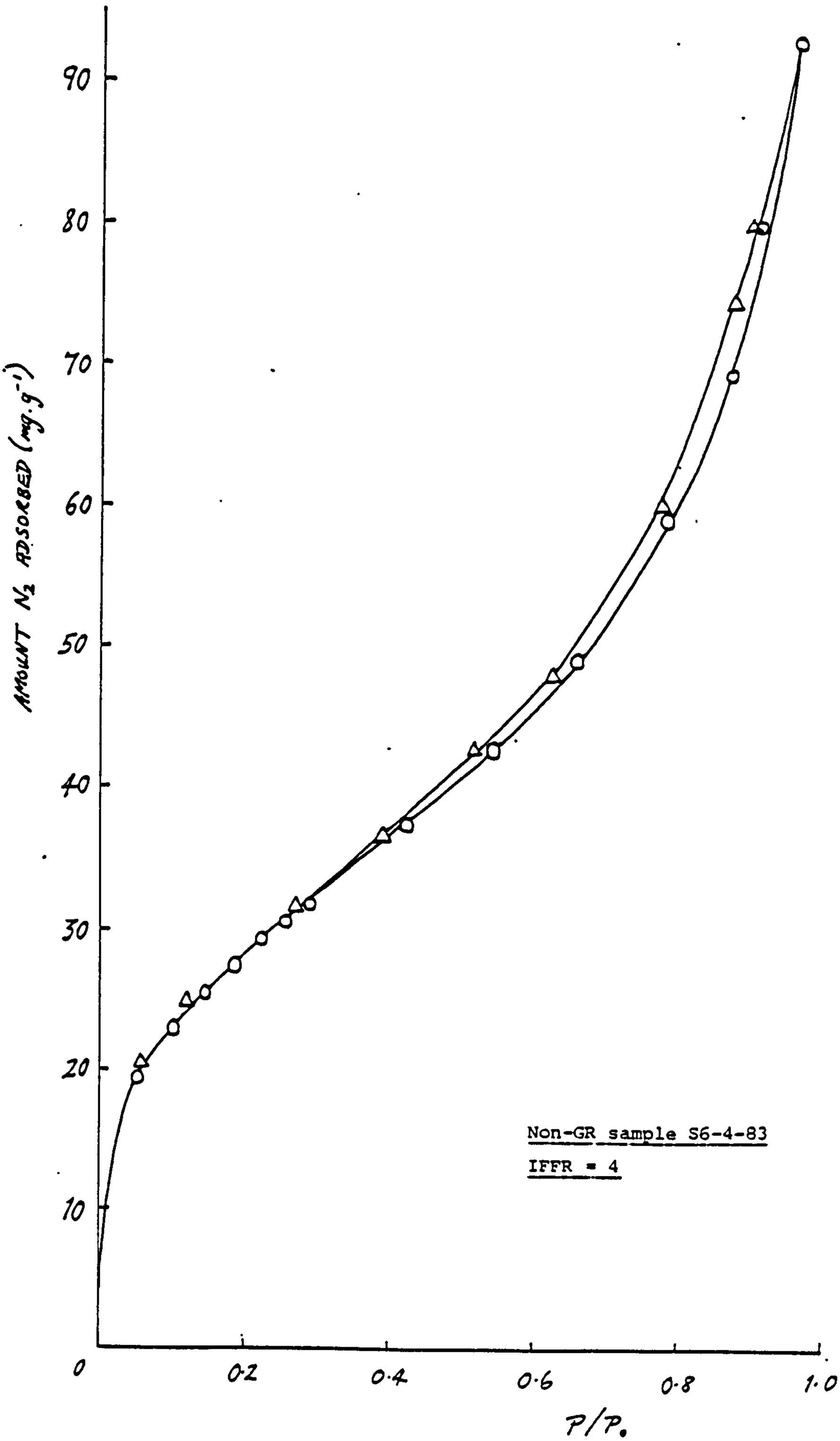

Non-GR sample S6-4-83

IFFR = 4

Fig 5.48 Typical N_2 adsorption isotherm of the non-GRs derived from 0.1 M $FeCl_2$.

(O - adsorption Δ - desorption)

Sample	IFFR	<Fe(III)> (mmole)	Surface Area ($m^2.g^{-1}$)
GR12	6	3.35	69.3
GR11	8	2.5	91.1
GR10	10	2.0	82.7
GR6	20	1.0	75.8
GR7	20	1.0	62.4
GR8	40	0.5	99.7

Table 5.47 Surface areas of chloride GRs (partially oxidised) derived from 0.1 M $FeCl_2$.

Sample	IFFR	<Fe(III)> (mmole)	Surface Area ($m^2.g^{-1}$)
S14-11-83	1	20	94.9
S30-3-83	4	5	89.7
S4-4-83	4	5	73.6
S6-4-83	4	5	82.5
S13-6-83	4	5	66.2

Table 5.48 Surface areas of non-GRs derived from 0.1 M $FeCl_2$.

$m^2.g^{-1}$) for both groups is characteristic of Fe(II)-derived oxides (Crosby, 1982; Crosby et al., 1983) i.e. significantly lower than the normal Fe(III) oxides (150-250 $m^2.g^{-1}$). The N_2 adsorption isotherms (Figs 5.47 and 5.48) confirm this view, being Type IV isotherms with hysteresis and characteristic of Fe(II)-derived material. The adsorption isotherms are very similar for both chloride GRs and the non-GRs. Thus the results so far show that the surface of the two categories are more or less the same. However, there is a difference between the chloride GRs and the sulphate GRs i.e. the surface area is generally greater for the chloride GRs (cf. 40-70 $m^2.g^{-1}$ for the sulphate GRs). It can be argued that this is not a direct comparison since the chloride GRs were partially oxidised. However, measurement of oxidised sulphate GRs show no change in the surface area, indicating that the surface is not altered by oxidation. Thus oxidised sulphate GRs would still have low surface areas.

The shape of the hysteresis loop for both chloride GRs and non-GRs conforms most closely to type B in the de Boer classification (de Boer, 1958), which is the same as the sulphate GRs. To reiterate, this type of hysteresis is associated with either slit-shaped pores or the space between parallel plates. The pore size distributions for both categories of material, as estimated from the hysteresis closure points and using equation 2.23, are

given in Tables 5.49 and 5.50, respectively. As with the sulphate GRs, the lower closure points on half of the chloride GR samples cannot be determined because the desorption points at the low relative pressure end have long equilibrium times, and thus the hysteresis loop does not completely close experimentally. This again is due to microporosity in the samples.

It can be seen from the tables that the pore sizes are usually in the mesopore range (20-500 A diameter) for both chloride GRs and non-GRs. There are some macropores (> 500 A diameter), and for the chloride GRs there is a degree of microporosity.

To sum up the surface area measurements, it can be stated that surface-wise there is very little difference between the chloride GRs (partially oxidised to completely oxidised) and the magnetic non-GRs. They also seem to have similar pore size and shape. It can also be said that there is a great similarity between the chloride GRs and the sulphate GRs in terms of surface and porosity (although the chloride GRs have a slightly larger surface area). This is not too surprising since the conditions of formation are very similar in respect to pH and concentration.

Sample	IFFR	Hysteresis Clos. P/P_o (approx.)	Pore Size Range, d (A)
GR12	6	0.30 - 0.96	30 - 500
GR11	8	* - 0.97	* - 670
GR10	10	0.30 - 0.95	30 - 400
GR6	20	0.30 - 0.95	30 - 400
GR7	20	0.25 - 0.96	20 - 500
GR8	40	* - 0.97	* - 670

* indicates that the lower limit cannot be determined.

Table 5.49 Pore size distributions for partially oxidised chloride GRs derived from 0.1 M $FeCl_2$.

Sample	IFFR	Hysteresis Clos. P/P_o (approx.)	Pore Size Range, d (A)
S14-11-83	1	0.40 - 0.93	30 - 290
S30-3-83	4	0.40 - 0.94	30 - 340
S4-4-83	4	0.40 - 0.92	30 - 260
S6-4-83	4	0.30 - 0.96	30 - 500
S13-6-83	4	0.25 - 0.97	20 - 670

Table 5.50 Pore size distributions for non-GRs derived from 0.1 M $FeCl_2$.

5.2.2e Mossbauer Spectroscopy

1) Chloride GRs synthesised from 0.1 M $FeCl_2$

(i) 77 K data

The 77 K Mb parameters for the wet, fresh precipitates of the chloride GRs are given in Table 5.51. Typical 77 K spectra are shown in Fig 5.49.

The chloride GR spectrum is composed of an Fe(II) and an Fe(III) quadrupole doublet. The ratio Fe(II)/Fe(III) (or FFR) in the spectra varies from 1.77 to 2.89, although there is no definite trend with IFFR (the general tendency is towards higher FFRs). The main difference between the chloride GR spectrum and that of the sulphate GR is the absence of any MHS. As with the sulphate GRs, the IS, QS and $1/2\Gamma$ seems to be invariant over the IFFR range studied. This is not surprising since these parameters are a measure of short-order interactions, and the environment around the ^{57}Fe nucleus would not be expected to change drastically with IFFR. The mean values are:-

(i) Fe(II) doublet: IS = 1.24 $\pm$ 0.10 mms^{-1}, QS = 2.80 $\pm$ 0.05 mms^{-1}, $1/2\Gamma$ = 0.19 $\pm$ 0.05 mms^{-1}

(ii) Fe(III) doublet: IS = 0.43 $\pm$ 0.10 mms^{-1}, QS = 0.46 $\pm$ 0.05 mms^{-1}, $1/2\Gamma$ = 0.17 $\pm$ 0.05 mms^{-1}.

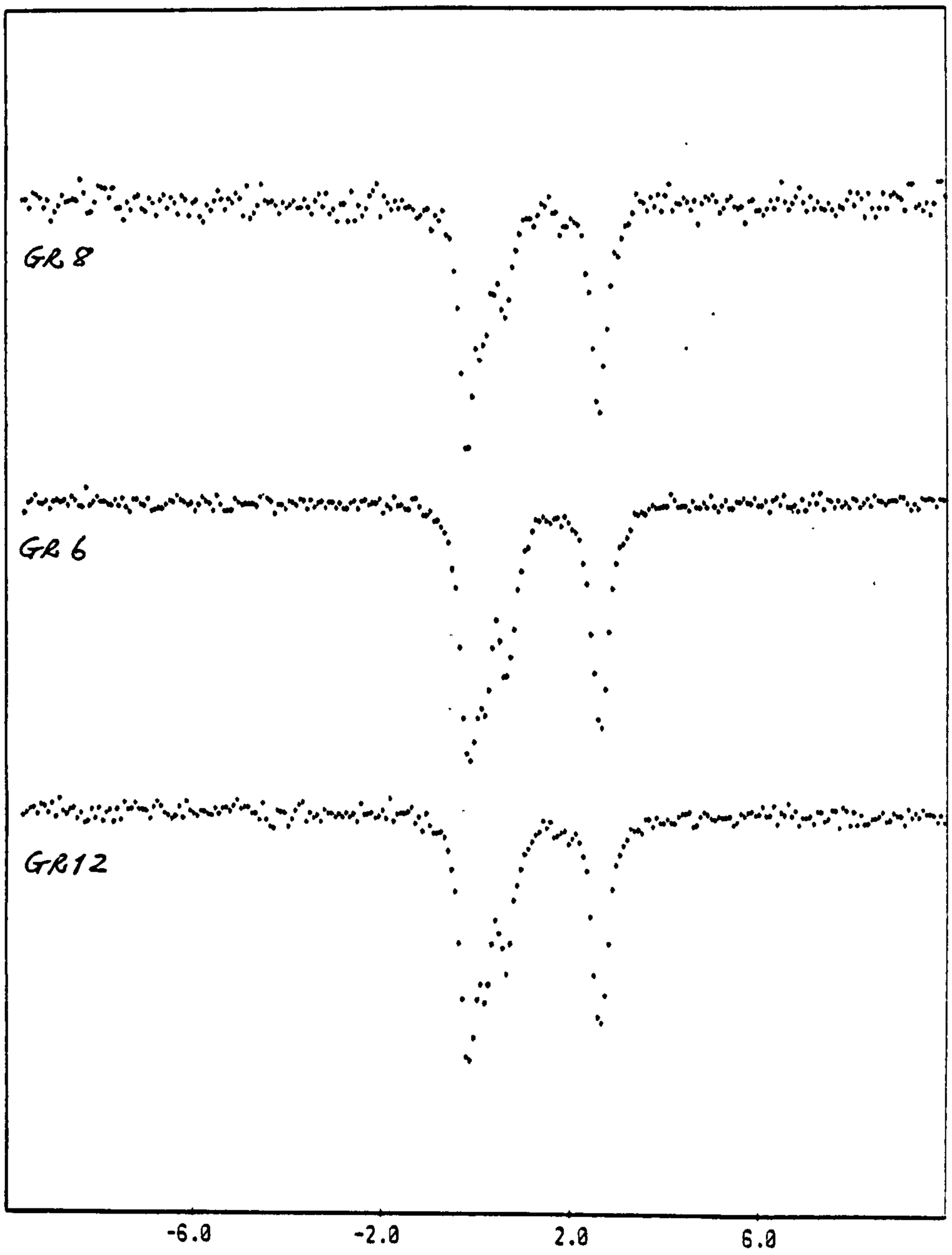

Fig 5.49 Typical 77 K Mb spectra of the wet, fresh precipitate of chloride GRs derived from 0.1 M $FeCl_2$.

Sample	IFFR	Fe(II) doublet			Fe(III) doublet			FFR
		δ	Δ	$\frac{1}{2}\Gamma$	δ	Δ	$\frac{1}{2}\Gamma$	
GR12	6	1.23	2.81	0.18	0.43	0.45	0.17	1.85
GR11	8	1.22	2.80	0.19	0.42	0.47	0.16	1.81
GR25	8	1.26	2.79	0.19	0.45	0.43	0.17	2.38
GR10	10	1.22	2.81	0.18	0.41	0.48	0.18	1.81
GR6	20	1.25	2.79	0.19	0.44	0.46	0.18	1.77
GR7	20	1.24	2.80	0.19	0.43	0.43	0.19	2.09
GR18	20	1.26	2.76	0.21	0.45	0.47	0.18	2.01
GR8	40	1.21	2.81	0.18	0.40	0.46	0.15	2.89
Mean		1.24	2.80	0.19	0.43	0.46	0.17	

Table 5.51 77 K Mb parameters for the wet, fresh precipitate of chloride GRs derived from 0.1 M $FeCl_2$.

Whilst the Fe(III) doublet here is virtually the same as that for the sulphate GRs, the Fe(II) doublet in the chloride GR is distinctively different with a slightly smaller QS. Thus obviously the Cl^- anions alter the environment the Fe nucleus enough for this to be noted on the Mb spectrum.

The IS and QS for the chloride GRs are very similar to that of the basic salts of $FeCl_2$ [as mentioned in section 5.2.2c, basic $FeCl_2$ has the general chemical formula $Fe(OH)_2.xFeCl_2$, where x is a variable].
The 77 K Mb spectrum of a basic $FeCl_2$ sample is shown in Fig 5.50. The corresponding Mb parameters are:- (i) Fe(II) doublet: IS = 1.13 $\pm$ 0.10 mms^{-1}, QS = 2.77 $\pm$ 0.05 mms^{-1}; (ii) Fe(III) doublet: IS = 0.29 $\pm$ 0.10 mms^{-1}, QS = 0.44 $\pm$ 0.05 mms^{-1}. In view of what was said in section 5.2.1e for the sulphate GRs, again the resemblance is not surprising.

The relative sharpness of the Mb peaks indicate that the chloride GR material investigated was crystalline. However, this crystallinity was not reflected in the XRD or even IR data because the samples deteriorated on vacuum-drying. Further oxidation in the dry state during the course of analysis rendered the samples even less crystalline.

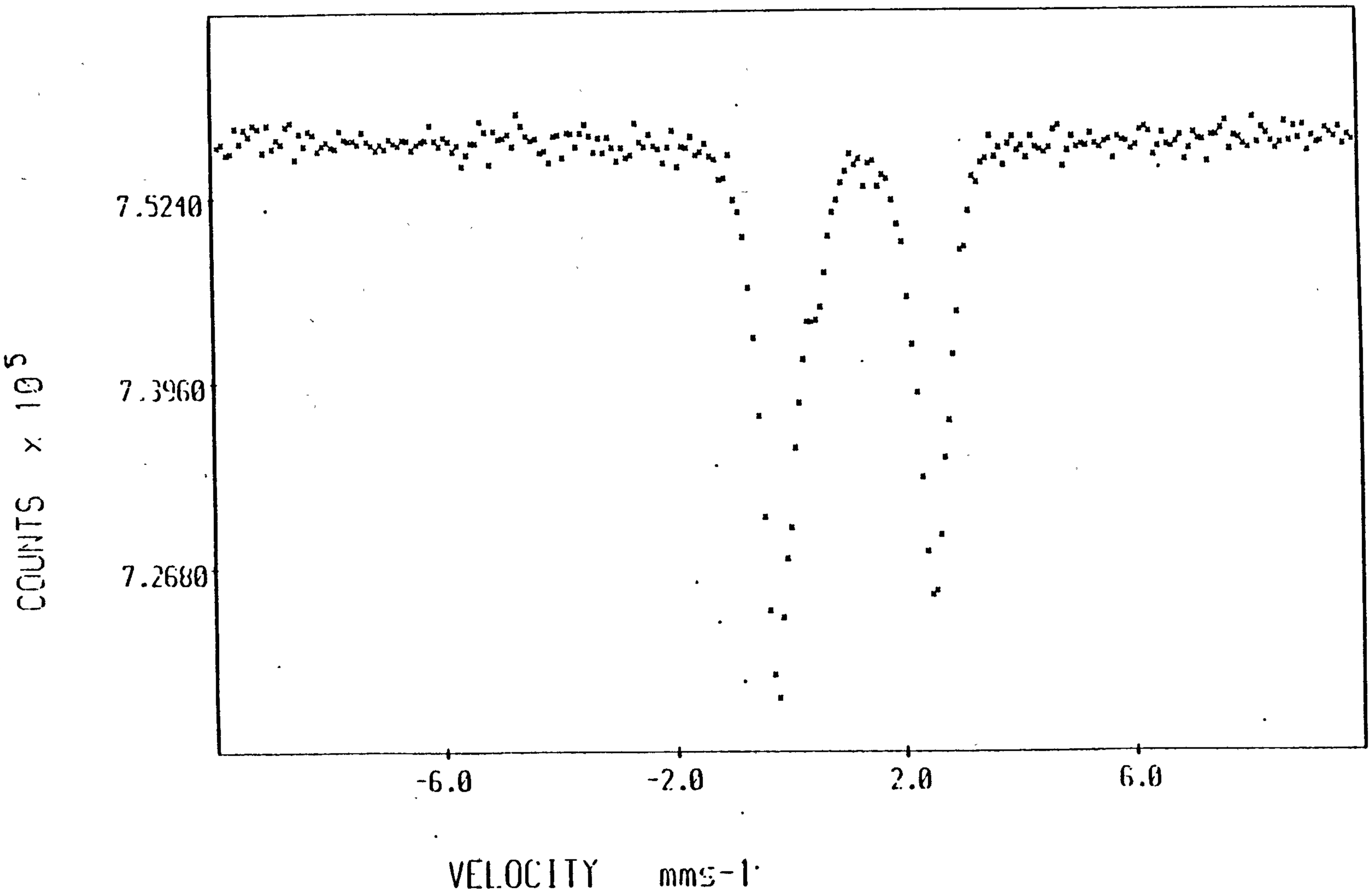

Fig 5.50 77 K Mb spectrum of a basic $FeCl_2$ sample.

The Mb parameters for the aged material (i.e. left overnight) are presented in Table 5.52. It can be seen that they remain more or less the same as the fresh precipitate. However, the FFR either increases or decreases but there is no trend with IFFR. This change in the FFR seems to correlate fairly well with the AAS data for the aged overnight samples (not presented in section 5.2.2a) i.e. in general, the increase in FFR corresponds to an increase in Fe(II) uptake while a decrease in FFR corresponds to a decrease in Fe(II) uptake. The change in FFR is thus evidently due to net adsorption of Fe(II) cations on, or the net loss of Fe(II) cations from, the surface of the precipitate. Which process is dominant probably depends on various factors such as time taken for chloride GR synthesis (related to amount of chloride GR produced) and the degree of oxidation occurring during the ageing process. Overall, the state of affairs in the chloride GR system is thus less complicated than in the sulphate GR system, where the magnetic component plays an important role in the ageing of the material. The actual spectra of the aged material is virtually identical to that of the fresh material.

On vacuum-drying, the chloride GR samples were partially oxidised (as mentioned in section 5.2.2b), and this shows up very well in the 77 K spectra for the dried material (Fig 5.51), where the increase in the Fe(III) component is clearly seen. The resolution of the lower (velocity)

Sample	IFFR	Fe(II) doublet			Fe(III) doublet			FFR
		δ	Δ	$\frac{1}{2}\Gamma$	δ	Δ	$\frac{1}{2}\Gamma$	
GR12	6	1.22	2.78	0.19	0.43	0.43	0.16	2.32
GR11	8	1.22	2.81	0.19	0.40	0.48	0.17	1.76
GR10	10	1.22	2.83	0.17	0.41	0.48	0.16	1.63
GR6	20	1.24	2.83	0.18	0.43	0.48	0.17	1.71
GR7	20	1.23	2.82	0.18	0.43	0.44	0.15	2.38
GR18	20	1.26	2.81	0.20	0.46	0.45	0.17	2.18
GR8	40	1.20	2.76	0.18	0.41	0.42	0.15	3.42
Mean		1.23	2.81	0.18	0.42	0.45	0.16	

Table 5.52 77 K Mb parameters for the wet, aged precipitate of chloride GRs derived from 0.1 M $FeCl_2$.

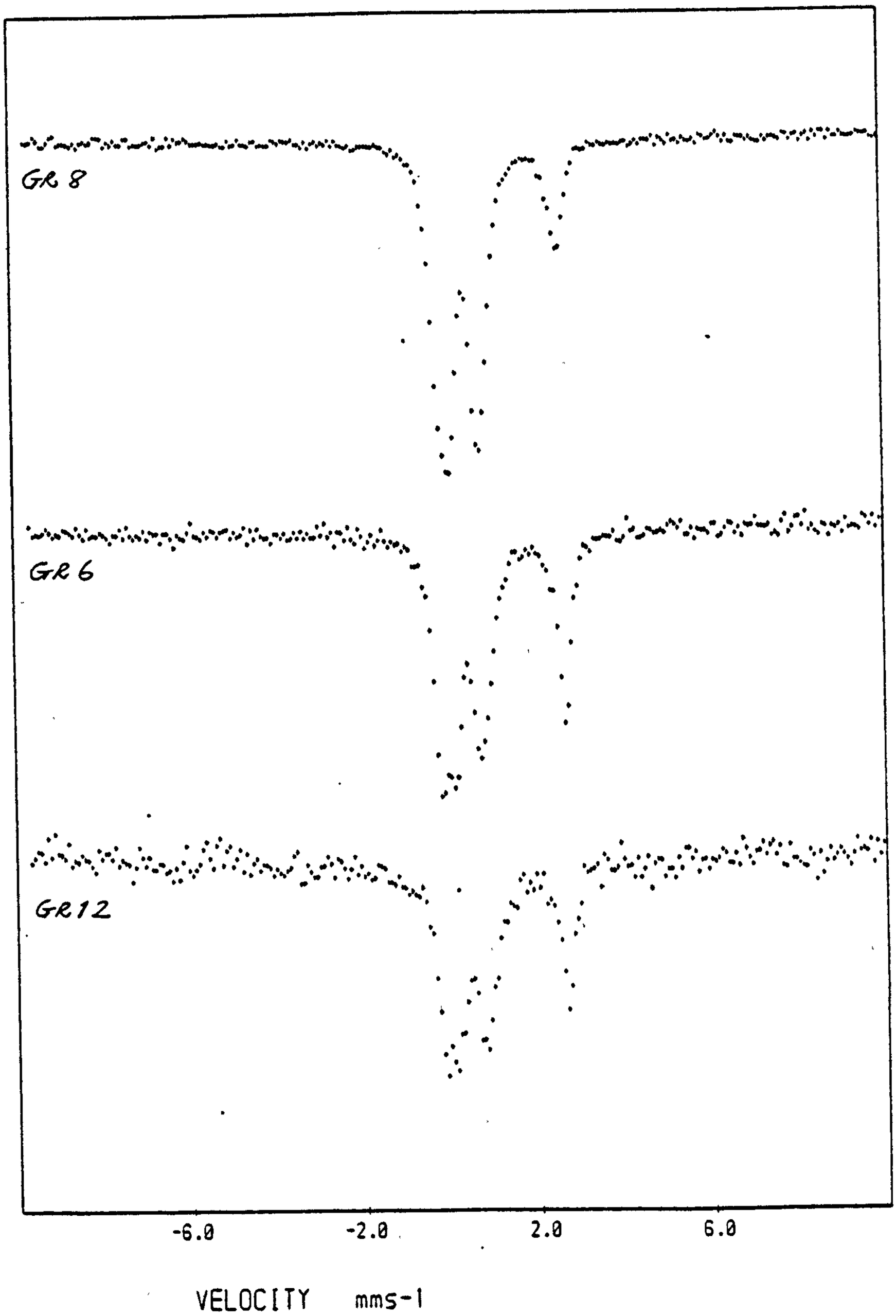

Fig 5.51 Typical 77 K Mb spectra of the dried, aged precipitate of chloride GRs derived from 0.1 M $FeCl_2$.

Fe(III) peak depends on the degree of oxidation. A few spectra also shows signs of a MHS which is superparamagnetically relaxed due to fine particle size. The MHS arises from the presence of akaganeite which has been converted from the chloride GR by oxidation.

The corresponding Mb parameters for the dried chloride GR samples are given in Table 5.53. The spectra were very difficult to curvefit because of distortion of line positions due to oxidation, and so the parameters have a larger error than with the sulphate GRs, although the values are still within the limits given. The partial oxidation of the samples is very evident in the reduced FFR values.

Some of the spectra had to be fitted with three Fe(III) doublets. Whether these doublets are real or not is open to debate. It is fairly certain that the third Fe(III) doublet is artificial since the IS is too high. However, the second doublet is probably real since it is similar to the secondary Fe(III) doublet of the oxidised material in some sulphate GR samples. Both the secondary Fe(III) doublets of chloride and sulphate GRs are similar to the secondary doublet required for the synthetic ferrihydrite produced in section 5.1 (see Table 5.1), and also of that used by Murad & Schwertmann (1980). The real answer probably lies in the fact that the distortion of the Mb line positions by oxidation results in a distribution of

Sample	IFFR	Fe(II) doublet			Fe(III) doublet			FFR
		δ	Δ	$\frac{1}{2}\Gamma$	δ	Δ	$\frac{1}{2}\Gamma$	
GR12	6	1.24	2.84	0.19	0.45	0.57	0.22	0.70
					(0.42	1.19	0.16)	-
					(1.10	0.71	0.22)	-
GR11	8	1.25	2.90	0.22	0.44	0.54	0.22	0.78
					(0.43	1.26	0.19)	-
					(1.16	0.92	0.22)	-
GR10	10	1.22	2.87	0.19	0.43	0.57	0.22	0.70
					(0.36	1.14	0.19)	-
					(1.07	0.71	0.23)	-
GR6	20	1.26	2.86	0.17	0.45	0.61	0.22	0.79
GR7	20	1.22	2.80	0.21	0.43	0.69	0.25	0.48
GR8	40	1.19	2.78	0.20	0.40	0.71	0.22	0.37
Mean		1.23	2.84	0.20	0.43*	0.62*	0.22*	

* values given here are for first Fe(III) doublet

( ) = Fe(III) doublet put in for curve fitting.

Table 5.53 77 K Mb parameters for the dried, aged & partially oxidised precipitate of chloride GRs derived from 0.1 M $FeCl_{\approx}$.

Fe(III) doublets (and also of Fe(II) doublets?). The Fe(III) doublets put in for curvefitting merely represent average values.

The ISs for both the Fe(II) and primary Fe(III) doublets of the dried chloride GR remain virtually the same as the wet precipitate. However, the QS for the Fe(II) doublet increases slightly (2.81 -> 2.84 mms^{-1}), although this change may be due to a larger error in the curvefitting procedure. Even if there was no change in QS, this would still contrast with the sulphate GRs where the QS decreases slightly on vacuum-drying. The QS for the primary Fe(III) doublet also increases (0.45 -> 0.62 mms^{-1}), and this increase is similar to that for the sulphate GRs. As mentioned in section 5.2.1e, the changes in the Mb parameters are most probably due to oxidation rather than to the drying process.

It was mentioned earlier that the spectra of the dried chloride GR samples showed signs of MHS due to the presence of akaganeite, which resulted from partial oxidation. The characteristic akaganeite spectrum can be clearly seen for the chloride GR material from sample GR12, which had been oxidised under storage in a test-tube sealed with N_2 (Fig 5.52). Because of this storage, the original chloride GR material acquired bulk magnetism from the conversion of part of the material to magnetite/maghemite. The latter phase can also be seen in

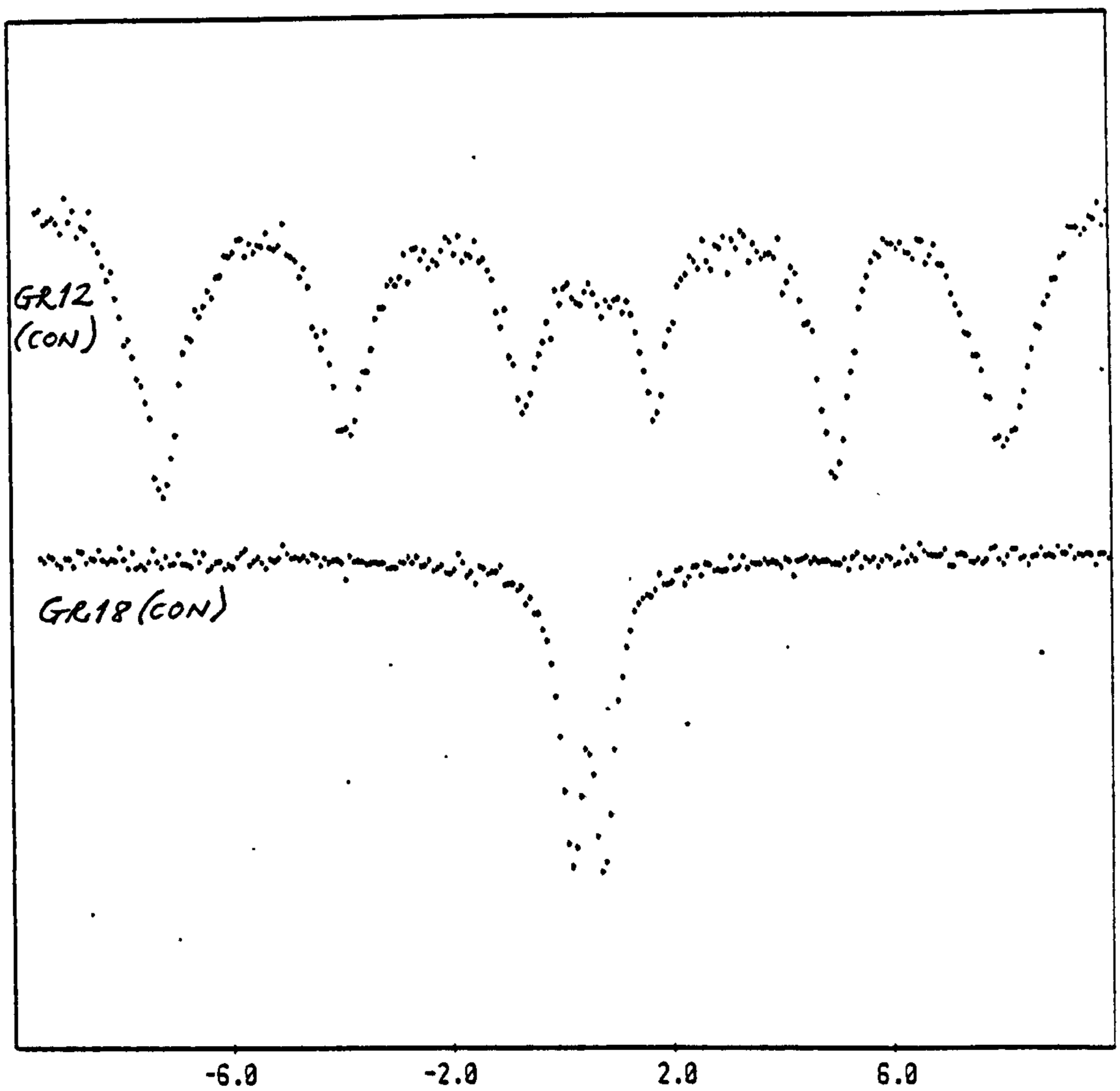

Fig 5.52 77 K Mb spectra of converted chloride GR samples:
(i) dry oxidation during storage in N_2
(ii) aged & oxidised in water.

the Mb spectrum since it gives rise to the asymmetry of the outer two pairs of peaks in the MHS. The existence of a magnetite/maghemite phase in the Mb spectrum supports further the XRD evidence. The MHS for the akaganeite component has the following values: IS = 0.47 ± 0.10 mms^{-1}, QS = −0.12 ± 0.10 mms^{-1} and B = 47.4 ± 0.5 T.

For comparison with the dry oxidation product of chloride GRs, the spectrum of the material from sample GR18, which was oxidised and aged under water, is also shown in Fig 5.52. This only gives a paramagnetic doublet which is consistent with lepidocrocite (as identified by XRD). The spectrum was fitted with two Fe(III) doublets whose values are:- (i) $Fe(III)_1$: {IS = 0.47 ± 0.10 mms^{-1}, QS = 0.53 ± 0.05 mms^{-1}, $1/2\Gamma$ = 0.21 ± 0.05 mms^{-1}}; and (ii) $Fe(III)_2$: {IS = 0.47 ± 0.10 mms^{-1}, QS = 0.94 ± 0.05 mms^{-1}, $1/2\Gamma$ = 0.23 ± 0.05 mms^{-1}}.

(ii) <u>RT data</u>

Because of the rapid oxidation of the chloride GRs in their dry state, it was not possible to obtain any reasonable RT spectrum of the dried material, which still had a Fe(II) component present. However, a fairly good spectrum of a wet, aged precipitate was obtained for

sample GR25 (Fig 5.53). This had the following Mb parameters:-

(i) Fe(II): {IS = 1.11 ± 0.10 mms^{-1}, QS = 2.48 ± 0.07 mms^{-1}, $1/2\Gamma$ = 0.22 ± 0.05 mms^{-1}}

(ii) Fe(III): {IS = 0.40 ± 0.10 mms^{-1}, QS = 0.36 ± 0.07 mms^{-1}, $1/2\Gamma$ = 0.21 ± 0.05 mms^{-1}}

As expected, all the parameters were shifted down in velocity and, in particular, that of the Fe(II) QS (2.80 -> 2.48 mms^{-1}). Apart from the Fe(II) QS, these Mb parameters are very similar to the corresponding RT Mb parameters for the sulphate GRs.

(iii) 4.2 K data

Mossbauer spectra at 4.2 K were obtained for only two samples of chloride GRs. The samples used were GR18 and GR25 (both wet, fresh precipitates). The raw spectra are shown in Fig 5.54 and, like the sulphate GRs, consist basically of (i) an Fe(III) magnetic hyperfine splitting with a small quadrupole interaction and (ii) an Fe(II) combined quadrupole and magnetic hyperfine splitting. Again the two hyperfine splittings are superimposed on each other, rendering analysis difficult. However, following the procedure outlined in section 5.2.1e, it was possible to obtain values for the Mb parameters

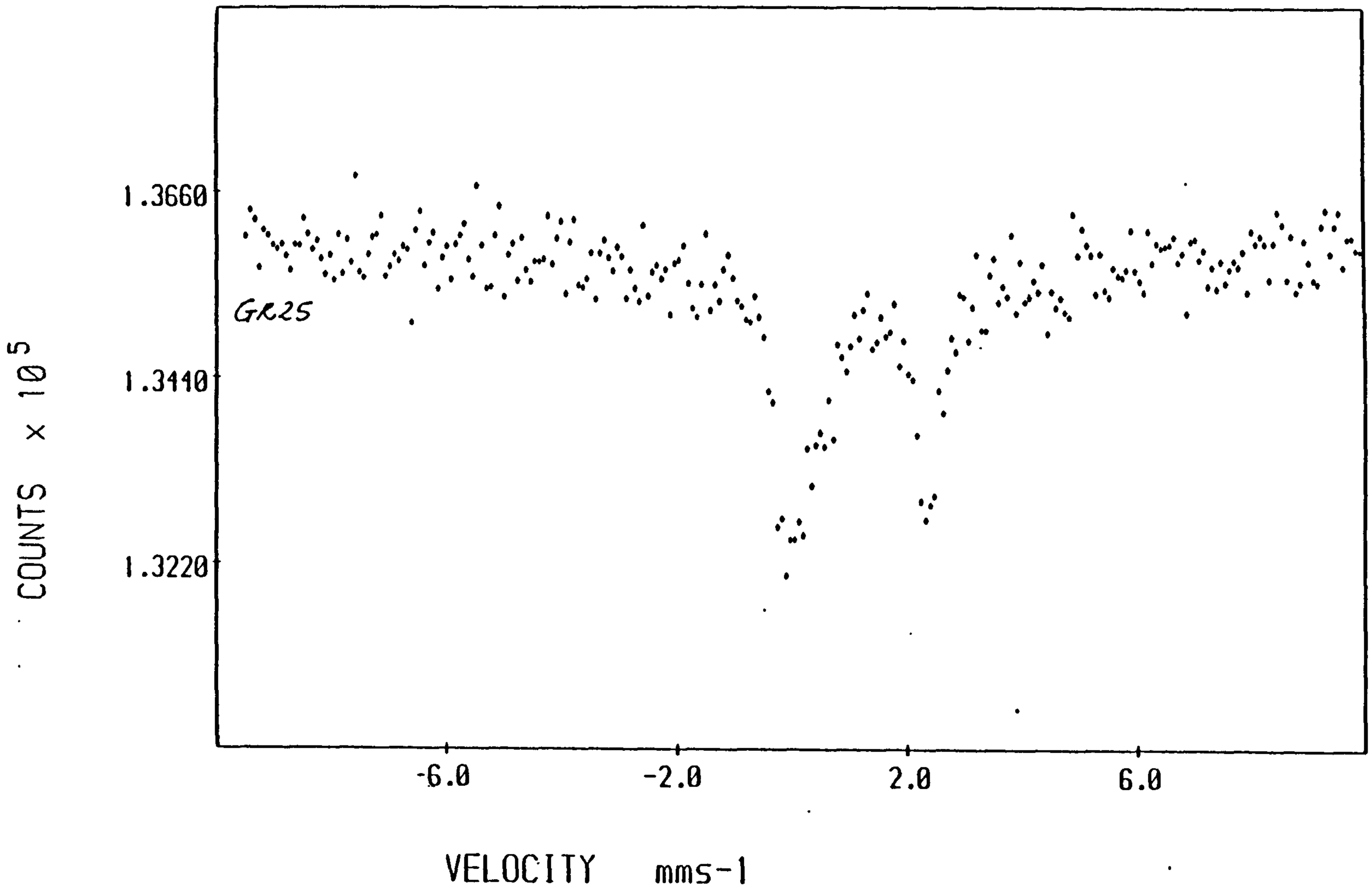

Fig 5.53 RT Mb spectrum of the wet, aged precipitate of a chloride GR sample derived from 0.1 M $FeCl_2$.

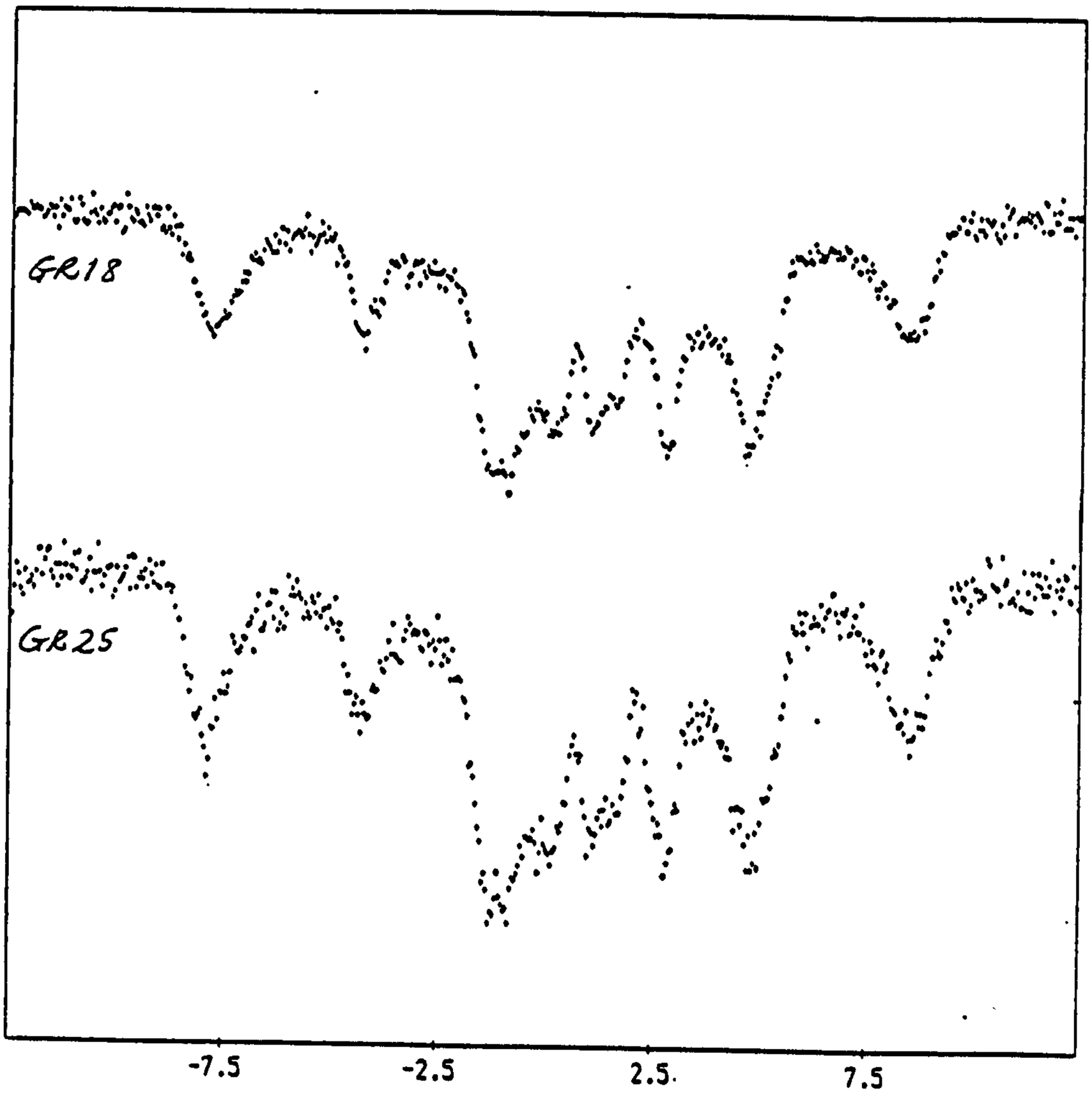

Fig 5.54 4.2 K Mb spectra of chloride GRs derived from 0.1 M $FeCl_2$.

relating to the Fe(II) hyperfine field (and also to the Fe(III) hyperfine field).

The best curves fitted for the Fe(II) hyperfine envelope of the two chloride GR samples are shown in Fig 5.55, and the Mb parameters corresponding to these fits are given in Table 5.54. It can be seen from Fig 5.55 that the fitted curves do not match the actual data closely. This is probably a reflection of the Fe(II) environment which is widely variant i.e. the short-range ordering is not uniform throughout, giving rise to a distribution of Fe(II) sites. Thus any curvefitting will be necessarily restricted to the best mean values. Nevertheless, the Mb parameters obtained give a very good indication of the Fe(II) environment. Both spectra are fitted with two Fe(II) hyperfine fields (B = 14.0 and 8.8 T, respectively) and, like the sulphate GRs, with an Fe(II) doublet. Apart from the relative intensities of these components, the parameters used for both chloride GR spectra were the same. Again the Fe(II) doublet must represent the contribution from a relaxing Fe(II) hyperfine field (Cuttler, private comm.). A relaxing Fe(II) hyperfine field may also account for the need to fit the spectra with two fields. The magnitude of the QS for the larger Fe(II) hyperfine field is very similar to that at 77 K (2.86 mms^{-1} at 4.2 K compared to 2.80 mms^{-1} at 77 K).

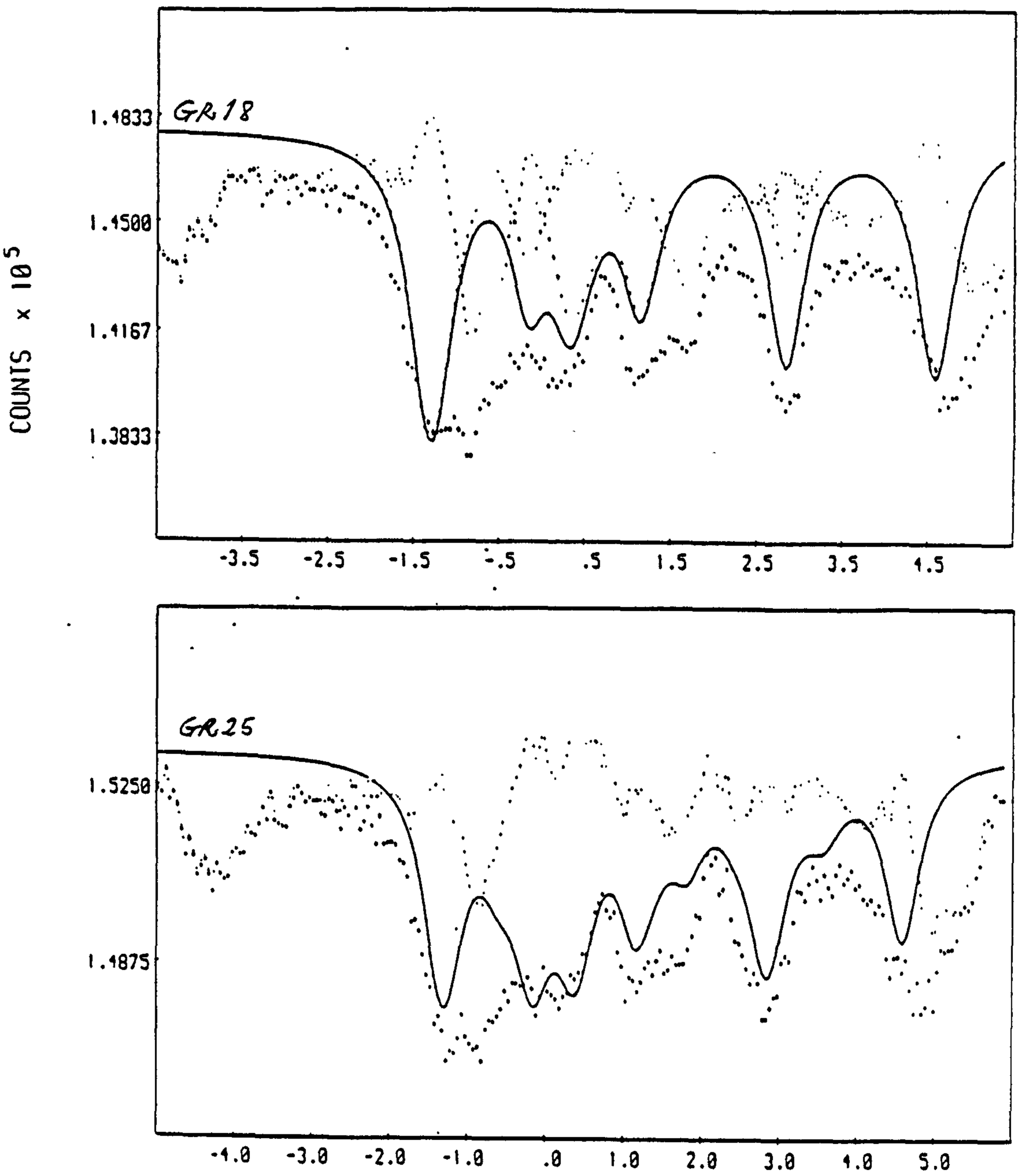

Fig 5.55 Partially-fitted 4.2 K spectra for the chloride GRs derived from 0.1 M $FeCl_2$.

Sample	Fe(II) Hyperfine Field								Fe(II) Doublet			
	δ	Δ	$\frac{1}{2}\Gamma$	η	θ	ϕ	B	%I	δ	Δ	$\frac{1}{2}\Gamma$	%I
GR18	1.31	-2.86	0.27	0	90	0	14.0	64	1.45	3.00	0.25	16
	1.30	-2.33	0.30	0	90	0	8.8	20				
GR25	1.31	-2.86	0.27	0	90	0	14.0	57	14.5	3.00	0.25	24
	1.30	-2.33	0.30	0	90	0	8.8	18				

Table 5.54 4.2 K Mb parameters for the Fe(II) hyperfine envelope of the chloride GR samples.

Sample	Fe(III) MHS		
	IS(mms^{-1})	QS(mms^{-1})	B(T)
GR18	0.47	0.00	49.2
GR25	0.47	0.00	49.2

Table 5.55 4.2 K Mb parameters for the Fe(III) MHS of chloride GR samples.

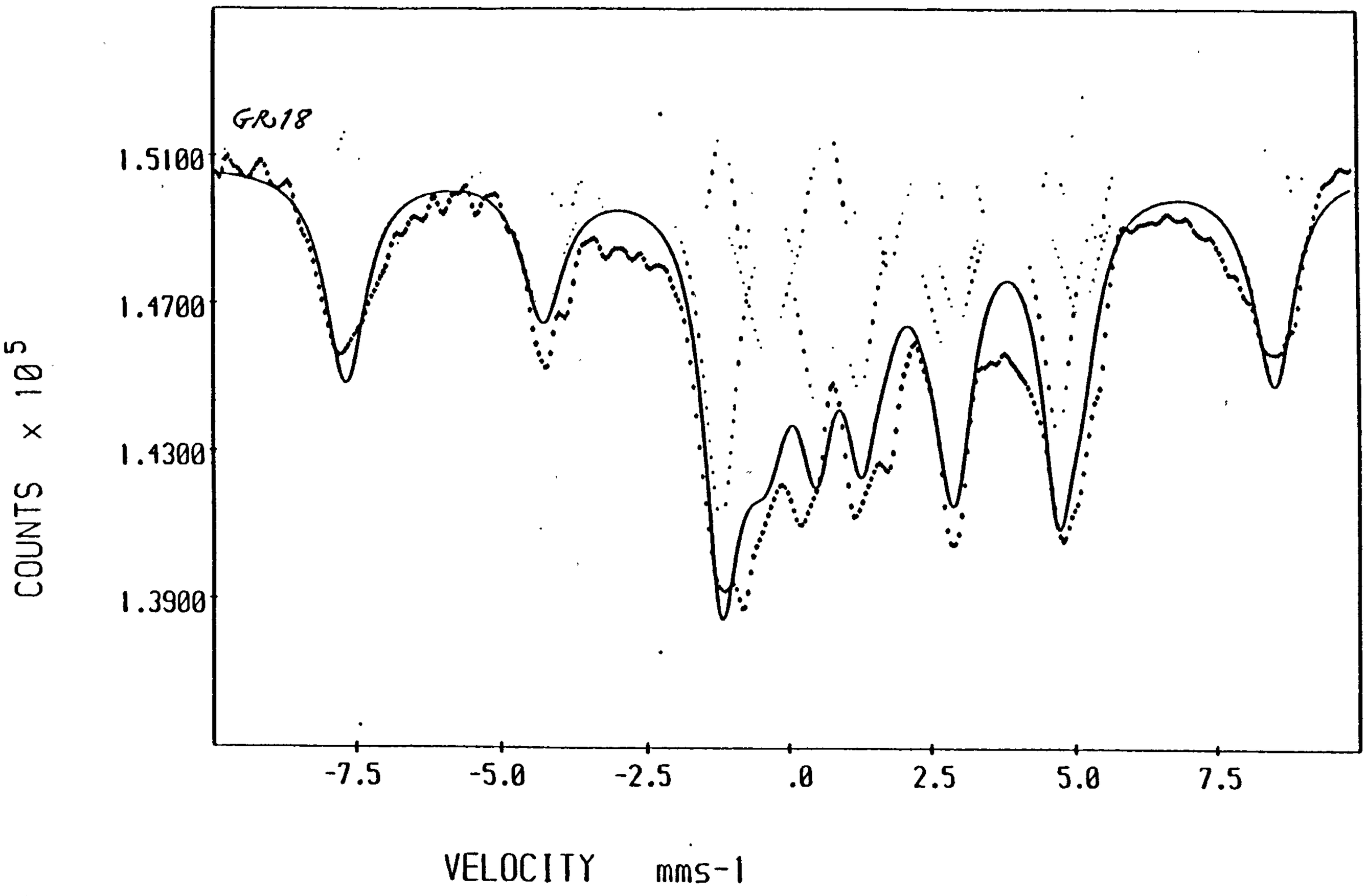

Fig 5.56 Completely-fitted 4.2 K Mb spectrum for a chloride GR sample derived from 0.1 M $FeCl_2$.

To take account of the Fe(III) MHS, the chloride GR spectra were curvefitted further using a distribution of Fe(III) MHS. Some slight adjustments of the relative intensities of the components in the Fe(II) hyperfine envelope was also made. The resultant fitted spectrum is shown in Fig 5.56 for sample GR18 only (the other is identical). The average values for the Mb parameters fitted to the Fe(III) peaks are given in Table 5.55. These values are consistent with that of the Fe(III) gel already discussed in section 5.2.1e.

At 4.2 K, this Fe(III) gel is magnetically ordered with mean values of IS ~ 0.4 mms^{-1} , QS ~ 0.0 mms^{-1} and B ~ 48 T. Thus it seems that the 4.2 K spectrum for the chloride GR is made up of a magnetically ordered Fe(II) component, showing a degree of relaxation, along with a magnetically ordered Fe(III) gel. Both components are paramagnetic at 77 K.

2) <u>Non-GRs synthesised from 0.1 M $FeCl_2$</u>

The Mb spectra for four out of the five non-GR samples (where IFFR = 4) are virtually identical in respect of the wet, fresh precipitate; the wet, aged precipitate and the dried material. The fifth sample, S14-11-83, behaves in a slightly different way because it has an IFFR = 1. Representative spectra for the types of material are

shown in Fig 5.57 for sample S6-4-83. The Mb parameters corresponding to these spectra are presented in Table 5.56.

At 77 K, the wet, fresh precipitate has a Mb spectrum similar to that of the corresponding sulphate GR material. That is, it consists of an Fe(III) MHS and two quadrupole doublets, one of Fe(II) and the other of Fe(III). The interesting point to note is that the Fe(II) quadrupole doublet has values of IS and QS very similar to that of the chloride GR (the QS is slightly lower at 2.76 mms^{-1}). This means that a chloride GR phase or one similar to it was formed. However, on ageing overnight this component along with the paramagnetic Fe(III) component almost completely disappears, as seen in the 77 K spectrum of the wet, aged material (Fig 5.57). The Fe(III) MHS that remains was identified as belonging to magnetite (not well-ordered), since the RT spectrum of the dried material gives the characteristically split outer two peaks at the low velocity end. Thus it seems, on ageing the fresh precipitate, any paramagnetic component (in particular, the Fe(II) doublet) becomes converted to magnetite. Hence it is apparent that any chloride GR-like phase forming under the conditions of IFFR = 4 (and < 4) is metastable. It is to be noted that the Mb data presented here has shown that the magnetic phase of the non-GR samples is magnetite rather than maghemite (at least of the original

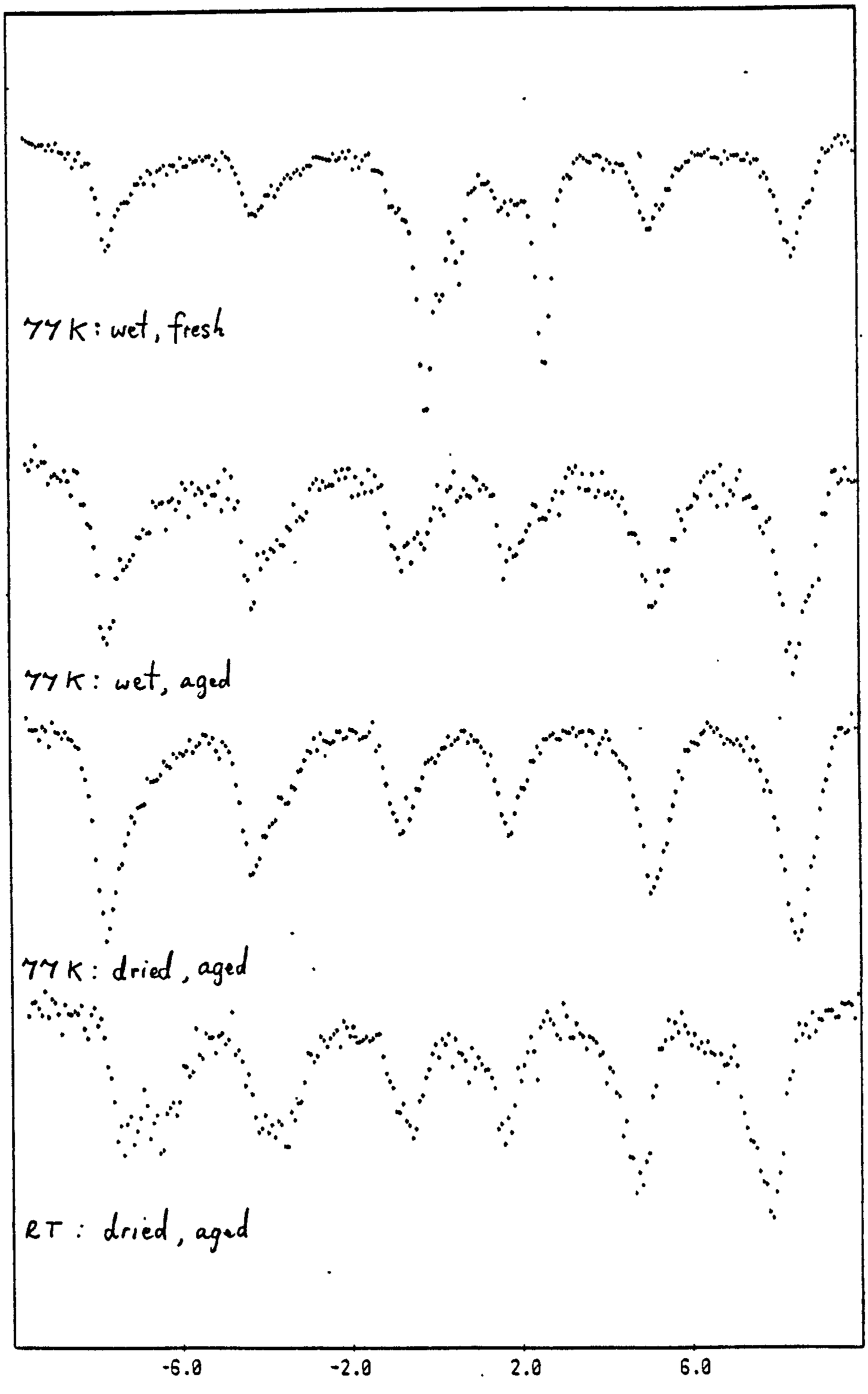

Fig 5.57 Mb spectra of a representative sample of non-GRs derived from 0.1 M $FeCl_2$. (Sample S6-4-83)

Precipitate	Temp. (K)	Component	δ (mms^{-1})	Δ (mms^{-1})	$\pm\frac{1}{2}\Gamma$ (mms^{-1})	B (T)
Wet,fresh	77	Fe(II)	1.24	2.76	0.18	-
		Fe(III)	0.46	0.43	0.15	-
		MHS	0.42	-0.05	-	49.9
Wet, aged	77	MHS	0.42	-0.06	-	50.0
Dried	77	MHS	0.39	-0.01	-	50.3
Dried	RT	MHS (outer)	0.38	-0.16	-	46.9

Table 5.56 Mb parameters of sample S6-4-83, representative of the non-GRs derived from 0.1 M $FeCl_2$.

material). The XRD seems to suggest maghemite, although the evidence is not clear cut. However, it must be said that XRD makes use of the dried material, which means that inevitably some oxidation (to maghemite) has occurred. The IR data also seem to indicate that magnetite rather than maghemite was formed.

Sample S14-11-83 (IFFR = 1) is only slightly different to the other samples in that it does not go through the metastable chloride GR-like phase. The 77 K spectrum of the wet, fresh precipitate consists only of the Fe(III) MHS (IS = 0.42 mms^{-1}, QS = -0.04 mms^{-1} & B = 49.9 T). This is not surprising in this case since <Fe(III)> was large and results in magnetite formation only.

5.3 Characterisation of the Al Green Rusts

The Al-GRs produced from both the $FeSO_4$ and $FeCl_2$ systems are presented here under one section since only a few samples of each type were made. The sample identities are given in Table 5.57. The $[Fe(II)]_I$ in both categories was 0.1 M. It is to be noted that pH maintenance at 7 was more difficult than in the corresponding Fe-GRs.

The fresh precipitate for the Al-GRs (both $FeSO_4$ and $FeCl_2$ systems) was milky to greyish blue in colour with a tinge of green. The vacuum-dried material was normally dark bluish-green to bluish-green in colour. The fresh precipitate was much more stable to oxidation in air than the Fe-GRs, with complete oxidation occurring in > 1-2 h (the colour changing to a yellowish-orange). The vacuum-dried material also had a similar stability, although greater for the $FeSO_4$ system than the $FeCl_2$ system, and the colour of the oxidation product was yellowish-orange in the $FeSO_4$ system but dark-brown in the $FeCl_2$ system. The contrast in stability between the Al- and Fe-GRs is shown up by the different degree of oxidation for the material stored under N_2 in sealed test-tubes. For the Al-GRs, the material still had a fairly deep green colour after 1 year's storage, whereas that for the Fe-GRs showed a great deal of deterioration.

Sample	Fe(II) source	IFAR	<Al(III)> (mmole)	pH maintained
GR23	$FeSO_4$	5	4	7.0 ± 0.3
GR17		10	2	7.2 ± 0.3
GR22		10	2	7.2 ± 0.3
Item47		50	0.5	7.0 ± 0.4
GR24	$FeCl_2$	5	4	7.1 ± 0.2
Item35		10	2.5	~ 7.0
GR19		20	1	7.0 ± 0.2

< > = amount of
IFAR = initial Fe(II)/Al(III) ratio

Table 5.57 Sample identities for Al-GRs derived from 0.1 M Fe(II).

5.3.1 Titration and AAS data

The consumption of alkali with time for the Al-GRs is much better defined than that for the Fe-GRs. The rate of consumption is rapid at the beginning but reaches a plateau at an abrupt juncture (Fig 5.58). The estimated equilibrium times are in the range 0.5-3.5 h which is shorter than that for the Fe-GRs (3-6 h).

The data giving the alkali consumption for the Al-GR samples is shown in Table 5.58. Looking at the values for the estimated equilibrium times, it seems also that the chloride Al-GRs were produced in a shorter time than the sulphate Al-GRs.

The variation in alkali consumption with IFAR (initial Fe(II)/Al(III) ratio) for the Al-GRs is shown by plots of alkali consumption v. <Al(III)> since $[Fe(II)]_I$ is again constant (Fig 5.59). The ln-ln plots of total NaOH consumption, $\langle NaOH \rangle_t$, and specific NaOH consumption, $\langle NaOH \rangle_s$, versus <Al(III)> both give fairly good straight lines. The graph shows that $\langle NaOH \rangle_t$ increases with <Al(III)> while $\langle NaOH \rangle_s$ decreases with <Al(III)>. The fact that the points seem to fit in with each other shows that the anion type is not of great importance in the synthesis of the Al-GRs. Linear least-squares fit of the two plots give the following relationships:

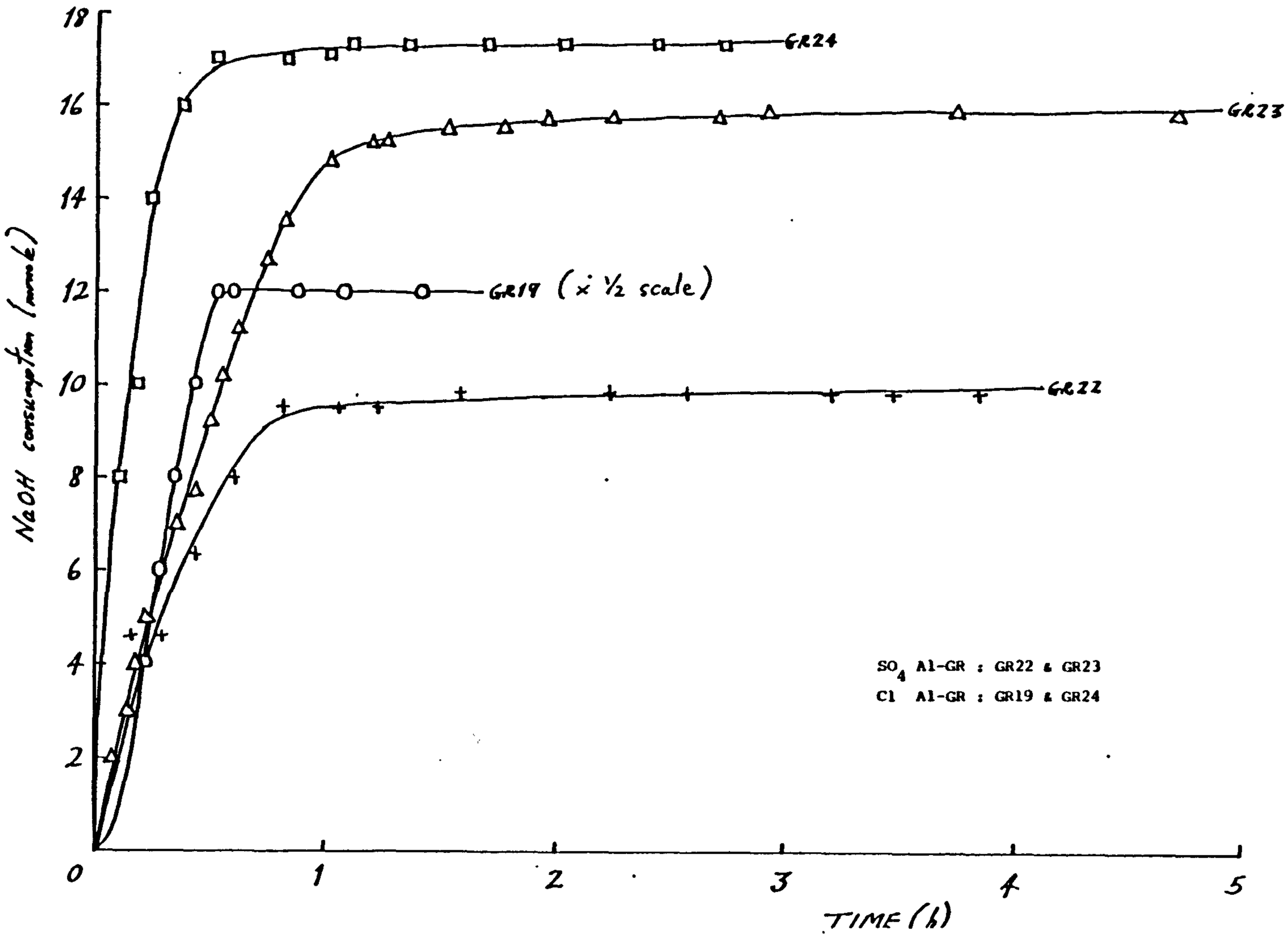

Fig 5.58 NaOH consumption v. time for typical Al-GR samples derived from 0.1 M Fe(II).

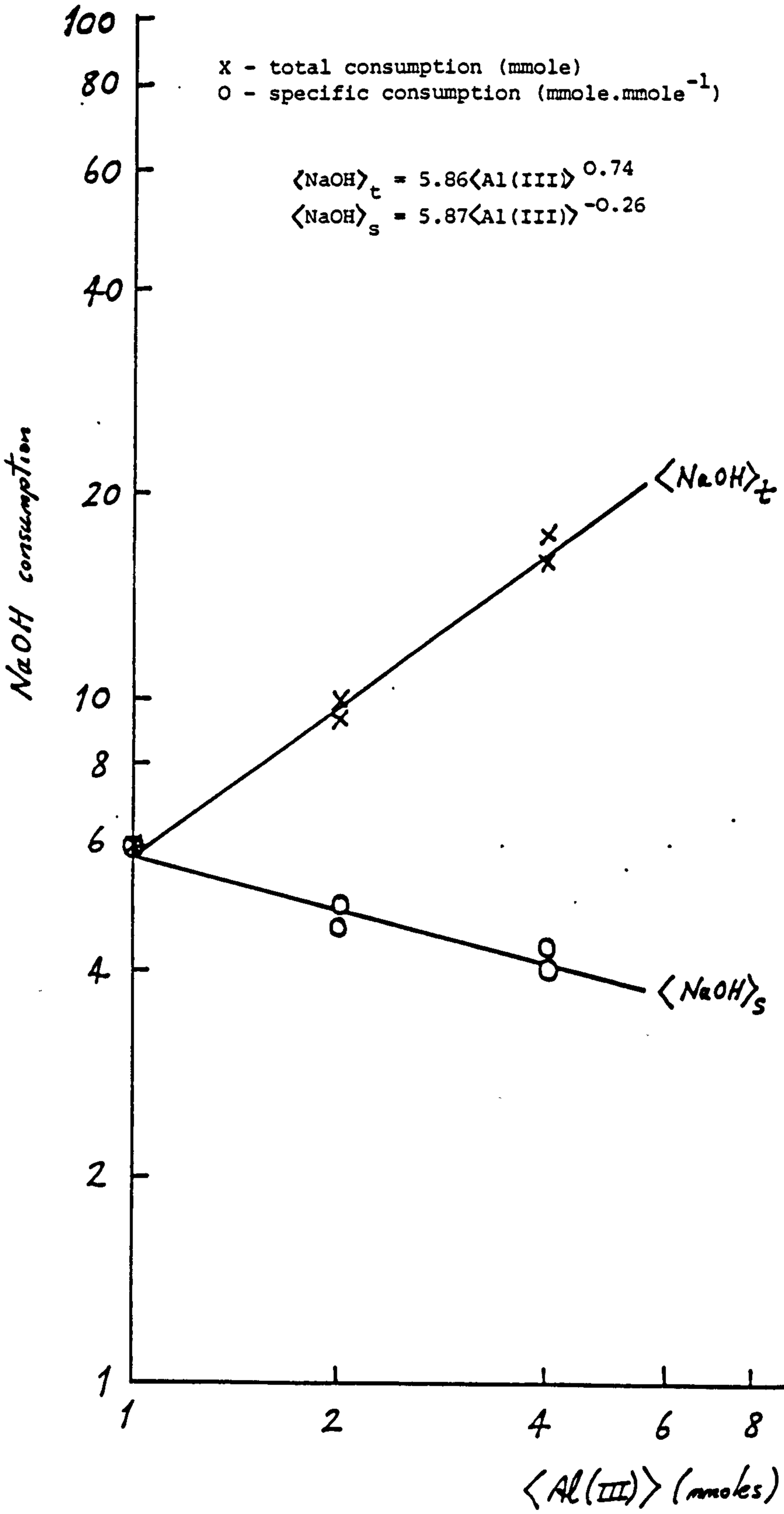

Fig 5.59 NaOH consumption v. <Al(III)> for Al-GRs derived from 0.1 M Fe(II).

Sample	Fe(II) Source	IFAR	⟨Al(III)⟩ (mmole)	$\langle NaOH \rangle_t$ (mmole)	$\langle NaOH \rangle_s$ (mmole.mmole^{-1})	Estimated eqm. time (h)
GR23	$FeSO_4$	5	4	16.00 ± 0.05	4.0	3.2
GR17	$FeSO_4$	10	2	9.30 ± 0.05	4.6	1.7
GR22	$FeSO_4$	10	2	9.90 ± 0.05	5.0	1.8
GR24	$FeCl_2$	5	4	17.30 ± 0.05	4.3	1.3
GR19	$FeCl_2$	20	1	6.00 ± 0.05	6.0	0.65

IFAR = Initial Fe(II)-Al(III) ratio

Table 5.58 Alkali consumption for Al-GRs derived from 0.1 M Fe(II).

Sample	Fe(II) Source	IFAR	⟨Al(III)⟩ (mmole)	$\langle Fe(II) \rangle_t$ (mmole)	$\langle Fe(II) \rangle_s$ (mmole.mmole^{-1})
GR23	$FeSO_4$	5	4	17.3	4.3
GR17	$FeSO_4$	10	2	16.8	8.4
GR22	$FeSO_4$	10	2	12.9	6.4
GR24	$FeCl_2$	5	4	13.9	3.5
GR19	$FeCl_2$	20	1	11.1	11.1

Table 5.59 Fe(II) uptake for Al-GRs derived from 0.1 M Fe(II).

$$\ln \langle NaOH\rangle_t = 0.74 \ln \langle Al(III)\rangle + 1.77 \qquad -5.22a$$

$$\rightarrow \quad \langle NaOH\rangle_t = 5.86 \langle Al(III)\rangle^{0.74} \qquad -5.22b$$

$$\ln \langle NaOH\rangle_- = -0.26 \ln \langle Al(III)\rangle + 1.77 \qquad -5.23a$$

$$\langle NaOH\rangle_- = 5.87 \langle Al(III)\rangle^{-0.26} \qquad -5.23b$$

As with the chloride Fe-GRs, the rate of increase in $\langle NaOH\rangle_t$ is greater than the rate of decrease in $\langle NaOH\rangle_-$.

The AAS data for Fe(II) uptake during the synthesis of the Al-GRs is presented in Table 5.59. A ln-ln graph of Fe(II) uptake v. $\langle Al(III)\rangle$ (Fig 5.60) shows that the total Fe(II) uptake, $\langle Fe(II)\rangle_t$, increases with $\langle Al(III)\rangle$ while the specific Fe(II) uptake, $\langle Fe(II)\rangle_-$, decreases with $\langle Al(III)\rangle$. The points for each of the plots do not give good linear correlation. Nevertheless, linear least-squares fit of the points were made, and the following relationships obtained:

$$\ln \langle Fe(II)\rangle_t = 0.22 \ln \langle Al(III)\rangle + 2.47 \qquad -5.24a$$

$$\rightarrow \quad \langle Fe(II)\rangle_t = 11.87 \langle Al(III)\rangle^{0.22} \qquad -5.24b$$

$$\ln \langle Fe(II)\rangle_- = -0.79 \ln \langle Al(III)\rangle + 2.47 \qquad -5.25a$$

$$\rightarrow \quad \langle Fe(II)\rangle_- = 11.87 \langle Al(III)\rangle^{-0.79} \qquad -5.25b$$

The rate of increase in $\langle Fe(II)\rangle_t$ is less than the rate of increase in $\langle NaOH\rangle_t$, with the consequence

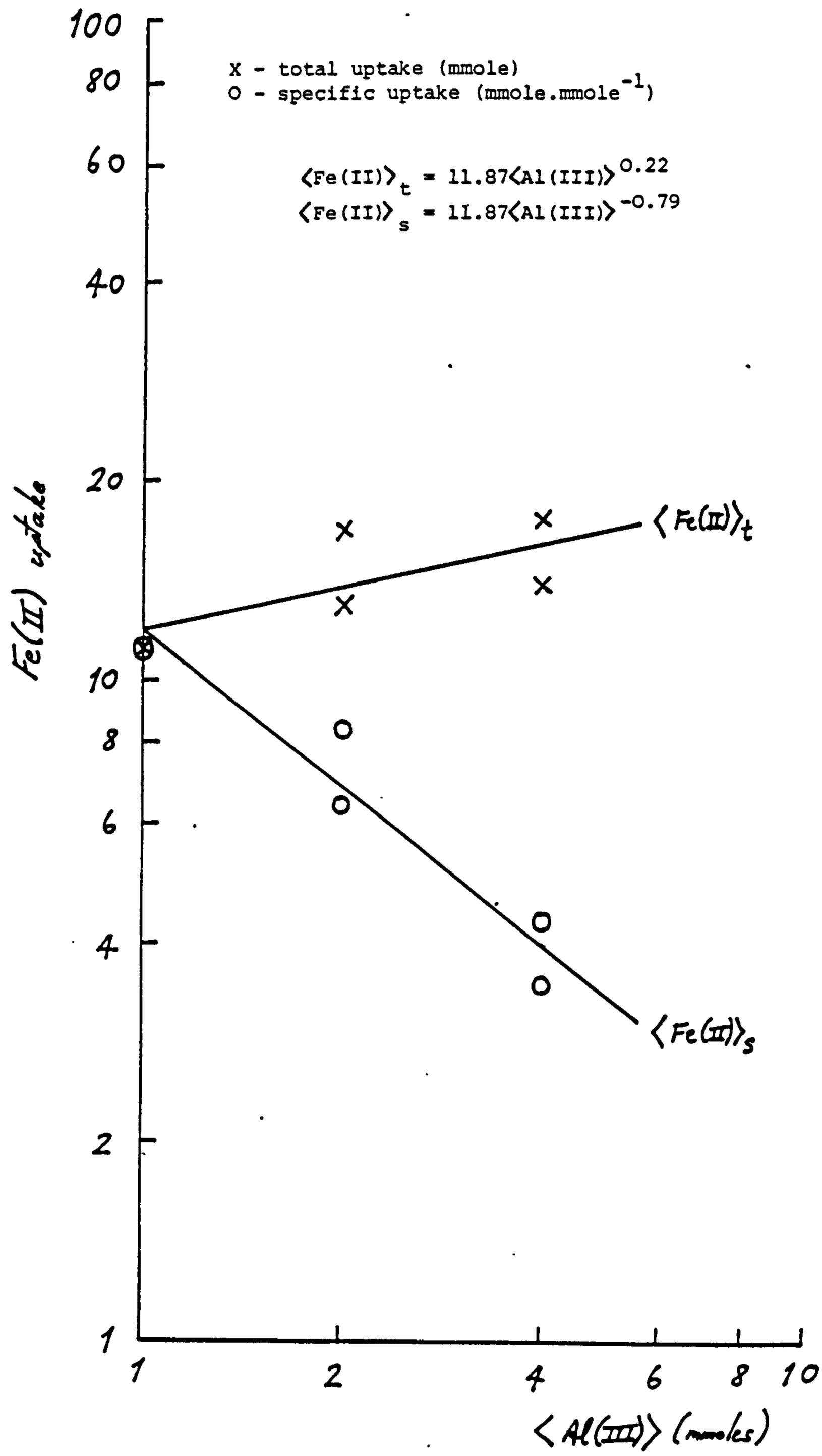

Fig 5.60 Fe(II) uptake v. <Al(III)> for Al-GRs derived from 0.1 M Fe(II).

that the rate of decrease in $\langle Fe(II)\rangle_w$ is much greater than the rate of decrease in $\langle NaOH\rangle_w$. The gradient of the $\langle Fe(II)\rangle_t$ line is almost the opposite of the gradient of the $\langle NaOH\rangle_w$. Similarly, the gradients of the $\langle Fe(II)\rangle_w$ and $\langle NaOH\rangle_t$ lines are virtually inverses of each other.

Freundlich and Langmuir isothermal plots were made of the Fe(II) uptake and gave scattered points, indicating that the uptake of Fe(II) cations is a non-adsorption process.

5.3.2 X-ray diffraction

The greater stability of the Al-GRs was reflected in their usage for XRD. This was particularly true for the sulphate Al-GRs which changed colour slowly from a bluish-green to a lime-green after a 2-3 h X-ray scan. The chloride Al-GRs changed colour quicker from a dark-green to a greenish, dark-brown in the same period. The sulphate Al-GR material was talc-like i.e. soft and fine-grained, while the chloride Al-GRs were harder and more coarse-grained. This difference was reflected in the X-ray peaks which were sharper in the case of the chloride Al-GRs and indicates a better crystallinity than the sulphate Al-GRs (Fig 5.61). Even so, compared to the Fe-GRs, the X-ray lines were very broad, indicating poor crystallinity, and thus the Al-GRs have a small particle size. Also, in the case of the $FeSO_4$ system, the XRD patterns for the Al-GRs do not have the extra lines of goethite that are present in the Fe-GR traces.

The X-ray d-spacings for the Al-GR samples are given in Table 5.60. It can be seen that the samples derived from 0.1 M $FeCl_2$, which has already been called "chloride Al-GRs", have X-ray lines consistent with a chloride GRI structure (see Table 5.40). Indeed, the two samples (GR24 & GR19) have lines similar to those obtained by Taylor & McKenzie (1980) for their Fe(II)-Al(III) hydroxy chloride samples. The d-spacings for sample GR23, derived from 0.1

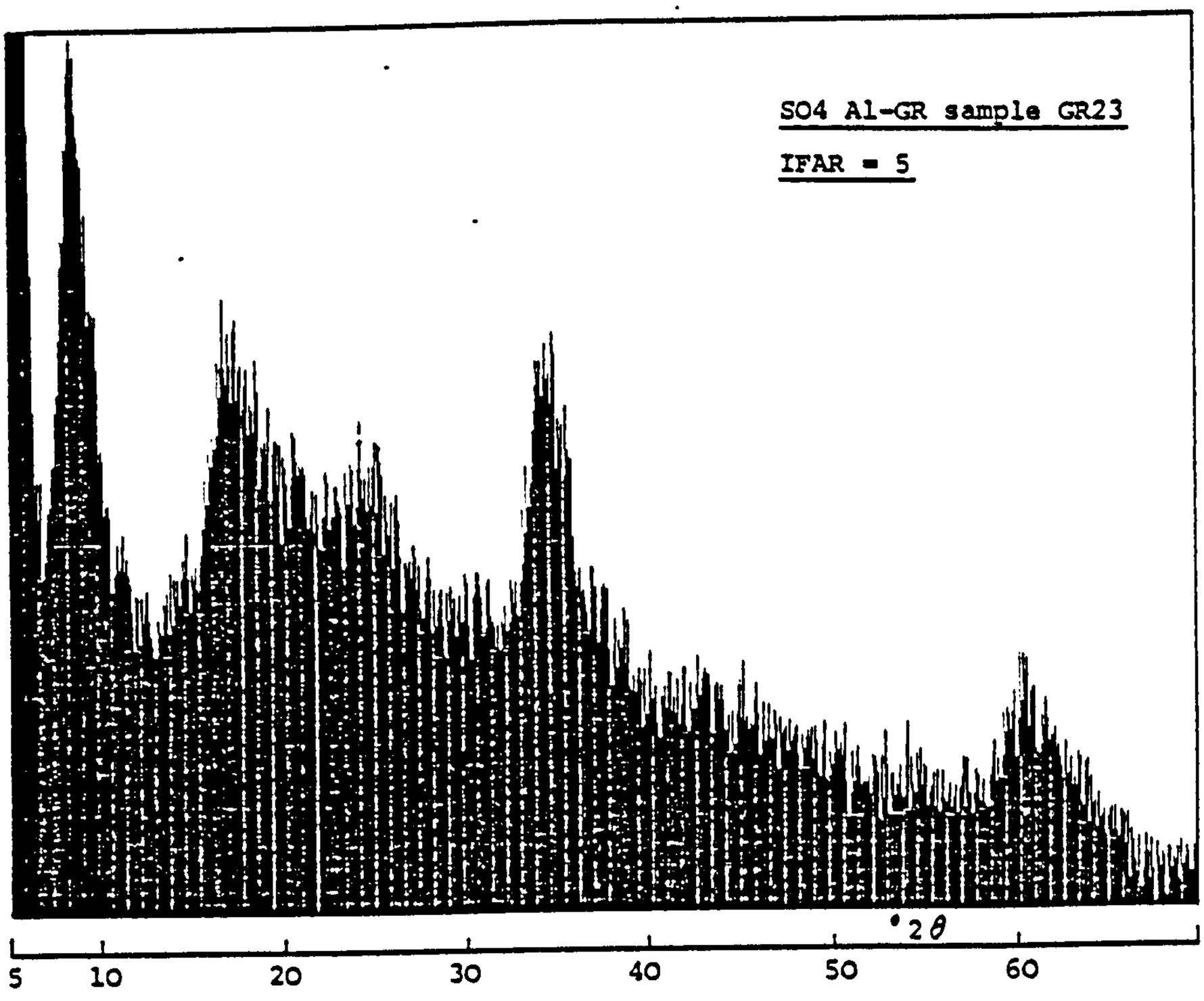

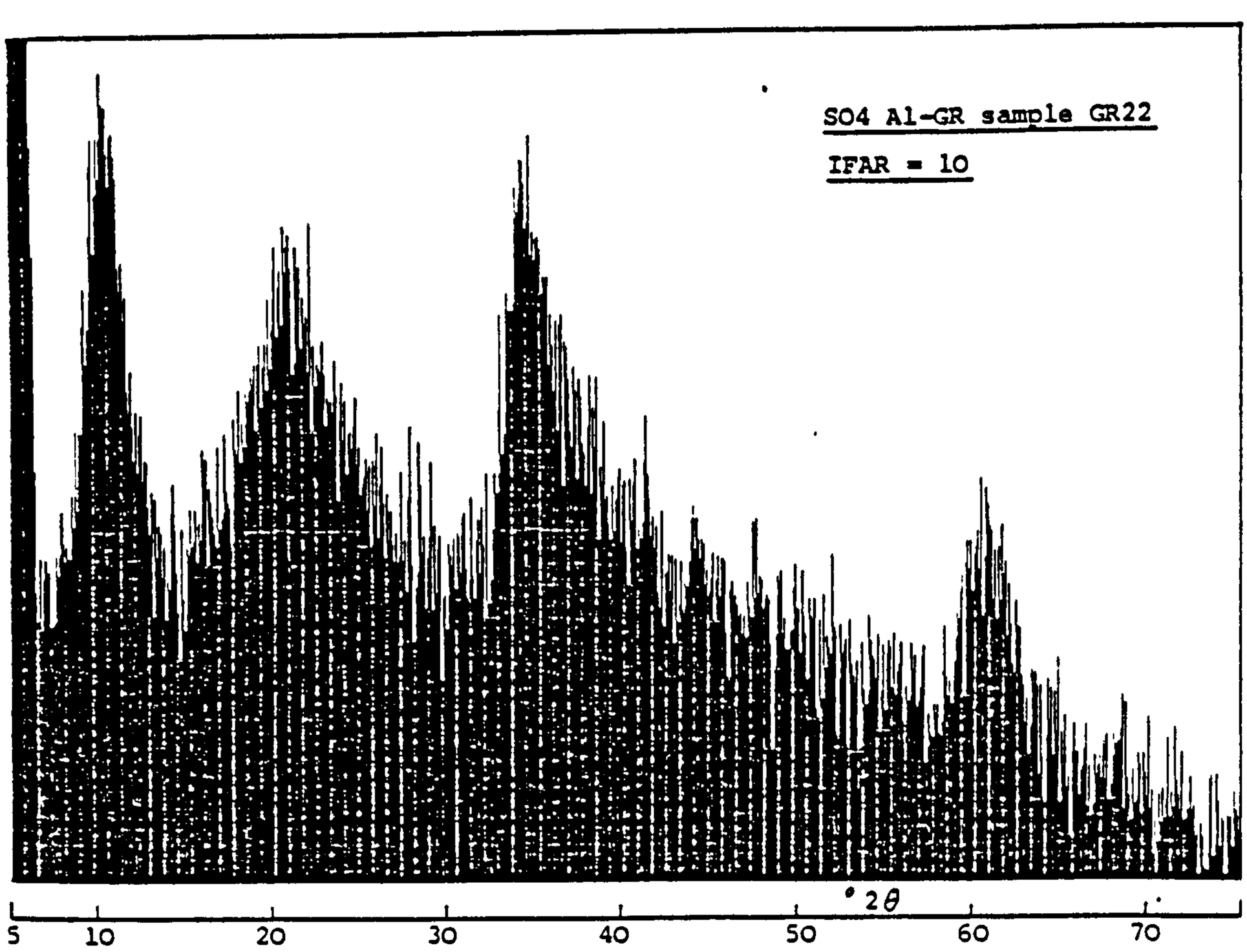

Fig 5.61 Typical X-ray diffractograms of Al-GRs derived from 0.1 M Fe(II).

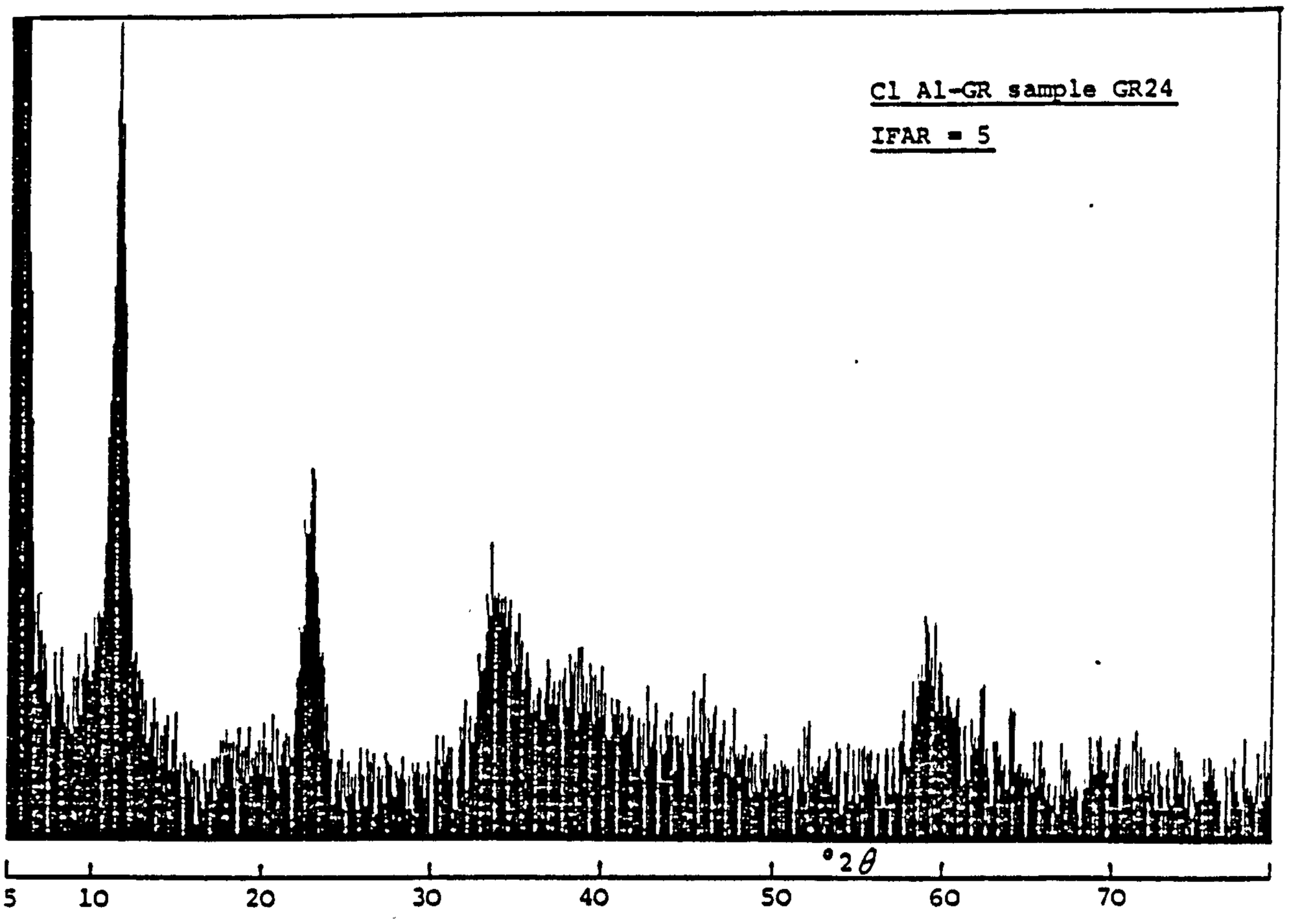

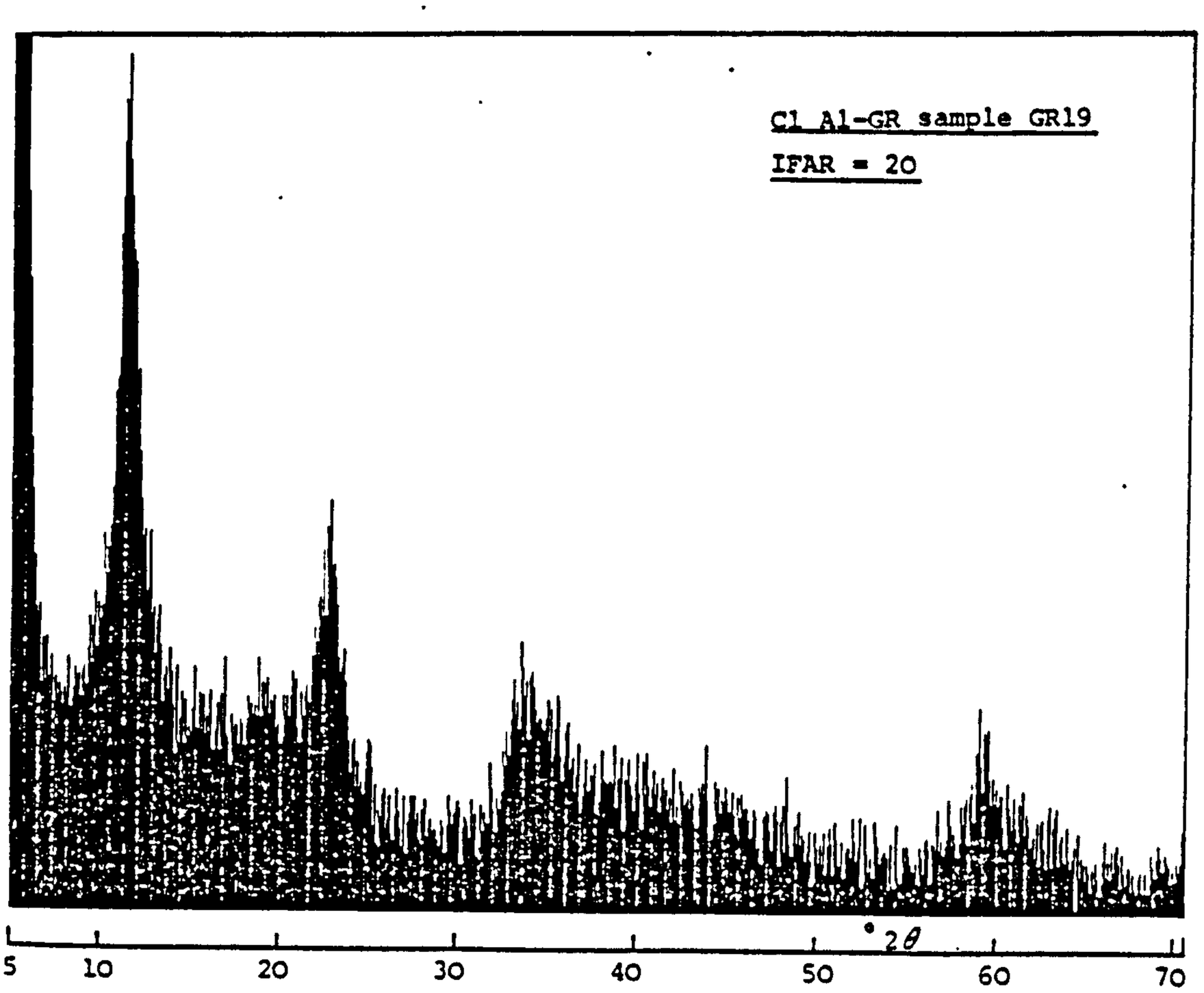

Fig 5.61 (cont'd) Typical X-ray diffractograms of Al-GRs derived from 0.1 M Fe(II).

Sample = GR23 Source = $FeSO_4$ IFAR = 5		Sample = GR17 Source = $FeSO_4$ IFAR = 10		Sample = GR22 Source = $FeSO_4$ IFAR = 10		Sample = GR24 Source = $FeCl_2$ IFAR = 5		Sample = GR19 Source = $FeCL_2$ IFAR = 20	
d-spacing (A)	Int	d-spacing (A)	Int	d-spacing (A)	Int	d-spacing (A)	Int	d-spacing (A)	Int
10.53	100(B)								
		8.94	100(B)	8.59	100(VB)				
5.22	48(VB)					7.76	100	7.76	100
		4.42	54(VB)	4.25	77(WB)				
						3.92	45	3.90	41(B)
3.60	23(VB)								
2.593	55(VB)	2.571	52(VB)	2.600	86(WB)	2.652	20(B)	2.652	25(VB)
						2.333	8(VB)		
1.535	29(VB)	1.504	25(VB)	1.530	51(VB)	1.563	21(B)	1.559	21(B)

B = broad V = Very

Table 5.60 X-ray d-spacings of Al-GRs derived from 0.1 M Fe(II).

M $FeSO_4$, is consistent with a sulphate GRII structure. The other two "sulphate Al-GR" samples (GR17 & GR22) do not have the characteristic low-angle lines at 10.5-10.9 A and 5.2-5.5 A, attributable to sulphate GRII. Instead, they have low-angle lines at 8.6-8.9 A and 4.2-4.4 A. The remaining lines seem to match up with those for sample GR23. By comparing the XRD spectra of sample GR23 and the other two "sulphate Al-GR" samples, it is apparent that the two low-angle lines have been shifted down in terms of d-spacing. Thus it seems reasonable to assume that the basic GRII structure has been formed but not to completion (since X-ray lines are missing), or else an imperfect structure was formed, for samples GR17 and GR22. In fact, the structure of GR23 is probably also incomplete which would explain the lower than expected d-spacings (cf. Taylor & McKenzie's sulphate Al-GR samples where all the lines of sulphate GRII were present). The two low-angle lines in samples GR17 and GR22 are not likely to be due to a contamination such as Fe(II) hydrogen sulphate hydrate [$Fe(SO_4)_3.H_2SO_4.8H_2O$] since (i) other reflections ascribed to the latter were missing and (ii) the XRD spectra for all three sulphate Al-GR samples are too consistent with each other. If samples GR17 and GR22 represent imperfectly formed sulphate GRII material, then this could also explain the line at ~ 8.8 A for some of the sulphate Fe-GR samples described in section 5.2.1b (e.g. GR13, GR14 & GR15). In other words, during GR

synthesis, some of the material produced did not have a completed sulphate GRII structure. This seems to apply particularly to sample GR21 where the basal d-spacing is at 7.90 A. Looking back at the way the synthesis had proceded, the explanation seems reasonable since the formation was slow and did not require much alkali.

The dried oxidation products of the Al-GRs depend on the Fe(II) system. For the $FeCl_2$ system, oxidation resulted in poorly-crystalline akaganeite (Table 5.61). This confirms the work of Taylor & McKenzie (1980). In the $FeSO_4$ system (samples GR23, GR17 & GR22), the oxidation products are more difficult to assess. The low-angle lines at 8.8-10.3 A indicate that the original structure is still present, although in a degraded form. The other lines are too few in number and too broad to correlate identification. They can be attributed to goethite or ferrihydrite (in the case of GR22, goethite seems to be the more appropriate).

Although dry oxidation of the chloride Al-GR samples has resulted in poorly-formed akaganeite, on wet oxidation under water, the material converted to a mixture of lepidocrocite and goethite. The X-ray d-spacings for material from sample GR24 which has been oxidised and aged in water for ~ 14 days is given in Table 5.62. Thus like the chloride Fe-GRs, the oxidation of the material has more than one pathway.

Sample = GR23 Source = $FeSO_4$ IFAR = 5		Sample = GR17 Source = $FeSO_4$ IFAR = 10		Sample = GR22 Source = $FeSO_4$ IFAR = 10		Sample = GR24 Source = $FeCl_2$ IFAR = 5		Sample = GR19 Source = $FeCl_2$ IFAR = 20	
d-spacing (Å)	Int	d-spacing (Å)	Int	d-spacing (Å)	Int	d-spacing (Å)	Int	d-spacing (Å)	Int
10.28	100(B)								
		9.12	100(B)	8.76	77(B)	7.63	100(B)	7.50	90(B)
						5.13	30	5.22(?)	40
		4.40	57(VB)	4.17(?)	65(VVB)				
3.90(?)	51(VVB)					3.83	45(B)		
								3.32	60
2.522	87(B)	2.536	59(B)	2.482	100(VB)	2.571	36(VB)	2.543	100
								2.287	35
								1.640(?)	35
		1.476	23(B)					1.488(?)	30

B = broad V = very

Table 5.61 X-ray d-spacings of oxidised Al-GRs derived from 0.1 M Fe(II).

Sample	GR24, IFAR = 5					
d-spacing	6.15	[4.70]	[4.12]	3.24	[2.430]	[1.918]
Intensity	37	22	41	75	100	35

[ ] = goethite lines

Table 5.62 X-ray d-spacings of converted chloride Al-GR sample which has been oxidised & aged in water.

5.3.3 Infrared Spectroscopy

The IR spectra of the Al-GRs are basically similar to those of the Fe-GRs i.e. they have OH/H_2O absorption in the regions 3960-2100 cm^{-1} & 1780-1230 cm^{-1} and, also, metal-OH, metal-O and anion absorption from 1300 cm^{-1} onwards (Fig 5.62). In the latter, diagnostic region, the IR absorption peaks are not well-developed showing that the samples have poor crystallinity, thus confirming the XRD data. A feature of the IR spectra of the Al-GRs is the large presence of water (either adsorbed or water of hydration) which is greater than that present in the Fe-GRs.

The IR absorption peaks and regions for the sulphate Al- and chloride Al-GRs are given in Tables 5.63 and 5.64, respectively. The main difference between the two types is the presence of the sulphate absorption band in the sulphate Al-GRs. For the sulphate Al-GRs, the main sulphate absorption occurs in the range 1300-950 cm^{-1} with peaks at ~ 1195, ~ 1111 and ~ 973 cm^{-1}. There is also a further peak at ~ 600 cm^{-1} associated with the sulphate group. Apart from sample Item47, which seems to have less water and sulphate present, all the sulphate Al-GR samples have similar IR spectra to that of basic $FeSO_4$ (see Fig 5.16). Since this is the case, the IR spectra of the sulphate Al-GRs are also similar to those of the sulphate

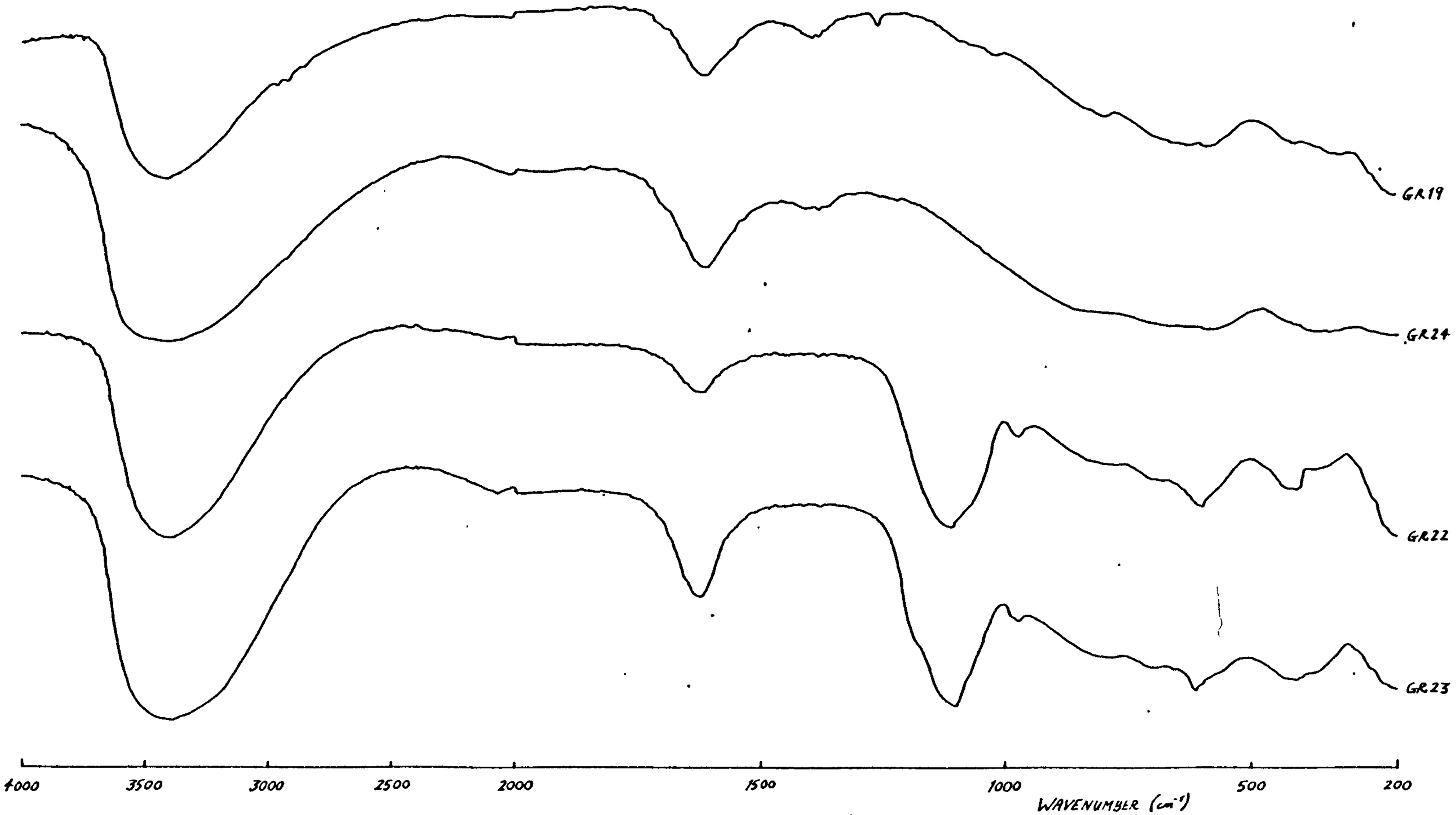

Fig 5.62 Typical IR spectra of Al-GRs. derived from 0.1 M Fe(II).

Sample = GR23 IFAR = 5	Sample = GR17 IFAR = 10	Sample = GR22 IFAR = 10	Sample = Item 47 IFAR = 50
Peaks (cm^{-1})			
3390 ± 50	3410 ± 40	3400 ± 40	3420 ± 30
1625 ± 10	1630 ± 10	1620 ± 10	1620 ± 10
1195 ± 20			
1098 ± 10	1115 ± 10	1110 ± 10	1120 ± 10
			1065 ± 20
970 ± 10	980 ± 10	973 ± 5	973 ± 10
700 ± 10	708 ± 10	700 ± 20	710 ± 15
610 ± 5	615 ± 5	600 ± 10	600 ± 10
415 ± 10	425 ± 10	413 ± 10	
Regions (cm^{-1})			
3940-2480	3720-2480	3820-2580	3700-2480
1770-1430	1730-1520	1760-1490	1730-1530
1300- 300	1280- 350	1290- 300	1260- 380

Table 5.63 IR absorption peaks and regions of sulphate Al-GRs derived from 0.1 M Fe(II).

Sample = GR24 IFAR = 5	Sample = Item 35 IFAR = 10	Sample = GR19 IFAR = 20
Peaks (cm^{-1})		
3430 ± 60	3380 ± 50	3410 ± 40
		(2950 ± 5)
		(2910 ± 5)
		(2850 ± 5)
1615 ± 10	1610 ± 10	1605 ± 10
1415(?)± 10	1450(?)± 20	
1370(?)± 10	1395(?)± 20	1390 ± 10
		1255 ± 5
		1082(?)± 15
		1012 ± 10
850(?)± 30	870 ± 20	
		793 ± 10
	680 ± 20	
585 ± 20	585 ± 20	580 ± 10
	418 ± 15	405 ± 10
375(?)± 20		
		3 5(?)± 20
Regions (cm^{-1})		
3960-2300	3700-2100	3760-2460
1780-1300	1720-1300	1740-1230
1200- 300	1180- 300	1170- 300

( ) = hydrocarbon pump oil contaminant

Table 5.64 IR absorption peaks and regions of chloride Al-GRs derived from 0.1 M Fe(II).

Fe-GRs but without the absorption peaks of goethite. In the case of the sulphate Fe-GRs, there is also an extra peak at 1131 cm^{-1} in the sulphate absorption region (Fig 5.14) which is not evident in the spectra of the sulphate Al-GRs. This indicates that the sulphate groups in the two types of material have slight differences in the S-O bonds. Since the extra peak does not occur in basic $FeSO_4$, it suggests that the differences are due to the presence of Fe(III) cations. Actually, the closer similarity of the IR spectra of basic $FeSO_4$ and the sulphate Al-GRs would also suggest that the presence of Fe(III) cations makes a difference to the structure of the GRs.

As already mentioned, there is very little feature in the 1200-200 cm^{-1} region for the IR spectra of the chloride Al-GR samples. The absorption peaks given in Table 5.64 for this region are hardly developed at all. This suggests that the chloride Al-GRs are more poorly-crystalline than the sulphate Al-GRs which contradicts the XRD data somewhat. Apart from the water absorption regions, the only other noticeable absorption area occurs in the range ~ 1480-1320 cm^{-1}. The absorption peak or peaks is/are similar to that occurring for the chloride Fe-GRs and thus probably associated with the Cl^- anions. There is also an unexplained peak at 1255 cm^{-1} in sample GR19, although this may be due to hydrocarbon pump oil contaminant (peaks at ~ 2900

cm^{-1}). The IR spectra of the chloride Al-GRs are similar to the spectra of basic $FeCl_2$ (see Fig 5.43). This is not surprising since basic $FeCl_2$ is less crystalline than chloride Fe-GRs and so shows less features from 1200 cm^{-1} onwards.

5.3.4 Surface Area Measurements

The surface areas determined for the Al-GRs are presented in Table 5.65 and adsorption isotherms typical of the two types are shown in Fig 5.63. Also given in Table 5.65 are the pore size distribution estimated from the hysteresis loop.

The N_2 adsorption isotherms are of Type IV for both categories of Al-GRs, and the shape is typical of Fe(II)-derived material (Crosby, 1982; Crosby et al., 1983). The shape of the hysteresis loop again conforms most closely to type B in the de Boer's classification (de Boer, 1958).

It can be seen quite clearly from Table 5.65 that there is a large difference in the surface areas between the sulphate and chloride Al-GRs. The latter group has a very low surface area of 3-12 $m^2.g^{-1}$ which is much lower than either the chloride Fe-GRs (~ 60-100 $m^2.g^{-1}$) or the sulphate Fe-GRs (~ 40-70 $m^2.g^{-1}$). The sulphate Al-GRs have a slightly higher surface area than the sulphate Fe-GRs, and there is no trend with IFAR nor <Al(III)>. In fact, the sulphate Al-GRs have similar surface areas to the hydrous Fe oxides derived from basic Fe(II) salts (see Appendix A). The surface area of the sulphate Al-GRs probably depend on the crystallisation rate during synthesis,

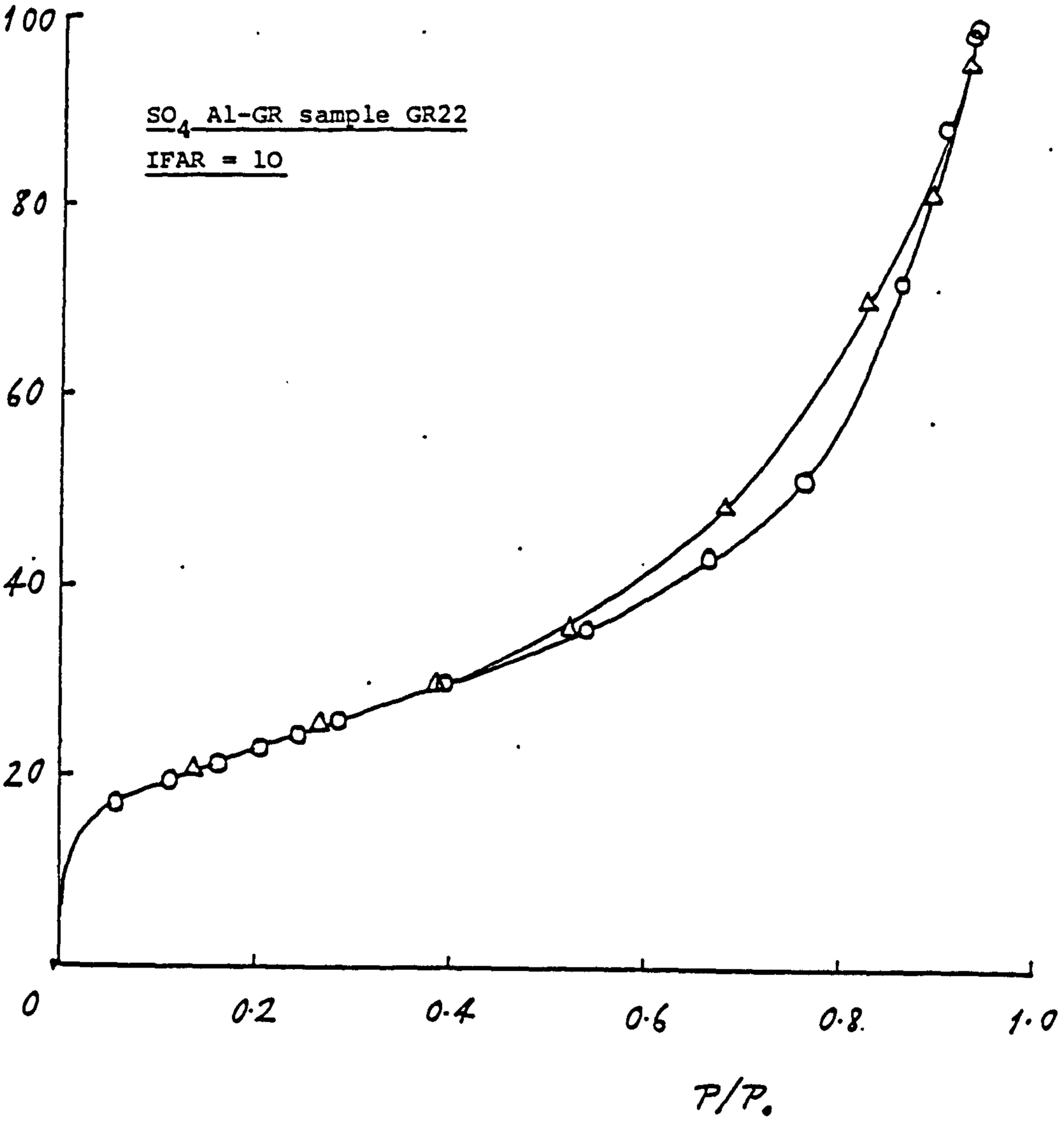

Fig 5.63 Typical N_2 adsorption isotherms of Al-GRs derived from 0.1 M Fe(II).

(O - adsorption △ - desorption)

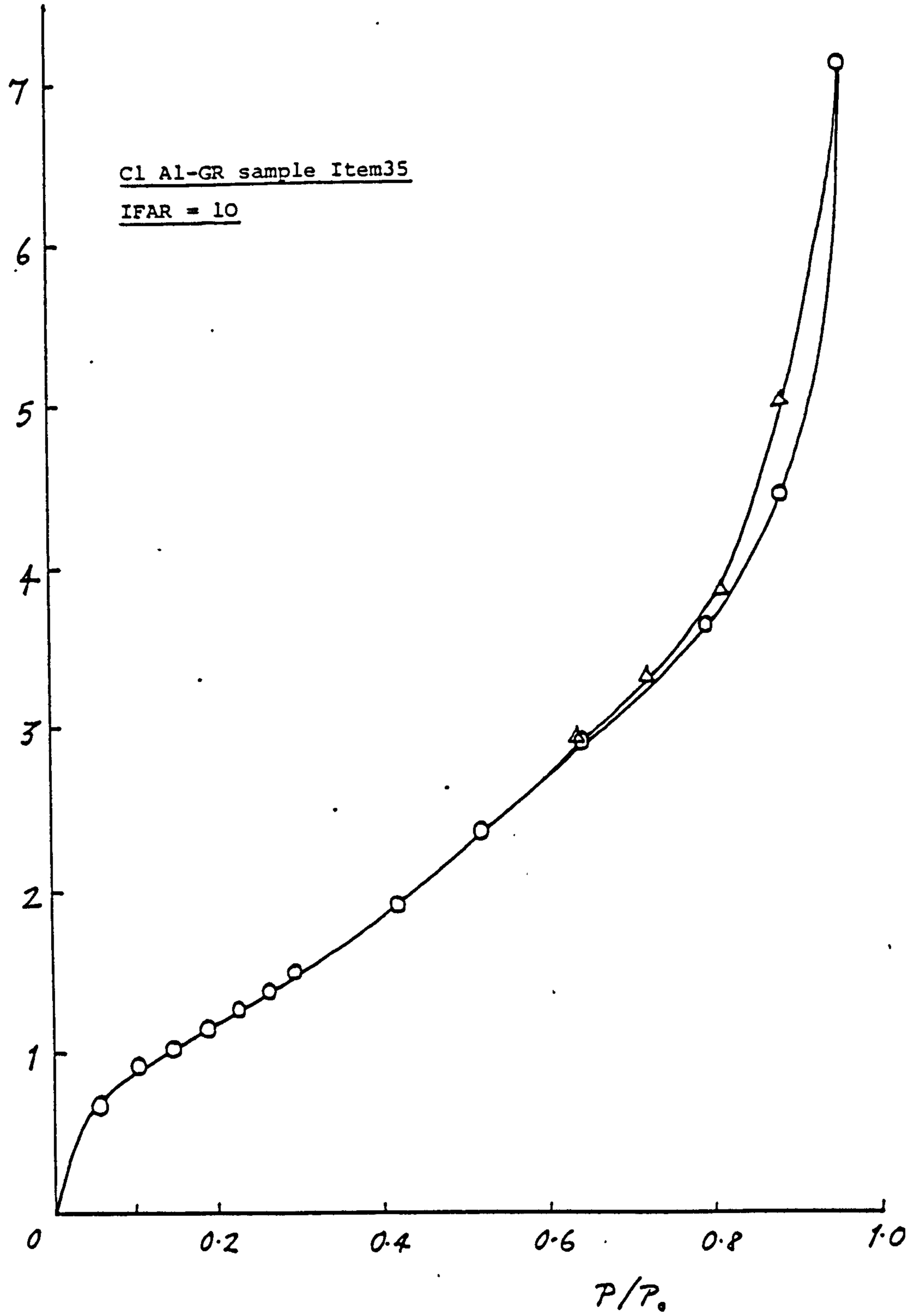

Fig 5.63 (cont'd) Typical N_2 adsorption isotherms of Al-GRs derived from 0.1 M Fe(II).

(O - adsorption $\triangle$ - desorption)

Sample	Fe(II) Source	IFAR	Al(III) (mmole)	Surface Area ($m^2.g^{-1}$)	Hystersis Closure P/P_o (approx)	Pore Size Range, d (A)
GR23	$FeSO_4$	5	4	47.7	* -0.96	* -500
GR17		10	2	107.7	0.38-0.98	30-990
GR22		10	2	65.8	0.40-0.94	30-340
Item 47		50	0.5	59.2	* -0.96	* -500
GR24	$FeCl_2$	5	4	11.3	—	—
Item 35		10	2.5	3.8	0.62-0.96	60-500
GR19		20	1	3.1	—	—

(* indicates that lower limit cannot be determined)

Table 5.65 Surface areas and pore size distribution for the Al-GRs derived from 0.1 M Fe(II).

which is generally the case with the sulphate Fe-GRs.

The pore size distribution between the sulphate and chloride Al-GRs is not very different, being in the mesopore range on the whole (even though it seems that the chloride Al-GRs have a higher value for the lower hysteresis closure point). However, the sulphate Al-GRs seem to have a certain degree of microporosity as the desorption points at low P/PO values have long equilibrium times. The rather low surface areas of the chloride Al-GRs is probably due to the absence of any micropores. Thus it appears that Al is incorporated somewhat differently in the structure of the two types of Al-GRs. It is interesting to note that Crosby et al. (1983) obtained a value of 6.4 $m^2.g^{-1}$ for the surface area of an iron oxide precipitated from water obtained from an acid mine stream. This water contained 1.9 $mg.L^{-1}$ Fe, of which 90% was in the Fe(II) form. Since natural waters probably contained dissolved Al, it is quite possible that a chloride Al-GR type phase was formed.

5.3.5 Mossbauer Spectroscopy

(i) 77 K and RT data

Mossbauer spectra at 77 K and RT, typical of the sulphate and chloride Al-GRs, are shown in Fig 5.64. The spectra shown are for samples GR22 and GR24. The two spectra for each type of Al-GR are of the wet, fresh precipitate and the dried, aged material, respectively.

From the two sets of spectra, it is clear that there is not a great deal of difference between the sulphate and chloride Al-GRs in terms of the Mossbauer effect (although sample GR22 shows a greater degree of oxidation when dried). The spectra of the fresh material consists only of an Fe(II) quadrupole doublet, while the spectra of the dried material also shows the presence of an Fe(III) quadrupole doublet arising from oxidation. There is no sign of any MHS for both types of material. This lack of MHS is consistent with the magnetic dilution effects of aluminium (Golden et al., 1979; Goodman & Lewis, 1981; Morup et al., 1980; Murad & Schwertmann, 1983; Srivastava & Sharma, 1972). The 77 K Mb spectra of the Al-GRs is, in fact, very similar to that of the basic Fe(II) salts (Figs 5.23 & 5.50).

The 77 K Mb parameters for both wet, fresh and dried, aged material are given in Tables 5.66 and 67,

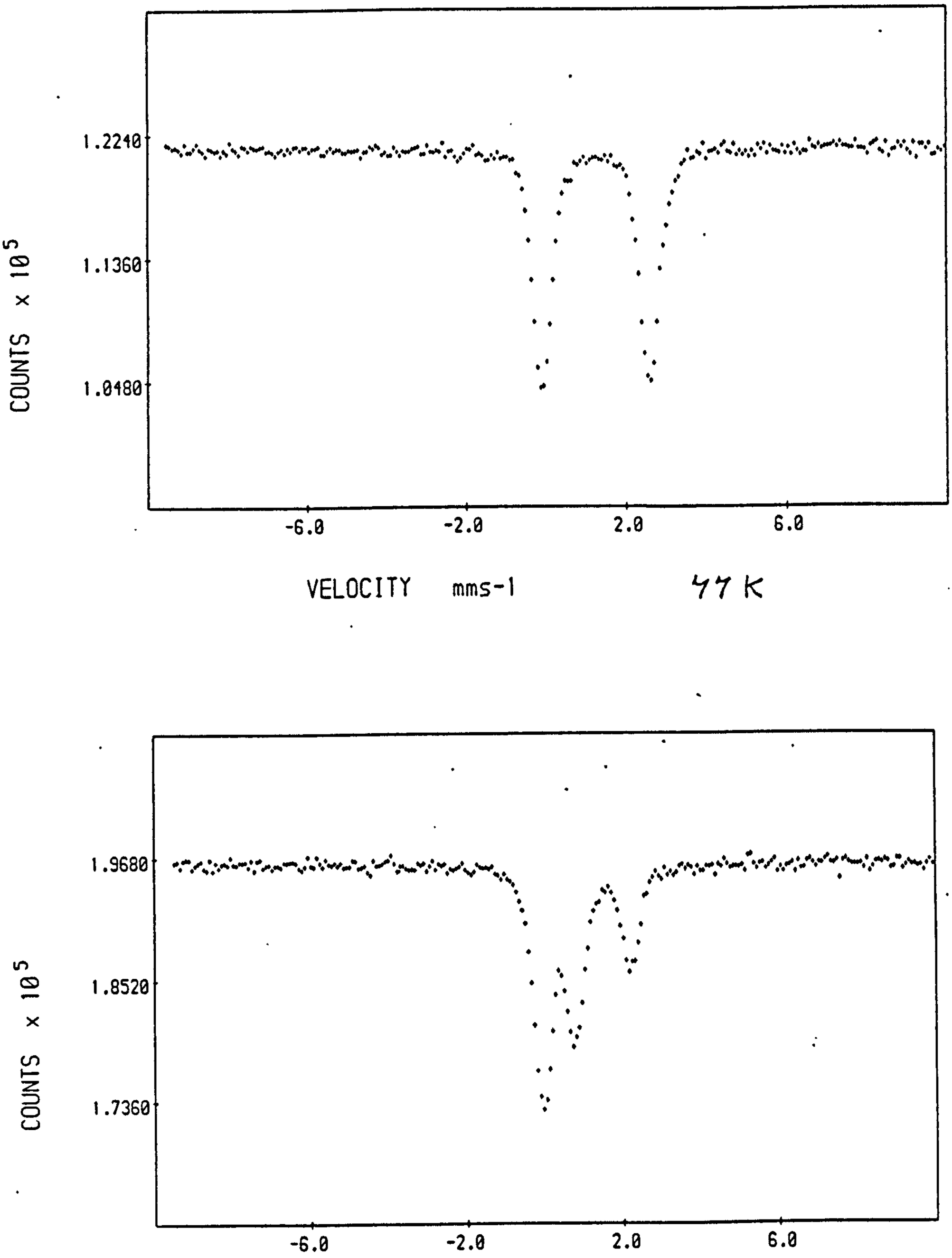

Fig 5.64 Mossbauer spectra at 77 K and RT of a typical sample of sulphate Al-GR. (Sample GR22)

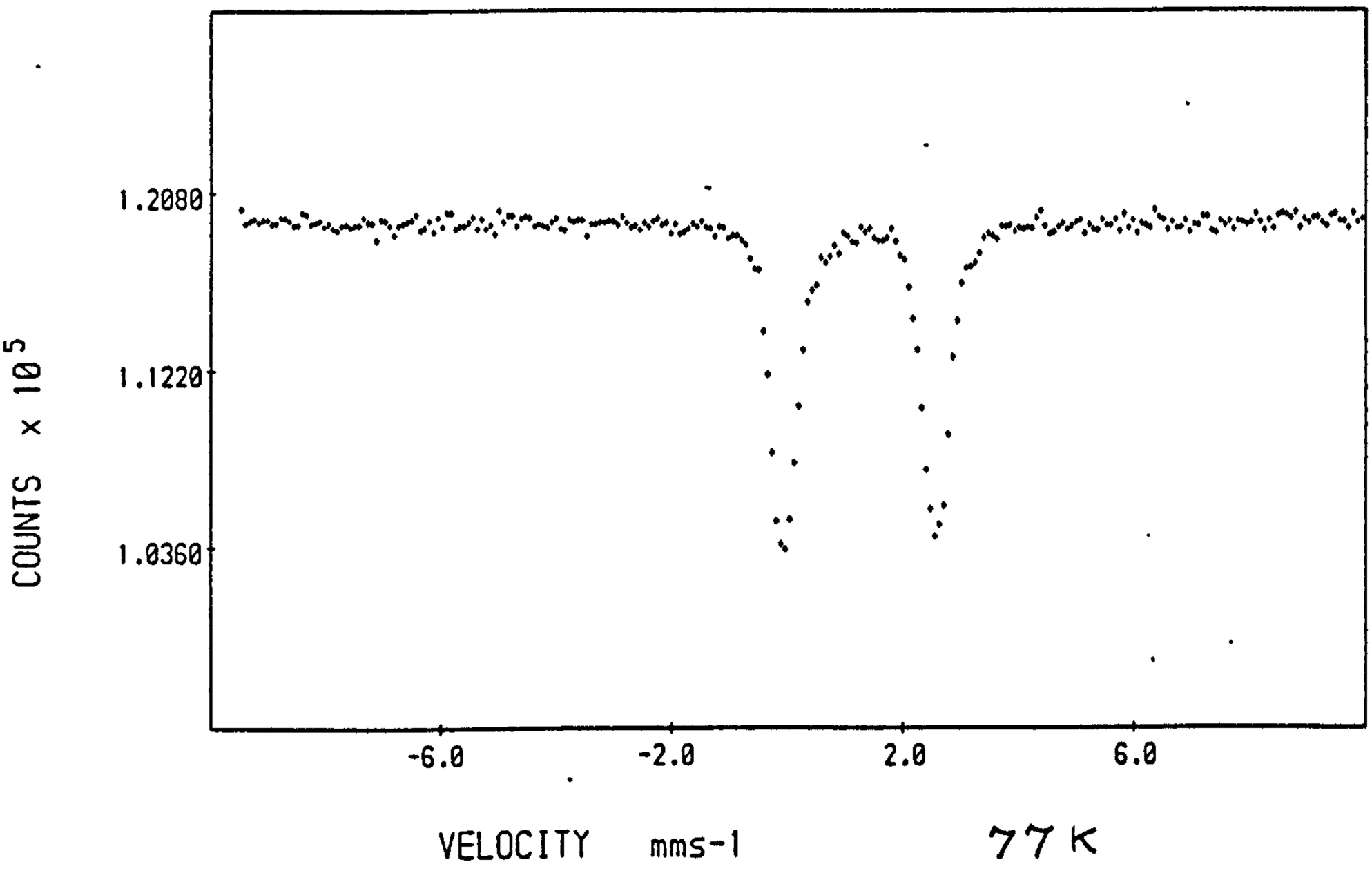

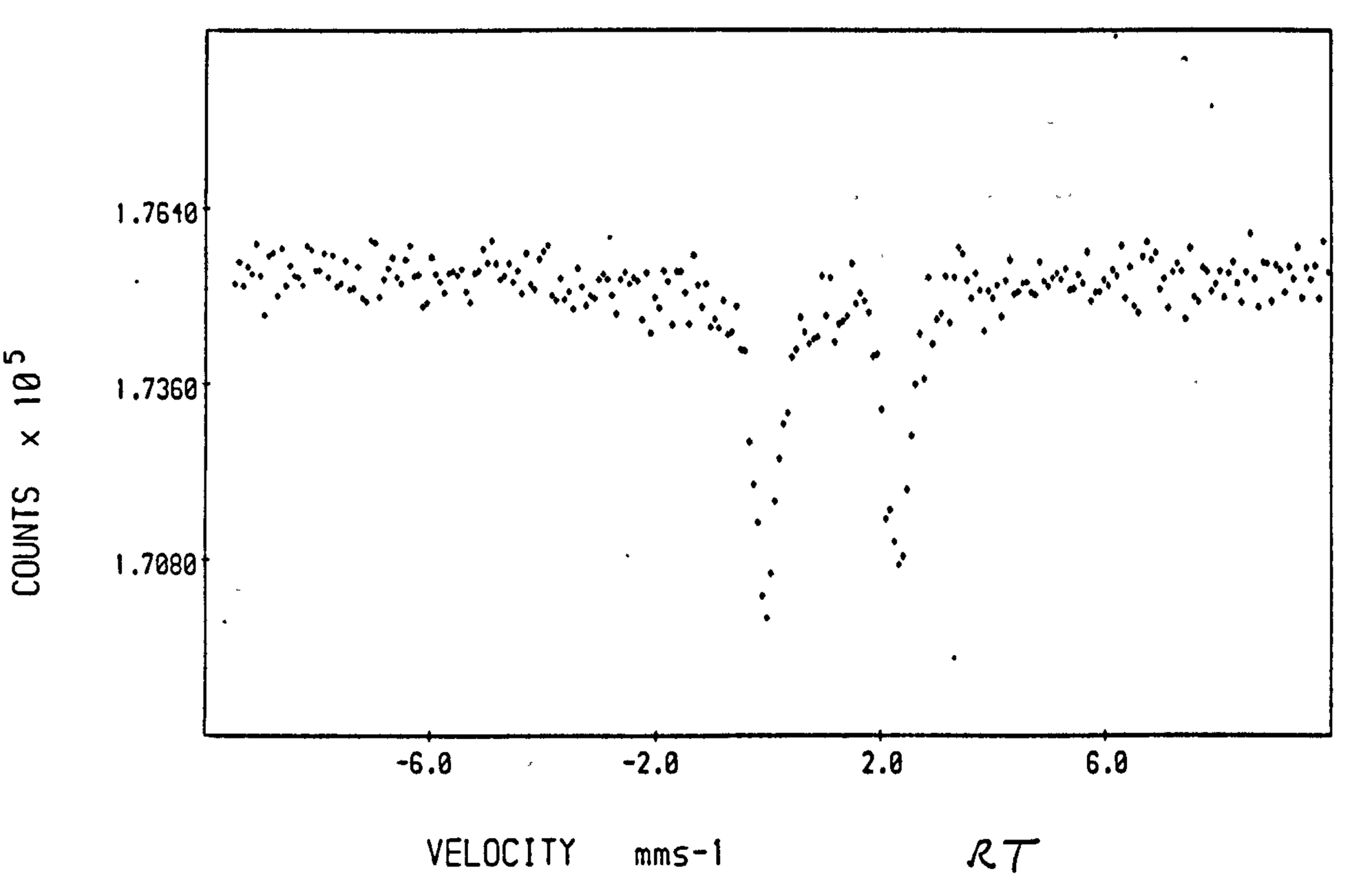

Fig 5.64 (cont'd) Mossbauer spectra at 77 K and RT of a typical sample of chloride Al-GR. (Sample GR24)

Sample	Fe(II) Source	IFAR	Fe(II) doublet		
			δ	Δ	$\frac{1}{2}\Gamma$
GR23	$FeSO_4$	5	1.24	2.67	0.26
GR17		10	1.21	2.67	0.22
GR22		10	1.24	2.67	0.25
Item 47		50	1.24	2.70	0.26
GR24	$FeCl_2$	5	1.24	2.63	0.26
Item 35		10	1.21	2.65	0.26
GR19		20	1.25	2.73	0.24
Mean			1.23	2.67	0.25

Table 5.66 77 K Mb parameters for the wet, fresh precipitate of Al-GRs derived from 0.1 M Fe(II).

Sample	Fe(II) Source	IFAR	Fe(II) doublet			Fe(III) doublet			FFR
			δ	Δ	$\frac{1}{2}\Gamma$	δ	Δ	$\frac{1}{2}\Gamma$	
GR23	$FeSO_4$	5	1.27	2.54	0.27	0.40	0.80	0.23	3.60
GR17		10	1.28	2.49	0.24	0.45	0.87	0.23	1.07
GR22		10	1.24	2.54	0.26	0.43	0.89	0.24	1.63
Item 47		50	1.27	2.45	0.26	0.45	0.83	0.24	0.28
GR24	$FeCl_2$	5	1.26	2.62	0.26	0.34	0.70	0.18	75.0
Item 35		10	1.32	2.48	0.38	0.42	0.76	0.42	0.25
Mean			1.27	2.52	0.28	0.42	0.81	0.26	

Table 5.67 77 K Mb parameters for the dried, aged precipitate of Al-GRs derived from 0.1 M Fe(II).

respectively. In the case of the wet, fresh material, the presence of any Fe(III) quadrupole component (as a result of oxidation) has been ignored since this is extremely small. It can be seen from Table 5.66 that the Mb parameters for the Fe(II) doublet are independent of the anion type and invariant over the range of IFAR used. The IS (mean = 1.23 ± 0.10 mms^{-1}) seems to be identical with that for the Fe-GRs but the QS is slightly smaller (mean = 2.67 ± 0.07 mms^{-1}). This latter fact is evidently due to the altered environment caused by the presence of the Al(III) cations, which may also account for the lack of difference between the sulphate and chloride Al-GRs. The $1/2\Gamma$ value (mean = 0.25 ± 0.05 mms^{-1}) is larger than the corresponding values for the Fe-GRs, and indicates poorer crystallinity.

The Mb parameters for the dried, aged material (Table 5.67) are affected to some extent by the drying process, and to a greater extent by oxidation. For instance, the Fe(II) QS seems to decrease with decreasing FFR (e.g. 2.45 mms^{-1} when FFR = 0.28 but 2.54 when FFR = 3.60 mms^{-1}). Evidently, oxidation causes a distortion at the Fe site. The mean $1/2\Gamma$ also increases (0.25 -> 0.28 mms^{-1}) indicating a decrease in crystallinity. The Fe(III) quadrupole component, arising from the oxidation of the Fe(II) material, has Mb parameters very similar to

those for amorphous Fe(III) oxides (see Bowen, 1979). This most certainly means that the change in QS on vacuum-drying for the Fe(III) quadrupole component in the Fe-GRs (~ 0.45 -> 0.62 mms^{-1}) is a direct result of oxidation rather than to the drying process.

The RT Mb parameters for the dried, aged material are given in Table 5.68. Again the FFR shows that the degree of oxidation varies from sample to sample. The Mb parameters may depend on the degree of oxidation. As expected, the IS and QS for both quadrupole components have decreased. The ISs for both Fe(II) and Fe(III) quadrupole components are similar to those for the Fe-GRs (both sulphate and chloride systems). However, the QS is slightly smaller at 2.29 ± 0.08 mms^{-1} (cf. ~ 2.5 mms^{-1} for Fe-GRs) and the Fe(III) QS is greater at 0.75 ± 0.08 mms^{-1} (cf. ~ 0.3-0.7 mms^{-1} for Fe-GRs). The difference is obviously due to the Al(III) cation which has a slightly smaller radius than the Fe(III) cation.

The results show that the Fe(III) sites participating in the formation of the GR structure clearly have a different environment to the Fe(III) sites arising from oxidation.

Sample	Fe(II) Source	IFAR	Fe(II) doublet			Fe(III) doublet			FFR
			δ	Δ	$\frac{1}{2}\Gamma$	δ	Δ	$\frac{1}{2}\Gamma$	
GR23	$FeSO_4$	5	1.12	2.25	0.26	0.32	0.66	0.23	2.93
GR17		10	1.12	2.28	0.23	0.36	0.78	0.21	0.25
GR22		10	1.07	2.27	0.27	0.36	0.78	0.25	0.66
GR24	$FeCl_2$	5	1.13	2.38	0.26	0.40	0.84	0.21	12.78
Item 35		10	1.14	2.28	0.23	0.34	0.71	0.23	0.07
Mean			1.12	2.29	0.25	0.36	0.75	0.23	

Table 5.68 RT Mb parameters for the dried, aged precipitate of Al-GRs derived from 0.1 M Fe(II).

Sample	Fe(II) Hyperfine Field								Fe(III) Doublet			
	δ	Δ	$\frac{1}{2}\Gamma$	η	θ	ϕ	B	%I	δ	Δ	$\frac{1}{2}\Gamma$	%I
GR17	1.41	-2.81	0.75	0	90	0	10.3	15.8	1.35	2.72	0.30	42.1
									1.35	3.30	0.15	42.1
GR19	1.41	-2.88	1.00	0	90	0	14.1	10.3	1.30	2.63	0.30	64.1
									1.35	3.30	0.30	25.6

All parameters in mms^{-1} except θ & ϕ, B (T) and η (dimensionless)

Table 5.69 4.2 K Mb parameters for Al-GR samples.

(ii) 4.2 K data

Mossbauer spectra at 4.2 K were obtained for one sample of sulphate Al-GR and one sample of chloride Al-GR. The samples used were GR17 and GR19 (both wet, fresh precipitates). The raw spectra are shown in Fig 5.65, and consist of (i) a large Fe(II) quadrupole doublet and (ii) a degree of hyperfine splitting due to Fe(II) combined quadrupole and magnetic interactions. There is no sign of any MHS from Fe(III) components which is what was expected since there was hardly any Fe(III) component at 77 K. Right away, it can be seen that the difference between the Fe-GRs and the Al-GRs is the lack of a large Fe(II) hyperfine component in the Al-GRs. This is evidently the result of the magnetic dilution effect of Al which results in relaxation of the Mossbauer lines.

The two Mb spectra were each curvefitted with two Fe(II) quadrupole doublets and a small Fe(II) hyperfine field. The latter was based on the values used for curvefitting the Fe(II) envelope in the Fe-GRs. The fitted spectra are shown in Fig 5.66 and the corresponding Mb parameters are given in Table 5.69. Looking at Fig 5.66, the fitted curves seem to be in good agreement with the actual points.

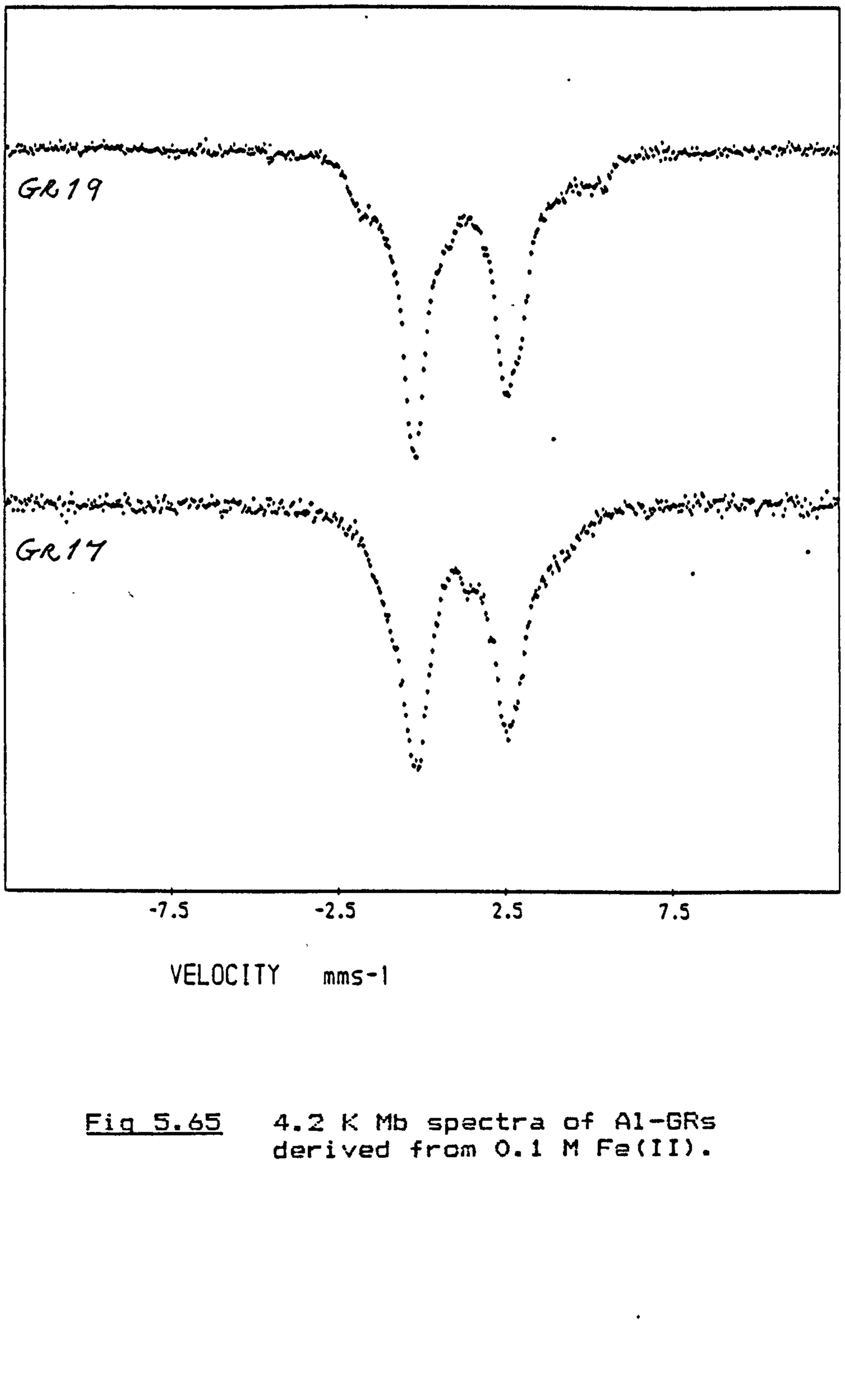

Fig 5.65 4.2 K Mb spectra of Al-GRs derived from 0.1 M Fe(II).

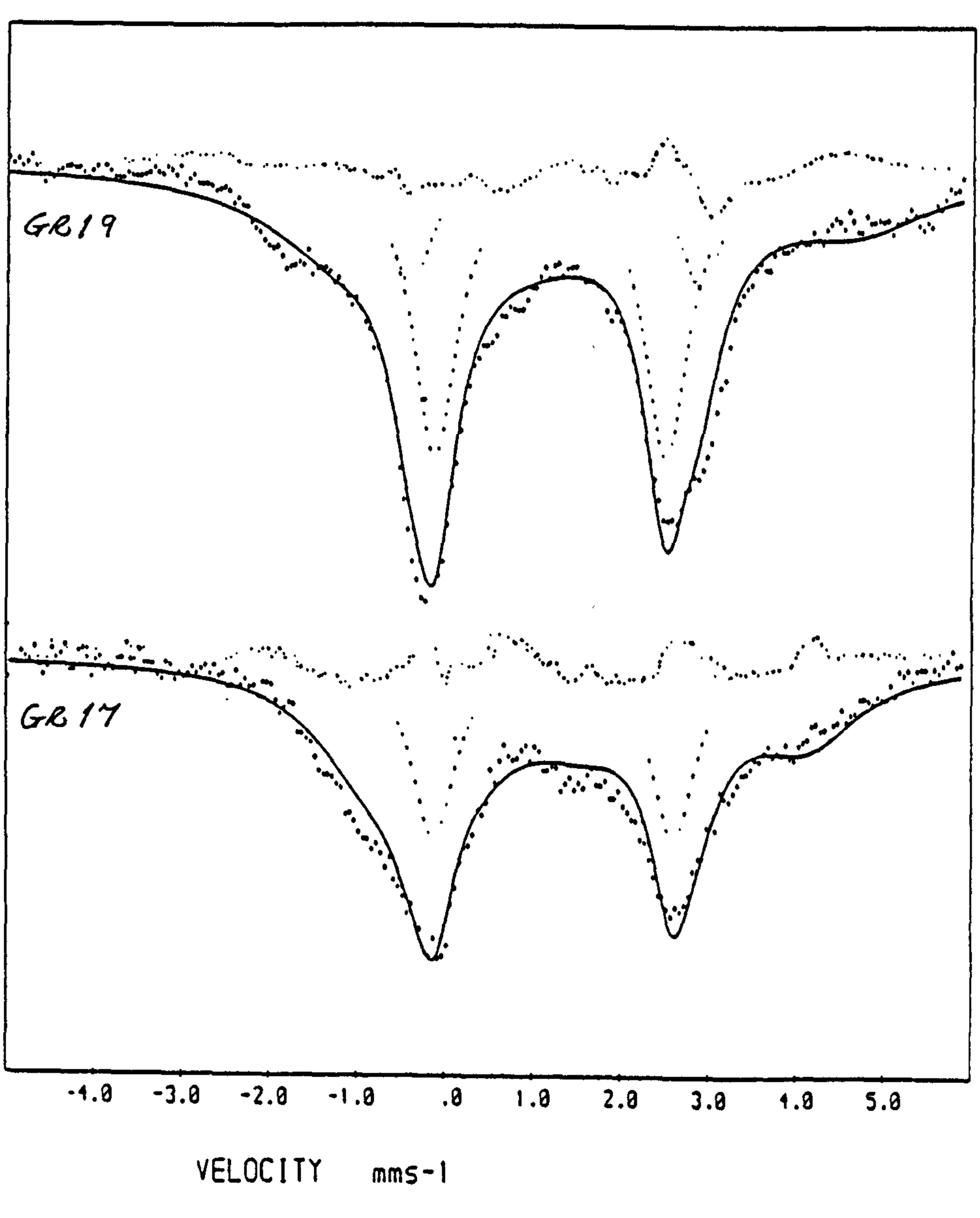

Fig 5.66 Fitted 4.2 K Mb spectra for the Al-GRs derived from 0.1 M Fe(II).

CHAPTER 6: CONCLUSIONS

In this concluding chapter, the three types of Green Rusts, sulphate Fe-GR, chloride Fe-GR and the Al-GRs (the sulphate and chloride Al-GRs are considered under one grouping as their properties are very similar), are compared in a summarily fashion to highlight the main similarities and differences. A generalised mechanistic interpretation of the results is then presented to account for the reactions and subsequent behaviour involved in the syntheses studied. The chapter ends with an appraisal of the significance of the work in this thesis and pointers to future study.

6.1 Comparison of sulphate Fe-GR, chloride Fe-GR and the Al-GRs

6.1.1 Titration and AAS data

1) NaOH consumption with time for all three types of material follows an exponential curve of the form $Y = Y_o[1-\exp(-kt)]$ where Y_o and k are constants. However, the curve for the Al-GRs reaches a plateau at a much earlier stage than the other two Green Rusts, thus indicating the synthesis reaction to have completed much more rapidly.

2) Total NaOH consumption and total Fe(II) uptake both increase with <Fe(III)> or <Al(III)> for all the types of Green Rusts.

3) Specific NaOH consumption was independent of <Fe(III)> for the sulphate Fe-GR but decreases in the other two cases.

4) Specific Fe(II) uptake decreases with <Fe(III)> or <Al(III)> for all the Green Rusts. This is to be expected since $[Fe(II)]_i$ was constant i.e. as the amounts of gel added increases the amount of Fe(II) available per unit mass of gel decreases.

Conversely, specific Fe(II) uptake increases with IFFR or IFAR [not surprising since IFFR and IFAR are proportional to the inverses of <Fe(III)> and <Al(III)>, respectively]. From this viewpoint, as IFFR or IFAR

increases the amount of Fe(II) available for uptake per unit mass of gel also increases.

5) The Freundlich isotherm for both sulphate and chloride Fe-GRs shows that the process of Fe(II) uptake was most likely due to physical adsorption and hence surface area related. It also shows that the surface in both cases was most probably not completely filled by adsorption of Fe(II) cations i.e. undersaturation of sites.

In the case of the Al-GRs, both Freundlich and Langmuir isotherms gave scatter points, indicating a non-physical (i.e. a non-Coulombic) process for the uptake of Fe(II) cations.

6.1.2 X-ray diffraction

1) X-ray diffractograms were sharpest for the sulphate Fe-GRs, followed by the chloride Fe-GRs and then finally the Al-GRs. This indicates that the sulphate Fe-GR samples were the most crystalline. In the case of the chloride Fe-GRs, the rapid deterioration of the samples by oxidation during analysis probably accounts for the poorly-resolved X-ray reflections.

There is a small difference between the sulphate Al-GRs and the chloride Al-GRs in that the latter gave sharper lines. However, both subgroups have distinctively fewer lines than the Fe-GRs (indicating a

poorer crystallinity).

2) Only the sulphate Fe-GRs have any discernible amount of contamination present in the unoxidised samples. This contaminant has been identified by XRD as goethite for the dried, aged precipitate; it is felt that, in the case of the wet, fresh precipitate, the phase which had Mossbauer parameters similar to that of goethite may not actually be goethite but a precursor, i.e. a protogoethite or a pseudogoethite, since it is somewhat metastable.

3) The XRD patterns for the sulphate Fe-GRs show that samples were more crystalline at high <Fe(III)>. This coincides with high total NaOH consumption and high total Fe(II) uptake (but low <NaOH>s and low <Fe(II)>s, respectively). The samples at high <Fe(III)> also appear to have less goethite impurity.

The X-ray diffractograms for the chloride Fe-GRs were too affected by oxidation for any trend with <Fe(III)> to show up.

4) Non-GRs were produced in the chloride Fe system at <Fe(III)> $\geq$ 5 mmoles (i.e. IFFR $\leq$ 4) for $[Fe(II)]_i$ = 0.1 M. The XRD data for the dried, aged samples show them to be either magnetite or maghemite. The X-ray lines were sharper and more intense than those for the chloride Fe-GR samples proper, thus indicating that they were more crystalline.

Non-GRs were only produced in the sulphate Fe system at $[Fe(II)]_i$ < 0.05 M for <Fe(III)> = 5

mmoles (IFFR < 2).

In addition, a non-GR (sample S7-2-83) was synthesised from the sulphate Fe system when NaOH was not added to maintain pH at 7. This is a very important result as it shows that alkali consumption was vital to the formation of a Green Rust precipitate.

5) In some samples of both sulphate Fe-GRs and sulphate Al-GRs, the X-ray diffractograms show up a refection around 7.9-8.9 A. This may be due to some contamination or linked to an imperfectly-formed or distorted crystal structure. The latter seems more likely as the oxidised samples show a line at ca. 9.0 A which is presumably from degraded GR material.

6) Under anoxic conditions, dried chloride Fe-GR samples undergo a solid state transformation to magnetite/maghemite. This does not occur with dried sulphate Fe-GR samples and so show that the difference in anion-type alters their behaviour accordingly. However, a sulphate Fe-GR sample (sample GR20) did convert to a mixture of goethite and magnetite under <u>wet</u> anoxic conditions. So it is apparent that transformation pathways are probably quite complex.

7) On dry oxidation, sulphate Fe-GR material converted to goethite while chloride Fe-GR material converted to akaganeite. Since the X-ray diffractograms were less well-defined, it cannot be ruled out that ferrihydrite was also present in the oxidised material. Ferrihydrite was probably present along with goethite in

the dry oxidation product of the sulphate Al-GRs. In the case of the chloride Al-GRs, the oxidation product was again akaganeite, although much less well-crystalline than that of the chloride Fe-GRs.

On wet oxidation, sulphate Fe-GR also converted to goethite whereas chloride Fe-GR converted to lepidocrocite. A sample of chloride Al-GR was found to convert to a mixture of lepidocrocite and goethite. Thus there are more than one oxidation pathway for both the chloride Fe-GRs and the chloride Al-GRs.

6.1.3 Infrared spectroscopy

1) IR spectra for all three types of Green Rusts have essentially the same profile in the region 4000-1500 cm^{-1}. This is not very surprising since the two main absorption peaks in this region (~ 3400 and ~ 1620 cm^{-1}) arise from molecular water and/or hydroxyl groups. In general, the chloride Fe-GR precipitates appear to be less hydrated than the other two types of material. The dominant factor here is probably the greater coordination of water by SO_4^{2-} anions.

2) The IR spectra of both sulphate Fe-GRs and sulphate Al-GRs have a distinguishing absorption region at 1280-950 cm^{-1} due to SO_4^{2-} anions. The precipitates derived from the chloride system do not have any strong absorption peak which can be definitely

ascribed to Cl^- anions.

3) The sulphate Fe-GR samples were further characterised by the strong IR absorption peaks (in the 1100-200 cm^{-1} region) arising from the presence of the goethite phase. Similarly, the chloride Fe-GR samples were further distinguished by having the characteristic absorption peaks of akaganeite in the same IR region. However, these latter absorption peaks were not as well-defined as those for the sulphate Fe-GRs, thus indicating again the poorer crystallinity of the chloride Fe-GRs (confirming the XRD data).

On the basis of all the IR data at hand, it is probably very difficult to distinguish between poorly-crystalline sulphate Fe-GRs and medium quality (or less) sulphate Al-GRs. A similar situation pertains with the two types of chloride Green Rusts.

4) Both the sulphate Fe-GRs and the sulphate Al-GRs have IR spectra which resemble closely the IR spectrum of basic $FeSO_4$ (ignoring the goethite peaks in the sulphate Fe-GRs). The sulphate Al-GRs have the greatest resemblance, indicating that the presence of Fe(III) cations makes a difference in structure. Similarly, both the chloride Fe-GRs and the chloride Al-GRs have IR spectra which resemble closely that of basic $FeCl_2$.

5) Oxidised samples in the case of the Fe-GRs tend to have less water and, in the case of the sulphate Fe-GRs, less SO_4^{2-} anions. The diagnostic peaks

in the region 1200-200 cm^{-1} were generally less well-defined, showing that the samples have degraded on oxidation.

6) The non-GR samples derived from the sulphate Fe system have roughly the same IR profile as the GR samples. However, they have considerably less water of hydration and the IR absorption region due to the SO_4^{2-} anions was less pronounced. The non-GRs produced in the chloride Fe system have very ill-defined IR profiles. The samples have a relatively small amount of hydration water, and the IR spectra show peaks in the 800-200 cm^{-1} region which are characteristic of magnetite.

6.1.4 Surface area measurements

1) The GRs produced from both the Fe(II)-Fe(III) and Fe(II)-Al(III) system have the same type of N_2 adsorption isotherm i.e. type IV with hysteresis in the BET classification which is associated with Fe(II)-derived precipitates. The hysteresis loops are similar and indicates slit-shaped pores or the space between parallel plates, according to the de Boer's classification.

2) In the Fe(II)-Fe(III) system, the sulphate GRs have surface areas in the range 40-65 m^2g^{-1} which is lower than that for the chloride GRs (60-100

m^2g^{-1}). This is reflected in the slightly greater stability to oxidation of the sulphate GRs.

In the Fe(II)-Al(III) system, it is the chloride GRs which have the lower surface areas (3-12 m^2g^{-1} compared to 45-110 m^2g^{-1} for the sulphate GRs). Indeed the values are also lower than those for the sulphate Fe-GRs.

Both the chloride Fe-GRs and the sulphate Al-GRs have surface areas similar to that for the hydrous Fe oxides derived from basic Fe(II) precipitates (~ 60-100 m^2g^{-1}). All the GR types have substantially lower surface areas than either the Fe(III)-derived oxides (> 150 m^2g^{-1}) or Fe(III) gel (> 300 m^2g^{-1}). The difference in surface area between the Fe-GRs and the Al-GRs is evidently due to the difference in the III state cation.

3) All the GR types show mesoporosity and also, with the exception of the chloride Fe(II)-Al(III) GRs, a degree of microporosity. The pore size ranges are as follows:

(i) sulphate Fe-GRs: 30-400 A

(ii) chloride Fe-GRs: 20-700 A

(iii) Al-GRs: 30-1000 A

The pore sizes for both types of Fe-GRs are very consistent over the range of conditions used in synthesising the samples i.e. it does not vary from sample to sample.

4) The non-GRs produced from the chloride

Fe(II)-Fe(III) system have similar surface and pore characteristics as the corresponding GRs themselves.

In the case of the sulphate Fe(II)-Fe(III) system, appendix A shows that surface area increases with decreasing $[Fe(II)]_I$.

6.1.5 Mossbauer spectroscopy

(This summary of Mossbauer data refers specifically to the wet, fresh and wet, aged precipitates unless otherwise stated.)

1) At 77 K, the Mossbauer spectra for the sulphate and chloride Fe-GRs are very similar to each other in that they consist of a paramagnetic Fe(II) doublet and a paramagnetic Fe(III) doublet. However, the sulphate Fe-GRs differ by having an extra magnetic hyperfine component present in their spectra. The Mb spectra for the Al-GRs consist only of a paramagnetic Fe(II) doublet.

In general, the spectra for the Fe-GRs have much better resolved Mb lines (halfwidths are smaller) than that for the Al-GRs, indicating better crystallinity as shown also by the XRD and IR data.

2) At 4.2 K, the Fe-GRs have a magnetically-ordered Fe(II) component as well as an Fe(III) hyperfine component. This magnetically-ordered

Fe(II) component is better resolved for the sulphate Fe-GRs (indicating a greater ordering in the latter). The Fe(II) MHS in the sulphate Fe-GRs was fitted with a single magnetic field whose magnitude was reckoned to be 12.5 ± 0.5 T. For the chloride Fe-GRs, two magnetic fields were fitted and their magnitudes were 8.8 ± 0.5 T and 14.0 ± 0.5 T, respectively.

The Fe(III) MHS had a magnitude of 50.4 ± 0.5 T for the sulphate Fe-GRs and 49.2 ± 0.5 T for the chloride Fe-GRs.

The Al-GRs have only a very slight magnetic ordering of the Fe(II) component at 4.2 K. This is no doubt due to the magnetic diluting effect of the Al cation.

3) At 77 K, the Mb parameters for the Fe(III) quadrupole doublet in both sulphate and chloride Fe-GRs are virtually identical, indicating a similar Mb environment. The important distinguishing feature is the QS for the Fe(II) quadrupole doublet. For the sulphate Fe-GRs, the QS = 2.93 ± 0.05 mms^{-1}; for the chloride Fe-GRs, QS = 2.81 ± 0.05 mms^{-1}. The IS for both types of material are also virtually the same. These parameters remain more or less the same at 4.2 K.

The 77 K Fe(II) QS for the Al-GRs (both subgroups) is 2.67 ± 0.07 mms^{-1} and the Fe(II) IS is similar to that for the Fe-GRs. However, as already mentioned, the halfwidth is slightly greater at 0.25 ± 0.05 mms^{-1} (cf. 0.16-0.18 mms^{-1} for Fe-GRs),

indicating poorer crystallinity.

4) The 77 K Mb spectra for both Fe-GRs and Al-GRs have a very similar appearance to that of the basic Fe(II) salts. Basic $FeSO_4$ has the following Mb parameters:

(i) Fe(II) doublet:- IS = 1.24 ± 0.10 mms^{-1}, QS = 2.92 ± 0.05 mms^{-1};

(ii) Fe(III) doublet:- IS = 0.43 ± 0.10 mms^{-1}, QS = 0.47 ± 0.05 mms^{-1}.

Basic $FeCl_2$ has the following Mb parameters:

(i) Fe(II) doublet:- IS = 1.13 ± 0.10 mms^{-1}, QS = 2.77 ± 0.05 mms^{-1};

(ii) Fe(III) doublet:- IS = 0.29 ± 0.10 mms^{-1}, QS = 0.44 ± 0.05 mms^{-1}.

5) The RT MB spectrum of a sample of sulphate Fe-GR shows relaxation of the MHS. Indeed it is almost totally collapsed. This would indicate the presence of fine-grained particles, contradicting somewhat the XRD data.

6) Mossbauer-wise, there is no distinguishing feature between the sulphate and chloride Al-GRs since Mossbauer spectroscopy only measures short-order interactions and the effect of the Al cation is to weaken the difference in anion-type.

7) The Mb spectra taken at 77 K and RT for the non-GRs derived from the chloride Fe(II)-Fe(III) system show that magnetite was produced (and most rapidly at

that).

8) The goethite or pseudogoethite phase present in the sulphate Fe-GRs seems to be metastable in the early stages after the completion of the GR synthesis experiment. This is presumably due to the onset of ageing in which the precipitate adjusts to the new ambient conditions. However, the manner in which this magnetic phase decreases or increases on ageing overnight, depending on IFFR, indicates that the goethite component is intimately associated with the GR phase.

9) The Mb spectra for the precipitates produced from $[FeSO_4]_I$ < 0.1 M shows that the goethite component becomes the dominant phase as $[Fe(II)]_I$ -> 0. The IR spectra for these samples still show the presence of SO_4^{2-} anions. Since goethite was not produced in the chloride Fe(II)-Fe(III) system, then the determining factor in the formation of a goethite phase is the SO_4^{2-} anions themselves. The SO_4^{2-} anions must co-ordinate the Fe(III) gel in such a way as to convert the gel to goethite. Of course, this is not the usual type of goethite since SO_4^{2-} anions become incorporated into the goethite structure.

6.2 Interpretation of results

6.2.1 The $FeSO_4$ system

The basic process involved in the formation of precipitates from the $FeSO_4$ system can be described by the following equation:

$$FeSO_4\ (aq.) + Fe(III)\ gel \xrightarrow[P(O_2)\to 0]{pH=7} SO_4\ GR\ (sol.) + goethite\ (sol.) \qquad -6.1$$

where $P(O_2)$ = partial pressure of oxygen.

The relative quantities of products formed obviously depend on the initial amounts of the reactants used i.e. $[FeSO_4]_I$ and $\langle Fe(III)\rangle$ or IFFR. Specifically, for the majority of syntheses studied in this thesis, the initial amounts used were (i) $[FeSO_4]_I = 0.1$ M and (ii) $1 \leq IFFR \leq 40$. (The subsequent discussion refers mainly to this regime.) For $[FeSO_4]_I \leq 0.025$ M and $IFFR \leq 1$, the precipitate produced was predominantly or virtually all goethite and the samples were labelled as non-GRs (samples S21-3-83 & S23-3-83). In addition, equation 6.1 would also depend on pH, $P(O_2)$ and to a lesser extent temperature. These factors can be ignored

since they are kept vigorously at constant levels during the synthesis experiments. However, in a control synthesis, alkali was not added to maintain pH at 7 in order to determine whether a Green Rust precipitate was still produced without alkali consumption. The result was that only goethite was formed (sample S7-2-83). This was a very important result because it showed that alkali consumption was required for the formation of Green Rust and, also, that goethite was the thermodynamically stable form to which equation 6.1 would end.

Another factor to consider is the time element. As virtually all the syntheses were allowed to proceed to their thermodynamic endpoint, it is the initial amounts of the reactants that would determine the time taken. So time is a consequence of the syntheses. However, if the syntheses were interrupted before the endpoint was reached, then the time interval taken would be a determining factor in the relative amounts of the products formed.

Since the two reactants in equation 6.1 were each initially at equilibrium at pH 7, and since alkali was required to maintain pH on subsequent mixing, the above menticned process appears to be a hydrolysis-precipitation reaction in which the Fe(III) gel induces hydrolysis of the $FeSO_4$ solution. This induced hydrolysis was probably initiated at the Fe(III)

gel surface-$FeSO_4$ solution interface. The assumption is reasonable since (i) Fe(III) gel has a highly active surface with regard to the adsorption of transition and heavy metal ions (Chukrov et al., 1972; Forbes et al., 1974 & 1976; Jenne, 1968; Schwertmann & Taylor,1977) - it has a specific surface area of ~ 400 m^2g^{-1} in the dry state for gels used in this thesis; (ii) the observed chemical changes were very rapid initially and then slowed down to equilibrium over the course of a few hours (Fig. 5.2), indicating an initial adsorption-type reaction; (iii) the Freundlich isotherm showed that Fe(II) removal from solution by the Fe(III) gel was most probably by physical adsorption; and (iv) the colour of the gel particles changed from dark-brown to bluish-green. Points (i) to (iii) suggest strongly that the initial stage of the induced hydrolysis, or rather the reaction immediately prior to the hydrolysis, was an adsorption process. Thus it seems that the first steps in the formation of the sulphate Fe-GRs involves an adsorption process, followed by hydrolysis of the $FeSO_4$ solution.

A simple and tentative model for the adsorption-hydrolysis reaction is as follows:

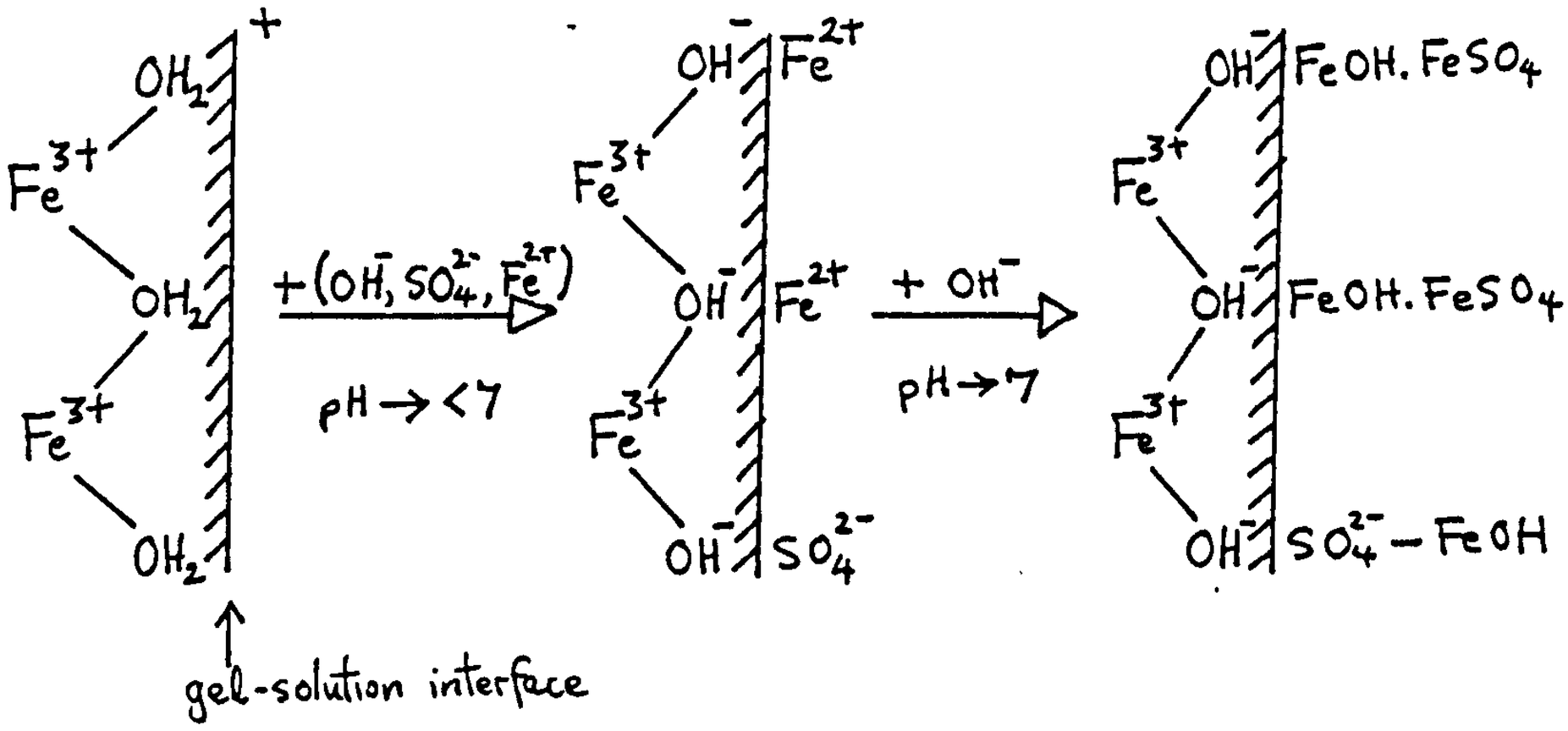

At pH 7, the surface of the Fe(III) gel must have a net postive charge [by the adsorption of potential-determining H^+ ions – counter ions such as Na^+ and NO_3^- are ignored in this discussion as they are known not to adsorbed specifically (Schwertmann & Taylor, 1977)] since the pH of zero point charge for amorphous Fe(III) oxides is ~ 8.0 (Crosby, 1982; Schwertmann & Taylor,1977). When the Fe(III) gel was introduced into the $FeSO_4$ solution, the equilibrium of the gel surface was upset by its new environment. In the near vicinity of the gel surface, OH^- and SO_4^{2-} anions were attracted towards the positively charged surface. The OH^- anions neutralise the surface at the sites of positive charge and the SO_4^{2-} anions probably become specifically adsorbed (Schwertmann & Taylor,1977). The relative amounts of OH^- and SO_4^{2-} anions

removed from solution was not determined, but it is assumed that the amount of SO_4^{2-} anions removed was significant. However, Appendix A does give a very good indication of the amount of SO_4^{2-} anions incorporated into the final precipitate - e.g. for sample GR1 (= Green Rust A), this was 18.5 % by weight of the sample (not forgetting that the samples are usually made up of two phases). Occurring simultaneously with and/or immediately after the removal of the above anions, Fe^{2+} cations were both preferentially adsorbed by displacing H^+ ions from the surface and, also, specifically adsorbed at surface sites which have become negatively charged (due to desorption of H^+ ions by OH^- ions). Since the surface area of the gel was large, the amount of ions removed from solution by the initial adsorption was probably also large. In particular, the rapid depletion of OH^- anions results in a rapid decrease in pH.

Evidence for the adsorption of ions by the Fe(III) gel at this early stage in the synthesis process comes from sample S7-2-83, which, as already mentioned, was produced from a synthesis when no alkali was added to maintain pH at 7. Mossbauer and IR spectra clearly show that both SO_4^{2-} and Fe^{2+} ions were taken onto the gel (see Figs 5.17 and 5.24). In addition, AAS shows that Fe^{2+} cations were removed in a considerable quantity (see Appendix B). Thus, it is quite clear that, before

alkali was added to maintain pH, Fe^{2+} and SO_4^{2-} ions were adsorbed by the gel surface. The amounts removed from solution probably follow an exponential growth curve with a fixed upper limit which depends upon the concentration of $FeSO_4$ and the amount of Fe(III) gel.

When alkali was subsequently added to maintain pH at 7, hydrolysis of the surface-adsorbed Fe^{2+} cations probably occurs which would explain the subsequent drop in pH. In the syntheses which produce a GR phase (i.e. when $[FeSO_4]_i \geq 0.025$ M and $1 \leq IFFR \leq 40$), this probably leads to the precipitation of basic $FeSO_4$, or a substance very similar to basic $FeSO_4$, onto the gel surface before the GR phase proper is formed. This is a reasonable assumption since (i) it is generally known from chemistry textbooks that basic Fe(II) salts can be obtained from the partial precipitation of Fe(II) solutions, and (ii) many previous works have either referred to or shown the existence of such compounds as intermediaries in the thermodynamic transition of Fe in the II oxidation state to the III oxidation state (Bernal et al., 1959; Evans, 1967; Misawa et al., 1973 & 1974; Murray, 1979; Schwertmann & Taylor, 1977). As mentioned previously in Chapter 5, basic $FeSO_4$ has a general chemical formula of $Fe(OH)_2.xFeSO_4$, where x is a variable. However, the NaOH consumption data shows that only ~ 1 mmole of

NaOH was used for every two mmoles of Fe(II) present in the GR phase, indicating a formula of $FeOH.xFeSO_4$. The extra OH group required for charge balance must probably come from the Fe(III) gel. For brevity, the term "basic $FeSO_4$" would be used from this point on to denote basic $FeSO_4$ and any closely related compounds.

Thus, basic $FeSO_4$ is probably a precursor phase of sulphate Fe-GR. This would explain the great similarity between the Mb Fe(II) QS of basic $FeSO_4$ and that of the sulphate Fe-GRs. Indeed, the Mb spectra of the latter may be considered as composed of a basic $FeSO_4$ component superimposed onto an Fe(III) gel component plus an Fe(III) MHS. Since sulphate Fe-GR is a bit more stable to oxidation than basic $FeSO_4$, the Fe(III) gel probably serves as a stabilising template for the latter. The reason why basic $FeSO_4$ and not, say, $Fe(OH)_2$ was preferentially precipitated is probably because this is the phase that has the lowest solubility at pH 7 and $[FeSO_4]_I \geq 0.025$ M. Pure $Fe(OH)_2$ is usually obtained at pH > 8 for this concentration of Fe(II) (Millward, private comm.).

[Incidentally, as noted in the experimental chapter, a small amount of precipitate (estimated to be 1-2% by weight of total Fe(II)) was produced in taking the fresh $FeSO_4$ solution up to pH 7. This precipitate was

probably basic $FeSO_4$. Since alkali consumption was directly related to the formation of GR, and since the specific NaOH consumption was constant with IFFR, the small quantity of precipitate present initially does not affect the end result of the synthesis. However, it is probably amongst the first material to be adsorbed onto the gel surface.]

Evidence for the precipitation of basic $FeSO_4$ comes from the Mb spectra of some of the GR samples. The wet precipitate also gave Mb lines which were consistent with those of $FeSO_4$ (e.g. for sample GR16, QS = 3.34 $\pm$ 0.05 mms^{-1} for this component at 77 K). In addition, many of the GR samples (and also those derived from 0.05 M $FeSO_4$) gave an X-ray line at ~ 8.8 A which can be attributed to the presence of $FeSO_4$ groups - materials with a substantial $FeSO_4$ component have a similarly-placed X-ray reflection e.g. Fe hydrogen sulphate hydrate, $Fe(SO_4)_3.H_2SO_4.8H_2O$. In the results chapter, it was speculated that the presence of this X-ray line in the sulphate Fe-GRs was due to an imperfect or distorted GRII structure. It may be that this is the case and that the basic $FeSO_4$ precipitate is sometimes too difficult to rearrange to obtain the normal crystal structure associated with GRII. It could, however, be equally the line arising from degraded GRI material - sample GR21 does not have the

low-angle reflection at ~ 10.9 A but has a line at 7.9 A as its basal line. On partial oxidation, the basal line increases to ~ 8.1 A. The Mb spectra does not show up the differences in basal d-spacings (the Fe(II) QS at 77 K for sample GR21 is identical to that for the other samples). Thus MbS shows that the $FeSO_4$ environment is the same regardless of whether the crystal structure is that of GRI or GRII.

In all of the 77 K Mb spectra of the wet precipitate for the sulphate Fe-GRs, there was no sign of any $Fe(OH)_2$ component, and this reinforces the premise that, initially, basic $FeSO_4$ was precipitated onto the Fe(III) gel surface.

So far, it has been stated that alkali addition to maintain pH at 7 probably results in the hydrolysis of the surface-adsorbed Fe^{2+} cations. However, this does not necessarily mean that all the Fe^{2+} cations were hydrolysed and subsequently used in the formation of the GR phase. The titration data shows that the specific alkali consumption was constant with IFFR at a value of approximately 1 mmole per mmole of Fe(III) gel. Since the control synthesis experiment (which produced sample S7-2-83) showed that alkali consumption was directly related to the formation of a sulphate GR phase, then this alkali consumption must result in a stoichiometric amount of Fe(II) being hydrolysed. Mossbauer spectroscopy

showed that, for the wet,fresh precipitates derived from the 0.1 M $FeSO_4$ system, the GR phase have FFR values in the range 0.9-2.5, depending upon IFFR. This indicates that 0.9-2.5 mmoles Fe(II) was hydrolysed by every mmole of alkali used. However, the AAS data shows that the specific Fe(II) removal increases with IFFR (or decreases with <Fe(III)>) - at IFFR = 40, it was very large, ~ 19 $mmole.mmole^{-1}$. This is not too surprising if it is assumed that the specific surface area was more or less constant, and so as <Fe(III)> decreases the amount of Fe(II) cations in solution per mmole of Fe(III) gel increases, and thus the specific Fe(II) removal also increases. Thus, at high values of IFFR, the amount of Fe(II) removed from solution exceeded greatly the quantity hydrolysed by the alkali. Therefore, there must be an excess amount of Fe(II) material which was not hydrolysed directly by the alkali consumption. This excess Fe(II) material obviously decreases as IFFR decreases e.g. at IFFR = 1 (sample GR20), specific Fe(II) removal was ~ 1.0 $mmole.mmole^{-1}$ and the Mb FFR was 0.9 for the wet, fresh precipitate. Since Mossbauer spectroscopy does not show up this excess Fe(II) material in the final precipitate, it must mean that they have been oxidised somehow during synthesis. Samples S7-2-83 and S21-3-83 show that the Fe(III) MHS was a result of the direct conversion of the gel itself and, in the process, any adsorbed Fe^{2+} cations are oxidised and probably incorporated into the structure. But as the

Fe(III) MHS is relatively small in the wet, fresh precipitates of most GR samples, only a small proportion of the excess Fe(II) removal can be accounted in this way. Most of the excess Fe(II) removal must reside in the GR phase. To account for the observed Mossbauer FFR values, the excess Fe(II) material must be partially oxidised through some unknown mechanism to give overall FFRs in the range 0.9-2.5. To recap: since alkali consumption does not match the Fe(II) removal, it must be concluded that only part of the surface-adsorbed Fe(II) material was hydrolysed at any given time during synthesis. The rest must be incorporated eventually into the final precipitate by some sort of structural rearrangement.

Thus the Fe(II) material taken up by the Fe(III) gel has three pathways: (i) it is utilised in the formation of the sulphate GR phase, (ii) it is utilised in the formation of the goethite phase, being oxidised in the process and (iii) it migrates into the gel bulk and becomes incorporated into the Fe(III) gel structure, being partially oxidised in the process. The amounts used in each case will, of course, depend on the initial conditions. The oxidation of the Fe(II) material in (ii) and (iii) by the Fe(III) gel is probably akin to the autocatalytic oxidation of Fe(II) solutions by Fe(III) oxide surfaces under oxic conditions (Sung & Morgan, 1980). The oxidation probably involves a charge-transfer

mechanism since this has been shown to occur in this type of synthesis (Cuttler, private comm.). Since the syntheses here were performed under anoxic conditions, the excess charge may be taken up by the surrounding water molecules via an agent such as the hydrated electron or perhaps SO_4^{2-} anions themselves. In point (iii) it is difficult to explain how a charge-transfer mechanism would partially oxidised the Fe(II) material so that the observed Mb FFRs are in the range 0.9-2.5. Another possibility is that the incorporated Fe(II) cations cannot be detected by MbS at 77 K because their recoil-free fraction becomes too small for MbS to be useful. However, this possibility seems unlikely given that frozen solutions produce more than adequate Mb spectra, and the Fe(II) caticns here are probably bonded to the gel atoms. In any case, sample S7-2-83 shows the presence of Fe(II) cations in its Mb spectrum.

For non-GR samples, such as S7-2-83 and S21-3-83, the Fe(II) material taken up becomes completely oxidised (and presumably fully incorporated) on ageing overnight (N.B. this is under anoxic conditions). These are samples where the wet, fresh precipitates do not have any GR material at all. When a GR phase was produced, obviously those Fe(II) cations which become part of the GR structure do not become oxidised. However, even when there was a great excess of Fe(II) material taken up (e.g. sample GR16),

there was no complete oxidation of the excess Fe(II) cations on ageing overnight. Thus, somehow, assuming that the recoil-free fraction was not reduced for the Fe(II) cations, the formation of a GR phase prevents the complete oxidation of the excess Fe(II) material. How this is brought about can only be speculated upon. Assuming a charge-transfer mechanism via the SO_4^{2-} anion, the sulphate GR phase may use the SO_4^{2-} anion to bridge to adjoining parts of the Fe(III) gel structure, and so inadvertently prevent the excess charge from entering solution.

As mentioned above, one of the pathways for the adsorbed Fe(II) cations leads to the formation of goethite. Since the formation of this goethite material was rather rapid in comparison with the usual goethites formed from Fe(III) sources (the precipitate had very good crystallinity in a matter of hours instead of days or even weeks), and as goethite was not produced in the $FeCl_2$ system (nor in the $Fe(HCO_3)_2$ system), there is a strong suggestion that the SO_4^{2-} anions are the agents which cause the formation of the goethite phase. The SO_4^{2-} anions are also different from the Cl^- anions in that they are specifically adsorbed by the Fe(III) gel surface. This is probably an important factor in initiating the conversion of the gel to goethite. They probably do this by co-ordinating the Fe(III) cations in

the gel with hydroxylated Fe(II) cations adsorbed on or near the surface in an octahedral configuration. Charge-transfer probably takes place through the co-ordinating SO_4^{2-} anions, leading to the oxidation of the Fe(II) cations. The excess charge may be removed by the surrounding solution via the hydrated electron, H_2O^-. The goethite so formed contains sulphate groups and thus is chemically different from the usual variety. Samples S7-2-83 and S21-3-83 are examples of this type of goethite. Since SO_4^{2-} anions are involved in forming both the goethite and sulphate GR phases, and by the nature of the hydrolysis-precipitation reaction, the two phases are probably structurally related in the overall matrix. In fact, electron micrographs taken of the wet; fresh precipitate of sulphate GR sample GR14 (IFFR = 20) show that goethite crystals were imbedded in larger hexagonal crystals of sulphate GR (Plates 1 & 2). This suggests that the goethite crystals either formed and grew within the larger GR crystals or else formed outside and then later envelopped by the growing GR crystals. The corresponding electron micrographs for sample GR20 (IFFR = 1) do not show any goethite crystals within the larger GR crystals (Plates 3 & 4), and confirms the 77 K Mb data i.e. that the wet, fresh precipitate contains little or no goethite component.

Further evidence that the goethite and GR phases are

Plate 1 Electron micrograph of the wet, fresh precipitate of sulphate Fe-GR sample GR14 (IFFR = 20).
Magnification: X 16000

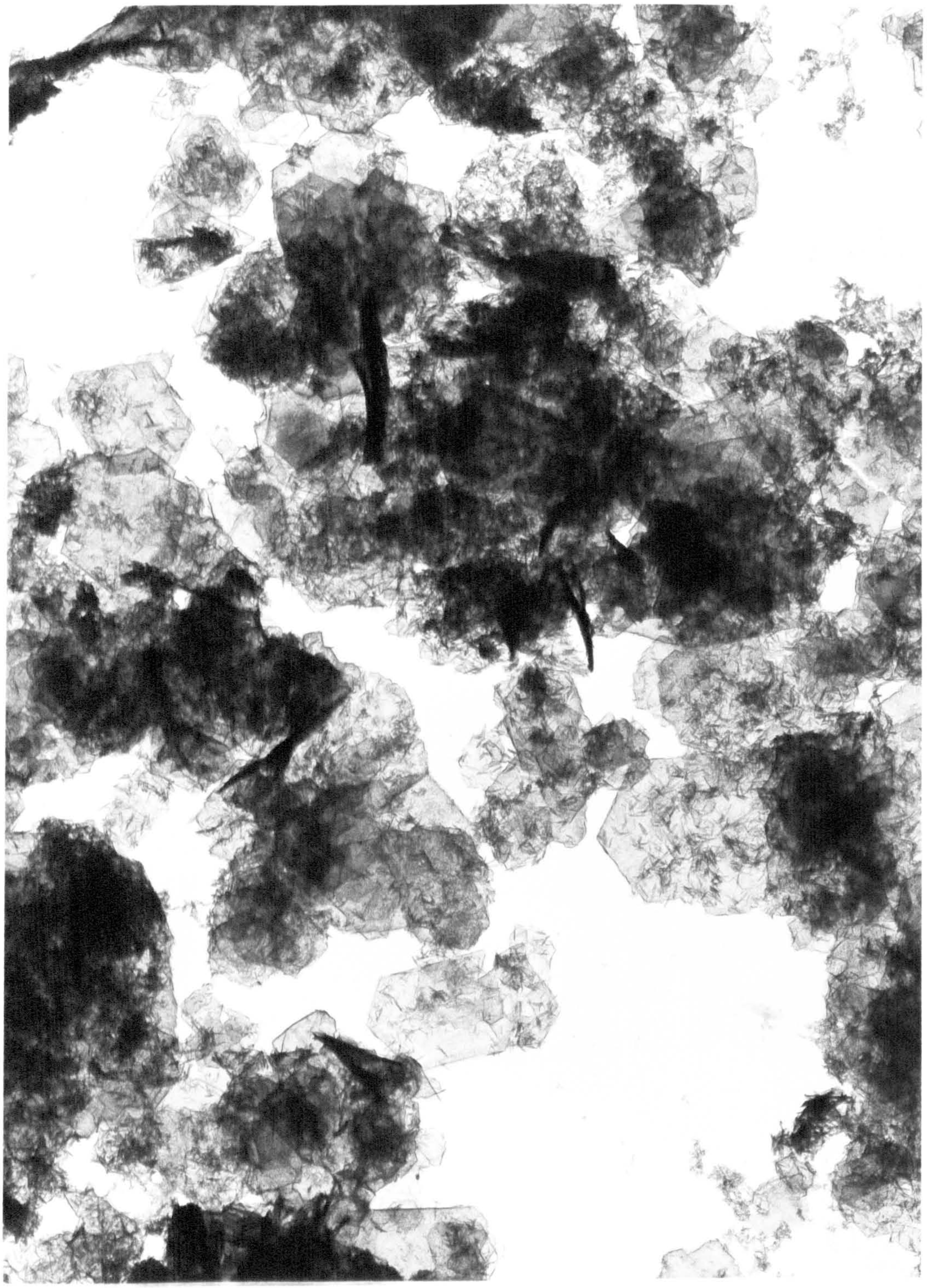

Plate 2 Electron micrograph of the wet, fresh precipitate of sulphate Fe-GR sample GR14 (IFFR = 20). Magnification: X 74000

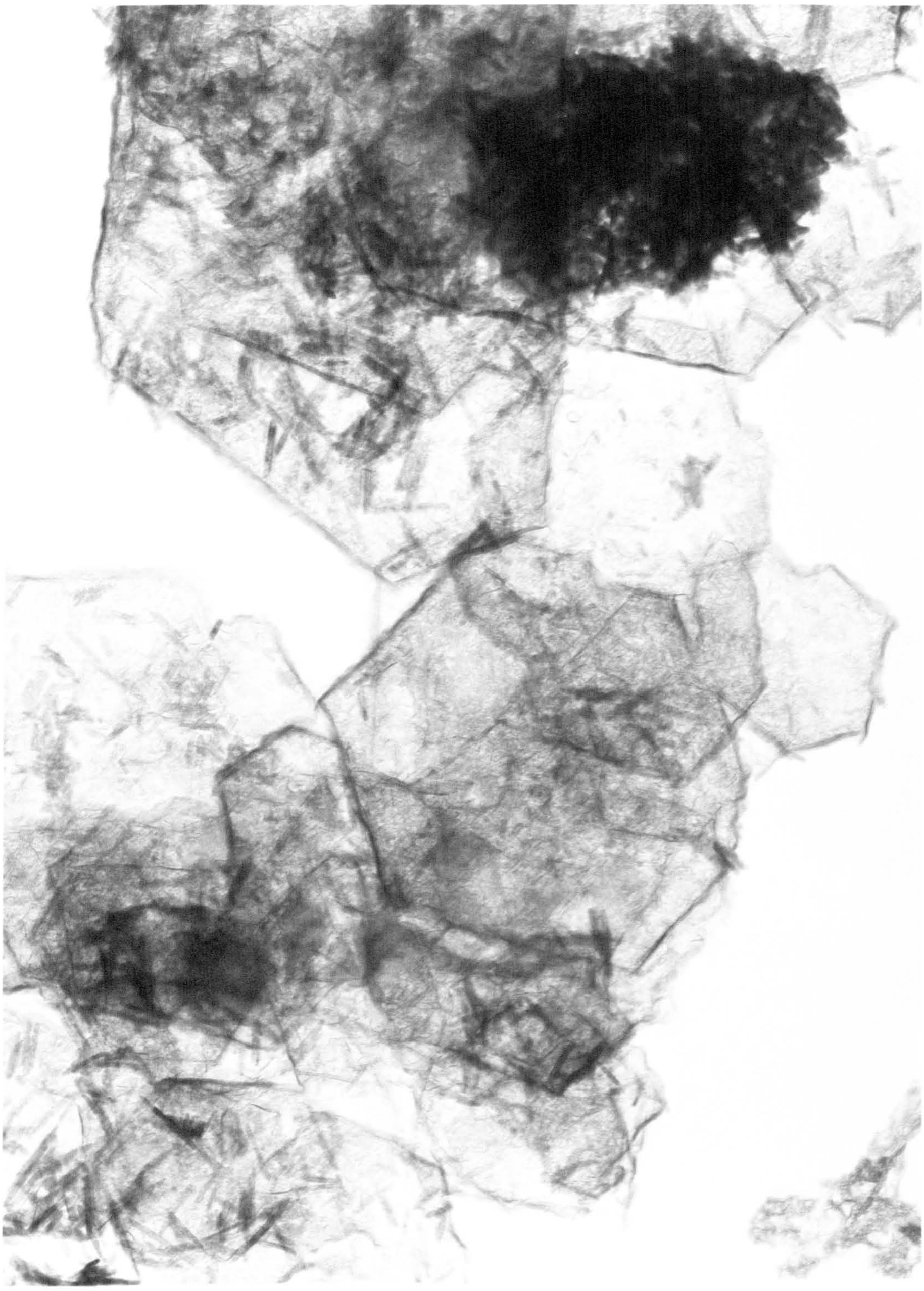

Plate 3 Electron micrograph of the wet, fresh precipitate of sulphate Fe-GR sample GR20 (IFFR = 1).
Magnification: X 16000

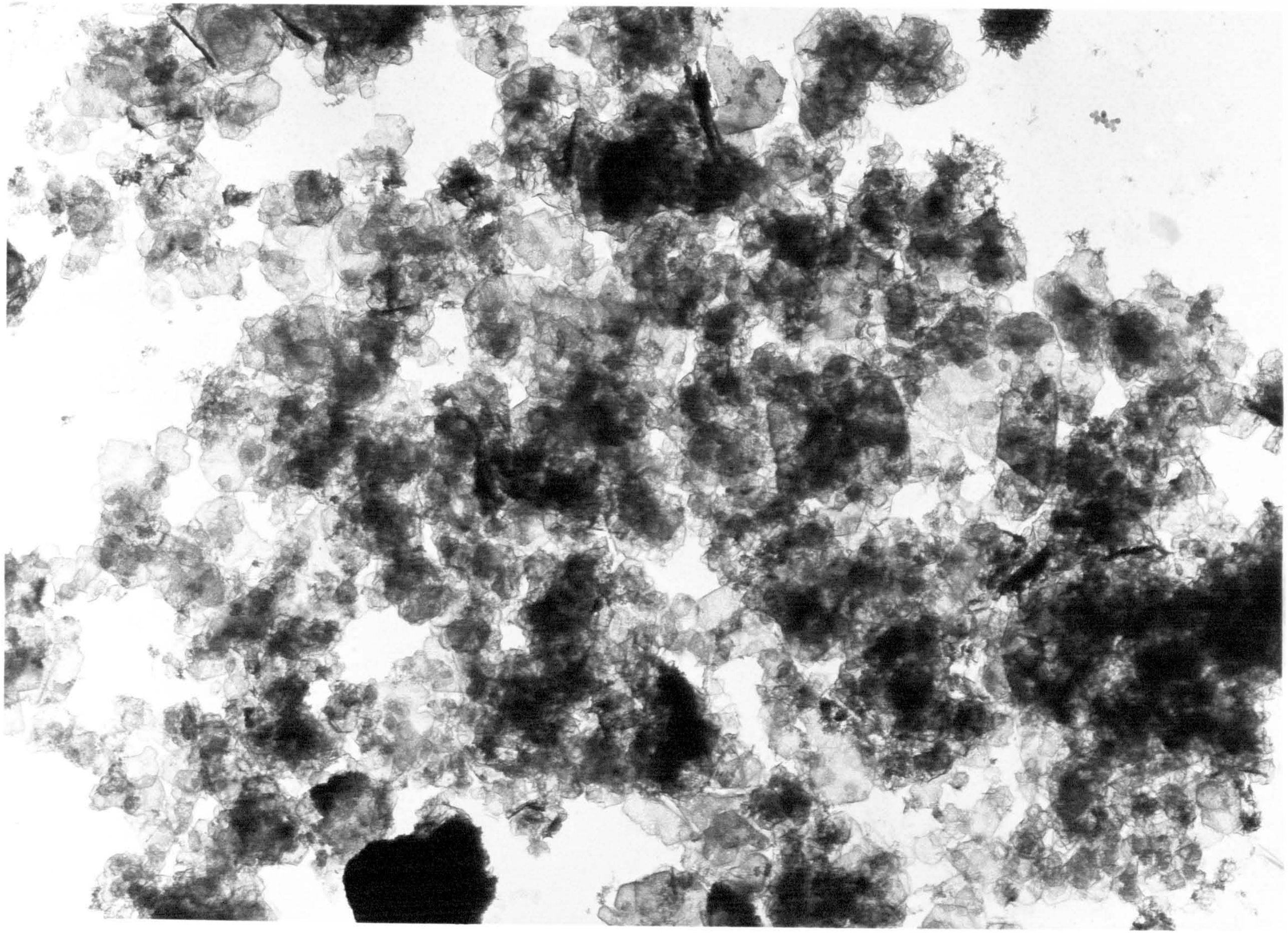

Plate 4 Electron micrograph of the wet, fresh precipitate of sulphate Fe-GR sample GR20 (IFFR = 1).
Magnification: X 74000

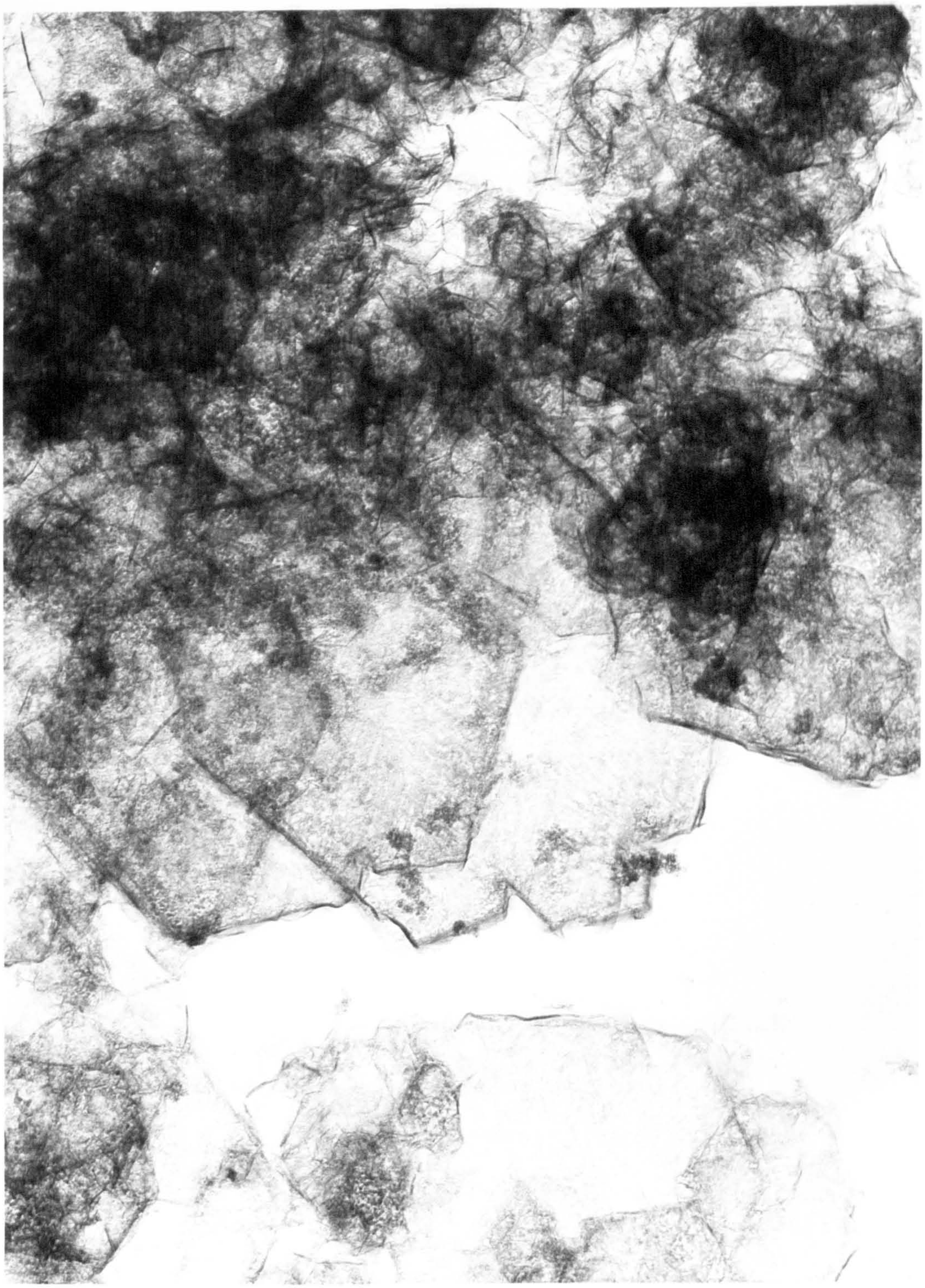

probably structurally related comes from the data on the oxidation products. Under both dry and wet oxidation conditions, the GR samples converted into a mixture of degraded GR material and goethite, with the latter the predominant component. In particular, infrared spectroscopy showed that dry oxidation results in reduced sulphate absorption peaks and less well-defined goethite absorption peaks. This indicates a deterioration in crystallinity of the goethite component, which can only be explained if the goethite phase was structurally intermixed with the GR phase. That is, when the Fe(II) cations in the latter oxidises, the subsequent change in bond lengths also distorts the bondings in the goethite structure to some degree. The above observation was not seen in the chloride Fe-GR samples, which do not have two phases present in the precipitate. In addition, the surface area measurements show that the GR samples, derived from 0.1 M $FeSO_4$, were remarkably consistent in terms of both surface area (40-65 m^2g^{-1}) and pore sizes (30-400 A diameter). This indicates that the GR and goethite phases were part of a well-defined matrix.

The fact that there are two types of sulphate groups in the GR samples (i.e. one type belonging to the GR phase and the other to the goethite phase) is indicated by the non-GR sample, S23-3-83, which actually contained a small amount of GR. The X-ray diffractogram for this sample

gave an X-ray reflection at 8.4 A which did not occur for the other non-GR samples (S7-2-83 & S21-3-83). From what has been said before, this X-ray line must be associated with the sulphate groups present in the GR phase.

So far, it can be seen that, for the syntheses which produced GR samples, the adsorption-hydrolysis reaction initiates two reactions, or rather two half-reactions in the light of equation 6.1. One leads to the formation of sulphate GR while the other gives rise to the formation of goethite. The rate of these half-reactions depends upon the surface area of the Fe(III) gel (which in turn depends on <Fe(III)>) and the concentration of the $FeSO_4$ solution. Since the half-reactions were surface area dependent, then the early stages of the synthesis would be faster as the number of ions adsorbed would be greater. As the synthesis progressed, less adsorption sites are available and so the half-reactions become progressively reduced. Hence the alkali consumption would also become gradually less with time.

Once the adsorption-hydrolysis reaction initiates the formation of the sulphate GR and goethite phases, the next stage probably involves consolidation and accommodation as the two phases come together. In the case of the GR phase, there would be rearrangement and restructuring of the precursor material (i.e. basic $FeSO_4$ and the Fe(III) gel component) to form the GR

crystal structure prior to this stage. To obtain the pyroaurite structure (Taylor, 1973), the Fe(III) gel component must rearrange to form brucite-like sheets with the SO_4^{2-} anions bridging the sheets. Support for the formation of brucite-like layers comes from the electron micrographs of samples GR14 & 20 (Plates 1-4). These clearly show that the hexagonal sulphate GR crystals are arranged in layers on top of each other, and must reflect the internal structural arrangement. In addition, according to the de Boer classification (de Boer, 1958), the hysteresis loops of the N_2 adsorption isotherms obtained for the sulphate GR samples may be associated with the spaces between parallel plates. This is precisely the situation shown by the electron micrographs. The consolidation and accommodation stage can be best described as a crystal growth stage in which the GR and goethite phases enlarge from their respective centres of formation.

As mentioned at the start of this section, the relative amounts of the products formed in equation 6.1 would depend on the initial conditions, $[FeSO_4]_i$ and IFFR. Since the former was usually constant at 0.1 M, the relative amount would depend on IFFR alone. For the wet, fresh precipitate, only a GR component was formed when IFFR = 1. At higher values of IFFR, the amount of goethite produced was quite substantial. However, there does not appear to be any trend with increasing IFFR.

On ageing overnight, there seems to be an unusual behaviour. At low values of IFFR the amount of goethite produced increases, while at high values of IFFR the amount of goethite actually decreases (the latter effect was demonstrated most dramatically in sample GR15, where the goethite component disappears virtually completely on ageing overnight). Corresponding to this pattern are the changes in the Mb FFR values. At low IFFR the Mb FFR values increases slightly on ageing overnight, while at high IFFR it decreases slightly. These anomalous behaviour patterns can be explain as follows. At low IFFR, the specific Fe(II) removal was also low and so virtually all the adsorbed Fe(II) cations were hydrolysed to form GR. There was little or no chance for any goethite material being formed. However, as <Fe(III)> was great, a large part of the gel would convert to goethite on ageing overnight (probably brought about by the penetration of the SO_4^{2-} anions into the gel bulk). This would result in the Mb FFR increasing (e.g for sample GR20, FFR increases from 0.9 to 1.5). At high IFFR, the specific Fe(II) removal was very high which would mean that there was a large excess of Fe(II) cations adsorbed. These would be oxidised and used to convert the Fe(III) gel into goethite. Thus the fresh precipitate would have a relatively large amount of goethite present. In fact, the large excess of Fe(II) cations results in less Fe(III) gel surface being

available for the formation of the sulphate GR phase. An alternative way of looking at this situation, is to say that the half-reaction producing the goethite phase was dominant over the other half-reaction producing the GR phase. Therefore, on ageing overnight, some of the goethite material would actually be used as a stabilising template by the GR component as the reaction mixture readjusts to the ageing conditions (once the synthesis had been completed, alkali was no longer added to maintain pH and the final precipitate was allowed to settle sealed in a containing vessel under N_2). This would probably disrupt the magnetic coupling in the goethite that was being used in his manner, and so reduce the MHS accordingly. The regained Fe(III) material would thus be observed by MbS as the Fe(III) gel part of the GR component. Therefore, the Mb FFR would decrease as well. From the preceding discussion, it is clear that the formation of sulphate GR can make use of a goethite as well as a Fe(III) gel surface.

To summarise the synthesis process in the $FeSO_4$ system: after the Fe(III) gel is added to the $FeSO_4$ solution, adsorption of Fe^{2+} and SO_4^{2-} ions occurs at the gel surface. The addition of alkali to maintain pH at 7 initiates the half-reactions represented in equation 6.1 at the gel surface, namely the formation of sulphate GR through a basic $FeSO_4$ precursor, and the formation of goethite with sulphate anions as the

co-ordinating groups. Equation 6.1 does not account adequately for all the Fe(II) cations taken up by the Fe(III) gel, unless it is assumed that the excess quantity is incorporated into the gel part of the GR phase in a partially oxidised form. Once the half-reactions are initiated, they will compete with each other, and their relative rates would depend on the starting conditions. The rate at which sulphate GR formation occurs is probably constant since this is pH dependent, and would explain why the specific alkali consumption was constant. Thus the only variable factor is the formation of the goethite phase and this probably depends on the amount of Fe(III) gel and hence on the surface area of the gel. The half-reactions would continue until all the available Fe^{2+} and SO_4^{2-} ions adsorbed onto the gel surface are used up. At this point (anything up to 6 h or more), little or no more alkali would be required and so the synthesis would be at a thermodynamic endpoint. The precipitate produced by the half-reactions at different adsorption sites would then build up until they interconnect to form larger aggregates. This would be analogous to the crystallisation of solutions by seeding. To form the pyroaurite structure, the Fe(III) gel component in the GR phase must rearrange to form brucite-like sheets containing the Fe^{2+} and SO_4^{2-} ions, and with the sheets bridged by SO_4^{2-} anions. The overall result here would be

a matrix containing both sulphate GR and goethite phases (see Plates 1 & 2).

6.2.2 The $FeCl_2$ System

The titration and AAS data for the syntheses carried out under the $FeCl_2$ system show that the formation of chloride~ Fe-GRs follow a similar pattern to the formation of the sulphate Fe-GRs. This is not surprising in view of the fact that the method of synthesis was identical in both cases. Thus most of the general interpretation and comments presented for the $FeSO_4$ system in section 6.2.1 also applies to the $FeCl_2$ system. In particular, the adsorption-hydrolysis model put forward as the mechanism which initiates the formation of the GR precipitate is also valid (apart from specific details such as anion-type). In this section, only the important differences between the $FeCl_2$ and $FeSO_4$ systems will be highlighted.

Since non-GR samples were also produced from the $FeCl_2$ system, the formation of precipitates can be best described by the following equations:

$$FeCl_2\ (aq.) + Fe(III)\ gel\ (sol.) \xrightarrow[P(O_2)->0]{pH=7} Cl\ GR\ (sol.) \qquad (IFFR \geq 6) \quad -6.2$$

$$FeCl_2\ (aq.) + Fe(III)\ gel\ (sol.) \xrightarrow[P(O_2)\to 0]{pH=7} [Cl\ GR\ (sol.)] + magnetite\ (sol.)$$

$$(IFFR \leq 4) \quad -6.3a$$

The initial conditions used were: (i) $[FeCl_2]_t$ = 0.1 M and (ii) $1 \leq IFFR \leq 40$.

In equation 6.3a, the chloride Fe-GR component is enclosed in square brackets to show that it was a very transitory phase. On ageing overnight it disappears completely (it probably takes less time than this). In fact, at IFFR = 1, the fresh precipitate did not contain any GR component at all (sample S14-11-83). Therefore,it may be better to simplify equation 6.3a to give:

$$FeCl_2\ (aq.) + Fe(III)\ gel\ (sol.) \xrightarrow[P(O_2)\to 0]{pH=7} magnetite\ (sol.)$$

$$(IFFR \leq 4) \quad -6.3b$$

It can be seen from the equations that non-GR samples were produced at IFFR $\leq$ 4 while chloride Fe-GR samples were formed at IFFR $\geq$ 6. This is in contrast to the $FeSO_4$ system, in which a stable GR phase was formed throughout an identical range of IFFR values, and at the same concentration of Fe(II) (i.e 0.1 M). However, the chloride Fe-GR samples produced were pure precipitates in that they were single-phase material. In contrast, the

sulphate Fe-GR samples produced from the 0.1 M $FeSO_4$ system nearly always contain a contaminating phase (i.e. goethite).

The significant difference between the $FeCl_2$ and $FeSO_4$ systems is obviously the difference in the anion-type. As stated in section 6.2.1, it is probably the presence of SO_4^{2-} anions which results in the formation of goethite in the $FeSO_4$ system. Conversely, in the $FeCl_2$ system, it is probably the presence of Cl^- anions which results in the formation of magnetite. This difference in anion-type would also account for the greater instability of the chloride Fe-GRs to oxidation. (Chloride anions are smaller and more electronegative than the SO_4^{2-} anions.) In addition, the difference in anion-type probably makes the chloride Fe-GR samples poorer in crystallinity (as shown by all the analytical techniques), and having larger surface areas (60-100 m^2g^{-1}). In fact, the poor crystallinity of the chloride Fe-GR samples is confirmed by an electron micrograph of the wet, fresh precipitate of sample GR18 (IFFR = 20). The amorphous nature of the material is shown clearly by the electron micrograph (Plate 5). The difference in anion-type would also affect the short-range interactions between the Fe atoms and results in poorer short-range ordering for the chloride Fe-GRs, as shown quite clearly in the 4.2 K Mb spectra of both

Plate 5 Electron micrograph of the wet, fresh precipitate of chloride Fe-GR sample GR18 (IFFR =20).

Magnification: X 5500

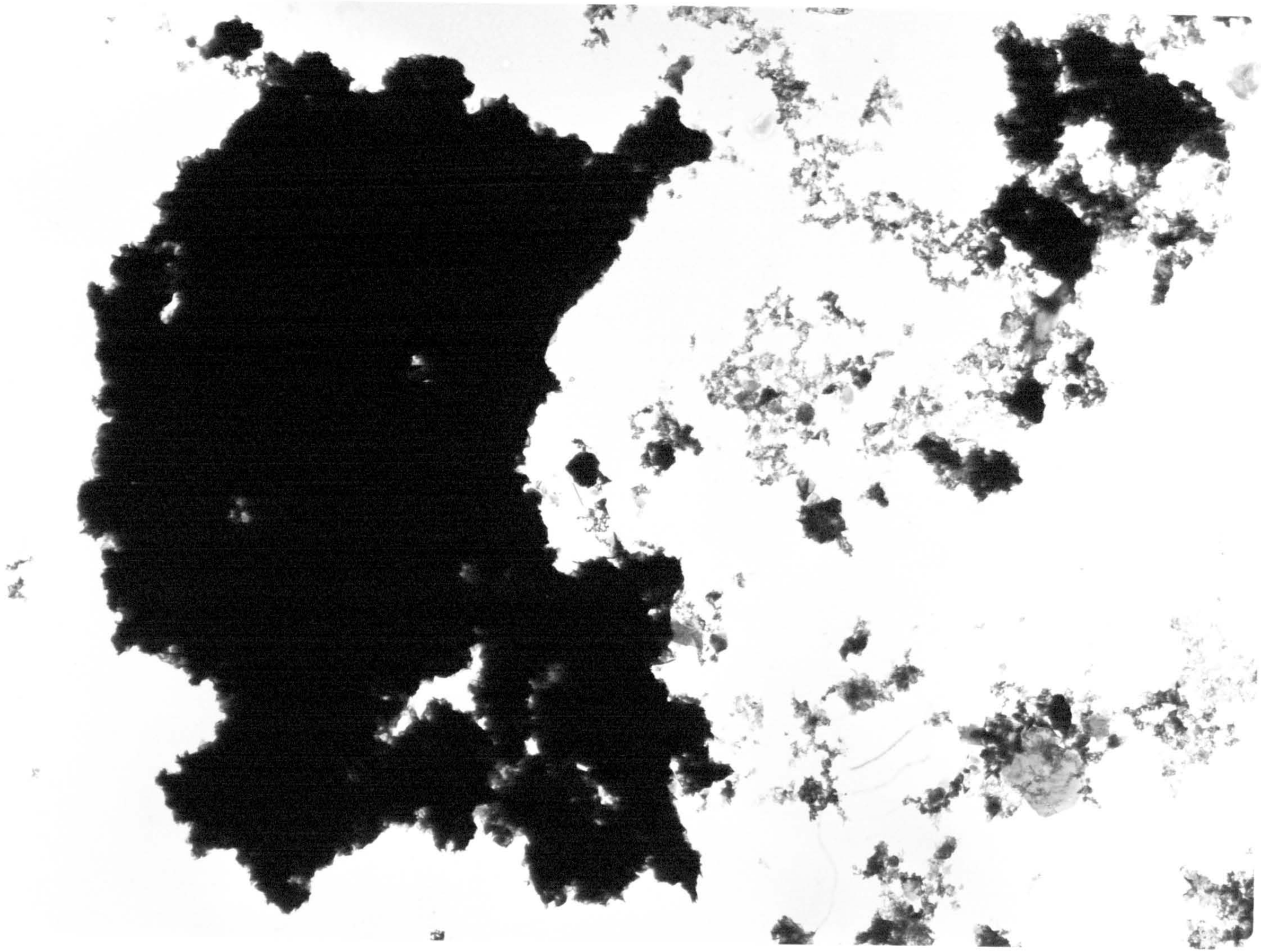

types of Fe-GRs (see Figs 5.28 & 5.54).

The non-GR samples show that any chloride Fe-GR phase, present initially, converts to magnetite very rapidly on ageing under wet, anoxic conditions. Also, a dried sample of chloride Fe-GR sample GR11, which was stored in a sealed test-tube under N_2, was found to have converted almost totally to magnetite on examination a few months later. Under oxidising conditions, chloride Fe-GR converts either to akaganeite (dry oxidation) or lepidocrocite (wet oxidation). Thus there must be a large degree of fluidity in the crystal structure of chloride Fe-GR. In contrast, sulphate Fe-GRs almost invariably transform to goethite on oxidation and ageing. This again must be attributable to the difference in anion-type (chloride anions being more chemically active). Chloride anions were probably not specifically adsorbed onto the Fe(III) gel during the adsorption-hydrolysis stage of the synthesis, and so would have less of an influence on the final nature of the GR precipitate.

As with the sulphate Fe-GRs, adsorption of ions occur once the Fe(III) gel was introduced into the $FeCl_2$ solution. The Freundlich isothermal plot for the chloride GR samples (i.e. IFFR $\geq$ 6) give a straight line, showing that the uptake of Fe(II) cations was probably due to physical adsorption. It is assumed that that the hydrolysis of the Fe(II) cations on or near the gel

surface results in the precipitation of the basic salt i.e. basic $FeCl_2$. However, there was no direct evidence from any of the analytical techniques, even from Mossbauer spectroscopy. But there is a remarkable similarity between basic $FeCl_2$ and the chloride Fe-GRs in terms of their Mb parameters.

The specific alkali consumption for the chloride Fe-GRs increases with IFFR (IFFR being proportional to the inverse of <Fe(III)>, on which the titration and AAS data in section 5.2.2a are quoted against) and so is somewhat different to that for the sulphate Fe-GRs, which is constant with IFFR. At any given IFFR value, the amount of alkali used was approximately $\geq$ 2 mmole for every mmole of Fe(III) gel (cf. ~ 1 mmole.mmole^{-1} for the sulphate Fe-GRs). This would suggest a formula of $Fe(OH)_2.xFeCl_2$ for any basic $FeCl_2$ formed.
Since specific Fe(II) removal also increases with IFFR (but at a much greater rate - see Figs 5.36 & 5.37), it is clear that the increased specific alkali consumption was a direct result of the greater Fe(II) hydrolysis arising from the increased specific Fe(II) uptake. However, this increased hydrolysis does not account for all the extra Fe(II) cations uptaken onto the Fe(III) gel. Since the synthesis system used was similar to that for the sulphate Fe-GRs, it can be assumed that the excess Fe(II) uptake was incorporated into the final precipitate in a similar fashion i.e. incorporated into

the gel bulk and then partially oxidised so that the observed Mb FFR values are ~ 2:1. The fact that the specific Fe(II) removal at high IFFR values is less than the corresponding parameter for the sulphate Fe-GRs probably indicates a slightly different Fe(III) gel surface, probably as a consequence of the different Fe(III) source used in the preparation of the gel (see sections 4.2.1 & 4.2.2).

To recap: the formation of the chloride Fe-GRs under the conditions used in this study probably involve very similar mechanisms to the formation of the sulphate Fe-GRs. Any differences can be attributed to the difference in anion-type.

6.2.3 The Al-GRs

As with the Fe-GRs, the synthesis process involved in the formation of the Al-GRs can be written as:

$$Fe(II)\ (aq.) + Al(III)\ gel\ (sol.) \xrightarrow[P(O_2)\rightarrow 0]{pH=7} Al\text{-}GR\ (sol.) \quad -6.4$$

The initial conditions used were: (i) $[Fe(II)]_I$ = 0.1 M, in the form of $FeSO_4$ and $FeCl_2$ and (ii) $5 \leq IFAR \leq 20$.

However, because of the limited database available for this system, only a few meaningful comments can be drawn from the results.

In their work on Al-GRs, Taylor & McKenzie (1980) proposed that the formation of Al-GRs arose from a precipitation reaction between the soluble hydroxy species of Fe and Al. For this to happen, the Al(III) gel would have had to redissolve into solution and react with the hydroxylated Fe(II) cations at the gel-solution interface. The titration data for the Al-GR samples produced in this study does not support this model and, in conjunction with the AAS data, showed that the formation of the Al-GRs was very like that of the Fe-GRs. However, the Freundlich isotherm plotted for the Al-GRs showed that the removal of Fe(II) from solution was

probably not due to any adsorption process. But overall, the data is not sufficient by itself to prove or disprove the case for the Taylor & McKenzie model.

In terms of Mossbauer spectroscopy, there was virtually no distinguishing difference between the sulphate and chloride Al-GRs. Both types give an Fe(II) quadrupole doublet at 77 K. [Incidentally, there was little or no sign of any Fe(III) quadrupole component, and so confirms the reliability of the methods used to prevent the occurrence of oxidation during synthesis.] However, the two subgroups were readily distinguished by X-ray diffractometry, although the samples were not very crystalline. In the case of the chloride Al-GRs, the XRD results contradicted the surface area measurements somewhat - surface areas of 3-11 m^2g^{-1} were found, suggesting good crystallinity. However, this may be due to a peculiarity of Al oxides with regard to the adsorption of N_2 used in the BET method - Crosby (1982 & 1983) obtained a surface area of 6 m^2g^{-1} for a natural sample derived from an Fe(II) source but containing a significant amount of Al. In fact, electron micrographs (Plates 6 & 7) of each type of Al-GR show that the morphology is similar to that of many amorphous iron oxides, and so support the XRD data.

Plate 6 Electron micrograph of the wet, fresh precipitate of sulphate Al-GR sample GR22 (IFFR = 10). Magnification: X 5500

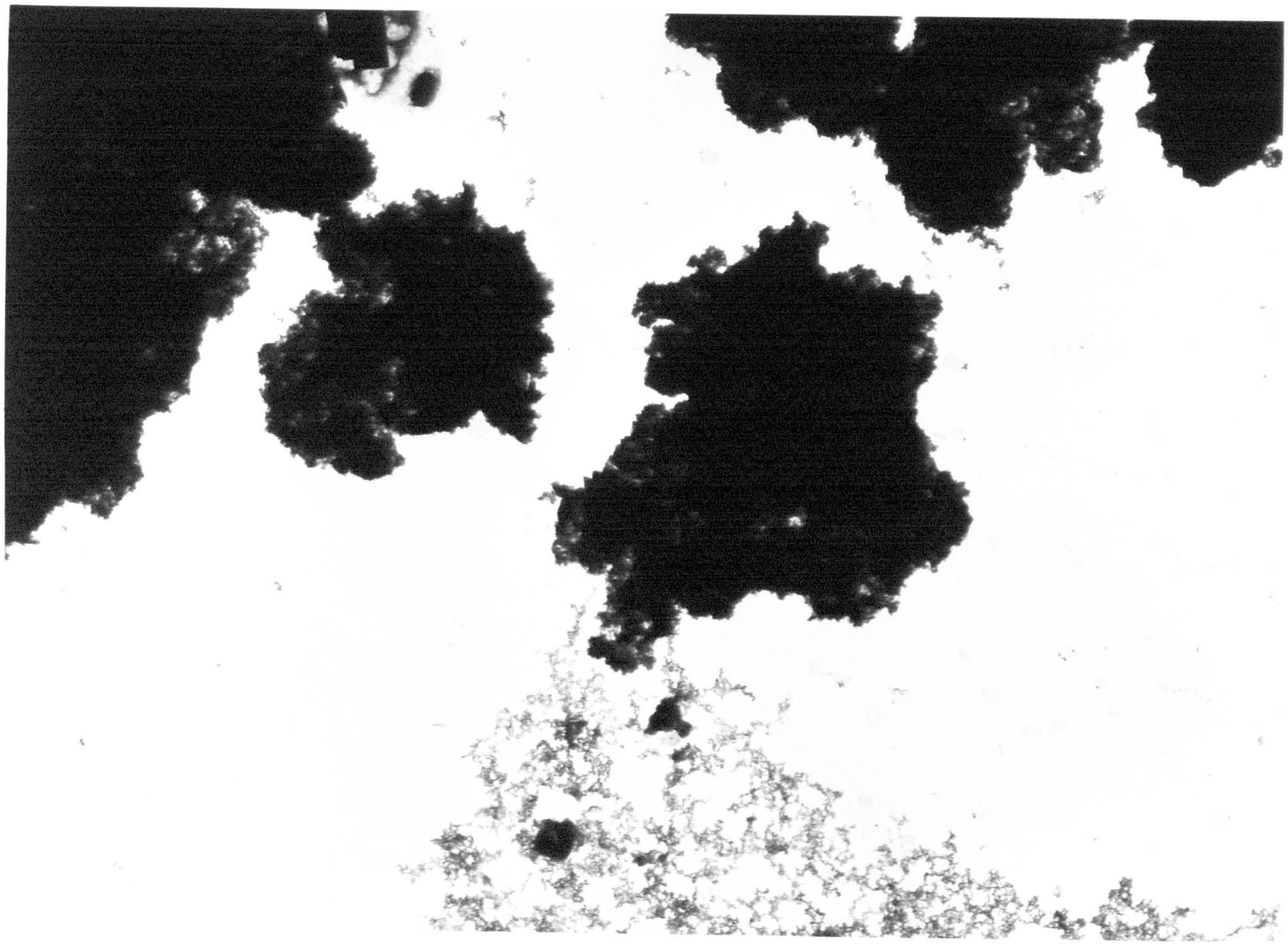

Plate 7 Electron micrograph of the wet, fresh precipitate of chloride Al-GR sample GR19 (IFFR = 20). Magnification: X 5500

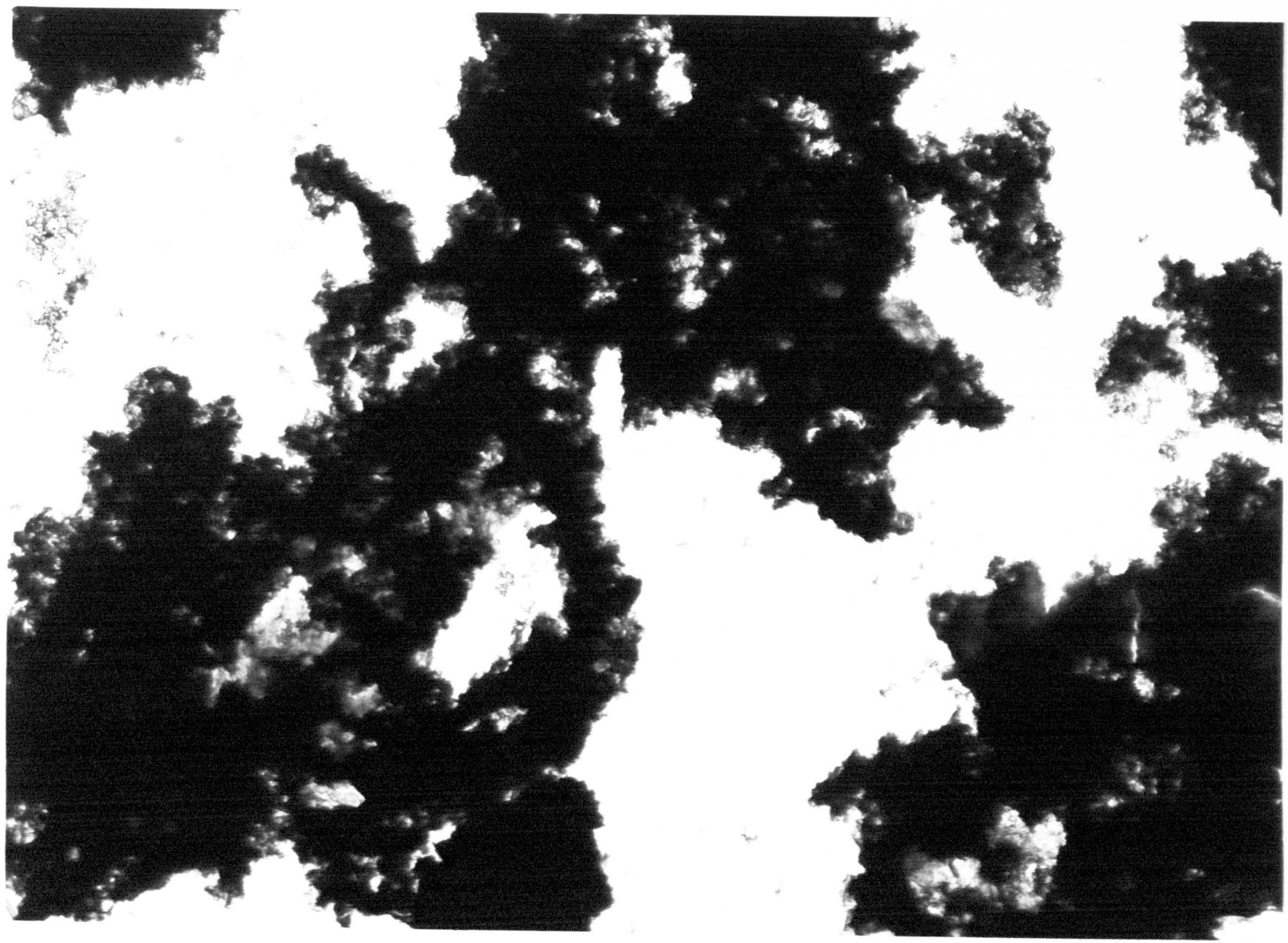

6.3 Conclusions

The work in this thesis has shown that Fe-GR compounds can be produced in a consistent fashion from Fe(II) solutions by the method of induced hydrolysis using Fe(III) gel at pH 7 and under anoxic conditions. A series of sulphate and chloride Fe-GR samples were synthesised, and characterised primarily by the analytical techniques of Mossbauer spectroscopy, X-ray diffractometry, infrared spectroscopy, and surface area measurements using the BET N_2 adsorption method. As far as was known at the time this work was carried out, the characterisation represents data on entirely novel materials and using techniques not considered before in the study of Green Rust compounds.

For diagnostic purposes, the most useful techniques have been X-ray diffractometry and Mossbauer spectroscopy. In fact, Mossbauer spectroscopy at 77 K and below was the only technique which could analyse the GR samples with little or no appreciable degree of oxidation occurring. This is an obvious advantage since the GR compounds are by nature very unstable to oxidation.

A few samples of the analogous Al-GR compounds were also synthesised but this did not add much insight into the nature and behaviour of the Fe-GRs.

The results in this thesis showed that the systems producing the Fe-GR compounds were of a highly complex nature, and that the amount of precipitate formed (if any) depended crucially on the starting conditions. For the 0.1 M $FeSO_4$ system, the GR formed was almost always accompanied by a goethite phase while, for the 0.1 M $FeCl_2$ system, pure GR material was only formed at IFFR $\geq$ 6. Any differences between the sulphate and chloride Fe-GRs can be attributed to the difference in anion-type.

The products of oxidation and ageing for the Fe-GRs indicate several transformation pathways, especially for the chloride Fe-GRs. Sulphate Fe-GRs converted to goethite on oxidation under both wet and dry conditions, while the chloride Fe-GRs converted to akaganeite on dry oxidation, and to lepidocrocite on wet oxidation. Under both wet and dry anoxic conditions, the chloride Fe-GRs converted to magnetite. In the case of the sulphate Fe-GRs, there was a suggestion that, under the right wet anoxic conditions, the material probably transformed into magnetite. These facts clearly demonstrate that the Fe-GRs are intermediaries in the thermodynamic transformation of Fe in the II oxidation state to Fe in the III oxidation state.

From what has been said already, the work in this thesis

may give more information on the rusting of iron and steel under poorly-oxygenated conditions (and the products formed), where Fe(II)-Fe(III) hydroxy compounds (i.e. GR-like) are known to be formed (Evans, 1967).

Although the initial Fe(II) concentrations used in the GR syntheses were at a much higher level than those normally encountered in the natural environment (e.g. sea floors and river estuaries), nevertheless under certain conditions the Fe(II) concentration may be high enough to enable GR or related compounds to be formed. This perhaps particularly applies to soil conditions where the concentration of Fe(II) in places can probably attain those used in this study. However, other factors such as pH and degree of oxygenation must also be right. Mossbauer spectra taken of a few samples of estuarine mud samples containing Fe suggest that compounds similar to the Fe-GRs or Al-GRs may have been formed. However, at this juncture in time, there is not sufficient data available. It would be interesting to see if GRs are formed at low concentrations of Fe(II) and, if so, how fast and how much.

In terms of anion-type, a few preliminary synthesis experiments showed that carbonate Fe-GRs were formed from iron(II) hydrogen carbonate [$Fe(HCO_3)_2$] solutions. The Mossbauer quadrupole splittings were of similar magnitude to those for the sulphate and chloride

Fe-GRs (at 77 K, the outer Fe(II) QS was ~ 2.88 ± 0.08 mms^{-1}). These preliminary syntheses indicate that many types of anion can be accommodated into the pyroaurite structure to form a GR compound, and has implications for the formation of GR compounds under a variety of natural conditions.

6.4 Further Work

The research work carried out in this thesis has made significant contributions to the documentation of the Fe-GR compounds. However, much remains to be done. Briefly, some of the more important extensions, relating to Fe-GR compounds and its synthesis, are as follows:

(i) to obtain a more complete study at $[Fe(II)]_i$ = 0.1 M, syntheses at the gaps in the IFFR values need to be undertaken in both the $FeSO_4$ and $FeCl_2$ systems.

(ii) to test the repeatability and reliability of the synthesis process, the syntheses already performed for both $FeSO_4$ and $FeCl_2$ systems at $[Fe(II)]_i$ = 0.1 M need to be repeated under the same initial conditions, at selected intervals of IFFR.

(iii) a series of syntheses (i.e. at different IFFR values) need to be carried out for a range of lower $[Fe(II)]_i$ values, particularly those approaching the levels in the natural environment.

(iv) time-dependent experiments, at various Fe(II) concentrations and IFFR values, to show the develcpment of the precipitates with time e.g. taking samples at

equal time intervals.

(v) radioisotopic tracer experiments to determine the fate of the excess Fe(II) cations uptaken by the Fe(III) gel i.e. whether they are in fact partially oxidised and incorporated into the gel structure.

(vi) further radioisotopic tracer experiments to confirm that charge-transfer does in fact occur during synthesis of the GRs in both $FeSO_4$ and $FeCl_2$ systems - to include control experiment in the Al system.

(vii) more control syntheses to show the type of precipitate produced when alkali is not added to maintain pH (as in sample S7-2-83).

(viii) syntheses using other anions e.g. CO_3^{-}, NO_3^{-}, I^{-}, Br^{-}, etc.

(ix) use of electron microscopy to study morphology of precipitates formed.

(x) more detailed and vigorous experiments on the products of oxidation and ageing.

(xi) complementary work on the Al-GR compounds and other possible GR compounds formed from suitable III state cations such as Mn^{3+} or Ni^{3+}.

(xii) work on other possible GR compounds derived from II state cations such as Mg^{2+} or Co^{2+}.

All in all, the above list represents a tremendous quantity of work which is required to be carried out, in order to well-document the Green Rust compounds. This is not surprising in view of the complex nature of the Fe(II)-Fe(III) system which has been revealed to some extent in this thesis.

REFERENCES

Allmann, R. (1968) "The crystal structure of pyroaurite." Acta. Cryst. B24, 972-977.

Annersten, H. & Hafner, S.S. (1973) "Vacancy distribution in synthetic spinels of the series Fe_3O_4-γ-Fe_2O_3." Z. Kristallogr. Bd. 137, 321-340.

Armstrong, R.J., Morrish, A.H. & Sawatsky, G.A. (1966) "Mossbauer study of ferric ions in the tetrahdral and octahedral sites of a spinel." Phys. Lett. 23, 414-415.

Bancroft, G.M. (1973) "Mossbauer Spectroscopy." McGraw-Hill Book Co., Maidenhead, UK.

Bando, Y., Kiyama, M., Yamamoto, N., Takada, T., Shinjo, T. & Takaki, H. (1965) "The magnetic properties of α-Fe_2O_3 fine particles." J. Phys. Soc. Japan 20, 2086.

Bannerjee, S.K., O'Reilly, W. & Johnson, C.E. (1967) "Mossbauer-effect measurements in FeTi spinels with local disorder." J. Appl. Phys. 38, 1289-1290.

Basta, E.Z. (1959) "Some mineralogical relationships in the system Fe_2O_3-Fe_3O_4 and the composition of titanomagnetite." Econ. Geol. 54, 698.

Bauman, L. (1976) "Introduction to Ore Deposits." Scottish Academic Press, Edinburgh.

Bauminger, R., Cohen, S.G., Marinov, A., Ofer, S. & Segal, E. (1961) "Study of the low-temperature transition in magnetite and the internal fields acting on iron nuclei in some spinel ferrites, using Mossbauer absorption." Phys. Rev. 122, 1447-1450.

Benjamin, M.M. (1983) "Adsorption and surface precipitation of metals on amorphous iron oxyhydroxide." Environ. Sci. Technol. 17, 686-696.

Bernal, J.D., Dasgupta, D.R. & Mackay, A.L. (1957) "Oriented transformations in iron oxides and hydroxides." Nature 180, 645-647.

Bernal, J.D., Dasgupta, D.R. & Mackay, A.L. (1959) "The oxides and hydroxides of iron and their structural inter-relationships." Clay Min. Bull. 4, 15-30.

Boekema, C., van der Woude, F. & Sawatsky, G.A. (1976) "A Mossbauer study of the conduction electron response in

doped magnetite." J. Phys. C (Sol. St. Phys.) 9, 2439-2448.

Bowen, H.J.M. (1966) "Trace Elements in Biochemistry." Academic Press, London.

Bowen, L.H. (1979) "Mossbauer spectroscopy of ferric oxide and hydroxides." Mossbauer Effect Ref. Data J. 2, 76-94.

Bowen, L.H. & Weed, S.B. (1981) "Mossbauer spectroscopic analysis of iron oxides in soil." in "Mossbauer Spectroscopy and its Chemical Applications." (eds. J.G. Stevens & G.K. Shenoy), Adv. Chem. Ser. 194, pp. 247-261.

Brauer, G. (1954) "Handbuch der Praparativen Anorganischen Chemie." F. Enke Verlag, Berlin, pp.1120.

Brindley, G.W. & Bish, D.L. (1976) "Green rust: a pyroaurite type structure." Nature 263, 353.

Brown, G. (1953) "The occurrence of lepidocrocite in some British soils." J. Soil Sci. 4, 220-228.

Brunauer, S., Deming, L.S., Deming, W.S. & Teller, E. (1940) "Theory of the van der Waals adsorption of gases." J. Am. Chem. Soc., 62, 1723-1732.

Brunauer, S., Emmett, P.H. & Teller, E. (1938) "Adsorption of gases in multimolecular layers." J. Am. Chem. Soc., 60, 309-319.

Carlson,L. & Schwertmann, U. (1980) "Natural occurrence of feroxyhite (δ'-FeOOH)." Clays Clay Min. 28, 272-280.

Carlson,L. & Schwertmann, U. (1981) "Natural ferrihydrites in surface deposits from Finland and their association with silica." Geochim. Cosmochim. Acta 45, 421-429.

Chambaere, D., Govaert, A., de Sitter, J. & de Grave, E. (1978) "A Mossbauer investigation of the quadrupole splitting in β-FeOOH." Sol. St. Comm. 26, 657-659.

Childs, C.W. & Johnston, J.H. (1980) "Mossbauer spectra of proto-ferrihydrite at 77 K and 295 K, and a reappraisal of the possible presence of akaganeite in New Zealand soils." Aust. J. Soil Res. 18, 245-250.

Chukhrov, F.V., Ermilova, L.P., Gorshkov, A.I., Zvyagin, B.B., Shukhlistov, A.P., Siderenko, O.V. & Balashova, V.V. (1976) "Uber die natur der eisenoxide in geologisch jungen bildungen." Chemie Erde 33,

109-124.

Chukhrov, F.V., Zvyagin, B.B., Gorshkov, A.I., Ermilova, L.P., Rudnitskaya, Ye.S. (1971) "Towe-Bradley's phase, a product of hypergenese alteration of ores." Izv. Akad. Nauk. SSSR, ser. geol., 1.

Chukhrov, F.V., Zvyagin, B.B., Ermilova, L.P. & Gorshkov, A.I. (1972) "New data on iron oxides inthe weathering zone." Proc. Int. Clay Conf., Madrid, 333-341.

Chukhrov, F.V., Zvyagin, B.B., Gorshkov, A.I., Ermilova, L.P. & Balashova, V.V. (1973) "Ferrihydrite." Int. Geol. Rev. 16, 1131-1143.

Chukhrov, F.V., Zvyagin, B.B., Gorshkov, A.I., Ermilova, L.P., Korovushkin, V.V., Rudnitskaya, Ye.S. & Yakubovskaya, N.Yu. (1977) "Feroxyhite, a new modification of FeOOH." Int. Geol. Rev. 19, 873-890.

Clarke, P.E., Nicholl, A.W. & Carlow, J.S. (1967) "A precision velocity generator suitable for Mossbauer experiments." J. Sci. Instr. 44, 1001-1004.

Cohen, R.L. (editor, 1976) "Applications of Mossbauer Spectroscopy." Vol. I, Academic Press, London.

Creer, K.M. (1962) "On the origin of the magnetisation of red beds." J. Geomagnetism and Geoelectricity 13, 86-100.

Cronan, D.S. (1976) "Manganese nodules and other ferro-manganese oxide deposits." in "Chemical Oceanography." Vol. 5 (editors J.P. Riley & R. Chester), Academic Press, New York, pp. 217-263.

Crosby, S.A. (1982) "The interaction of phosphate with iron oxyhydroxides in simulated estuarine conditions." Ph.D. thesis, Plymouth Polytechnic, Plymouth, UK.

Crosby, S.A., Butler, E.I., Turner, D.R., Whitfield, M., Glasson, D.R. & Millward, G.E. (1981) "Phosphate adsorption onto iron oxyhydroxides at natural concentrations." Environ. Technol. Letts. 2, 371-378.

Crosby, S.A., Glasson, D.R., Cuttler, A.H., Butler, E.I., Turner, D.R., Whitfield, M. & Millward, G.E. (1983) "Surface areas and porosities of Fe(II)- and Fe(II)-derived oxyhydroxides." Environ. Sci. Technol. 17, 709-713.

Cuttler, A.H. (1980) "A Mossbauer and electron paramagnetic resonance study of the oxyhydroxides δ- and δ'-FeOOH and the identification of this material as a

contamination of a Blackpool Kaolin." (unpublished).

Cuttler, A.H. (1981) Private communication.

Cuttler, A.H. (Private comm.)

Dasgupta, D.R. & Mackay, A.L. (1959) "β-Ferric oxyhydroxide and Green Rust." J. Phys. Soc. Japan 14, 932-935.

Dasgupta, D.R. (1961) "Topotactic transformations in iron oxides and oxyhydroxides." Indian J. Phys. 35, 401-419.

Davis, J.A. (1982) "Adsorption of natural dissolved organic matter at the oxide/water interface." Geochim. Cosmochim. Acta 46, 2381-2393.

De Boer, J.H. (1958) "The shape of capillaries." in "The Structure and Properties of Porous Materials." (ed. J.H. de Boer), Butterworths, London, pp. 68-94.

Deer, W.A., Howie, R.A. & Zussman, J. (1962) "Rock Forming Minerals." Vol. 5, Longmans, London.

Dezsi, I. & Fodor, M. (1966) "On the antiferromagnetism of α-FeOOH." phys. stat. sol. 15, 247-254.

Dezsi, I., Keszthelyi, L., Kulgawczuk, D., Molnar, B. & Eissa, N.A. (1967) "Mossbauer study of β- and δ-FeOOH and their disintegration products." phys. stat. sol. 22, 617-629.

Elderfield, H. (1976) "Hydrogenous material in marine sediments: excluding manganese nodules." in "Chemical Oceanography." Vol. 5 (editors J.P. Riley & R. Chester), Academic Press, New York, pp. 137-215.

Evans, U.R. (1967) "The mechanism of rusting." Quart. Revs. 21, 29-42.

Fitzpatrick, R.W. & Schwertmann, U. (1982) "Al-substituted goethite - an indicator of pedogenic and other weathering environments in South Africa." Geoderma 27, 335-347.

Forbes, E.A., Posner, A.M. & Quirk, J.P. (1974) "The specific adsorption of inorganic Hg(II) species and Co(III) complex ions on goethite." J. Colloid Interface Sci. 49, 403-409.

Forbes, E.A., Posner, A.M. & Quirk, J.P. (1976) "The specific adsorption of divalent Cd, Co, Cu, Pb and Zn on goethite." J. Soil Sci. 27, 154-166.

Forsyth, J.B., Hedley, I.G. & Johnson, C.E. (1968) "The magnetic structure and hyperfine field of goethite (α-FeOOH)." J. Phys. C (Proc. Phys. Soc.) ser. 2, 1, 179-188.

Francome, M.H. & Rooksby, H.P. (1959) "Structure transformations effected by the dehydration of diaspore, goethite, and delta ferric oxide." Clay Min. Bull. 4, 1-14.

Gancedo, J.R., Martinez, M.L. & Oton, J.M. (1976) "Mossbauer spectroscopy study of corrosion products of iron with ammonium nitrate in aqueous solutions." J. de Phys. 37, C6, 297-299.

Gangas, N.H., Simopoulos, A., Kostikas, A., Yassoglou, N.J. & Filippaki, S. (1973) "Mossbauer studies of small particles of iron oxides in soil." Clays Clay Min. 21, 151-160.

Garrels, R.M. & MacKenzie, F.T. (1971) "Evolution of Sedimentary Rocks." W.W. Norton & Co., New York.

Gendler, T.S., Kuz'min, R.N. & Urazaeva, T.K. (1976) "Study of the Mossbauer effect in hydrogoethite." Sov. Phys. Crystallogr. 21, 440-444.

Gibbs, M.M. (1979) "A simple method for the rapid

determination of iron in naturals waters." Water Res. 13, 295-297.

Gibb, T.C. (1976) "Principles of Mossbauer Spectroscopy." Chapman and Hall, London.

Glasson, D.R. (1956) "The production of active solids by thermal decomposition: Part VIII. Calcination of calcium hydroxides." J. Chem. Soc., 1506-1510.

Glemser, O. & Gwinner, E. (1939) "Uber eine naue ferromagnetische modifikation des eisen (III) -oxydes." Z. Anorg. Chem., 240, 163-171.

Gloyna, E.F. & Eckenfelder, W.W. (eds. 1970) "Water Quality Improvement by Physical and Chemical Processes." Water Resource Symposium, Austin, Texas.

Goldberg, E.D. (1954) "Chemical scavengers of the sea." J. Geol. 62, 249-265.

Golden, D.C., Bowen, L.H., Weed, S.B. & Bigham, J.M. (1979) "Mossbauer studies of synthetic and soil-occurring aluminium-substituted goethite." Soil Sci. Soc. Am. J. 43, 802-808.

Goodman, B.A & Lewis, D.G. (1981) "Mossbauer spectra of aluminous goethite (α-FeOOH)." J. Soil Sci.

32, 351-363.

Govaert, A., Dauve, C., de Grave, E. & de Sitter, J. (1976a) "On the effective magnetic hyperfine field in naturally occurring goethite." Sol. St. Comm. 18, 389-390.

Govaert, A., Dauve, C., Plinke, P., de Sitter, J., de Grave, E. & Robbrecht, G. (1976b) "Analysing iron ores with Mossbauer spectroscopy." Bull. Soc. Chim. Belg. 85, 251-259.

Greenwood, N.N. & Gibb, T.C. (1976) "Mossbauer Spectroscopy." Chapman and Hall, London, pp. 240-257.

Gregg, S.J. & Sing, K.S.W. (1982) "Adsorption, Surface area and Porosity." 2nd edition, Academic Press, London.

Grimes, N.W. & Collett, A.J. (1971) "Infrared absorption spectra of ferrites." Nature (Phys. Sci.) 230, 158.

Hrynkiewicz, A.Z. & Kulgawczuk, D.S. (1963) "Hyperfine structure of the 14.4 kev gamma line of ^{57}Fe in some iron oxyhydroxides investigated with the Mossbauer effect." Acta Phys. Polon. 24, 689-692.

Hrynkiewicz, A.Z., Kulgawczuk, D.S. & Tomala, K. (1965)

"Antiferromagnetism of α-FeOOH investigated with the Mossbauer effect." Phys. Lett. 17, 93-95.

Ito, A., Ono, K. & Ishikawa, Y. (1963) "A study of the low temperature transition in magnetite." J. Phys. Soc. Japan 18, 1465-1472.

Jenne, E.A. (1968) "Controls on Mn, Fe, Co, Ni, Cu, and Zn concentrations in soils and water: the significant role of hydrous Mn and Fe oxides." in "Trace Inorganics in Water", Adv. Chem. Ser., pp. 337-387.

Johnson, C.E. (1962) "The Mossbauer Effect." Cryogenics 2, 129-135.

Johnson, C.E. (1969) "Antiferromagnetism of γ-FeOOH: a Mossbauer effect study." J. Phys. C (Sol. St. Phys) 2. 1996-2002.

Johnston, J.H. & Glasby, G.P. (1982) "A Mossbauer spectroscopic and X-ray diffraction study of the iron mineralogy of some sediments from the Southwestern Pacific Basin." Marine Chem. 11, 437-448.

Johnston, J.H. & Lewis, D.G. (1983) "A detailed study of the transformation of ferrihydrite to hematite in an aqueous medium at 92° c." Geochim. Cosmochim. Acta 47, 1823-1831.

Kauffman, K. & Hazel, F. (1975) "Mossbauer spectroscopy of aged ferric oxide gels." J. Colloid Interface Sci. 51, 422-426.

Kinniburgh, D.G., Jackson, M.L. & Syers, J.K. (1976) "Adsorption of alkaline earth, transition and heavy metal cations by hydrous oxide gels of iron and aluminium." Soil Sci. Soc. Am. J. 40, 796-799.

Kistner, O.C. & Sunyar, A.W. (1960) "Evidence for quadrupole interaction of Fe^{57m} and influence of chemical binding on nuclear gamma-ray energy." Phys. Rev. Lett. 4, 412-415.

Krauskopf, K.B. (1956) "Factors controlling the concentrations of thirteen rare metals in seawater." Geochim. Cosmochim. Acta 9, 1-26.

Krupyanskii, Y.F. & Suzdalev, J.P. (1974) "Size effects in fine particles of Fe_3O_4." J. de Phys. 35, C6, 407-410.

Kundig, W. (1967) "Evaluation of Mossbauer Spectra for ^{57}Fe." Nucl. Instr. Methods 48, 219-228.

Kundig, W., Bommel, H., Constabaris, G. & Lindquist, R.H. (1966) "Some properties of supported small

α-Fe_2O_3 particles determined with the Mossbauer effect." Phys. Rev. 142, 327-333.

Kundig, W. & Hargrove, R.S. (1969) "Electron hopping in magnetite." Sol. St. Comm. 7, 223-227.

Langmuir, D. & Whittemore, D.O. (1971) "Variations in the stability of precipitated ferric oxyhydroxides." in "Non-equilibrium Systems in Natural Water Chemistry." (ed. J.D. Hem), A.C.S. Symposium Series 106, Washington, D.C., pp. 209-234.

Lepp, H. (ed., 1975) "Geochemistry of Iron." Benchmark Papers in Geology, Vol. 18, Dowden, Hutchinson & Ross, Pennsylvania.

Lewis, D.G. & Schwertmann, U. (1979) "The influence of Al on iron oxides: III. Preparation of Al goethites in M KOH." Clay Min. 14, 115-126.

Lijklema, L. (1980) "Interaction of orthophosphate with iron(III) and aluminium hydroxides." Environ. Sci. Tech. 14, 537-541.

Lipka, J., Morup, S. & Topsoe, H. (1977) "Mossbauer effect studies of superparamagnetic Fe_3O_4." Bratislava Conference on Magnetism.

Logan, N.E., Johnston, J.H. & Childs, C.W. (1976) Mossbauer spectroscopic evidence for akaganeite (.-FeOOH) in New Zealand soils." Aust. J. Soil Res. 14, 217-224.

Loseva, G.V. & Murashko, N.V. (1972) "Dehydration mechanism of β- and δ- iron hydroxides." Izv. Akad. Nauk. SSSR Neorg. Mater. 8, 485-487.

Lowell, S. (1979) "Introduction to Powder Surface Area." Wiley-Interscience, New York.

Mackay, A.L. (1960) "Some aspects of the topochemistry of the iron oxides and hydroxides." Proc. 4th Int. Symp. on the Reactivity of Soilds, Amsterdam (ed. J.H. de Boer, Elsevier, London). pp. 571-583.

Mason, B. & Berry, L.G. (1968) "Elements of Mineralogy." W.H. Freeman & Co., San Francisco.

McGill, I.R., McEnaney, B. & Smith, D.C. (1976) "Crystal structure of green rust formed by corrosion of cast iron." Nature 259, 200-201.

McNab, T.K., Fox, R.A. & Boyle, A.J.F. (1968) "Some magnetic properties of magnetite (Fe_3O_4) microcrystals." J. Appl. Phys. 39, 5703-5711.

Mehra, O.P. & Jackson, M.L. (1960) "Iron oxide removal from soils and clays by a dithionate-citrate system buffered with sodium bicarbonate." Clays Clay Min. Z, 317-327.

Millward, G.E. (private comm.)

Millward, G.E. & Moore, R.M. (1982) "The adsorption of Cu, Mn and Zn by iron oxyhydroxides in model estuarine solutions." Water Res. 16, 981-985.

Minkova, A. & Schunck, J.P. (1975) "Study of superfine γ-FeOOH layers by means of Mossbauer effect." Proc. Bulg. Acad. Sci. 28, 1171-1173.

Misawa, T., Hashimoto, K. & Shimodaira, S. (1973) "Formation of Fe(II)1-Fe(III)1 intermediate green complex on oxidation of ferrous ion in neutral and slightly alkaline sulphate solutions." J. Inorg. Nucl. Chem. 35, 4167-4174.

Misawa, T., Hashimoto, K. & Shimodaira, S. (1974) "The mechanism of formation of iron oxide and oxyhydroxides in aqueous solutions at room temperature." Corrosion Sci. 14, 131-149.

Morup, S., Dumesic, J.A. & Topsoe, H. (1980) "Magnetic microcrystals." in "Applications of Mossbauer

Spectroscopy." Vol. II (ed. R.L. Cohen), Academic Press, London, pp. 1-53.

Murad, E. (1979) "Mossbauer and X-ray data on β-FeOOH (akaganeite)." Clay Min. 14, 273-283.

Murad, E. & Schwertmann, U. (1980) "The Mossbauer spectrum of ferrihydrite and its relation to those of other iron oxides." Am. Mineral. 65, 1044-1049.

Murad, E. & Schwertmann, U. (1983) "The influence of aluminium substitution and crystallinity on the Mossbauer spectra of goethite." Clay Min. 18, 301-312.

Murad, E. & Taylor, R.M. (1984) "The Mossbauer spectra of hydroxycarbonate Green Rusts." Clay Min. 19, 77-83.

Murray, J.W. (1979) "Iron oxides." in "Marine Minerals." (ed. R.G. Burns), Mineral. Soc. Am. Short Course Notes 6, pp. 47-98.

Nakamura, T., Shinjo, T., Endoh, Y., Yamamoto, N., Shiga, M. & Nakamura, Y. (1964) "Fe^{57} Mossbauer effect in ultra fine particles of α-Fe_2O_3." Phys. Lett. 12, 178-179.

Nicholls, D. (1973) "Iron." in "Comprehensive

Inorganic Chemistry." Vol. 3 (ed. J.C. Bailar), Pergamon Press, London, pp. 979-1051.

Noike, T., Nakamura, K. & Matsumoto, J. (1983) "Oxidation of ferrous iron by acidophilic iron-oxidising bacteria from a stream receiving acid mine drainage." Water Res. 17, 21-27.

Norrish, K. & Taylor, R.M. (1961) "The isomorphous replacement of iron by aluminium in soil goethite." J. Soil Sci. 12, 294-306.

Ono, K. & Ito, A. (1962) "Mossbauer study of the internal field of Fe^{57} in α-Fe_2O_3." J. Phys. Soc. Japan 17, 1012-1017.

Pawluk, S. (1972) "Measurement of crystalline and amorphous iron removal in soils." Can. J. Soil Sci. 52, 119-123.

Povitskii, V.A., Makarov, E.F., Murashko, N.V. & Salugin, A.N. (1976a) "Mossbauer study of superparamagnetic δ-FeOOH and its transformation into α-Fe_2O_3." phys. stat. sol. 33, 783-787.

Povitskii, V.A., Salugin, A.N., Makarov, E.F. & Baldokhin, Y.V. (1976b) "Mossbauer investigation of the magnetic structure of hematite containing a small

amount of chromium." Sov. Phys. -Sol. St. 18, 958-959.

Read, H.H. (1973) "Rutley's Elements of Mineralogy." 26th edition, Thomas Murby & Co., London.

Rendon, J.L. & Serna, C.J. (1981) "Ir spectra of powder haematite: effects of particle size and shape." Clay Min. 16, 375-381.

Rossiter, M.J. & Hodgson, A.E.M. (1965) "A Mossbauer study of ferric oxy-hydroxides." J. Inorg. Nucl. Chem. 27, 63-71.

Russell, J.D. (1979) "Infrared spectroscopy of ferrihydrite: evidence for the presence of structural hydroxyl groups." Clay Min. 14, 109-114.

Saraswat, I.P., Vajpei, A.C., Garg, V.K., Sharma, V.K. & Prakash, N. (1979) "Characterisation and thermal transformation of ferric oxide hydrate gel." J. Colloid Interface Sci. 73, 373-380.

Schwertmann, U. & Fischer, W.R. (1973) "Natural 'amorphous' ferric hydroxide." Geoderma 10, 237-247.

Schwertmann, U & Taylor, R.M. (1972) "The

transformation of lepidocrocite to goethite." Clays Clay Min. 20, 151-158.

Schwertmann, U. & Taylor, R.M. (1977) "Iron oxides." in "Minerals in Soil Environments." (eds. J.B. Dixon & S.B. Weed), Soil Sci. Soc. Am., Madison, Wisconsin, pp. 145-179.

Schwertmann, U. & Taylor, R.M. (1979) "Natural and synthetic poorly crystallised lepidocrocite." Clay Mineral. 14, 285-293.

Schwertmann, U. & Thalmann, H. (1976) "The influence of [Fe(II)], [Si], and pH on the formation of lepidocrocite and ferrihydrite during oxidation of aqueous $FeCl_2$ solutions." Clay Min. 11, 189-200.

Sidgwick, N.V. (1950) "The Chemical Elements and Their Compounds." Vol. II, Oxford University Press, London, pp. 1319.

Shinjo, T. (1966) "Mossbauer effect in antiferromagnetic fine particles." J. Phys. Soc. Japan 21, 917-922.

Srivastava, B.N. & Singh, R.P. (1974) "Mossbauer spectroscopic study of thermal transformation of ferric

hydroxide to α-Fe_2O_3." Indian J. Pure Appl. Phys. 12, 311-313.

Srivastava, B.N. & Sharma, R.P. (1972) "Magnetic dilution effects on Morin phase transition in hematite." phys. stat. sol. 49, 135-146.

Stumm, W. & Morgan, J.J. (1981) "Aquatic Chemistry." 2nd edition, Wiley-Interscience, New York.

Sung, W. & Morgan, J.J. (1980) "Kinetics and product of ferrous iron oxygenation in aqueous systems." Environ. Sci. Technol. 14, 561-568.

Takada, T., Kiyama, M., Bando, Y., Nakamura, T., Shiga, M., Shinjo, T., Yamamoto, N., Endoh, Y. & Takaki, H. (1964) "Mossbauer study of α-, β-, and γ-FeOOH." J. Phys. Soc. Japan 19, 1744.

Taylor, H.F.W. (1973) "Crystal structures of some double hydroxide minerals." Mineral. Mag. 39, 377-389.

Taylor, R.M. (1980) "Formation and properties of Fe(II)Fe(III) hydroxy-carbonate and its possible significance in soil formation." Clay Min. 15, 369-382.

Taylor, R.M. & McKenzie, R.M. (1980) "The influence of aluminium on iron oxides: VI. The formation of Fe(II)-Al(III) hydroxy-chlorides, -sulphates, and -carbonates as new members of the pyroaurite group and their significance in soils." Clays Clay Min. 28, 179-187.

Taylor, R.M. & Schwertmann, U. (1974) "Maghemite in soils and its origin: II. Maghemite synthesis at ambient temperature and pH 7." Clay Min. 10, 299-310.

Taylor, R.M. & Schwertmann, U. (1978) "The influence of aluminium on iron oxides: Part I. The influence of Al on Fe oxide formation from the Fe(II) system." Clays Clay Min., 26, 373-383.

Tipping, E. (1981) "The adsorption of aquatic humic substances by iron oxides." Geochim. Cosmochim. Acta 45, 191-199.

Towe, K.M. & Bradley, W.F. (1967) "Mineralogical constitution of colloidal 'hydrous ferric oxides'." J. Colloid Interface Sci. 24, 384-392.

Van der Giessen, A.A. (1966) "The structure of iron (III) oxide-hydrate gels." J. Inorg. Nucl. Chem. 28, 2155-2159.

Van der Giessen, A.A., Rensen, J.G. & van Wieringen, J.S. (1968) "A study of the constitution and freezing behaviour of iron oxide-hydrate gels by means of the Mossbauer effect." J. Inorg. Nucl. Chem. 30, 1739-1744.

Van der Kraan, A.M. & van Loef,J.J. (1966) "Superparamagnetism in submicroscopic α-FeOOH particles observed by the Mossbauer effect." Phys. Lett. 20, 614-616.

Van der Marel, H.W. (1951) "Gamma ferric oxide in sediments." J. Sediment. Petrol. 21, 12-21.

Van der Woude, F. (1966) "Mossbauer effect in α-Fe_2O_3." phys. stat. sol. 17, 417-432.

Van Dongen Torman, J., Jagannathan, R. & Trooster, J.M. (1975) "Analysis of ^{57}Fe Mossbauer hyperfine spectra." Hyperfine Interactions 1, 135-144.

Vertes, A., Korecz, L. & Burger, K. (1979) "Mossbauer Spectroscopy." Elsevier Scientific Publishing Co., Amsterdam.

Verwey, E.J.W., Haayman, P.W. & Romeijn, F.C. (1947) "Physical properties and cation arrangement of oxides with spinel structures: II. Electronic conductivity." J.

Chem. Phys. 15, 181-187.

Vlasov, A.Ya., Loseva, G.V., Makarov, E.F., Murashko, N.V., Petukhov, E.P. & Povitskii, V.A. (1970a) "Mossbauer spectroscopy and X-ray diffraction study of the thermal conversion of δ-FeOOH to α-Fe_2O_3." Sov. Phys. -Sol. St. 12, 1177-1180.

Vlasov, A.Ya., Loseva, G.V., Murashko, N.V. & Petukhov, E.P. (1972) "Change in the crystal structure of iron β-hydroxide in its thermal conversion into haematite." Russian J. Inorg. Chem. 17, 482-483.

Vlasov, A.Ya., Loseva, G.V., Murashko, N.V. & Rubosuev, M.N. (1970b) "Electron microscopy study of the thermal phase transition of β- and δ-FeOOH into α-Fe_2O_3." Izv. Vuz. Fiz. 7, 917-918.

Von Weirman, P.P. (1908) Kolloid Z. 2, 199-203.

Voznyuk, P.O. & Dubinin, V.N. (1973) "Magnetic structure of extremely small antiferromagnetic particles of β-FeOOH." Sov. Phys. -Sol. St. 15, 1265-1266.

Weiser, H.B., Milligan, W.O. & Cook, E.L. (1946) "Beta iron(III) oxide 1-hydrate." Inorg. Syntheses 2, 215-216.

Yamamoto, N., Shinjo, T., Kiyama, M., Bando, Y. & Takada, T. (1968) "Mossbauer effect study of α-FeOOH and β-FeOOH; making use of oriented particles." J. Phys. Soc. Japan 25, 1267-1271.

APPENDIX A

Published work

Thermochimica Acta, 82 (1984) 231–240
Elsevier Science Publishers B.V., Amsterdam – Printed in The Netherlands

VACUUM BALANCE AND RELATED STUDIES OF GREEN AND RED RUSTS

A.H. CUTTLER, D.R. GLASSON and V. MAN

John Graymore Chemistry Laboratories, Department of Environmental Sciences, Plymouth Polytechnic, Plymouth PL4 8AA, Devon, England

ABSTRACT

Green and red rusts are formed when iron is partially or completely oxidised. Analogues of the rusts may be precipitated from iron(II) and iron(III) salt solutions treated with alkali under reducing or oxidising conditions. Variations in surface area and porosity have been investigated by gravimetric nitrogen gas sorption, using vacuum microbalance techniques.

Freshly-precipitated red rusts, hydrous iron(III) oxide, have surface areas of about 200-400 m^2g^{-1}. When they are added to iron(II) hydroxide suspensions kept at pH 7, the green Fe(II)-Fe(III) rusts formed have lower surface areas of about 40-100 m^2g^{-1}, depending on the initial iron(II) sulphate concentrations.

INTRODUCTION

The commonest type of rust seen on the surface of corroded iron is red to reddish-brown in colour, when the iron is mainly in the Fe(III) state, as hydrous iron(III) oxide. For iron to rust at room temperature, both water and oxygen must be present. In air, rusting becomes appreciable above 50 % humidity and the corrosion is severe at 80 % humidity (1). Rusting is initiated by the electrochemical processes of iron, $2Fe \rightarrow 2Fe^{2+} + 4e$, and dissolved oxygen in the water, $O_2 + 2H_2O + 4e \rightarrow 4OH^-$, leading to formation of iron(II) hydroxide, $Fe(OH)_2$. The water acts catalytically as an electron carrier and further oxidation of Fe^{2+} to Fe^{3+} and subsequent hydrolysis produces iron(III) hydroxide, often formulated as $Fe(OH)_3$. Although this is empirically the same as Fe_2O_3, $3H_2O$, the water of constitution does not normally exceed that of Fe_2O_3, H_2O. Additional water is present as adsorbed water, often in gel form, so that no characteristic trihydrate crystal lattice has been found, analogous to those of the alumina trihydrates. The emoirical Fe_2O_3,H_2O is really an iron(III) oxyhydroxide, FeOOH, of which there are 5 crystal forms known, viz. α, β, γ, δ and δ'. Thus the term hydrous iron(III) oxide covers both water of constitution and adsorbed water and also defines red rust.

Green rusts may be formed if there is insufficient oxygen for complete oxidation of the iron. Thus in steel reinforcements in concrete piles, access of air is insufficient to oxidise the iron fully to the Fe(III) state and surface films are commonly black (Fe_3O_4) or sometimes white, green or yellow

0040-6031/84/$03.00

($Fe(OH)_2$ and basic salts containing some Fe(III) iron), changing rapidly to red on exposure to air. Similarly in soils coloured by iron oxides, anoxic regions contain green layers where red hydrous iron(III) oxides have been partially reduced to the iron(II) state.

The term "green rusts" is used in a general way to describe any green oxide material resulting from the corrosion of iron. However, iron(II) hydroxide, $Fe(OH)_2$, is white when pure and becomes green on partial oxidation or when it forms basic salts with acid radicals, e.g., sulphate formed from sulphur dioxide pollution in the atmosphere. Thus green rusts are essentially mixed hydrous Fe(II)-Fe(III) oxides. There is some chemical combination between the Fe(II) and Fe(III) oxides producing material with a characteristic crystal lattice and definite chemical formula within stoicheiometric limits (2, 3). This material is termed "Green Rust" with capitals G and R to distinguish it from the non-stoicheiometric green rusts. In the Green Rust crystal lattice, some of the OH^- groups can be replaced by SO_4^{2-} radicals (from basic Fe(II) salts) without extensive modification of the lattice structure; similarly, there may be replacement by carbonate CO_3^{2-} radicals.

Analogues of the rusts may be precipitated from solutions of iron(II) and iron(III) salts treated with alkali under reducing or oxidising conditions. In the present research, the composition, surface activity and porosity of green and red rusts have been investigated using thermogravimetric, electrochemical, Mössbauer and infra-red spectroscopic techniques in conjunction with X-ray diffractometry and vacuum microbalance techniques. Changes in surface area and porosity of the rusts during their production and ageing have been determined by gravimetric nitrogen gas sorption.

EXPERIMENTAL

Preparation of samples

Iron(III) oxyhydroxides (red rust analogues) are precipitated from Fe(III) salt solutions by addition of alkali mainly at pH levels of about 1. Iron(II) hydroxides precipitate from Fe(II) salt solutions mainly at pH 6-7. Thus green rusts are prepared best by keeping the pH just above 7 to avoid dissolution of iron(II) hydroxide. These principles are illustrated in the following preparations.

(a) Samples of iron(III) oxyhydroxide red rusts were precipitated from solutions of 0.1M.$FeCl_3$ by addition of M.KOH. The pH was taken to about 11, so that virtually all of the iron would have come out of solution. One sample was then left to age in solution for approximately 8 months. Subsequently, the precipitate was removed, washed twice with distilled water and acetone to arrest ageing (4), before being dried in air at room temperature. As shown by the X-ray, Mössbauer and infra-red spectra, the end-product was a sample of well-crystalline

goethite (α-FeOOH).

(b) Two samples of hydrous iron(II) oxides were precipitated from solutions of 0.1M.$FeSO_4$ and 0.1M.$FeCl_2$ with M.KOH and 0.1M.NaOH, respectively, under anoxic conditions (nitrogen bubbling of solutions in an enclosed vessel). The green precipitates were washed with nitrogen-saturated acetone in a nitrogen-filled glove-box and then vacuum dried. The precipitates were so unstable to oxidation that even these procedures resulted in some oxidation of the material, so that they were lime-green to yellow after vacuum drying. The dried materials were stored in sealed test-tubes under nitrogen until required. The X-ray diffraction traces showed both samples to be amorphous, but in accordance with earlier electro-chemical evidence (from pH changes during precipitation (5)), they consisted mainly of $Fe(OH)_2$ with some basic Fe(II) salts and Fe(III) impurities. The instability of the basic salts to form $Fe(OH)_3$ as more alkali is added during preparation probably accounts for the low crystallinity of the final products.

(c) Samples of green rusts, mixed Fe(II)-Fe(III) hydrous oxides, were made by the addition of hydrous iron(III) oxide suspension to solutions of iron(II) sulphate under anoxic conditions. The hydrous iron(III) oxide suspensions were made by the addition of 0.1M.NaOH to 50 cm^3 0.1M.$FeCl_3$ or $Fe(NO_3)_3$ until the pH was approximately 7.0-7.5. Iron(II) sulphate solutions of 0.1M, 0.05M, 0.025M and 0.01M concentrations were taken to just above pH 7 by addition of M.KOH in the presence of flowing nitrogen. Thus the initial ratios of Fe(II):Fe(III) ions were 5:1, 2:1, 1:1 and 0.4:1 respectively. The resulting Fe(II) and Fe(III) hydrous oxide suspensions were mixed by magnetic stirring and also by the nitrogen bubbling. The pH was maintained at just above 7 by adding more alkali as required. Depending on the initial ratio of Fe(II):Fe(III), the original greenish-brown mixed suspensions acquired colours ranging from dark-green to murky-green after 2-3 hours. The precipitates were removed by means of separating funnels and centrifuging in stoppered test-tubes, before being washed with nitrogen-saturated acetone and finally vacuum dried. X-ray diffraction traces of the two samples with initial Fe(II):Fe(III) ratios of 5:1 and 2:1 identified them as true Green Rust compounds with some contamination of goethite.

The Green Rusts have been defined as mixed Fe(II)-Fe(III) hydroxy compounds with basic formula $Fe_x^{2+} - Fe_y^{3+} (O^{2-}_y, OH^-_{2x+y})$, where x = 1.45-1.6 and y = 0.9-2.55 and some of the OH^- groups can be replaced by anions such as Cl^-, Br^-, SO_4^{2-} or CO_3^{2-} etc. Thus the ratios of Fe(II):Fe(III) are in fixed ranges, viz., 4:1 to 2:1 to 0.75:1. Accordingly, the remaining two samples prepared with low initial Fe(II):Fe(III) ratios of 1:1 and 0.4:1 were shown by X-ray diffraction and infra-red spectroscopy to be mainly goethite. Nevertheless, all four of the precipitates showed an infra-red absorption band for sulphate at 1100-1250 cm^{-1}. The Mössbauer spectra of the samples show the presence of

both Fe^{2+} and Fe^{3+} ions along with a magnetic hyperfine field due to goethite. The decrease in Fe(II):Fe(III) ratios in the precipitates as the initial Fe(II):Fe(III) ratios decrease is very evident in the Mössbauer spectra.

Gravimetric nitrogen gas sorption

The surface areas of the samples were determined by a gravimetric gas sorption technique (6), using nitrogen adsorption at -196 °C recorded on a CI Electronics Microforce Mark 2B balance. The samples were outgassed in vacuo at room temperature beforehand and their dry weights were between 100-250 mg. Balance sensitivity ranges used were 0-2.5 mg, 10 mg and 100 mg for measuring the nitrogen uptake. The adsorption isotherms also indicated any porosity present (from hysteresis) and pore size ranges.

Thermogravimetric and titrimetric analysis

The total iron content of the hydrous Fe(II)-Fe(III) oxide samples was determined by TG, calcining portions at 1000 °C for 1-2 h to give a residue of α-Fe_2O_3. The % Fe^{2+} was determined by dissolving a portion of the sample in 6M.HCl and titrating the solution with 0.005M.$Ce(SO_4)_2$. The ferroin indicator was sufficiently sensitive at this low concentration, but required a blank determination correction of about 0.2-0.3 cm^3.

The % SO_4^{2-} was determined by dissolving a portion of the sample in 6M.HCl and adding barium chloride to precipitate the sulphate as $BaSO_4$ for gravimetric determination.

RESULTS AND DISCUSSION

The adsorption isotherms for the hydrous iron oxide samples are shown in Fig. 1-4. The isotherms give linear B.E.T. plots from which the calculated specific surface areas are shown in Table 1. The chemical compositions of the hydrous Fe(II)-Fe(III) oxides are given in Table 2.

In Fig. 1, the adsorption isotherms are shown for (i) hydrous Fe(II) oxide precipitated from $FeSO_4$, (ii) hydrous Fe(II) oxide precipitated from $FeCl_2$, and (iii) well-crystalline goethite precipitated from $FeCl_3$. They are all type IV.

Isotherm (iii) shows adsorption hysteresis above a relative pressure of 0.5, indicating an almost full range of mesopores (3 to 50 nm diameter). The surface area of this 8-months aged goethite is 149 m^2g^{-1}. Samples of freshly-produced material have higher specific surfaces of 200-400 m^2g^{-1}. Thus it is apparent that ageing in solution has improved the crystallinity of the goethite. The freshly-prepared samples with the highest surface areas (ca. 400 m^2g^{-1}) give type I isotherms (Fig. 2), indicating some microporosity (pores below 2 nm diameter). The micropores evidently disappear on ageing leaving only meso and macropores, so that the isotherms change to type IV. When iron (III)

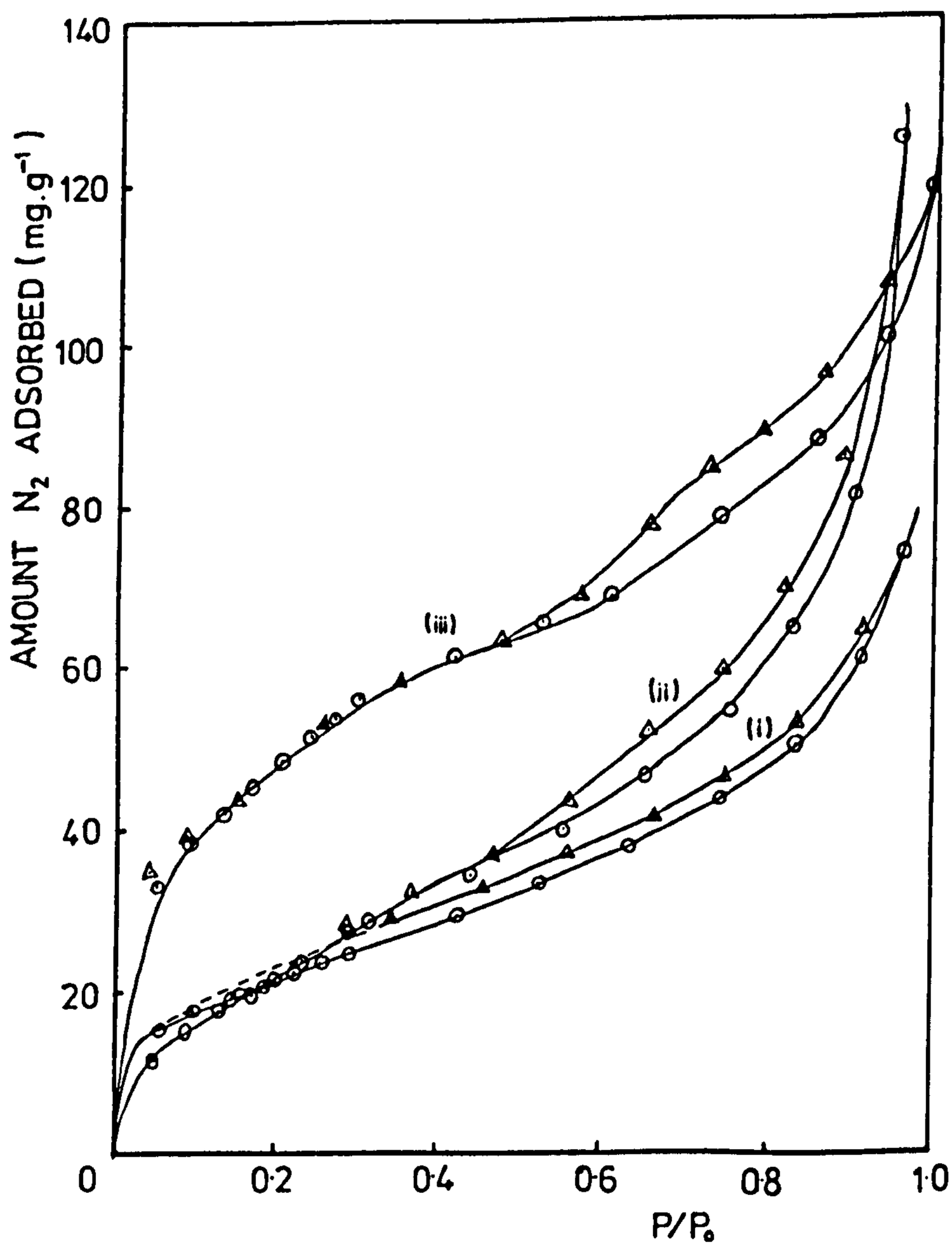

Key: (i) hydrous Fe(II) oxide precipitated from $FeSO_4$
(ii) hydrous Fe(II) oxide precipitated from $FeCl_2$
(iii) hydrous Fe(III) oxide precipitated from $FeCl_3$ and aged 8 months to well-crystalline goethite
⊙ adsorption points △ desorption points

Fig. 1. Comparison of nitrogen adsorption isotherms at -196 °C between Fe(II)-derived and Fe(III)-derived hydrous oxides

TABLE 1

Surface areas of hydrous iron oxides

No.	Sample Description	Derivation	Initial Fe(II):Fe(III) ratio	Specific surface, m^2g^{-1}
1	Hydrous Fe(II) oxide	0.1M.$FeSO_4$	—	64
2	Hydrous Fe(II) oxide	0.1M.$FeCl_2$	—	76
3	Hydrous Fe(III) oxide	0.1M.$FeCl_3$	—	149
4	Hydrous Fe(II)-Fe(III) oxide (Green Rust A)	0.1M.$FeSO_4$	5:1	44
5	Hydrous Fe(II)-Fe(III) oxide (Green Rust B)	0.05M.$FeSO_4$	2:1	55
6	Hydrous Fe(II)-Fe(III) oxide (green rust A)	0.025M.$FeSO_4$	1:1	98
7	Hydrous Fe(II)-Fe(III) oxide (green rust B)	0.01M.$FeSO_4$	0.4:1	93

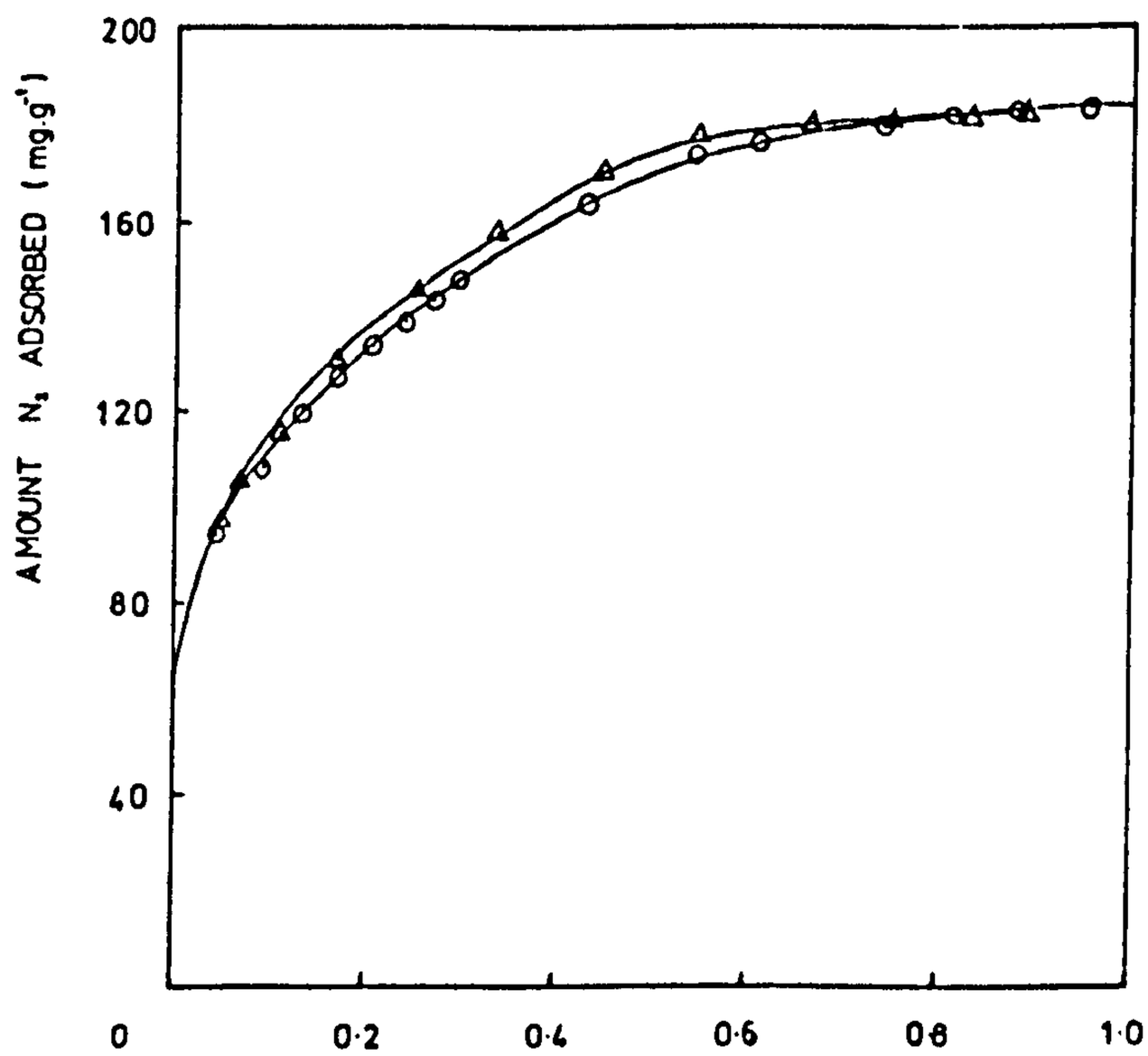

⊙ adsorption points △ desorption points

Fig. 2. Nitrogen adsorption isotherm at -196 °C on a freshly-prepared hydrous Fe(III) oxide. (S = 170 m^2g^{-1})

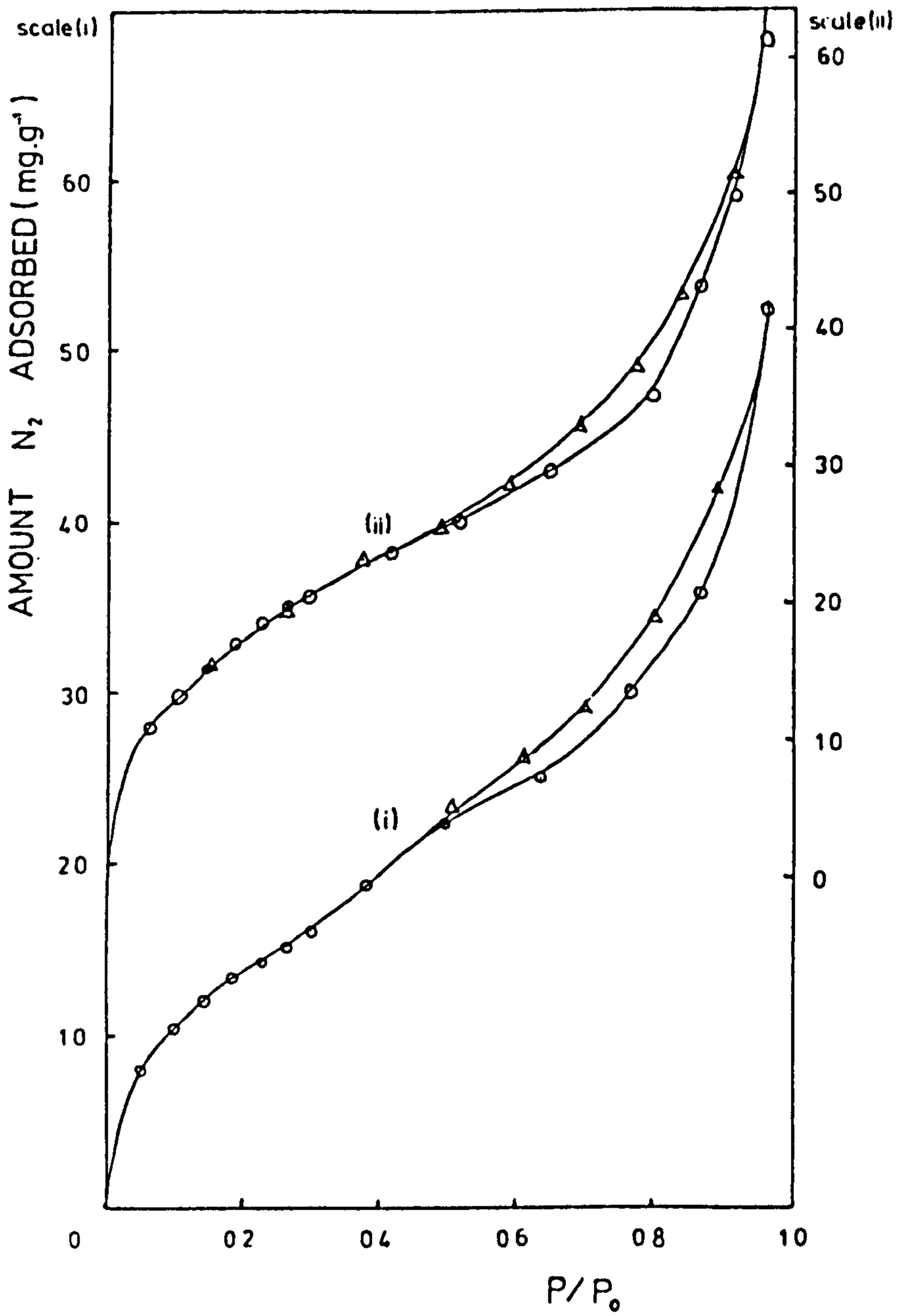

Key:-
(i) Green Rust A from 0.1M.$FeSO_4$ with an initial Fe(II):Fe(III) ratio of 5:1.
(ii) Green Rust B from 0.05M.$FeSO_4$ with an initial Fe(II):Fe(III) ratio of 2:1.

FIG. 3. Nitrogen adsorption isotherms at -196 ^{0}C for Green Rusts.

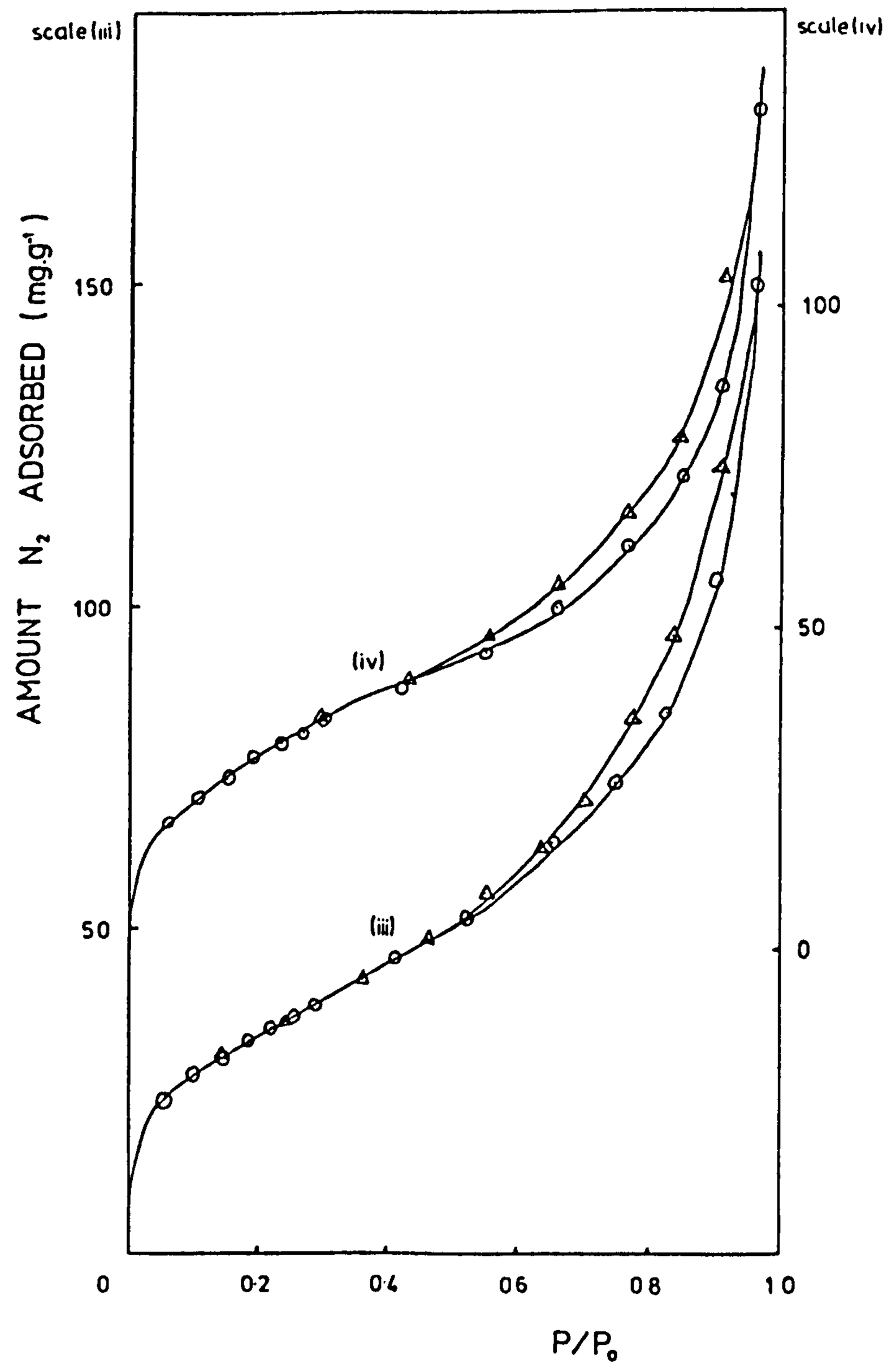

Fig. 4. Nitrogen adsorption isotherms at -196 ^{o}C for green rusts from 0.025 and 0.01M.$FeSO_4$ with lower initial Fe(II):Fe(III) ratios of 1:1 and 0.4:1.

TABLE 2

Chemical analysis of the hydrous Fe(II)-Fe(III) oxides

Sample	Initial Fe^{2+} : Fe^{3+} ratio	SO_4^{2-}	% Fe^{2+}	% Fe^{3+}	% total Fe
Green Rust A	5:1	18.5	12.7	42.5	55.2
Green Rust B	2:1	15.2	8.3	41.5	49.8
green rust A	1:1	10.0	2.4	51.4	53.8
green rust B	0.4:1	-	0.7	55.8	56.5

oxyhydroxide is precipitated from very dilute $FeCl_3$ solutions (ca. 10^{-5}M), the rate of nucleation is slower and less active samples are produced (nearer 200 m^2g^{-1}). Thus Crosby et al (7, 8) have shown that these iron(III) oxyhydroxides on ageing increase their surface areas to a maximum before decreasing in the normal way. This has been ascribed to the conversion of the initially-precipitated δ-FeOOH to the more stable goethite, α-FeOOH, which subsequently ages.

The two hydrous iron oxides derived from the Fe(II) salts have adsorption isotherms which also show practically the full range of mesopores. Some of the desorption points at the low relative pressures on isotherm (i) have long equilibrium times and hence the hysteresis loop does not completely close experimentally. The initial material precipitated from the Fe(II) solutions was dark green in colour and very unstable to oxidation. Thus the nitrogen sorption measurements were therefore of the almost completely oxidised material, cf. Table 2. However, these Fe(II)-derived hydrous oxides have much lower surface areas (60-80 m^2g^{-1}) than the aged goethite which was Fe(III)-derived. So even though the final state of the iron in both types of materials is mainly or completely III, the initial iron state must be important to the microstructure of the end-product and hence to its surface area and porosity.

In Fig. 3 and 4, the adsorption isotherms are shown for the four hydrous Fe(II)-Fe(III) oxides with initial Fe^{2+}:Fe^{3+} ratios ranging from 5:1 to 0.4:1. The surface areas (Table 1) of the Green Rusts (samples 4 and 5) are considerably lower than what would be expected from corresponding mixtures of Fe(II)- and Fe(III)-derived oxides (cf. samples 1 and 3). This indicates that the Green Rust structures are markedly different from those of the materials from which they have been produced, as confirmed by X-ray diffraction. The two remaining green rust samples (6 and 7), prepared with low initial Fe(II):Fe(III) ratios of 1:1 and 0.4:1 were shown by X-ray diffraction to be mainly goethite; accordingly their surface areas are much higher than those of the Green Rusts, viz., 98 and 93 m^2g^{-1} compared with 44 and 55 m^2g^{-1}. Nevertheless, the surface areas in the 90-100 m^2g^{-1} range still fall short of those for goethite samples directly precipitated from Fe(III) salt solutions (140 m^2g^{-1} upwards), but they

are more comparable with products from hydrolysis and oxidation of Fe(II) salt solutions 80-120 m^2g^{-1}), as found by Crosby et al (7, 8). At the lowest concentrations, 10^{-5}-10^{-3}M, and with no goethite (or δ-FeOOH convertible to goethite) present initially, the Fe(II) salts hydrolyse and oxidise to form mainly γ-FeOOH, lepidocrocite. But at somewhat higher concentrations and with goethite (or ferrihydrite, δ-FeOOH) present initially, the products are mainly goethite, α-FeOOH, suggesting that there has been some crystal growth on the added goethite ("seeding out") which would reduce its surface area.

The magnitude and variation of the % SO_4^{2-} in Table 2 show that sulphate is an important factor in the formation of Green Rusts. It is likely that the sulphate comes out of solution at the same time as the iron(II) hydroxide to form basic sulphate precipitates, which react with the surface of the iron(III) oxyhydroxide. Since the Green Rusts have comparatively low surface areas, the higher concentrations of sulphate evidently promote coagulation and crystal growth with loss of surface and porosity.

REFERENCES

1 U.R. Evans, Quart. Revs., Lond., 21 (1967) 29
2 J.D. Bernal, D.K. Dasgupta and A.L. Mackay, Clay Miner. Bull., 4 (1959) 15-30
3 R.M. Taylor and R.M. McKenzie, Clays and Clay Minerals, 28 (1980) 179-187
4 D.R. Glasson, J. appl. Chem., Lond., 10 (1960) 38-42
5 H.T.S. Britton, Hydrogen Ions, Chapman and Hall, London, 1955, Vol. 2, pp. 61-66
6 D.R. Glasson, J. chem. Soc., 1956, pp. 1506-1510
7 S.A. Crosby, D.R. Glasson, G.E. Millward, E.I. Butler, D.R. Turner and M. Whitfield, Environmental Technology Letters, 2 (1981) 371-378; idem., Amer. J. Environmental Sci. Technology, 17 (1983) in press
8 J.G. Marsh, S.A. Crosby, D.R. Glasson and G.E. Millward, Thermochim. Acta, (1984), this volume.

APPENDIX B

Sample	IFFR	$[FeSO_4]_I$ (M)	$\langle Fe(II)\rangle_t$ (mmole)	$\langle Fe(II)\rangle_w$ (mmole.mmole^{-1})
S21-3-83	0.4	0.01	1.34	0.27
S23-3-83	1	0.025	4.04	0.81
GR3	2	0.05	9.06	1.81
GR4	2	0.05	9.38	1.88
S7-2-83	5	0.10	13.04	2.61

< > = amount of (t = total, s = specific)
<Fe(III)> = 5 mmole

Appendix B Fe(II) uptake for sulphate GRs and non-GRs derived from $\leq$ 0.1 M $FeSO_4$.